

THE TRAP-LOADED CYLINDRICAL ANTENNA

by
Dean Lance Smith

A dissertation submitted in partial fulfillment
of the requirements for the degree of
Doctor of Philosophy
(Electrical Engineering)
in The University of Michigan
1972

Doctoral Committee:

Professor John A. M. Lyon, Co-Chairman
Professor Chen-To Tai, Co-Chairman
Professor Chiao-Min Chu
Professor Ralph E. Hiatt
Associate Professor Roger D. Low

ABSTRACT

THE TRAP-LOADED CYLINDRICAL ANTENNA

by
Dean Lance Smith

Co-Chairmen: John A. M. Lyon and Chen-To Tai

The trap-loaded cylindrical antenna is a cylindrical antenna having one or more traps located in its arms. The traps are either parallel inductor-capacitor circuits or short-circuited transmission line stubs that are designed to be anti-resonant (have essentially an infinite input impedance) at some particular frequency. The location and the anti-resonant frequency of the traps are selected to enhance some property of the antenna.

Historically, two types of trap-loaded cylindrical antennas have been given specific names. A trap-loaded cylindrical antenna designed to give a radiation pattern and input impedance similar to that of a half-wave dipole on several frequencies that are approximately integral multiples of one another is called the trap antenna. A trap-loaded cylindrical antenna with traps spaced at approximately integral multiples of one-half the wave length corresponding to the anti-resonant frequency of the trap is called a Franklin antenna or Franklin array.

This study was confined to the properties of trap-loaded cylindrical antennas that contained only one trap in each arm. The effect of the length of the outer section,

length of the inner section, diameter of the cylinder, characteristic impedance or inductance-capacitance ratio of the trap, feed-gap width and trap-gap width on the input impedance, radiation pattern and current distribution were studied both experimentally and with the aid of two numerical solutions of an integral equation for the current distribution.

The conclusions drawn from this study are that the design procedure for the trap antenna described by Greenberg (1956), adjusting the anti-resonant frequency of the trap to control the upper resonant frequency and adjusting the length of the outer section to control the lower resonant frequency, is indeed valid. Graphs suitable for designing trap antennas using this procedure are available for the first time in this thesis. Furthermore, it was shown that the characteristic impedance or inductance-capacitance ratio of the trap can also be adjusted to vary the lower resonant frequency of the antenna. Design graphs using this procedure are also available for the first time in this thesis. This study also showed that a relatively wide range of upper to lower antenna resonant frequency ratios can be obtained while still maintaining radiation patterns and input impedances close to those of a half-wave dipole at both frequencies. Graphs are available showing the trade off in pattern shape and input impedance that must be made to obtain resonant frequency ratios other than 2 to 1.

It was discovered that the Franklin antenna must be operated somewhat below the nominal design frequency, have the spacing between traps shortened somewhat, or possibly (this was not fully explored in the thesis) have the trap tuned somewhat above the nominal design frequency for it to have a radiation pattern similar to a co-linear array of half-wave dipoles. Furthermore, the thicker the antenna, the more pronounced this effect is. While the nominal design was discovered to give an input impedance nearly resistive and near 70 ohms (for a dipole), any of the above modifications studied resulted in a non-resonant, highly capacitive input impedance.

Greenberg, Arthur (1956), "Simple Trap Construction for the Multiband Antenna," QST, v. 40, n. 10, pp. 18-19, 120.

ACKNOWLEDGEMENTS

The author wishes to thank the members of his committee, and in particular its co-chairmen, Professors Lyon and Tai, for their many helpful suggestions and their patience. He also appreciates the time and trouble Mr. Yu-Ping Liu and Mr. Tommy C. Tong took to discuss the numerical solution of integral equations. The author also wishes to thank Miss Rosslyn Cannon and Mr. Charles Loftis who assisted with some of the measurements and Mr. Chester Grabowski who did such an excellent job of constructing the current probe used in the current distribution measurements. Above all, the author would like to thank his wife, Dr. Patricia Linda Smith, for her patience and wit.

TABLE OF CONTENTS

ACKNOWLEDGEMENTS	ii
TABLE OF CONTENTS	iii
LIST OF ILLUSTRATIONS	v
LIST OF APPENDICES	xii
I INTRODUCTION	1
1.1 Statement of Problem	1
1.2 History of Problem	3
1.3 Solution of Problem	6
II THEORETICAL SOLUTION	7
2.1 Derivation of Integral Equation	7
2.2 Solution of Integral Equation	15
2.3 Subsections and Point Matching	18
2.4 Polynomial and Point Matching	26
2.5 Radiation Pattern	33
III EXPERIMENTAL PROCEDURE	34
3.1 Model Details	35
3.2 Impedance Measurements	41
3.3 Radiation Patterns	46
3.4 Current Distribution	48
IV RESULTS	51
4.1 Consistency Checks	52
4.2 Discussion	63
V CONCLUSIONS	94

REFERENCES	96
APPENDICES	98
A: Additional Input Impedances	98
B: Selected Radiation Patterns	132
C: Selected Current Distributions	135
D: Photographs	149

LIST OF ILLUSTRATIONS

Figure		Page
1-1	Illustration of the Symmetric Trap-Loaded Cylindrical Antenna	2
2-1	Application of the Compensation Theorem to the Trap-Loaded Cylindrical Antenna	8
2-2	Geometry of the Trap-Loaded Cylindrical Antenna	10
3-1	Construction of a 34.8 Ohm Transmission Line Trap	36
3-2	Impedance Measurement Set-Up (Copper Tubing Series)	43
3-3	Impedance Measurement Set-Up (2x4 Frame Series)	45
3-4	Radiation Pattern Measurement Set-Up	47
3-5	Current Distribution Measurement Set-Up	49
4-1	Convergence of the Theoretical Solutions for a Half-Wave Dipole Antenna	54
4-2	Convergence of the Theoretical Solutions for a Trap Antenna at the Anti-Resonant Frequency of the Trap	55
4-3	Convergence of the Theoretical Solutions for a Franklin Antenna at the Anti-Resonant Frequency of the Trap	56
4-4	Input Impedance of a Monopole Antenna	58
4-5	Input Impedance of a Dipole Antenna	59
4-6	Amplitude of the Current Distribution on a Half-Wave Dipole	61
4-7	Phase of the Current Distribution on a Half-Wave Dipole	62
4-8	Input Impedance of a Trap Antenna with a 34.8 Ohm Transmission Line Trap	64
4-9	Input Impedance of a Trap Antenna with a 34.8 Ohm Transmission Line Trap	65

Figure		Page
4-10	Input Impedance of a Trap Antenna with a 53 Ohm L-C Trap	67
4-11	Linear Power Radiation Patterns of a Trap Antenna as a Function of Frequency Normalized to the Anti-Resonant Frequency of the Trap	68
4-12	Amplitude of the Current Distribution on a Trap Antenna at the Anti-Resonant Frequency of the Trap	69
4-13	Phase of the Current Distribution on a Trap Antenna at the Anti-Resonant Frequency of the Trap	70
4-14	Input Impedance of a Franklin Antenna with a 34.8 Ohm Transmission Line Trap	72
4-15	Input Impedance of a Franklin Antenna with a 34.8 Ohm Transmission Line Trap	73
4-16	Input Impedance of a Franklin Antenna with a 53 Ohm L-C Trap	74
4-17	Linear Power Radiation Patterns of a Franklin Antenna as a Function of Frequency Normalized to the Anti-Resonant Frequency of the Trap	75
4-18	Amplitude of the Current Distribution on a Franklin Antenna at the Anti-Resonant Frequency of the Trap	76
4-19	Phase of the Current Distribution on a Franklin Antenna at the Anti-Resonant Frequency of the Trap	77
4-20	Linear Power Radiation Patterns of a Trap Antenna When the Trap is Anti-Resonant	78
4-21	Linear Power Radiation Patterns of a Franklin Antenna When the Trap is Anti-Resonant	78
4-22	Linear Power Radiation Patterns of a Franklin-Like Trap-Loaded Cylindrical Antenna as a Function of Length When the Trap is Anti-Resonant	80
4-23	Input Impedance for a Franklin Antenna as a Function of L/λ_0 Where the Trap is Anti-Resonant	81

Figure		Page
4-24	The First Two Resonant Frequencies of a Trap-Loaded Cylindrical Antenna as a Function of the Length of the Outer Arm	83
4-25	The First Two Resonant Frequencies of a Trap-Loaded Cylindrical Antenna as a Function of the Length of the Inner Arm	85
4-26	The First Two Resonant Frequencies of a Trap-Loaded Cylindrical Antenna as a Function of the Characteristic Impedance of the Trap	86
4-27	The First Resonant Frequency of a Trap Antenna as a Function of the Inductive Reactance of the Trap	88
4-28	The First Two Resonant Frequencies of a Trap Antenna as a Function of the Feed Gap Width	89
4-29	The First Two Resonant Frequencies of a Trap Antenna as a Function of the Trap Gap Width	90
4-30	The First Two Resonant Frequencies of a Trap Antenna as a Function of the Antenna Radius	91
4-31	The First Two Resonant Frequencies of a Franklin Antenna as a Function of the Antenna Radius	92
A-1	Input Impedance of a Trap-Loaded Cylindrical Antenna with a 34.8 Ohm Transmission Line Trap, $L/s = 1\frac{1}{4}$, $s = \lambda_0/4$	99
A-2	Input Impedance of a Trap-Loaded Cylindrical Antenna with a 34.8 Ohm Transmission Line Trap, $L/s = 1\frac{1}{2}$, $s = \lambda_0/4$	100
A-3	Input Impedance of a Trap-Loaded Cylindrical Antenna with a 34.8 Ohm Transmission Line Trap, $L/s = 1\text{-}3/4$, $s = \lambda_0/4$	101
A-4	Input Impedance of a Trap-Loaded Cylindrical Antenna with a 34.8 Ohm Transmission Line Trap, $L/s = 2\frac{1}{4}$, $s = \lambda_0/4$	102
A-5	Input Impedance of a Trap-Loaded Cylindrical Antenna with a 34.8 Ohm Transmission Line Trap, $L/s = 2\frac{1}{2}$, $s = \lambda_0/4$	103

Figure		Page
A-6	Input Impedance of a Trap-Loaded Cylindrical Antenna with a 34.8 Ohm Transmission Line Trap, $L/s = 2-3/4$, $s = \lambda_0/4$	104
A-7	Input Impedance of a Trap-Loaded Cylindrical Antenna with a 34.8 Ohm Transmission Line Trap, $L/s = 3\frac{1}{4}$, $s = \lambda_0/4$	105
A-8	Input Impedance of a Trap-Loaded Cylindrical Antenna with a 34.8 Ohm Transmission Line Trap, $L/(L - s) = 1\frac{1}{2}$ and $(L - s) = \lambda_0/4$	106
A-9	Input Impedance of a Trap-Loaded Cylindrical Antenna with a 34.8 Ohm Transmission Line Trap, $L/(L - s) = 1-3/4$ and $(L - s) = \lambda_0/4$	107
A-10	Input Impedance of a Trap-Loaded Cylindrical Antenna with a 34.8 Ohm Transmission Line Trap, $L/(L - s) = 2\frac{1}{4}$ and $(L - s) = \lambda_0/4$	108
A-11	Input Impedance of a Trap-Loaded Cylindrical Antenna with a 34.8 Ohm Transmission Line Trap, $L/(L - s) = 2\frac{1}{2}$ and $(L - s) = \lambda_0/4$	109
A-12	Input Impedance of a Trap Antenna with a 53 Ohm Inductor-Capacitor Trap	110
A-13	Input Impedance of a Trap Antenna with a 53 Ohm Inductor-Capacitor Trap	111
A-14	Input Impedance of a Trap Antenna with a 53 Ohm Inductor-Capacitor Trap	112
A-15	Input Impedance of a Franklin Antenna with a 53 Ohm Inductor-Capacitor Trap	113
A-16	Input Impedance of a Franklin Antenna with a 53 Ohm Inductor-Capacitor Trap	114
A-17	Input Impedance of a Franklin Antenna with a 53 Ohm Inductor-Capacitor Trap	115
A-18	Input Impedance of a Trap Antenna with a 88.5 Ohm Inductor-Capacitor Trap	116
A-19	Input Impedance of a Trap Antenna with a 88.5 Ohm Inductor-Capacitor Trap	117
A-20	Input Impedance of a Franklin Antenna with a 88.5 Ohm Inductor-Capacitor Trap	118
A-21	Input Impedance of a Franklin Antenna with	119

Figure		Page
	a 88.5 Ohm Inductor-Capacitor Trap	
A-22	Input Impedance of a Trap Antenna with a 18.5 Ohm Transmission Line Trap	120
A-23	Input Impedance of a Trap Antenna with a 62.5 Ohm Transmission Line Trap.	121
A-24	Input Impedance of a Trap Antenna with a 100 Ohm Transmission Line Trap	122
A-25	Input Impedance of a Franklin Antenna with a 18.5 Ohm Transmission Line Trap	123
A-26	Input Impedance of a Franklin Antenna with a 62.5 Ohm Transmission Line Trap	124
A-27	Input Impedance of a Franklin Antenna with a 100 Ohm Transmission Line Trap	125
A-28	Input Impedance of a Trap Antenna with a 34.8 Ohm Transmission Line Trap and a 2/16 Inch Feed Gap Width	126
A-29	Input Impedance of a Trap Antenna with a 34.8 Ohm Transmission Line Trap and a 3/16 Inch Feed Gap Width	127
A-30	Input Impedance of a Trap Antenna with a 34.8 Ohm Transmission Line Trap and a 4/16 Inch Feed Gap Width	128
A-31	Input Impedance of a Trap Antenna with a 34.8 Ohm Transmission Line Trap and a 2/16 Inch Trap Gap Width	129
A-32	Input Impedance of a Trap Antenna with a 34.8 Ohm Transmission Line Trap and a 3/16 Inch Trap Gap Width	130
A-33	Input Impedance of a Trap Antenna with a 34.8 Ohm Transmission Line Trap and a 4/16 Inch Trap Gap Width	131
B-1	Linear Power Radiation Patterns of a Series of Trap-Loaded Cylindrical Antennas at the Anti-Resonant Frequency of the Trap as a Function of the Antenna Length to Trap Location Ratio	133
B-2	Linear Power Radiation Patterns of a Series of Trap-Loaded Cylindrical Antennas at the	134

Figure		Page
	Anti-Resonant Frequency of the Trap as a Function of the Antenna Length to Outer Section Length Ratio	
C-1	Current Distribution for a Trap-Loaded Cylindrical Antenna at the Anti-Resonant Frequency of the Trap, $L = (5/16)\lambda$, $L/s = 1\frac{1}{4}$	136
C-2	Current Distribution for a Trap-Loaded Cylindrical Antenna at the Anti-Resonant Frequency of the Trap, $L = (3/8)\lambda$, $L/s = 1\frac{1}{2}$	137
C-3	Current Distribution for a Trap-Loaded Cylindrical Antenna at the Anti-Resonant Frequency of the Trap, $L = (7/16)\lambda$, $L/s = 1\text{-}3/4$	138
C-4	Current Distribution for a Trap-Loaded Cylindrical Antenna at the Anti-Resonant Frequency of the Trap, $L = (1/2)\lambda$, $L/s = 2$	139
C-5	Current Distribution for a Trap-Loaded Cylindrical Antenna at the Anti-Resonant Frequency of the Trap, $L = (9/16)\lambda$, $L/s = 2\frac{1}{4}$	140
C-6	Current Distribution for a Trap-Loaded Cylindrical Antenna at the Anti-Resonant Frequency of the Trap, $L = (5/8)\lambda$, $L/s = 2\frac{1}{2}$	141
C-7	Current Distribution for a Trap-Loaded Cylindrical Antenna at the Anti-Resonant Frequency of the Trap, $L = (11/16)\lambda$, $L/s = 2\text{-}3/4$	142
C-8	Current Distribution for a Trap-Loaded Cylindrical Antenna at the Anti-Resonant Frequency of the Trap, $L = (3/4)\lambda$, $L/s = 3$	143
C-9	Current Distribution for a Trap-Loaded Cylindrical Antenna at the Anti-Resonant Frequency of the Trap, $L = (13/16)\lambda$, $L/s = 3\frac{1}{4}$	144
C- 10	Current Distribution for a Trap-Loaded Cylindrical Antenna at the Anti-Resonant Frequency of the Trap, $L = (3/8)\lambda$, $L/(L-s) = 1\frac{1}{2}$	145

Figure		Page
C-11	Current Distribution for a Trap-Loaded Cylindrical Antenna at the Anti-Resonant Frequency of the Trap, $L = (7/16) \lambda$, $L/(L-s) = 1-3/4$	146
C-12	Current Distribution for a Trap-Loaded Cylindrical Antenna at the Anti-Resonant Frequency of the Trap, $L = (9/16) \lambda$, $L/(L-s) = 2\frac{1}{4}$	147
C-13	Current Distribution for a Trap-Loaded Cylindrical Antenna at the Anti-Resonant Frequency of the Trap, $L = (5/8) \lambda$, $L/(L-s) = 2\frac{1}{2}$	148
D-1	Copper Tubing Series of Antennas	150
D-2	2x4 Series of Antennas	151
D-3	2x4 Antenna Mounted on Ground Plane	152
D-4	Inductor-Capacitor Trap	153
D-5	Copper Tubing Trap Antenna Mounted on Ground Plane	154
D-6	Radiation Pattern Measurement on a Trap Antenna	155
D-7	Current Probe and Trap Antenna	156
D-8	Assembled and Dis-Assembled Special Short Circuit	157

LIST OF APPENDICES

Appendix		Page
A	Additional Input Impedances	98
B	Selected Radiation Patterns	132
C	Selected Current Distributions	135
D	Photographs	149

INTRODUCTION

1.1 Statement of Problem

The problem of this dissertation is to determine the current distribution, input impedance, and radiation pattern of the trap-loaded cylindrical antenna as functions of the antenna length, trap location, antenna radius and characteristic impedance or inductance to capacitance ratio of the trap. Figure 1-1 illustrates a typical symmetric trap-loaded cylindrical antenna.

The antenna has a total length of $2L$, the traps are located a distance, s , from the center, and the diameter of the antenna is $2a$. The surface of the antenna is assumed to be perfectly conducting and both the source and the trap are assumed to be very small. The trap, Z_L , is either a parallel inductor-capacitor circuit or a short-circuited quarter-wave transmission line. The trap is usually adjusted to be anti-resonant when s is a quarter of a wavelength.

If L is approximately three quarters of a wave length, the antenna is more commonly referred to as the Franklin array or the Franklin antenna. Its radiation pattern is assumed to be similar to that of a colinear array of three half-wave dipoles. If L is approximately half a wave length, the antenna is what is usually referred to as a trap antenna. The radiation pattern of the antenna is assumed to be similar to that of a half-wave dipole both

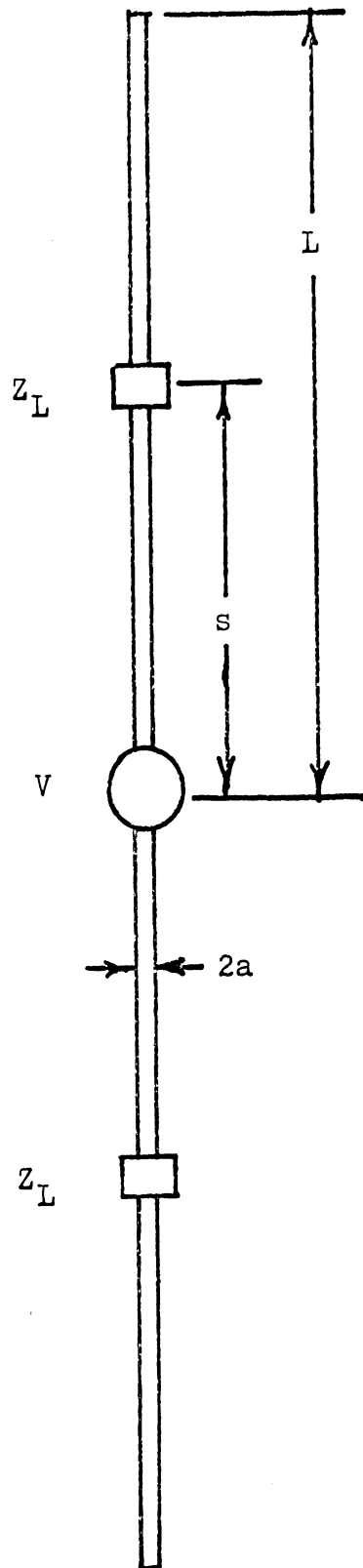


Figure 1-1: Illustration of the Symmetric Trap-Loaded Cylindrical Antenna

when the trap is anti-resonant and also at approximately one half the anti-resonant frequency of the trap. To avoid confusion throughout the remainder of this dissertation, the term "trap antenna" will be used specifically to refer to an antenna where s is a quarter wave length and L a half wave length when the trap is anti-resonant; the term "Franklin antenna" will be used to refer specifically to an antenna where s is a quarter wave length and L three-quarters of a wave length when the trap is an open circuit. The general terms "trap-loaded antenna" or "trap-loaded cylindrical antenna" will be used to refer to the general antenna depicted in Figure 1-1, of which the trap and Franklin antennas are special cases.

1.2 History of the Problem

Various types of trap-loaded cylindrical antennas have been used almost from the conception of radio. The Franklin array is a typical example of a trap-loaded cylindrical antenna used in the early days of radio as a wireless telegraphy antenna (Williams, 1950). Even today it is frequently used as a radio amateur antenna (ARRL, 1968). The trap of a Franklin array is usually constructed out of a shorted transmission line stub. The input impedance of the array at resonance is believed to be about 300 ohms (ARRL, 1968) and the current distribution is assumed to be sinusoidal and of equal amplitude on both the main section ($|z| \leq s$) and the parasitic elements ($s \leq |z| \leq L$)

(Williams, 1950).

Harrington (1968, Sec. 6.2) has obtained the current, input impedance and radiation pattern of an antenna very similar to a Franklin array by numerical means. The antenna consists of an asymmetrically driven cylindrical antenna with one shorted transmission line segment used as a load impedance. Harrington's results indicate that the current distribution is approximately sinusoidal but that the current amplitude on the parasitic element is somewhat less than on the driven element.

ARRL (1968), Bell (1963), Shafer (1958) and Greenberg (1956) have all described how to construct trap antennas for the short wave amateur bands. A parallel inductance-capacitance circuit is used as a trap. Some experimental data on the input impedance are presented in these references, but generally the articles are written to instruct a radio amateur on how to design a specific antenna which the authors "cut and tried" until it operated as desired. Indeed, the authors are interested in multiple trap antennas that resonate at several frequencies.

Of course, below the anti-resonant frequency of the trap, the trap acts as an inductance. Hence, the trap-loaded cylindrical antenna acts as an inductance-loaded cylindrical antenna. The inductance-loaded cylindrical antenna has been used for many years as a foreshortened antenna. The inductance loading permits a symmetric

cylindrical antenna to resonate at a frequency lower than that corresponding to a half wave length. (See ARRL, 1968 for example.)

While the center-loaded cylindrical antenna has been studied extensively (See Harrington, 1968, Sec. 6.3 for example and additional references) and a study has been made of resistive loading used principally to produce a short traveling wave antenna (Altshuler, 1961), there has been very little done to develop the theory of the trap-loaded cylindrical antenna or to make systematic measurements of its properties. Schelkunoff and Friis (1952, p. 236) discuss the general theory of an impedance-loaded antenna very briefly. However, they confine their discussion to observing that the loading is usually assumed to be small enough so that the current is constant through the impedance. Hence the voltage drop across the impedance can be expressed in terms of

$$V_L = I(s) Z_L \quad (1.1)$$

where V_L is the voltage drop across the impedance, Z_L , and $I(s)$ is the current at the impedance.

Lin et al. (1970) have looked at reactance loadings for short antennas (L less than 0.1 wave length.) Lin and his associates solved the integral equation for the current based on the King-Wu difference kernel and used the solution to determine optimum load impedances. The selection of optimum loading impedances was based on the criteria of "enhanced" radiation, the radiation being

enhanced when the input impedance was either purely resistive or the maximum input resistance possible, or when the directivity was a maximum.

1.3 Solution of the Problem

Plots illustrating how the input impedance and resonant frequencies of a trap-loaded cylindrical antenna vary as functions of length, radius, trap location and characteristic impedance or inductance-capacitance ratio of the trap were obtained both theoretically and experimentally. Comparisons of theoretical and experimental radiation patterns and current distributions were also made.

The theoretical solution was obtained by formulating an integral equation for the current distribution on the antenna by using the compensation theorem to obtain an equivalent voltage source for the trap and the slice generator approximation for the sources. The integral equation was solved numerically by two techniques. The first technique, which seemed to produce the more accurate results, was the method of subsections using a constant current assumption in each subsection and point matching to evaluate the unknown current distribution. The second technique was the polynomial current approximation using point matching to evaluate the coefficient of each term of the polynomial.

II

THEORETICAL SOLUTION

2.1 Derivation of Integral Equation

Maxwell's equations for a homogeneous isotropic medium specialized to $e^{+j\omega t}$ time dependence may be written as

$$\nabla \times \bar{E} = -j\omega\mu\bar{H} \quad (2.1)$$

$$\nabla \times \bar{H} = j\omega\epsilon\bar{E} + \bar{J} \quad (2.2)$$

$$\nabla \cdot \bar{D} = \rho \quad (2.3)$$

and

$$\nabla \cdot \bar{H} = 0 \quad (2.4)$$

where \bar{E} is the electric field, \bar{H} is the magnetic field, \bar{J} is the current density and ρ is the charge density. If the terminals of the trap are small enough, the compensation theorem of circuit theory may be applied to the impedance; that is, the impedance may be replaced by an equivalent voltage source, V_L , assigned the value

$$V_L = -Z_L I(s) = -Z_L I(-s). \quad (2.5)$$

Figure 2-1 illustrates the assumed polarity of the voltage source and the direction of the current. Thus an integral equation for the current distribution on the antenna can be written in terms of the three voltage sources: the driving voltage, V , and the two sources associated with the impedances, V_L .

The integral equation for the current on the trap-loaded cylindrical antenna can be derived from Maxwell's

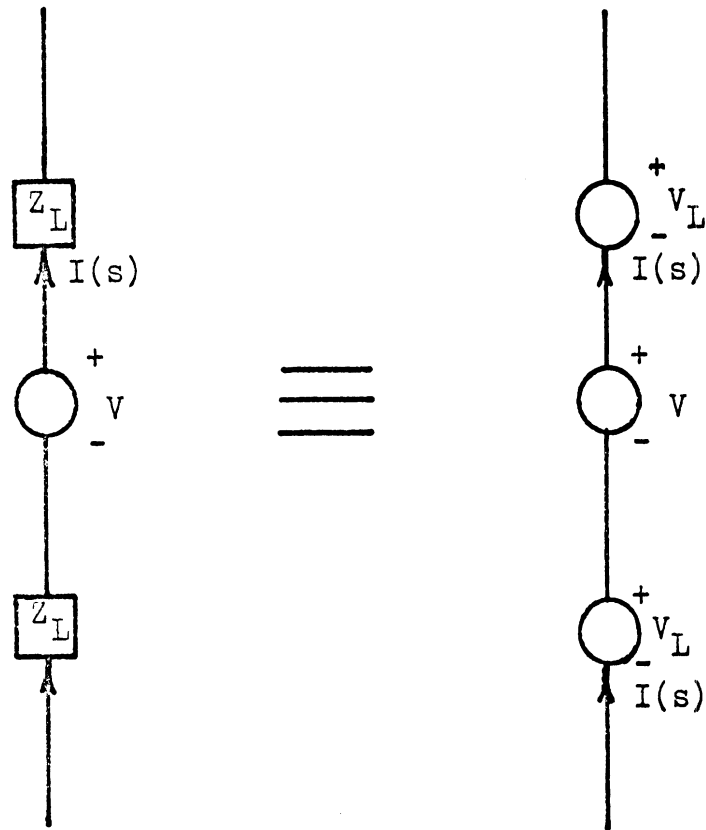


Figure 2-1: Application of the Compensation Theorem to Trap-Loaded Cylindrical Antenna

equations by first defining the vector potential as

$$\bar{\mathbf{H}} = \mu^{-1} \nabla \times \bar{\mathbf{A}} \quad (2.6)$$

where $\bar{\mathbf{A}}$ is the vector potential. It can be shown that the vector potential satisfies the following wave equation,

$$\nabla^2 \bar{\mathbf{A}} + k^2 \bar{\mathbf{A}} = -\mu \bar{\mathbf{J}} \quad (2.7)$$

provided the Lorentz condition holds, and that the solution of this wave equation is

$$\bar{\mathbf{A}} = \frac{\mu}{4\pi} \int \frac{\bar{\mathbf{J}} e^{-jk|\bar{\mathbf{R}}-\bar{\mathbf{R}}'|}}{|\bar{\mathbf{R}}-\bar{\mathbf{R}}'|} dV' \quad (2.8)$$

where the prime coordinates indicate those associated with the current density. It can also be shown that

$$\bar{\mathbf{E}} = -j\omega \left[\bar{\mathbf{A}} + k^{-2} \nabla \nabla \cdot \bar{\mathbf{A}} \right] \quad (2.9)$$

(See Van Bladel, 1964, Sec. 7.8, for example.)

Consider the case of an antenna constructed out of a perfect conductor. Figure 2-2 illustrates the orientation of the circular cylindrical coordinate system used to study the antenna. Assuming that the currents on the ends of the antenna can be neglected, then only currents on the lateral surface of the antenna need to be considered. The driving points of the antenna will be considered to be infinitesimally small gaps so that the fields in the gap can be expressed in the form

$$\bar{\mathbf{E}} = -V \delta(|z| - s) \hat{\mathbf{z}} \quad (2.10)$$

where V is the voltage across the gap and $\delta(z)$ is the delta function.

As a result of these assumptions, it follows that the vector potential has only

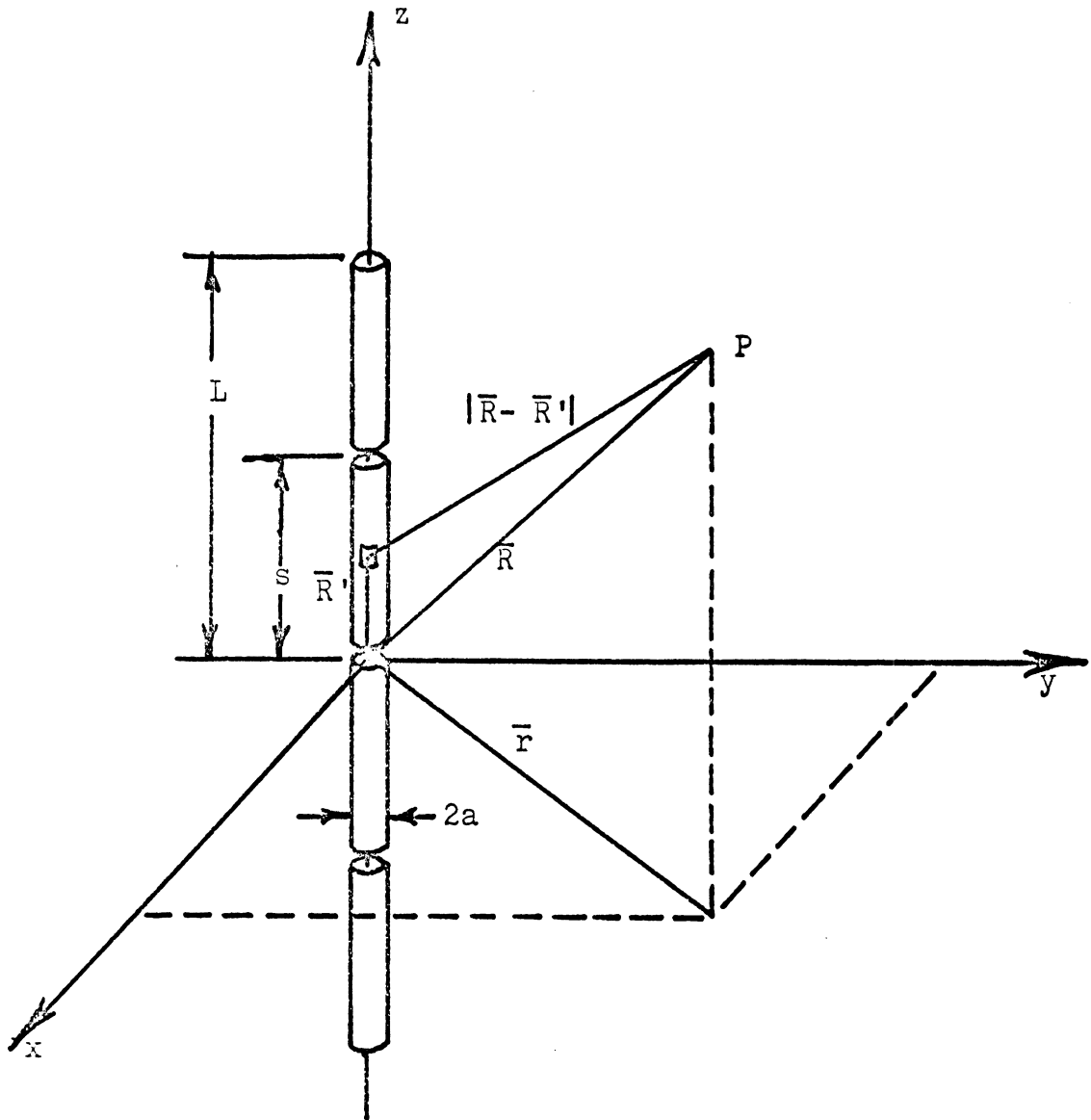


Figure 2-2: Geometry of the Trap-Loaded Cylindrical Antenna

an axial component, since the current density has only an axial component. Thus the axial component of the vector potential may be written as

$$A_z = \frac{\mu}{4\pi} \int_{S'} \frac{J_s(z') e^{-jk|\bar{R}-\bar{R}'|}}{|\bar{R}-\bar{R}'|} dS' \quad (2.11)$$

where $J_s(z)$ is the surface current density on S' , the antenna surface. The axial component of the expression for the electric field may be written in terms of the vector potential as

$$E_z = -j\omega \left[A_z + k^{-2} \frac{\partial^2 A_z}{\partial z^2} \right] \quad (2.12)$$

On the surface of the antenna, the electric field is everywhere zero, since it is tangential to the surface, except at the sources, where it is $-V\delta(z)$, $-V_L\delta(z-s)$ and $-V_L\delta(z+s)$. Thus equation (2.12) becomes

$$\begin{aligned} -V\delta(z) - V_L \left[\delta(z-s) + \delta(z+s) \right] = \\ -j\omega \left[1 + k^{-2} \frac{\partial^2}{\partial z^2} \right] A_z \end{aligned} \quad (2.13)$$

where the vector potential, \bar{A} , is evaluated on the surface. Substituting equation (2.11) into equation (2.13) and noting that $|\bar{R}-\bar{R}'|$ is evaluated on the surface results in an integral equation for the current,

$$\begin{aligned} V\delta(z) + V_L \left[\delta(z-s) + \delta(z+s) \right] = \\ \frac{j\omega\mu_0}{4\pi} \left[1 + k^{-2} \frac{\partial^2}{\partial z^2} \right] \int_{S'} K(z, z') J_s(z') dS' \end{aligned} \quad (2.14)$$

where

$$K(z, z') = \frac{e^{-jk|\bar{R}-\bar{R}'|}}{|\bar{R}-\bar{R}'|} \quad (2.15)$$

Up to this point, $|\bar{R} - \bar{R}'|$ has not been written explicitly to avoid confusion. The term can be written as

$$|\bar{R} - \bar{R}'| = \sqrt{2a^2(1 - \cos \phi') + (z - z')^2}. \quad (2.16)$$

This makes K , the kernel of the integral equation, very complex. The assumption usually made at this point is that a , the radius of the cylinder, is much smaller than a wave length. Thus the retardation effects across the diameter of the cylinder can be ignored and the integral equation becomes

$$V\delta(z) + V_L \left[\delta(z - s) + \delta(z + s) \right] = \quad (2.17)$$

$$\frac{j\omega\mu_0}{4\pi} \left[1 + k^{-2} \frac{d^2}{dz^2} \right] \int_{-L}^L K(z, z') I(z') dz'$$

where

$$K(z, z') = \frac{e^{-jk\sqrt{a^2 + (z - z')^2}}}{\sqrt{a^2 + (z - z')^2}} \quad (2.18)$$

and $I(z)$ is the current on the antenna. The current satisfies the boundary conditions

$$I(L) = 0 \quad (2.19)$$

and

$$I(z) = I(-z). \quad (2.20)$$

In spite of the simplification of the kernel, the

integral equation (2.17) is not in a very convenient form to solve numerically even though it has been solved for the case of $V_L = 0$ by Harrington (1967, 1968.) Equivalent forms of equation (2.17) can be formulated which will drastically reduce the computer time necessary to obtain a good solution.

The problems with the form of equation (2.17) are as follows. 1) It contains delta functions which, because they are not well behaved, are difficult to expand in a rapidly converging series of functions. 2) The equation contains a Green's Function (the kernel is a Green's function) whose behavior is almost singular when z' is in the vicinity of z . 3) It contains derivatives which for some methods of solution can contribute to round off error. 4) The boundary conditions on the current are not included in the integral equation, thus making the computer programming more complex.

The first, third and fourth inconveniences can be alleviated somewhat by setting

$$F(z) = \frac{j\omega\mu_0}{4\pi} \int_{-L}^L K(z, z') I(z') dz'. \quad (2.21)$$

Thus F must satisfy the differential equation

$$\left[k^{-2} \frac{d^2}{dz^2} + 1 \right] F(z) = V_L \left[\delta(z-s) + \delta(z+s) \right] + V\delta(z). \quad (2.22)$$

A homogeneous solution for $F(z)$, $F_h(z)$, is

$$F_h(z) = A \sin kz + B \cos kz . \quad (2.23)$$

A particular solution for $F(z)$, $F_p(z)$, can be written in terms of the homogeneous solution by means of variation of parameters. The result is that

$$F_p(z) = k \int_c^z \frac{[V\delta(z') + V_L\delta(z' - s) + V_L\delta(z' + s)]}{\sin k(z - z')} dz' \quad (2.24)$$

where c is some constant. Thus the total solution for $F(z)$ is

$$\begin{aligned} F(z) &= F_h(z) + F_p(z) \\ &= k \int_c^z \frac{[V\delta(z') + V_L\delta(z'-s) + V_L\delta(z'+s)]}{\sin k(z - z')} dz' \\ &\quad + A \sin kz + B \cos kz . \end{aligned} \quad (2.25)$$

Since the current, $I(z)$, is symmetric with respect to z and the kernel of the integral, K , has the property that $K(z, z') = K(-z, -z')$, then $F(z)$ must also be symmetric with respect to z . Thus

$$F(z) = k \int_0^z \frac{[V\delta(z') + V_L\delta(z'-s) + V_L\delta(z'+s)]}{\sin k(z - z')} dz' + B \cos kz. \quad (2.26)$$

Assuming the delta function at $z'=0$ is split equally between the positive and negative axes, equation (2.26) can be rewritten as

$$F(z) = \frac{kV}{2} \sin k|z| + B \cos kz , \quad -s \leq z \leq s \quad (2.27)$$

$$= \frac{kV}{2} \sin k|z| + kV_L \sin k(|z|-s) + B \cos kz, \quad |z| \geq s$$

or as

$$\begin{aligned} F(z) &= \frac{kV}{2} \sin k|z| + u_{-1}(|z| - s) kV_L \sin k(|z|-s) \\ &\quad + B \cos kz \end{aligned} \quad (2.28)$$

where $u_{-1}(z)$ is the unit step function.

Hence the integral equation becomes

$$\frac{-j2\pi V}{\eta_0} \sin k|z| - \frac{j4\pi V_L}{\eta_0} u_{-1}(|z| - s) \quad (2.29)$$

$$\sin k(|z| - s) + C \cos kz = \int_{-L}^L K(z, z') I(z') dz'$$

where η_0 is the intrinsic impedance of free space and C is a new arbitrary constant. Substituting equation (2.5) into equation (2.29) and rearranging terms gives

$$\frac{-j2\pi V}{\eta_0} \sin k|z| + \frac{j4\pi V_L I(s)}{\eta_0} u_{-1}(|z| - s) \sin k(|z| - s)$$

$$+ C \cos kz = \int_{-L}^L K(z, z') I(z') dz' \quad (2.30)$$

where the left hand side of the equation is the inhomogeneous term.

2.2 Solution of Integral Equation

Equation (2.30) can be solved numerically by either of the analytic techniques pointed out by King (1967): iteration, Hallén's method being one method of iteration, and Fourier series, which is the classical way of solving inhomogeneous Fredholm integral equations of the first kind. Equation (2.30) can also be solved numerically by the method of moments, of which the Fourier series solution can be shown to be a special case (Harrington, 1967, 1968.)

The general case of the Fredholm integral equation of the first kind has been solved numerically by Ullman and Ullman (1966) both by iteration and by Fourier-trigono-

metric series. The Fredholm integral equation of the first kind arising from the scattering of a plane wave by a cylindrical antenna has also been solved by iteration and Fourier-trigonometric series by Harrison et al. (1967). In both cases, the kernel was approximated before solving by iteration. Ullman and Ullman, not too surprisingly, found that the Gaussian quadrature method of numerical integration gave the most efficient method of solving the problem.

Other techniques of numerical solution have also been used to reduce the amount of computer time necessary to obtain acceptable answers. Richmond (1965) improved the behavior of the Green's function by making the substitution of the form

$$z - z' = a \tan \theta' \quad (2.31)$$

in an integral equation with a kernel similar to the kernel in equation (2.30) and then used the Newton-Cotes method of numerical integration. This seemed to reduce computation time since it improved the behavior of the Green's function.

Hickman et al. (1966) reformulated the integral equation by adding and subtracting $\int_{-L}^L K(z, z') I(z) dz'$ and then performing the integration by Gaussian quadrature using a point matching method. They report that 19 subdivisions gave adequate convergence. Although not made clear in the reference, it does appear that the solution is a first order iteration method.

All of these techniques can be thought of as different applications of the method of moments. Using the jargon of the method of moments, equation (2.30) can be put in the form

$$\mathcal{L}f = g \quad (2.32)$$

where the unknown function, f , is $I(z)$; the known function, g , is the left hand side of equation (2.30); and the linear operator, \mathcal{L} , is defined by

$$\mathcal{L}f = \int_{-L}^L K(z, z') I(z') dz' . \quad (2.33)$$

A suitable inner product between f and g , $\langle f, g \rangle$, can be defined as

$$\langle f, g \rangle = \int_{-L}^L f g dz . \quad (2.34)$$

The unknown function, f , can be expanded in a suitable set of basis functions, $\{f_m\}$, with the aid of the inner product such that

$$f = \sum_m \alpha_m f_m \quad (2.35)$$

where

$$\alpha_m = \langle f, f_m \rangle . \quad (2.36)$$

Substituting this approximate representation of f into equation (2.30) gives

$$\sum_m \alpha_m \mathcal{L}f_m = g. \quad (2.37)$$

Expanding both sides of this equation in a suitable set of weight functions, $\{w_n\}$, gives

$$\sum_n \sum_m \alpha_m \langle w_n, \mathcal{L}f_m \rangle = \sum_n \langle w_n, g \rangle \quad (2.38)$$

and solving equation (2.38) for the $\{\alpha_m\}$ and substituting into equation (2.32) gives the approximate solution for f (Harrington, 1968), Sec. 1.3).

Three observations on the quality of the approximate solution can be made at this point. First, if the weight and basis sets are complete sets, then the approximate solution will become exact if enough terms are used. Second, using a finite number of weight and basis functions is equivalent to finding the approximate solution by a Rayleigh-Ritz variational procedure (Harrington, 1968, Sec. 1.8). Third, the better the weight and basis functions approximate the unknown function, the quicker is the convergence of the approximate solution to the exact solution.

Two solutions were obtained by the method of moments: one by the method of subsections and point matching using delta functions as the approximating functions, and the other by polynomial series and point matching. Each will be discussed in a separate section.

2.3 Subsections and Point Matching

The method of subsections and point matching consists of dividing the range of the variable into equal subsections and then assuming that the unknown function is some simple type of function in each subsection. The unknown coefficients are then evaluated by point matching.

In this dissertation, the functions were assumed to be delta functions located in the center of each subsection.

This is similar to one of the approaches used by Mei (1965) and Harrington (1967, 1968) although with a slightly different boundary condition. Liu and Sengupta (1971) have also used subsections and point matching but have assumed that the unknown functions were simple polynomials.

The set of basis functions, $\{f_m\}$, has the form

$$f_m = I_m \Delta z \delta(z - z_m) \quad (2.39)$$

where $\delta(z)$ is the Dirac delta function,

$$\Delta z = 2L/M, \quad (2.40)$$

$$z_m = m \Delta z - \Delta z/2 - L \quad (2.41)$$

and M is the total number of subsections. The index, m , is assumed to start with $m=1$. The set of weight functions, $\{w_n\}$, has a form similar to the set of basis functions and thus

$$w_n = \delta(z - z_n) \quad (2.42)$$

where

$$z_n = z_m. \quad (2.43)$$

This choice of basis functions can be thought of as equivalent to dividing the range of the integral in equation (2.30) into intervals and then assuming that 1) both the Green's function and the current are constant in the interval and that 2) they both take on their values at the midpoint of the interval. The choice of weight functions corresponds to forcing both sides of equation (2.30) to agree at the midpoint of each section. This approach differs from Mei's method in that instead of assuming that the current is constant and integrating the Green's function, an approximate value of the integral of the Green's function

is obtained by assuming the Green's function is constant and multiplying its value by the length of the interval.

An advantage of both sets of functions is that the integrals produced in evaluating the unknown coefficients, $\{I_m\}$, are closed form analytical expressions. Therefore no numerical integrations need be performed.

The experience of others using the Mei solution is favorable (Mei, 1965, Harrington, 1967, 1968). Since the delta function solution is really the Mei solution with the modification that the integral of the Green's function is replaced with the approximate integral of the Green's function, an approximation that becomes more exact as the number of subsections is increased, the delta function solution would also be expected to give good results.

Furthermore, both the weight and basis sets are complete sets (Harrington, 1968). Thus convergence is assured if enough terms are taken. The rate of convergence can be estimated by increasing the number of functions in the set and observing the amount of change in the solution.

Expanding the current in terms of the basis set of functions gives

$$I(z) = \sum_m I_m \Delta z \delta(z - z_m) . \quad (2.44)$$

Substituting this into the integral equation gives

$$\frac{-2\pi jV}{\eta_0} \sin k|z| + \frac{j4\pi I(s)Z_L}{\eta_0} \sin k(|z|-s) u_{-1}(|z|-s)$$

$$+ C \cos kz = \Delta z \sum_m K(z, z'_m) I_m . \quad (2.45)$$

Expanding equation (2.45) in terms of the weight functions and taking the inner product using z_m for z'_m gives

$$\sum_m \left\{ \frac{-2\pi jV}{\eta_0} \sin k|z_n| + \frac{j4\pi I(s)Z_L}{\eta_0} \sin k(|z_n| - s) \right. \\ \left. u_{-1}(|z_n| - s) + C \cos kz_n \right\} = \Delta z \sum_n \sum_m K(z_n, z'_m) I_m , \quad (2.46)$$

which is the matrix equation for the approximate expression for the current.

A careful examination of equation (2.46) will reveal that it is indeterminate. In addition to the set of unknowns $\{I_m\}$, there are also the unknowns $I(s)$ and C . One of the additional equations needed to make the $\{I_m\}$ unique is the boundary condition on the current,

$$I(L) = 0.$$

Note that equation (2.46) cannot be satisfied exactly by equation (2.47) since to require the current to be zero at the end of the outermost subsection would require that the current be zero in the entire subsection. Therefore an approximation of equation (2.47) is used. The approximation should become exact as the number of subsections becomes infinite.

The simplest approximation is, of course, to set the current at the first sample point equal to zero, that is let

$$I_1 = 0. \quad (2.48)$$

This is the technique used by Harrington (1967, 1968) and Mei (1965). For the number of subdivisions used by Mei and Harrington, on the order of 40 to 80, this is a reasonable approximation. However, for a number of subdivisions on the order of 20, as was used in this dissertation for reasons explained in Chapter 4, the error introduced by this approximation may not be insignificant.

If the current on the first two sample points, $I(z_1)$ and $I(z_2)$ is taken as I_1 and I_2 , respectively, then by linear extrapolation the boundary condition can be expressed as

$$\frac{I_2 - I_1}{z_2 - z_1} = \frac{I_1}{z_1 - L} \quad (2.49)$$

or

$$(z_2 - L) I_1 - (z_1 - L) I_2 = 0 \quad (2.50)$$

where z_1 and z_2 are the first and second sample points. The condition that $I(-L)=0$ is not needed because of symmetry.

The final equation needed is merely the identity

$$I(s) = I(z) \Big|_{z=s} \quad (2.51)$$

Since there is in general no reason why s need be one of the sample points of a finite set of basis functions, the exact relationship given in equation (2.51) could prove disastrous if used in the approximate solution. The number of sample points could conceivably be very very large and yet it is probable that the direct use of equation (2.51) would require that $I(s) = 0$, a completely unsatisfactory

result. Of course as the number of points becomes infinite, the probability of $I(s)$ taking some non-zero value would approach one.

This problem can be avoided by using an approximate definition for $I(s)$ that becomes exact for a complete set of basis functions. The simplest approximation is

$$I(s) = I(z_{\tilde{m}}) \quad (2.52)$$

where $z_{\tilde{m}}$ is chosen to be the z_m closest to s . However, a more accurate approximation and one more in keeping with the end condition used is

$$I(s) = \frac{s - z_{\tilde{m}}}{z_{\tilde{m}+1} - z_{\tilde{m}}} \left[I_{\tilde{m}+1} - I_{\tilde{m}} \right] + I_{\tilde{m}} \quad (2.53)$$

or

$$(z_{\tilde{m}+1} - z_{\tilde{m}}) I(s) - (s - z_{\tilde{m}}) I_{\tilde{m}+1} - (z_{\tilde{m}+1} - s) I_{\tilde{m}} = 0 \quad (2.54)$$

where $z_{\tilde{m}}$ and $z_{\tilde{m}+1}$ are the sample points closest to s . In effect, $I(s)$ is found by a first degree interpolation polynomial passing through the sample points closest to s .

If equation (2.46) is rearranged as

$$\sum_n \frac{j2\pi V}{\eta_0} \sin k|z_n| = \sum_n \left\{ \frac{j4\pi I(s) Z_{\perp}}{\eta_0} \sin k|z_n| - s) u_{-1}(|z_n| - s) + C \cos kz_n - \Delta z \sum_m K(z_n, z_m) I_m \right\}, \quad (2.55)$$

then $I(s)$ and C can be treated as unknowns along with $\{I_m\}$. Equations (2.50) and (2.54) can be added to the matrix equation in equation (2.55) to produce a matrix equation of the form

$$\begin{bmatrix}
 K_{11} & K_{12} & \dots & K_{1\tilde{m}} & K_{1\tilde{m}+1} & \dots & K_{1M} & \Psi_1 & \Upsilon_1 \\
 K_{21} & K_{22} & \dots & K_{2\tilde{m}} & K_{2\tilde{m}+1} & \dots & K_{2M} & \Psi_2 & \Upsilon_2 \\
 \vdots & \vdots & & \vdots & \vdots & & \vdots & \vdots & \vdots \\
 \vdots & \vdots & & \vdots & \vdots & & \vdots & \vdots & \vdots \\
 K_{\tilde{n}1} & K_{\tilde{n}2} & \dots & K_{\tilde{n}\tilde{m}} & K_{\tilde{n}\tilde{m}+1} & \dots & K_{\tilde{n}M} & \Psi_{\tilde{n}} & \Upsilon_{\tilde{n}} \\
 K_{\tilde{n}+1\ 1} & K_{\tilde{n}+1\ 2} & \dots & K_{\tilde{n}+1\ \tilde{m}} & K_{\tilde{n}+1\ \tilde{m}+1} & \dots & K_{\tilde{n}+1\ M} & \Psi_{\tilde{n}+1} & \Upsilon_{\tilde{n}+1} \\
 \vdots & \vdots & & \vdots & \vdots & & \vdots & \vdots & \vdots \\
 \vdots & \vdots & & \vdots & \vdots & & \vdots & \vdots & \vdots \\
 K_{N1} & K_{N2} & \dots & K_{N\tilde{m}} & K_{N\tilde{m}+1} & \dots & K_{NM} & \Psi_N & \Upsilon_N \\
 (z_2-L) & (L-z_1) & \dots & 0 & 0 & \dots & 0 & 0 & 0 \\
 0 & 0 & \dots & (s-z_{\tilde{m}+1}) & (z_{\tilde{m}}-s) & \dots & 0 & (z_{\tilde{m}+1}-z_{\tilde{m}}) & 0
 \end{bmatrix}$$

$$\begin{bmatrix}
 I_1 \\
 I_2 \\
 \vdots \\
 \vdots \\
 I_{\tilde{m}} \\
 I_{\tilde{m}+1} \\
 \vdots \\
 \vdots \\
 I_M \\
 I(s) \\
 c
 \end{bmatrix}
 =
 \begin{bmatrix}
 \Theta_1 \\
 \Theta_2 \\
 \vdots \\
 \vdots \\
 \Theta_{\tilde{n}} \\
 \Theta_{\tilde{n}+1} \\
 \vdots \\
 \vdots \\
 \Theta_N \\
 0 \\
 0
 \end{bmatrix}
 \quad (2.56)$$

where

$$\Theta_n = \frac{j2\pi V}{\eta_0} \sin k|z_n| \quad (2.57)$$

$$\Psi_n = \frac{j4\pi Z_L}{\eta_0} \sin k(|z_n| - s) u_{-1}(|z_n| - s) \quad (2.58)$$

$$\gamma_n = \cos kz_n \quad (2.59)$$

$$K_{nm} = -\Delta z K(z_n, z_m) = -\Delta z \frac{e^{-jk\sqrt{a^2 + (z_n - z_m)^2}}}{\sqrt{a^2 + (z_n - z_m)^2}} \quad (2.60)$$

and

$$N = M. \quad (2.61)$$

This augmented matrix equation can then be solved for the $\{I_m\}$, $I(s)$ and C .

The input impedance can then be determined from the current distribution given by the $\{I_m\}$ by

$$Z_{in} = \frac{V}{I_i} \quad (2.62)$$

where $i = (M+1)/2$ if M is odd. However, if M is even, none of the points is located at the origin. The value of the current in a subsection adjacent to the origin could be used to calculate the input impedance, but a more accurate approach for M relatively small is to do a linear extrapolation through the points closest to the origin. This approach has the programming advantage that it reduces to equation (2.62) for M odd. However, since the current distribution can have a cusp at the origin, the extrapolation must be done through the two points closest to the origin on the same side of the origin. The result is that

$$I_{in} = I_i - \frac{z_i}{z_i - z_{i+1}} (I_i - I_{i+1}) \quad (2.63)$$

where

$$i = \begin{cases} (M + 1)/2, & \text{if } M \text{ is odd} \\ (M/2) + 1, & \text{if } M \text{ is even} \end{cases} \quad (2.64)$$

and

$$Z_{in} = \frac{V}{I_{in}} \quad (2.65)$$

2.4 Polynomial and Point Matching

The polynomial approximation consists of approximating the current by an M^{th} degree polynomial with undetermined coefficients. The coefficients are then determined by point matching. This is an approach first used by Popovic (1970) to determine the current distribution on a cylindrical antenna.

The set of basis functions, $\{f_m\}$, has the form

$$f_m = I_m (1 - |z|/L)^m \quad (2.66)$$

where m is greater than zero. This form of the basis functions has the convenient property that each basis function satisfies the boundary condition at $z=L$. The set of weight functions, $\{w_n\}$, has a form similar to those used in Sec. 2.3,

$$w_n = \delta(z - z_n) \quad (2.67)$$

where

$$z_n = (n - 1)\Delta z \quad (2.68)$$

$$\Delta z = L/N \quad (2.69)$$

and N is the total number of points. Note that for convenience all z_n will be taken as greater than zero since the current is symmetrical.

An advantage of the polynomial approximation is that a fairly low order polynomial can accurately approximate the current distribution on a linear cylindrical antenna. This reduces the number of simultaneous equations that need to be solved. Another advantage is that both the basis and weight functions are complete sets of functions. Thus convergence is assured if enough terms are taken and the rate of convergence can be estimated by increasing the number of functions in the set and observing the amount of change in the solution.

A disadvantage of the polynomial approximation is that integrals produced in evaluating the unknown coefficients do not have a closed analytic form and must therefore be evaluated numerically. This numerical integration is very time consuming for accurate evaluations of the integral. Indeed, as a result of the lengthy numerical integrations required, much of the time saved by solving a smaller matrix equation may be lost evaluating the integrals.

Expanding the current in terms of the basis set of functions gives

$$I(z) = \sum_{m=1}^M I_m (1 - |z|/L)^m. \quad (2.70)$$

Notice that the boundary condition on the current at $z=L$ and symmetry are automatically satisfied by the choice of basis functions.

Substituting this into the integral equation gives

$$\frac{-j2\pi V}{\eta_0} \sin k|z| + \frac{j4\pi Z_L}{\eta_0} \sin k(|z|-s) u_{-1}(|z|-s)$$

$$\sum I_m (1-s/L)^m + C \cos kz = \sum I_m \int_{-L}^L K(z, z') (1-|z'|/L)^m dz'. \quad (2.71)$$

Expanding equation (2.71) in terms of the weight functions gives

$$\begin{aligned} & \sum_n \left\{ \frac{-j2\pi V}{\eta_0} \sin k|z_n| + \frac{j4\pi Z_L}{\eta_0} \sin k(|z_n| - s) \right. \\ & \left. u_{-1}(|z_n| - s) \sum_m I_m (1-s/L)^m + C \cos kz_n \right\} \\ & = \sum_n \sum_m I_m \int_{-L}^L K(z_n, z') (1-|z'|/L)^m dz'. \quad (2.72) \end{aligned}$$

By suppressing the summation signs, equation (2.72) can be rearranged as

$$\begin{aligned} \frac{j2\pi V}{\eta_0} \sin k|z_n| & = \left\{ - \int_{-L}^L K(z_n, z') (1-|z'|/L)^m dz' \right. \\ & + \frac{j4\pi Z_L}{\eta_0} \sin k(|z_n| - s) u_{-1}(|z_n| - s) (1-s/L)^m \left. \right\} I_m \\ & + C \cos kz_n \quad (2.73) \end{aligned}$$

if C is treated as an unknown along with the $\{I_m\}$. Note that no additional relations are needed since each basis function vanishes at the end of the antenna and the value of the current at the trap is determined explicitly in the expression. However, there are $M+1$ unknowns and therefore the number of sample points, N , must satisfy the relationship

$$N = M + 1. \quad (2.74)$$

Equation (2.73) can be put in a more explicit matrix form by rewriting it as

$$\begin{bmatrix} K_{11} & \cdots & K_{1M} & \gamma_1 \\ \cdot & & \cdot & \cdot \\ \cdot & & \cdot & \cdot \\ K_{M1} & \cdots & K_{MM} & \gamma_M \\ K_{N1} & \cdots & K_{NM} & N \end{bmatrix} \begin{bmatrix} I_1 \\ \cdot \\ \cdot \\ I_M \\ C \end{bmatrix} = \begin{bmatrix} \Phi_1 \\ \cdot \\ \cdot \\ \Phi_M \\ \Phi_N \end{bmatrix}$$

where

$$K_{nm} = - \int_{-L}^L K(z_n, z') (1 - |z'|/L)^m dz' \quad (2.76) \\ + \frac{j4\pi Z_L}{\eta_0} \sin k(|z_n| - s) u_{-1}(|z_n| - s) (1-s/L)^m$$

$$\gamma_n = \cos kz_n \quad (2.77)$$

$$\Phi_n = \frac{j2\pi V}{\eta_0} \sin k|z_n|. \quad (2.78)$$

There appears to be no known optimum sampling strategy so the $\{z_n\}$ were chosen to be equally spaced along one-half of the antenna. Once the $\{I_m\}$ are known, $I(0)$ can be evaluated directly from equation (2.70) and the input impedance, Z_{in} , can be obtained from

$$Z_{in} = \frac{V}{I(0)}. \quad (2.79)$$

Evaluating the coefficients of the matrix introduces the problem of numerically evaluating integrals of the form

$$I = \int_{-L}^L (1 - |z'|/L)^m \frac{e^{-jk\sqrt{a^2 + (z-z')^2}}}{\sqrt{a^2 + (z-z')^2}} dz'. \quad (2.80)$$

Richmond's (1965) approach works well for $m=0$, a case not of interest here. Only eight to ten point Gaussian quadrature formulas were necessary to evaluate the integral in

equation (2.80) to within 1% of what appeared to be a final value for $m=0$. However, for $m \neq 0$, even a 64 point Gaussian quadrature formula did not appear to give adequate convergence.

The best approach, discovered after much trial and error, is to add and subtract a term similar to the real part of the integral in equation (2.80) that can be analytically integrated in a closed form. The difference between the integrand of equation (2.80) and the additional term can then be adjusted to suppress the near singularity. Hence the difference term can be numerically integrated rather rapidly.

The integral to be added and subtracted, I_a , that gave the best results is

$$I_a = \int_{-L}^L \frac{(1 - |z|/L)^m}{\sqrt{a^2 + (z - z')^2}} dz' \quad (2.81)$$

which can be integrated analytically with the help of entry 38, p 1070 of Westman (1964) into the closed form

$$I_a = (1 - |z|/L)^m \ln \frac{(z+L) + \sqrt{(z+L)^2 + a^2}}{(z-L) + \sqrt{(z-L)^2 + a^2}}. \quad (2.82)$$

Addition and subtraction of I_a in equation (2.80) gives

$$I = \int_{-L}^L \frac{(1 - |z|/L)^m e^{-jk\sqrt{a^2 + (z - z')^2}} - (1 - |z|/L)^m}{\sqrt{a^2 + (z - z')^2}} dz' + I_a. \quad (2.83)$$

Since the value of z significantly affects the number

of terms required to evaluate the integral in equation (2.83) to a given degree of accuracy, the computer program itself was written to select the number of terms needed to supply a given degree of accuracy. The trapezoid rule is more amenable to this kind of automatic programming than Gaussian quadrature. Hence the trapezoid rule is used to perform the integration even though more terms are required to obtain a given degree of accuracy with it than with Gaussian quadrature.

The procedure is to select an initial number of intervals (10), perform the integration, then double the number of intervals, perform another integration, and compare the change in the value of the integral. If the change is more than a given tolerance (1%), then the number of intervals is doubled again, a new value of the integral calculated, and a new comparison made, and so on, until either the desired accuracy is achieved, or a maximum number of intervals is surpassed (640). If the latter condition prevails, Richardson's rule (Carnahan and Wilkes, 1968) is used to improve the estimate of the answer. Specialized to the case of two estimates for the integral, I_1 and I_2 , where I_2 is based on twice the number of intervals used for I_1 , Richardson's rule reduces to

$$I = \frac{4}{3} I_2 - \frac{1}{3} I_1 \quad (2.84)$$

where I is the best estimate of the integral.

The procedure also takes advantage of the property

of the trapezoid rule that doubling the number of intervals to $2N$ only requires N additional samplings of the function to be integrated (Carnahan and Wilkes, 1968). Thus some of the efficiency of Gaussian quadrature can be retained without the necessary storage of the Gaussian coefficients and sample points.

A problem arises in evaluating I_a for $(|z-L|/a)$ greater than 100; most computers will give an error return indicating attempted division by zero. The problem lies in the denominator of the logarithmic term which is very small, but not zero. An excellent approximation can be used that prevents error returns by expanding the radical in the denominator in terms of the binomial expansion and then retaining the first two terms. The result is that

$$\sqrt{(z-L)^2 + a^2} = |z-L| + \frac{a^2}{2|z-L|} \quad (2.85)$$

Substituting this approximation into the denominator gives

$$(z-L) + \sqrt{(z-L)^2 + a^2} = \frac{a^2}{2|z-L|} \quad (2.86)$$

Thus I_a becomes

$$I_a = (1 - |z|/L)^m \ln \frac{2|z-L| \left[(z+L) + \sqrt{(z+L)^2 + a^2} \right]}{a^2} \quad (2.87)$$

For $|z-L|/a = 100$, the error in this approximation is on the order of 0.01% and decreases rapidly for $|z-L|/a$ greater than 100.

2.5 Radiation Pattern

The far zone electric field from a linear radiator is given by

$$E_{\theta} = \frac{j\eta_0 \sin \theta}{2 R \lambda} \int_{-L}^L I(z) e^{-jkz \cos \theta} dz \quad (2.88)$$

(Jasik, 1961) where the current, $I(z)$, is a complex expression. This integral can be evaluated in a number of ways, but probably the easiest, and the one most in keeping with the first method of solution for the current distribution is to assume that the current has the form given in equation (2.39). Substituting this into equation (2.88) gives

$$E_{\theta} = \frac{j\eta_0 \sin \theta}{2 R \lambda} \Delta z \sum_{m=1}^M I_m e^{-jkz_m \cos \theta} \quad (2.89)$$

The power radiation pattern, $P(\theta)$, is proportional to

$$P(\theta) = \sin^2 \theta \left| \sum_{m=1}^M I_m e^{-jkz_m \cos \theta} \right|^2 \quad (2.90)$$

The power radiated at any angle can be calculated for a number of angles and the results normalized to the largest value.

This method of calculating the radiation pattern can be interpreted physically as assuming that the current distribution is an array of small dipoles. For the polynomial method of solution for the current distribution, the resulting distribution is evaluated at a convenient number of points along the antenna and the result is substituted into equation (2.90) to obtain the radiation pattern.

III

EXPERIMENTAL PROCEDURE

Two sets of trap-loaded cylindrical antennas were constructed so that measurements of the input impedance, radiation patterns and current distribution could be compared with the theory. One set of antennas was constructed out of 3/8 inch O.D. copper tubing and used several transmission line traps. All three types of measurements were made on this series of antennas to determine how its properties varied as the length of the outer section, length of the inner section, trap impedance, trap gap capacitance and feed gap capacitance were varied.

The other series of antennas was supported on 2x4 frames and used inductor-capacitor traps. The input impedance was measured on this series of antennas to determine how the input impedance varied as a function of the diameter of the cylinder.

If the dimensions of the two series are measured in terms of wave length, the two series overlap, although they were designed to operate in different frequency ranges. The copper tubing antennas were measured from 0.3 to 2.0 GHz. and their traps were designed to be anti-resonant at 1.5 GHz. The 2x4 frame series, however, was measured over a frequency range of 30 to 130 MHz. and the traps were designed to be anti-resonant at 100 MHz. (Photographs of the two series are included in Appendix D.)

3.1 Model Details

The copper tubing models were constructed out of 3/8 inch x 0.040 inch semi-hard copper tubing. Each monopole was constructed in two sections, one of which contained a trap. Figure 3-1 illustrates the construction of the trap. The interior of the trap was filled with paraffin ($\epsilon_r=2.25$) so that both the inner and outer lengths of the trap were a quarter wave length at 1.5 GHz. and the impedance looking in the terminals of the trap was essentially an open circuit at that frequency. Traps with characteristic impedances of 18.5, 34.8 and 62.5 ohms were constructed using, respectively, 3/16, 1/8 and 1/16 inch brass rod stock for center conductors. 10-24, 5-40 and 0-80 NC screw threads were used, respectively, for the threaded ends of the center conductors. The short circuit was constructed out of 19/64 inch brass rod stock that was soldered in place with 60-40 lead-tin solder. Both ends of the plug were drilled and tapped to accept screw threads, one end to accept the center conductor and the other end to accept a 10-24 NC thread that was used to facilitate mounting.

The trap sections were used both as inner and outer sections. The non-trap section was constructed out of the 3/8 x 0.040 copper tubing and had a 19/64 inch diameter 1/4 inch long plug soldered in place at one end to accept the threaded center conductor of the trap. If used as an inner section, another plug was soldered in place at the

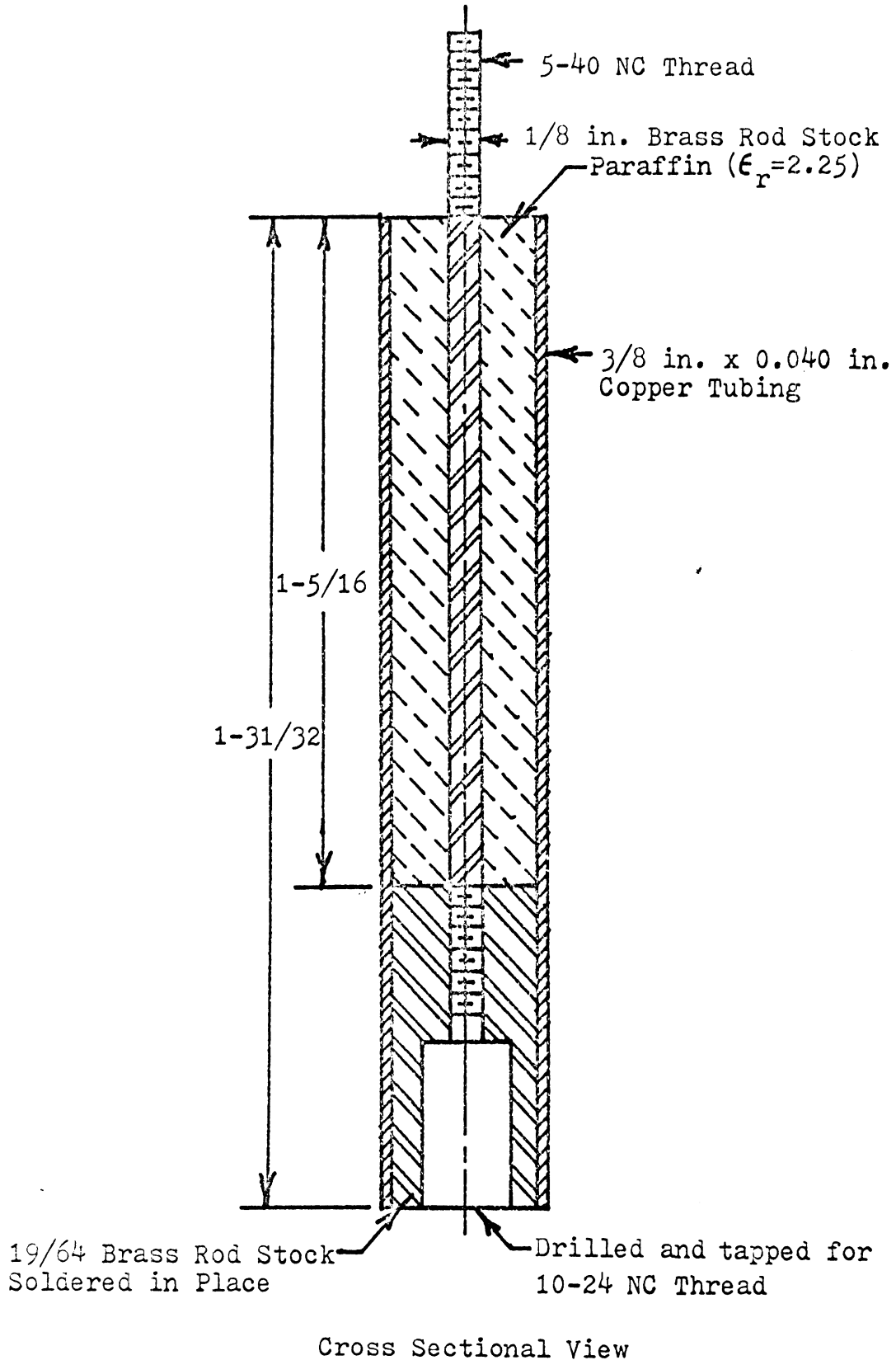


Figure 3-1: Construction of a 34.8 Ohm Transmission Line Trap

opposite end of the non-trap section. This additional plug was drilled and tapped to facilitate mounting. All sections were constructed slightly longer than necessary. Their end faces were then turned down in a lathe until the length was within 0.005 inch of the stated value.

Inner sections $63/64$, $1-61/128$, $1-31/32$, $2-59/128$ and $2-61/64$ inches long ($1/8$, $3/16$, $1/4$, $5/16$ and $3/8$ wave lengths at 1.5 GHz.) were constructed to determine how the properties of the antenna varied as the length of the inner section was varied. Outer sections $63/128$, $63/64$, $1-61/128$, $1-31/32$, $2-59/128$, $2-61/64$, $3-57/128$, $3-15/16$ and $4-55/128$ inches long ($1/16$, $1/8$, $3/16$, $1/4$, $5/16$, $3/8$, $7/16$, $1/2$ and $9/16$ wave lengths at 1.5 GHz.) were constructed to determine how the properties of the antenna varied as the length of the outer section varied.

The outer shell of the trap and the non-trap sections were electrically isolated from each other by $1/16$ inch thick G-10 epoxy-fiberglass laminate ($\epsilon_r=4.0$) washers. All measurements (unless otherwise stated) were made with one washer at both the trap and the feed (two at the feed for dipole measurements.) The study of how the trap and feed gap capacitances affected the results was made by adding additional washers.

The 2x4 series of antennas were all supported with 2x4 fir supports. Both trap and Franklin antennas were constructed in four different diameters. The antennas were constructed using number 35 AWG (5.615 mils) copper wire,

number 14 AWG (64.08 mils) tinned copper wire, 5/8 inch diameter by 0.058 inch thick 5061-T6 alloy aluminum tubing and a 5-5/8 inch diameter "birdcage" constructed out of number 14 AWG copper wire.

The "birdcage" consisted of eight number 14 AWG copper wires equally spaced on a 5-5/8 inch circle with copper foil end caps on both sides of the feed and trap gaps. Because of the narrow spacing between the wires, the "birdcage" is electrically equivalent to 5-5/8 inch copper tubing, which was impractical to use.

The "birdcage" was strung between 1/2 inch exterior plywood disks 6 inches in diameter that were glued in position on a 2x4 support with hide glue and gluing blocks. The gluing blocks were nailed in position with brads which were all located interior to the antenna so that the nails would not affect the antenna performance.

The outer and inner sections were constructed separately and bolted together with four 1/4 inch nylon bolts. The bolts, all located interior to the "birdcage," held together a flush lap joint in the 2x4 supports. Separate outer sections were built for the Franklin and trap antennas and a common inner section was used.

The inner and outer sections of the 5/8 inch tubing antennas were also constructed separately and bolted together with 1/4 inch nylon bolts. The outer section was placed over a 1/2 inch diameter piece of G-10 epoxy-fiberglass laminate tubing and bolted in place with two

1/4 inch nylon bolts. The fiberglass tubing was inserted in the lower section and bolted in place with two additional 1/4 inch nylon bolts. The lower section was bolted to an 8-1/2 inch long 2x4 at the base, again with two 1/4 inch nylon bolts. Like the 5-5/8 inch diameter antennas, separate outer sections were made for both the trap and Franklin antennas while the inner section was shared.

Complete and separate trap and Franklin antennas were constructed out of number 14 and 35 wire. The wire was mounted with Q-Dope (polystyrene dissolved in a volatile solvent) to 2x4 supports running the length of the antennas. All wood used in constructing the eight antennas was given two coats of polyurethane exterior varnish to reduce dimensional instability.

All inner sections and the outer sections of the trap antennas were 29.5 inches long (1/4 wave length at 100 MHz., the anti-resonant frequency of the trap). The outer sections of the Franklin antennas were 59.0 inches long (1/2 wave length at 100 MHz.). All feed and trap gaps were 15/16 inch. Care was taken to insure that all dimensions were maintained within 1/64 of an inch.

Thus, the 5-5/8 inch diameter antennas were scale models of the copper tubing trap and Franklin antennas described earlier, except for the difference in trap construction. Moreover, the 5/8 inch tubing, number 14 wire and number 35 wire antennas were also scale models, except that their diameters were approximately 1/10, 1/100 and

1/1000 the diameter of the copper tubing antennas.

The inductor-capacitor traps used on these models were constructed out of 5% silvered mica capacitors and number 14 AWG tinned copper wire. The capacitors were selected to provide the desired capacitance and the inductors were wound out of one to three turns of wire (depending on the inductance needed) using a pencil as a form. The inductors were expanded or compressed until the traps were anti-resonant at 100 MHz. in a test circuit before the traps were mounted on the antenna. Traps with "characteristic impedances" ($\sqrt{L/C}$ ratios) of 53 and 88.5 ohms were constructed and tested. These ratios give the same equivalent inductance at one-half the anti-resonant frequency (which is approximately the lower resonant frequency of the trap antenna) as will 34.8 and 62.5 ohm transmission line stubs.

This relationship between transmission line and inductor-capacitor traps results from noting that the input impedance of a transmission line trap is given by

$$Z_t = j Z_0 \tan kl \quad (3.1)$$

where k is the wave number,

$$k = \omega/v = 2\pi/\lambda, \quad (3.2)$$

Z_0 is the characteristic impedance, ω the radian frequency, v the velocity of propagation, and l the line length from the short circuit to the terminals. The impedance of a parallel inductor-capacitor circuit is given by

$$Z_{LC} = \frac{j\omega L}{1 - \omega^2 LC} \quad (3.3)$$

where L is the inductance and C the capacitance. By designating the anti-resonant frequency as ω_0 , noting that

$$\omega_0 = 1/\sqrt{LC} \quad (3.4)$$

and normalizing the radian frequency to the resonant frequency, the impedance of a parallel inductor-capacitor trap becomes

$$Z_{LC} = \frac{j(\omega/\omega_0) \mathcal{Y}}{1 - (\omega/\omega_0)^2} \quad (3.5)$$

where

$$\mathcal{Y} = \sqrt{L/C} \quad (3.6)$$

the "characteristic impedance" of the inductor-capacitor trap.

At one-half the anti-resonant frequency ($k\ell = \frac{1}{2}(\pi/2) = \pi/4$),

$$Z_t = j Z_0 \quad (3.7)$$

and

$$Z_{LC} = j \ 2\mathcal{Y}/3 . \quad (3.8)$$

Thus

$$\mathcal{Y} = 3 Z_0/2 . \quad (3.9)$$

3.2 Impedance Measurements

All impedance measurements in the 0.3 to 2.0 GHz. range were made on monopoles in a 9 foot cube anechoic chamber located in the G.G. Brown Building. The chamber has provisions for mounting a 1/8 inch thick by 4 foot square aluminum ground plane on one side of the chamber

in place of a panel of absorber. The absorber of the chamber has a minimum reflection coefficient of -30 db. down to 0.5 GHz. and previous experience with the chamber indicates that it gives useable results down to 0.1 GHz.

The monopoles were screwed to a threaded stud soldered to the center conductor of a UG-58/U bulkhead type N connector. The connector was modified by turning down the shoulder on the face abutting the ground plane so that it would fit flush with the surface of the ground plane.

The impedance was measured by the comparison method using a Hewlett-Packard type 8410A Network Analyzer in the circuit illustrated in Figure 3-2. The known impedance to which the monopole was compared was a special short circuit constructed out of another UG-58/U bulkhead connector modified as described above. The connector was mounted tightly on two 1/8 inch thicknesses of aluminum sheet, one to simulate the 1/8 inch thick ground plane, and the other to act as a short circuit. The latter had a hole drilled in it to accept the center conductor of the connector with a force fit.

All impedance measurements in the 30 to 130 MHz. range were made on monopoles mounted on top of a 1/8 inch thick, 10 foot square aluminum ground plane mounted 9-1/2 feet above the roof of the G. G. Brown Building. The monopoles were bolted with four 3/8 inch bolts to a base in the form of a cross. The arms of the cross were 23 inches across and the base was given two coats of

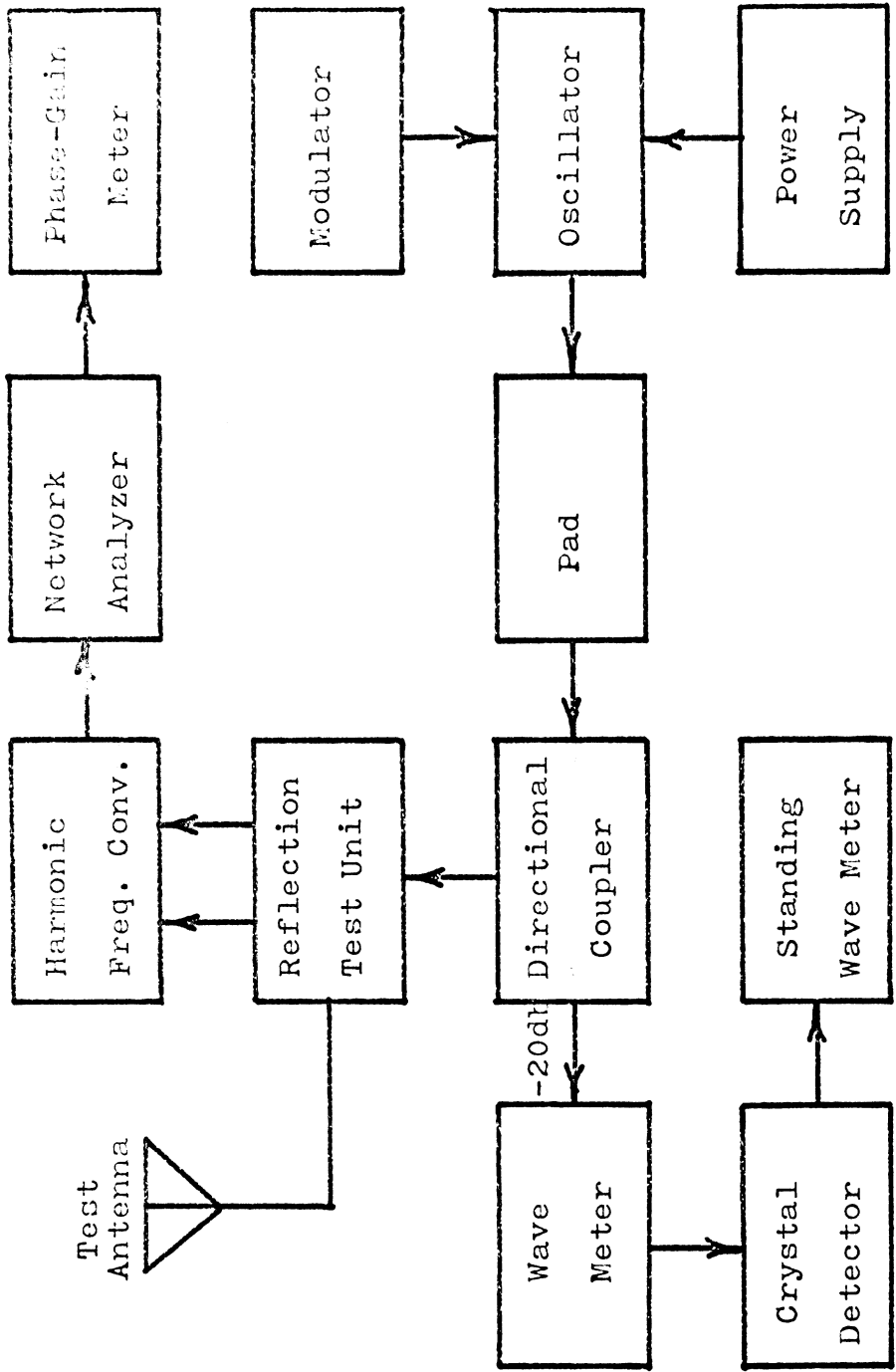


Figure 3-2: Impedance Measurement Set-Up (Copper Tubing Series)

polyurethane exterior varnish to minimize dimensional instability.

All monopoles were positioned directly over a bulk-head connector which was located in the center of the ground plane. The number 14 and 35 wire antennas were soldered directly to the center conductor of the connector. The 5/8 inch tubing and the "birdcage" antennas were connected to a piece of number 14 wire that was soldered to the center conductor of the connector.

The impedance was measured by the comparison method using a Hewlett-Packard type 8405A Vector Voltmeter in the circuit illustrated in Figure 3-3. The known impedance to which the impedance was compared was the same special short circuit described earlier. However, it was mounted at the end of a piece of RG-8 coaxial cable identical in length to the cable used to connect the monopole to the equipment located in a penthouse under the ground plane.

As a further control on accuracy, the anti-resonant frequency of the trap was checked after each impedance measurement session. If the resonant frequency had changed, the trap was adjusted and the data retaken.

The gap and feed capacitances of the copper tubing antennas were measured by two different techniques. The feed gap capacitance was measured by placing a 10-24 hexagonal brass nut, which was 3/8 inch across the points, on the threaded stud of the mount on the ground plane. The nut held a 1/16 inch thick G-10 washer in place. The

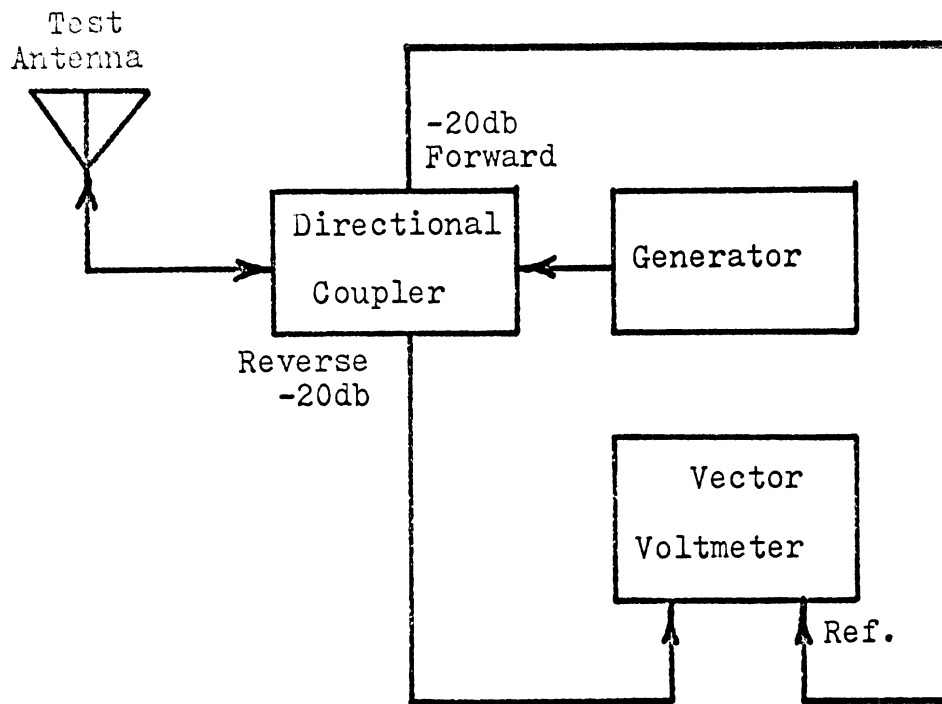


Figure 3-3: Impedance Measurement Set-Up (2x4 Frame Series)

reactance of the capacitance was then measured using the procedure to measure the input impedance of the copper tubing monopoles.

The value of the trap gap capacitance was measured by constructing a structure similar to a trap attached to a non-trap section, except that the brass center conductor of the trap was replaced by a threaded G-10 dielectric rod. The capacitance of the similar structure was then measured on a Tektronix type 130 LC meter. The capacitance was then corrected by the factor of $4/5$ to account for the change in the dielectric constant of the G-10 washer between audio frequencies and microwave frequencies.

3.3 Radiation Patterns

The radiation patterns were measured on dipoles on the 50 foot antenna range located on the roof of the G. G. Brown Building. The antennas were a minimum of 40 feet above the roof of the building and the transmitting antenna for this range is a log-periodic antenna with a beam width narrow enough so that reflections are insignificant. Figure 3-4 illustrates the circuitry used.

The test antennas were mounted on a 8 inch long by $3/8$ inch wide rod of G-10 epoxy-fiberglass laminate that was $1/8$ inch thick. The G-10 rod was used in place of feed washers. The G-10 rod was bolted with two $1/4$ inch nylon bolts to a 10 foot 2x2 fir mast which in turn was bolted to the table of the antenna range rotator. All

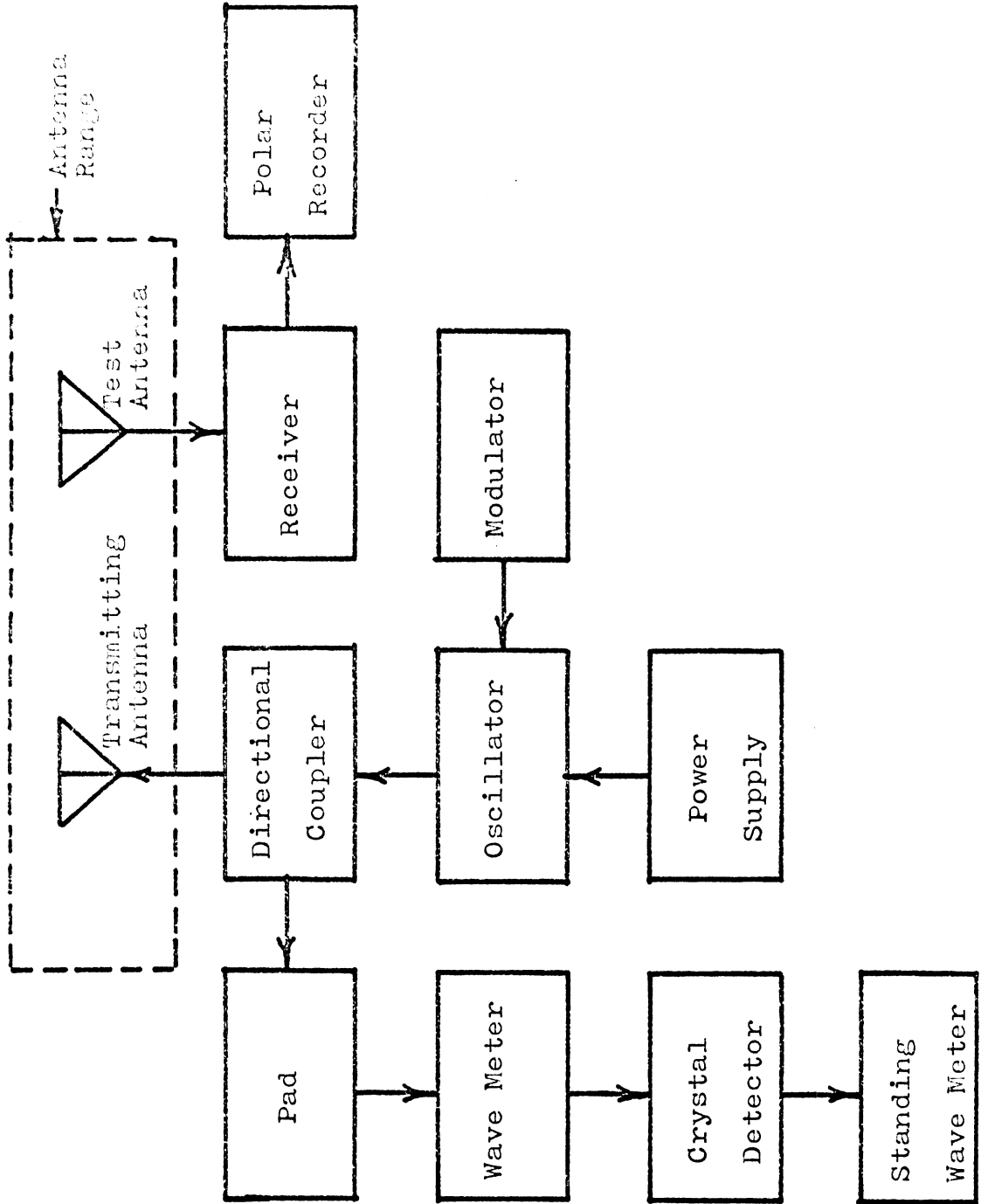


Figure 3-4: Radiation Pattern Measurement Set-Up

patterns taken were horizontal polarizations in the plane of the electric field vector.

The dipoles were fed through an Anzac H-9 hybrid, which is a broadband 180° hybrid. A special balanced line from the hybrid to the antenna was constructed out of RG-58A/U coaxial cable. The cables from the opposite output ports of the hybrid were stripped of their outer insulation and taped together with electrical tape so that their outer conductors would be in continuous contact. Just short of the antenna, the outer conductors were cut away to reveal the inner conductors, which were connected to the antenna through terminal lugs. The faces of the G-10 rod were machined down to accept the terminal lugs as inserts, without disturbing the $1/8$ inch feed gap width. A 10-24 NC threaded G-10 rod was used to hold the two halves of the dipole together, in addition to securing the antenna to the mast and holding the terminal lugs in place.

3.4 Current Distribution

The current distribution was measured in the 9 foot cube anechoic chamber described in Section 3.2. Figure 3-5 illustrates how a Hewlett-Packard type 8411A Network Analyzer was used to measure the relative amplitude and phase of the current distribution.

The probe used to measure the current was an 0.108 inch O. D. shielded loop constructed out of 0.027 inch

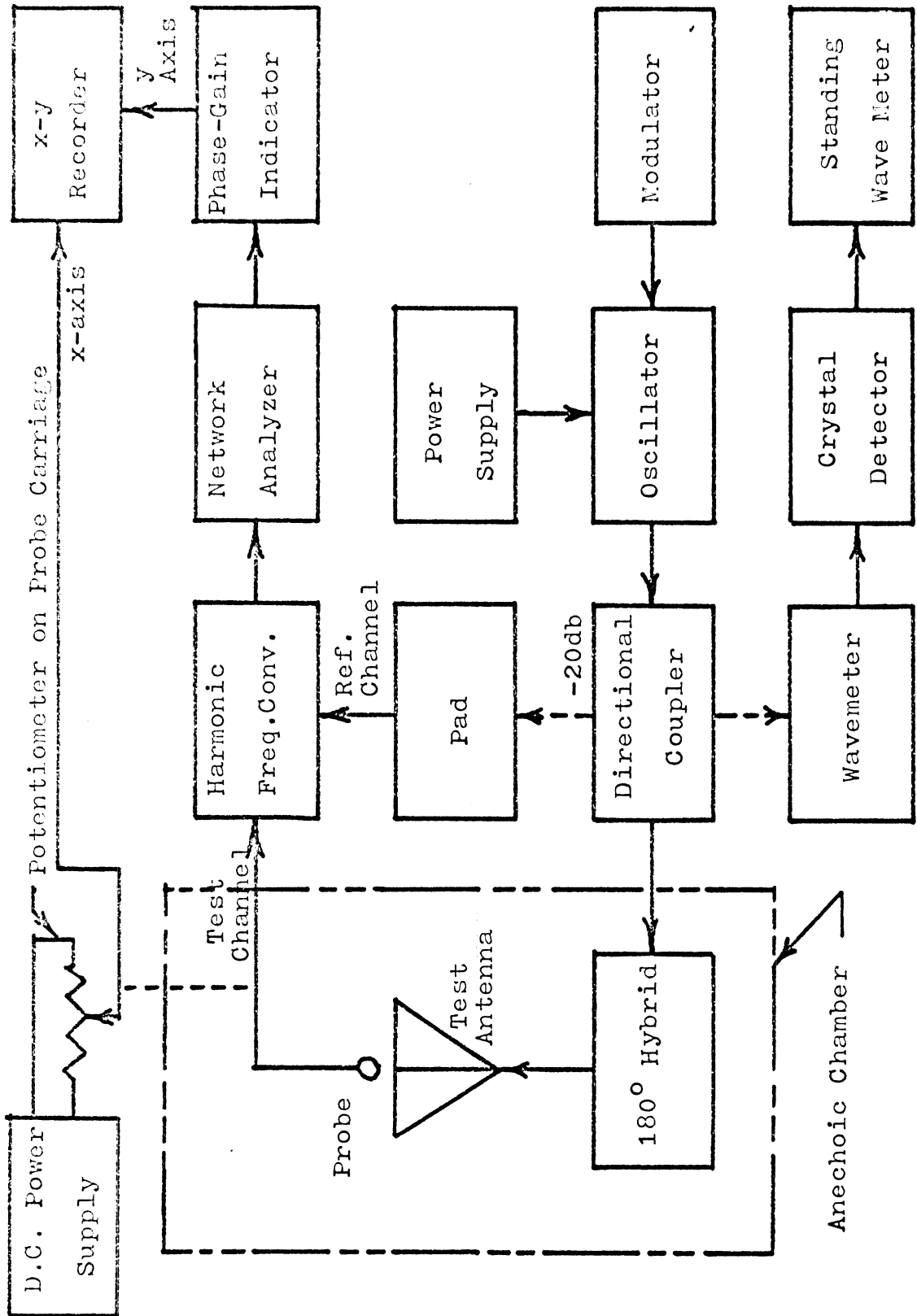


Figure 3-5: Current Distribution Measurement Set-Up

C. D. coaxial cable. The probe was coated with Q-Dope to insulate it from the antenna under measurement when they came in contact. The antenna under measurement was supported on styrofoam blocks in the center of the chamber. Care was taken to level the antenna so that the probe would neither lift off the surface of the antenna, nor bind while being moved along the antenna.

The position of the probe was controlled by a selsyn motor system which drove the probe carriage across the chamber. Position information was obtained from the voltage on the wiper arm of the potentiometer across which a constant voltage was impressed. The potentiometer was mounted on the probe carriage and was driven by a rubber wheel resting on the top of the chamber. The probe was swept along the length of the antenna slowly enough to prevent it from oscillating like a pendulum.

IV RESULTS

The trap antenna was found to produce a radiation pattern resembling a half-wave dipole pattern at its first two resonant frequencies and an input impedance in the vicinity of 70 ohms at both resonances. The three element Franklin antenna was found to produce a radiation pattern near its second resonant frequency similar to a collinear array of three half-wave dipoles. However, the fatter the antenna, the farther below the second resonance the desired pattern occurred; and the further below resonance the desired pattern occurred, the more capacitive the input impedance became from its approximately 70 ohms at the second resonance.

The design procedure for a trap antenna described by Greenberg (1956) in connection with a multiple trap antenna (adjusting the trap to obtain the exact upper resonant frequency desired and then changing the length of the outer section to adjust the lower resonance) was found to be valid. However, plots in Section 4.2 also permit the inductor-capacitor ratio of a lumped element trap or the characteristic impedance of a transmission line trap to be specified as a means of controlling the lower resonant frequency.

Section 4.1 describes checks made on the consistency of the theoretical solutions and the experimental data.

Section 4.2 describes how the properties of a trap-loaded cylindrical antenna vary as a function of the parameters and gives the details of how the input impedance and radiation patterns vary as a function of frequency for both the trap and Franklin antennas, along with the current distribution of these two antenna at their second resonant frequency.

4.1 Consistency Checks

Several checks were run on both the theoretical calculations and the experimental procedure to insure consistency and accuracy of the results presented in the next section. The short circuits used for the impedance measurements were checked over a wide range of frequencies and compared with standard short circuits for accuracy of their amplitude and phase responses. They were found to agree with the standards within 0.1 db in amplitude and 1.0 degree in phase. Over most of the frequency range checked, there was no noticeable disagreement with the standards at all.

The reference cable used for the impedance measurements on the 10 foot square ground plane was checked for consistency with the measurement cable over the 30 to 130 MHz. range of operation by measuring the same short circuit at the end of each cable. The magnitudes of the reflection coefficients were found to agree within 0.04 and the phase within 1.7 degrees.

A special adapter was constructed to permit the 34.8 ohm traps to be connected to a coaxial line so that the anti-resonant frequency of the traps could be measured. The traps were designed to be open circuits at 1.5 GHz. The most accurate trap (and the one used in all the impedance measurements) was found to be anti-resonant at 1.505 GHz. (a 0.33% error). The other trap was anti-resonant at 1.525 GHz. (a 1.67% error).

A half-wave dipole antenna was used for many consistency checks since its properties are reasonably well known. The theoretical half-wave dipole current distribution was studied as a function of the number of matching points to determine how rapidly the theoretical solutions converged. Figure 4-1 shows how the input impedance varies as the number of points increases. Figures 4-2 and 4-3 show the same study made on the input impedance of a trap and a Franklin antenna when the trap is anti-resonant. These plots, along with the current distributions on which they are based, were studied to determine convergence.

Note that for $N=40$, the delta function solution starts to diverge and that for $N=5$ the polynomial solution starts to diverge. The divergence in the delta function solution is caused by the subsection size, Δz , being on the order of the radius. As a result, the first few terms of the coefficient matrix off the diagonal are not small compared with the diagonal terms, and round off error appears. The round off error introduces "noise" into a plot of the current

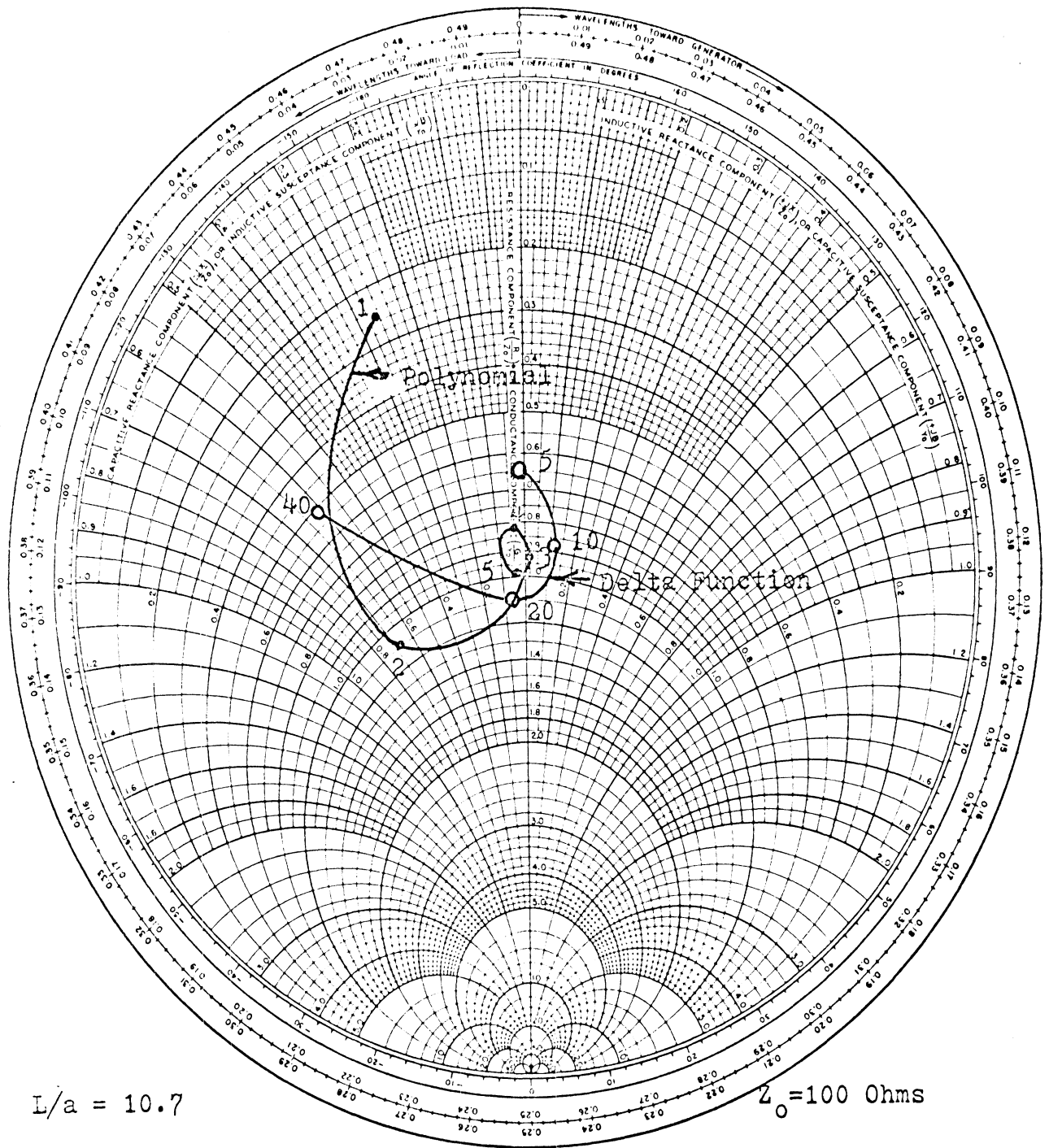


Figure 4-1: Convergence of the Theoretical Solutions for a Half-Wave Dipole Antenna

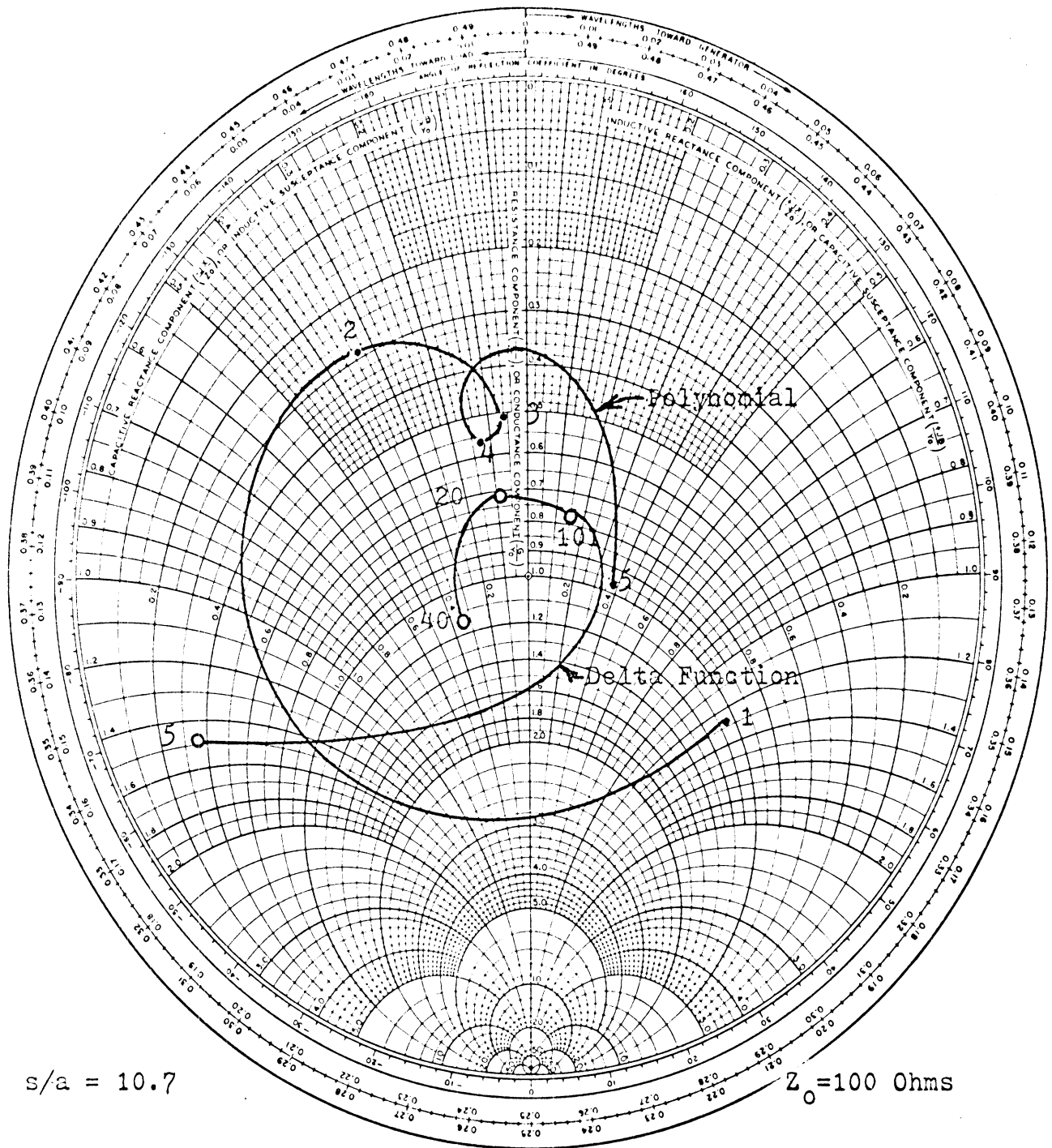


Figure 4-2: Convergence of the Theoretical Solutions for a Trap Antenna at the Anti-Resonant Frequency of the Trap

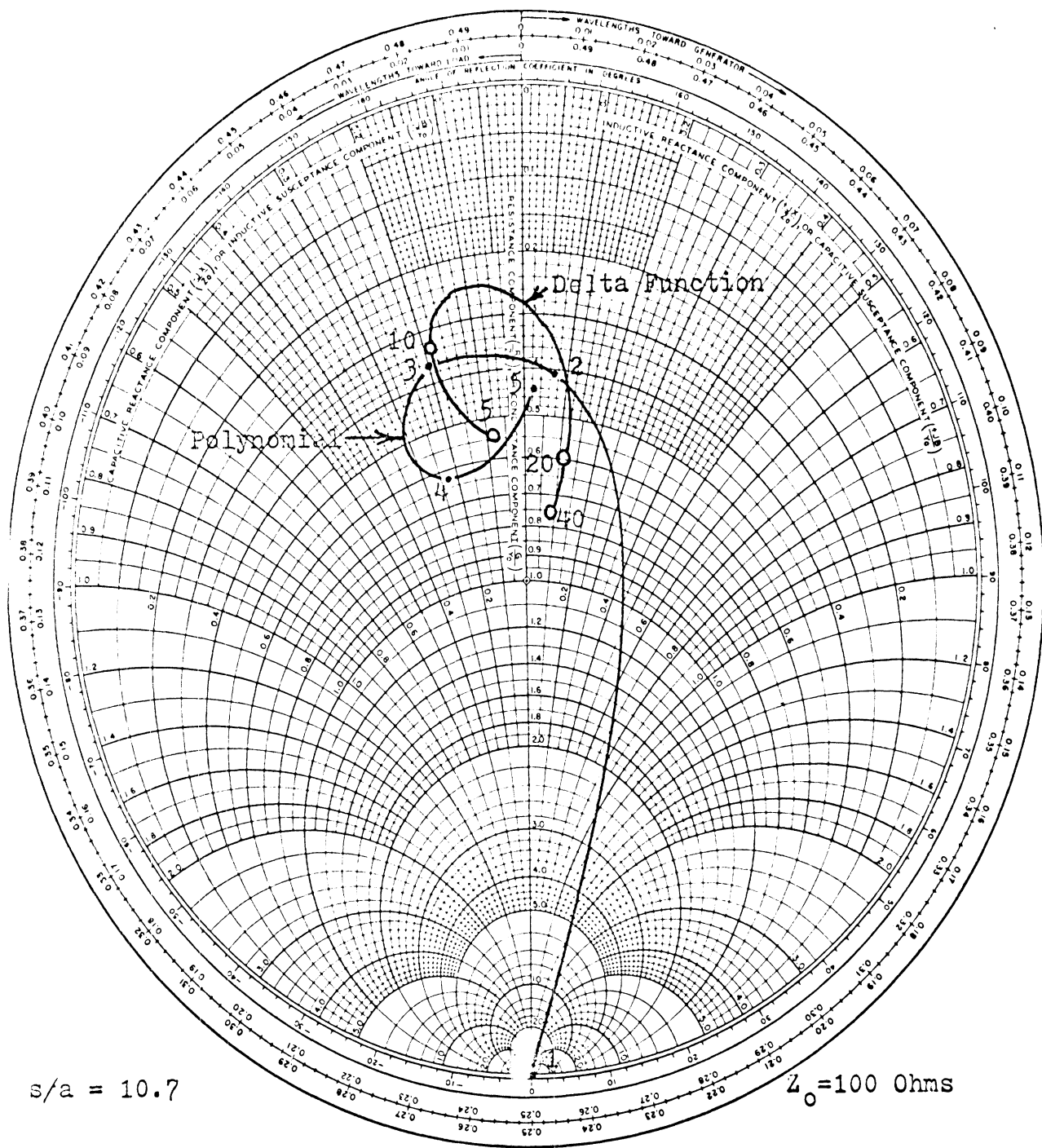


Figure 4-3: Convergence of the Theoretical Solutions for a Franklin Antenna at the Anti-Resonant Frequency of the Trap

distribution and the input impedance.

Note also that for $N=5$, the polynomial solution starts to diverge, but for a different reason. For N less than 4, the integrations needed to evaluate the coefficients of the matrix can be evaluated within an estimated accuracy of 1%. For N equal to 4, one or two terms (usually those resulting from matching points close to the end of the antenna) occasionally fail to give integration accuracy within 1%. For N equal to 5, some of the integration error estimates are over 2% and the real parts of some of the input impedances become negative.

To insure that the computer programs for both numerical solutions were working correctly, some of the results were calculated by hand and compared with the computer output. As a further check, the computer output for a half-wave dipole was compared with one result obtained by Mei (1965) and with the experimental results obtained by Brown and Woodward as reproduced by C-T Tai in Chapter 3 of Jasik (1961).

Half-wave monopoles were measured in both the 0.3 to 2.0 GHz. range and in the 30 to 130 MHz. range and compared with both the delta function and the polynomial solutions. Figure 4-4 shows the input impedance of both experimental antennas and Figure 4-5 shows the results for both theoretical solutions plotted as a function of f/f_0 , where f_0 is the frequency where L is a quarter wave-length.

The greatest discrepancy between the two theoretical

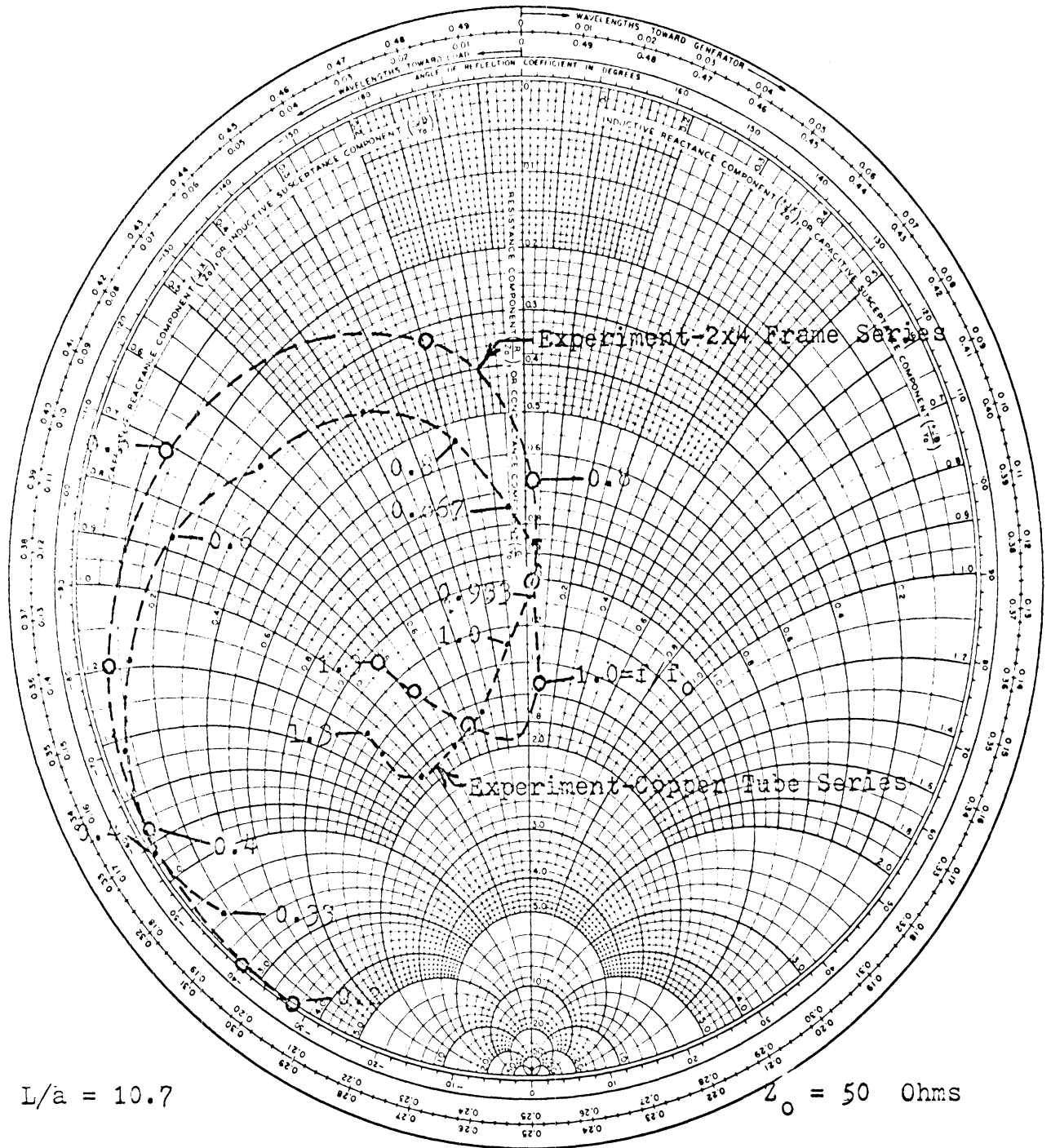


Figure 4-4: Input Impedance of a Monopole Antenna (f_0 is the Frequency Where L is a Quarter-Wave Length)

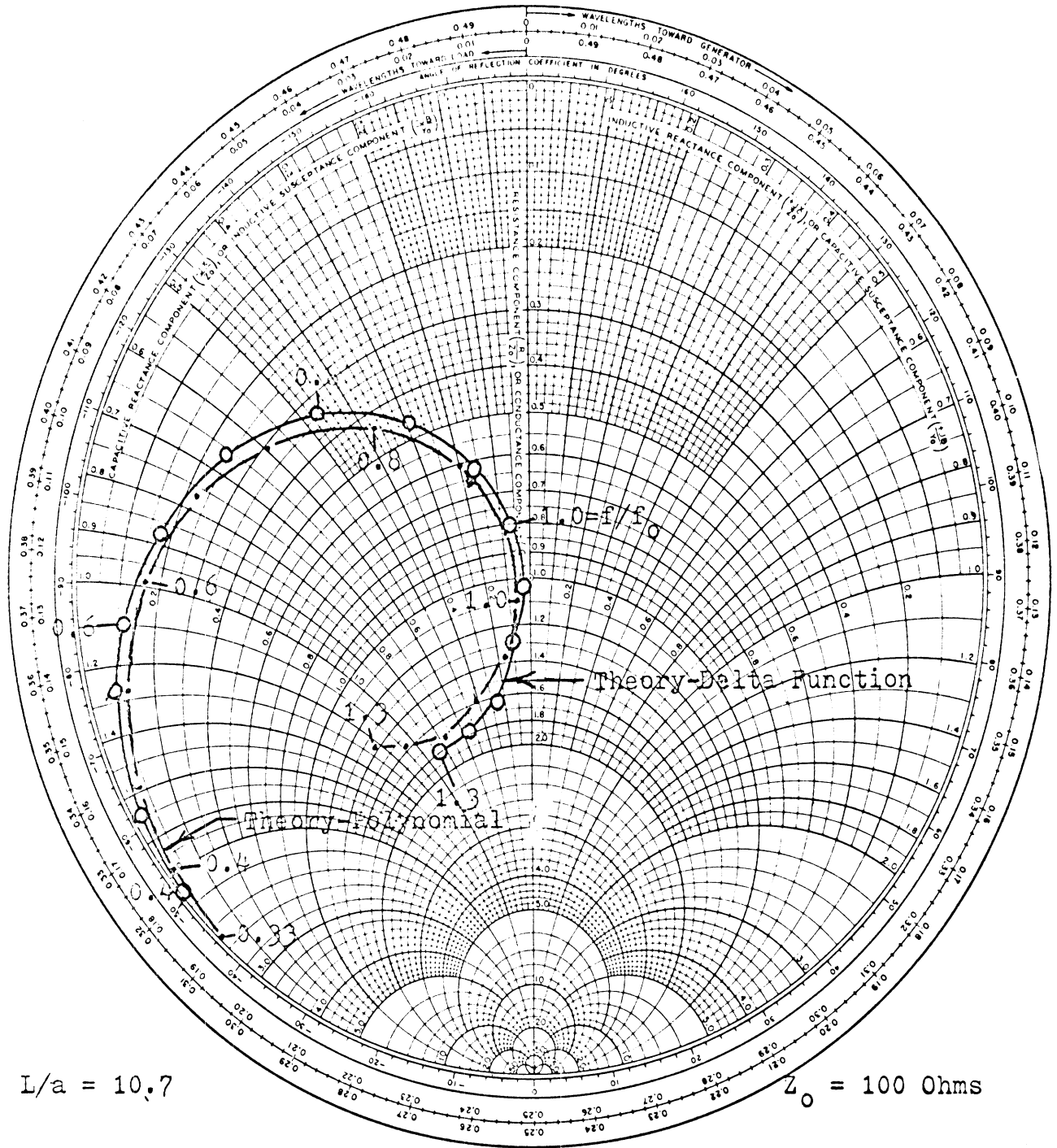


Figure 4-5: Input Impedance of a Dipole Antenna (f_0 is the Frequency Where L is a Quarter-Wave Length)

solutions occurs for frequencies where the computer program could not accurately evaluate the integrals of the polynomial solution. The delta function solution gives better agreement with experimental results, and has an added advantage that the computer program costs less to run than does the program for the polynomial solution.

The discrepancy in the experimental solutions, particularly for f/f_0 greater than 1.0 is probably due to the influence of the feed gap capacitance of the copper tubing models. This capacitance was measured at several frequencies between 1.0 and 2.0 GHz. The average of the values measured was 1.21 pf. This compares with 1.20 pf. calculated using a formula given on p. 133 of Westman (1964). This capacitance would have a reactance of 181 ohms at f_0 , which is 1.5 GHz.

To check the accuracy of the current distribution measurements, a half-wave dipole was measured and compared with both theoretical solutions. The results are shown in Figures 4-6 and 4-7. Most of the discrepancy between the experimental and theoretical curves occurs at the feed point. The apparent discrepancy in the phase curve at the ends of the antenna is a combination of two phenomena. First, the phase for the theoretical solutions is not defined at the ends of the antenna since the amplitude of the current is zero. Second, the breaks in the experimental phase curve near the ends are a result of the current measuring probe being finite instead of infinitesimally small. The consequence is that the probe averages the

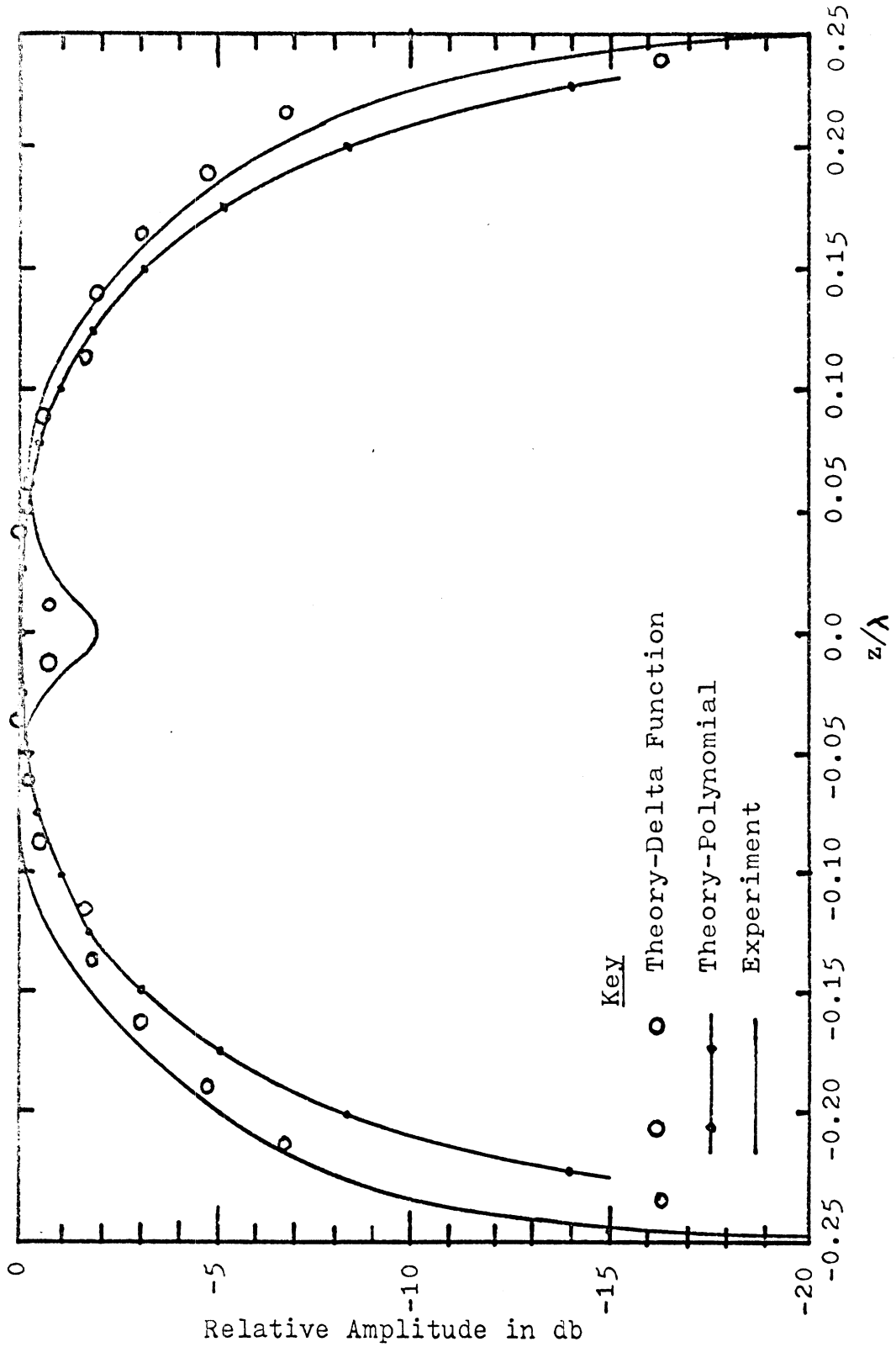


Figure 4-6: Amplitude of the Current Distribution on a Half-Wave Dipole

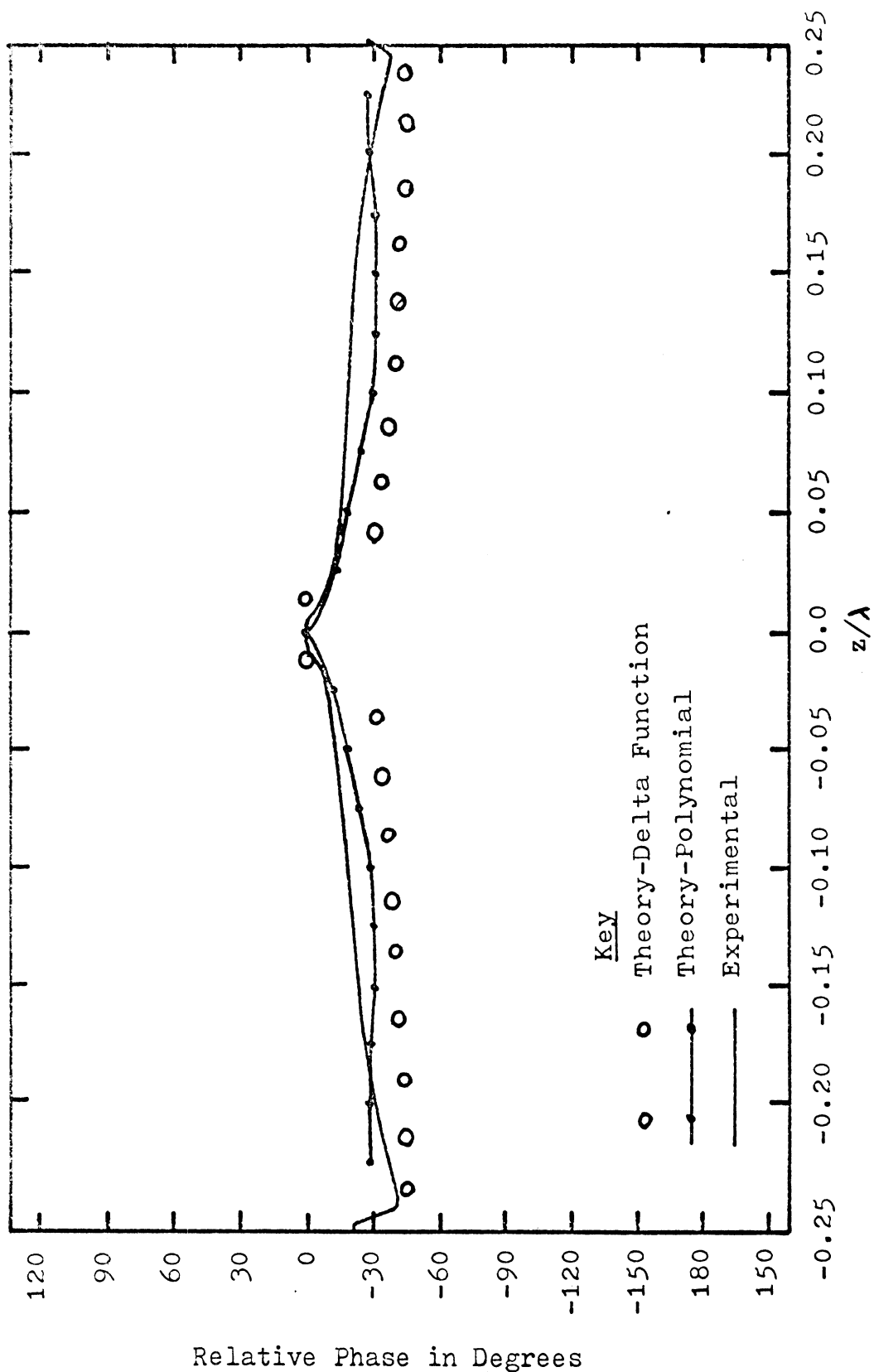


Figure 4-7: Phase of the Current Distribution on a Half-Wave Dipole

value of the current over its small but finite width. The breaks in the phase curve just off the ends of the antenna correspond to where the probe just starts to contact the antenna. The breaks in the phase curve closer to the center of the antenna correspond to where the entire probe is just barely on the dipole.

4.2 Discussion

The input impedance of a 34.8 ohm transmission line trap antenna is given in Figures 4-8 and 4-9. Figure 4-8 compares both the delta function and the polynomial theoretical solutions, while Figure 4-9 illustrates the corresponding experimental results for a copper tube model.

This discrepancy between theory and experiment was eventually traced to the trap gap capacitance. The trap gap capacitance was sufficient to detune the trap of the experimental model and lower its resonant frequency from a design of 1.5 GHz. to an estimated 1.21 GHz. Taking the detuning effect of the measured 1.27 pf. trap gap capacitance into account in the theoretical solution, as illustrated in Figure 4-9, results in very good agreement between theory and experiment.

The only remaining discrepancy between theory and experiment can be explained by the feed gap capacitance. Correcting the experimental data for the 1.21 pf. capacitance measured resulted in too much correction. A value of about half that measured gave optimum agreement between theory and experiment.

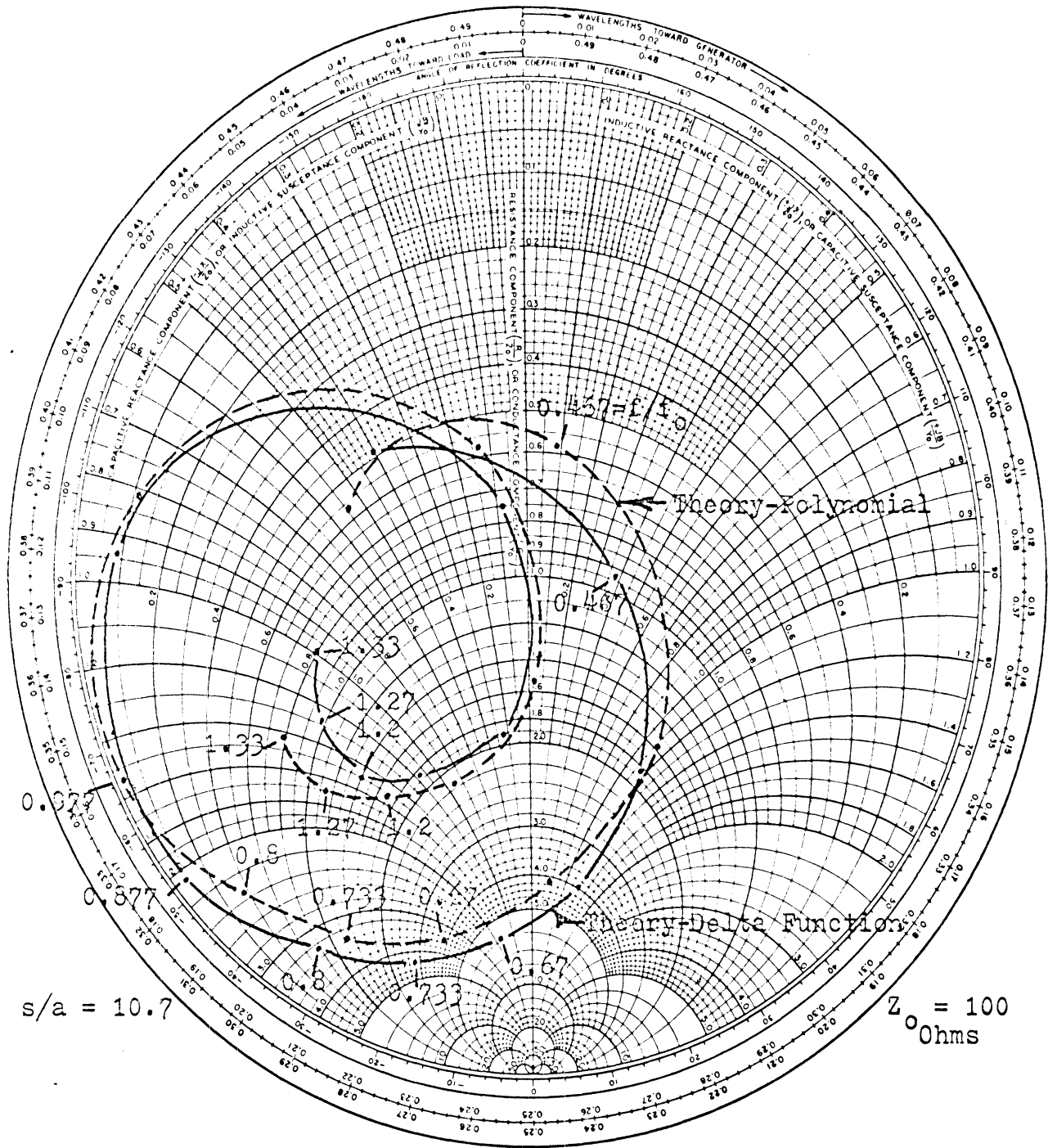


Figure 4-8: Input Impedance of a Trap Antenna with a 34.8 Ohm Transmission Line Trap

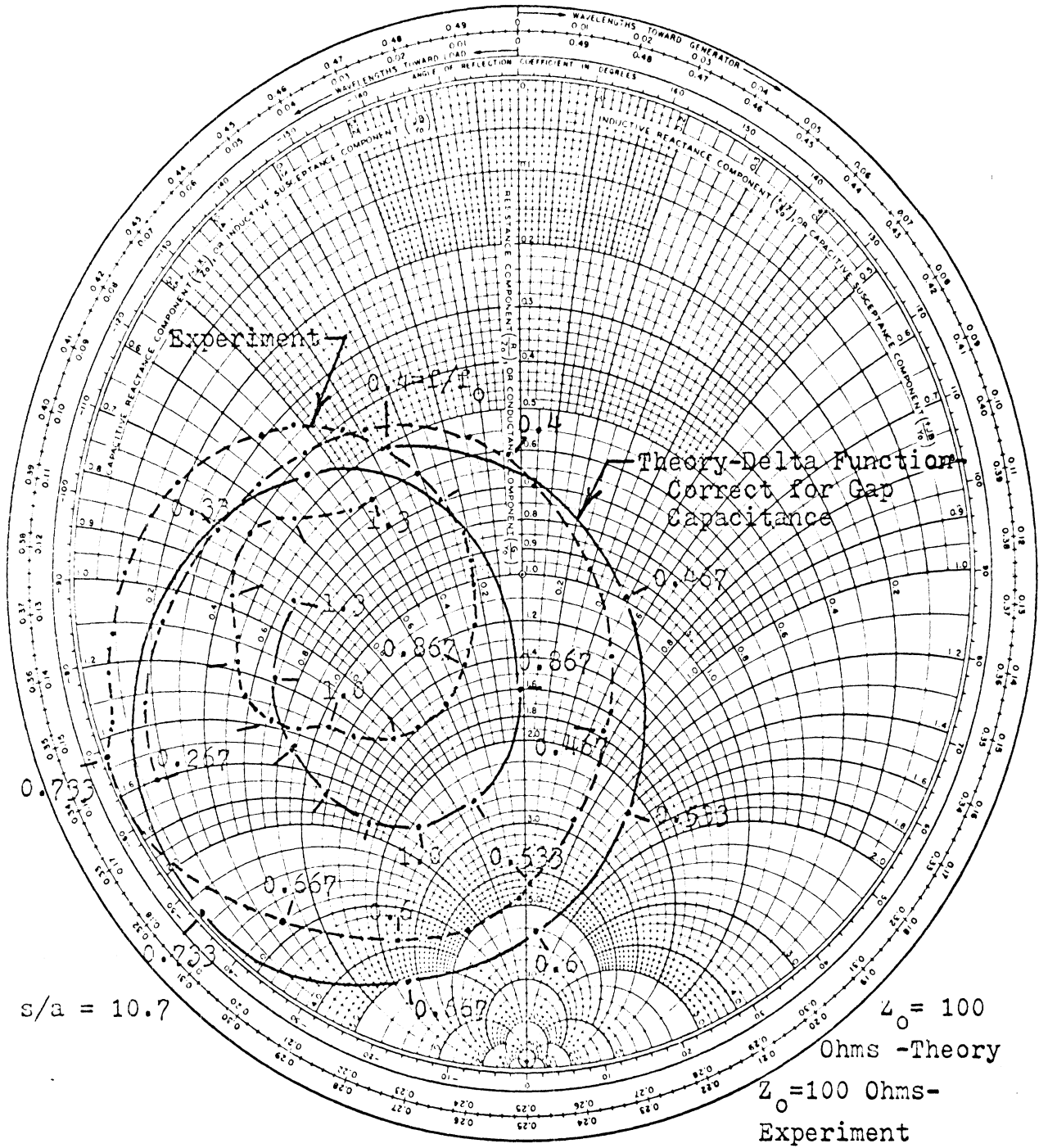
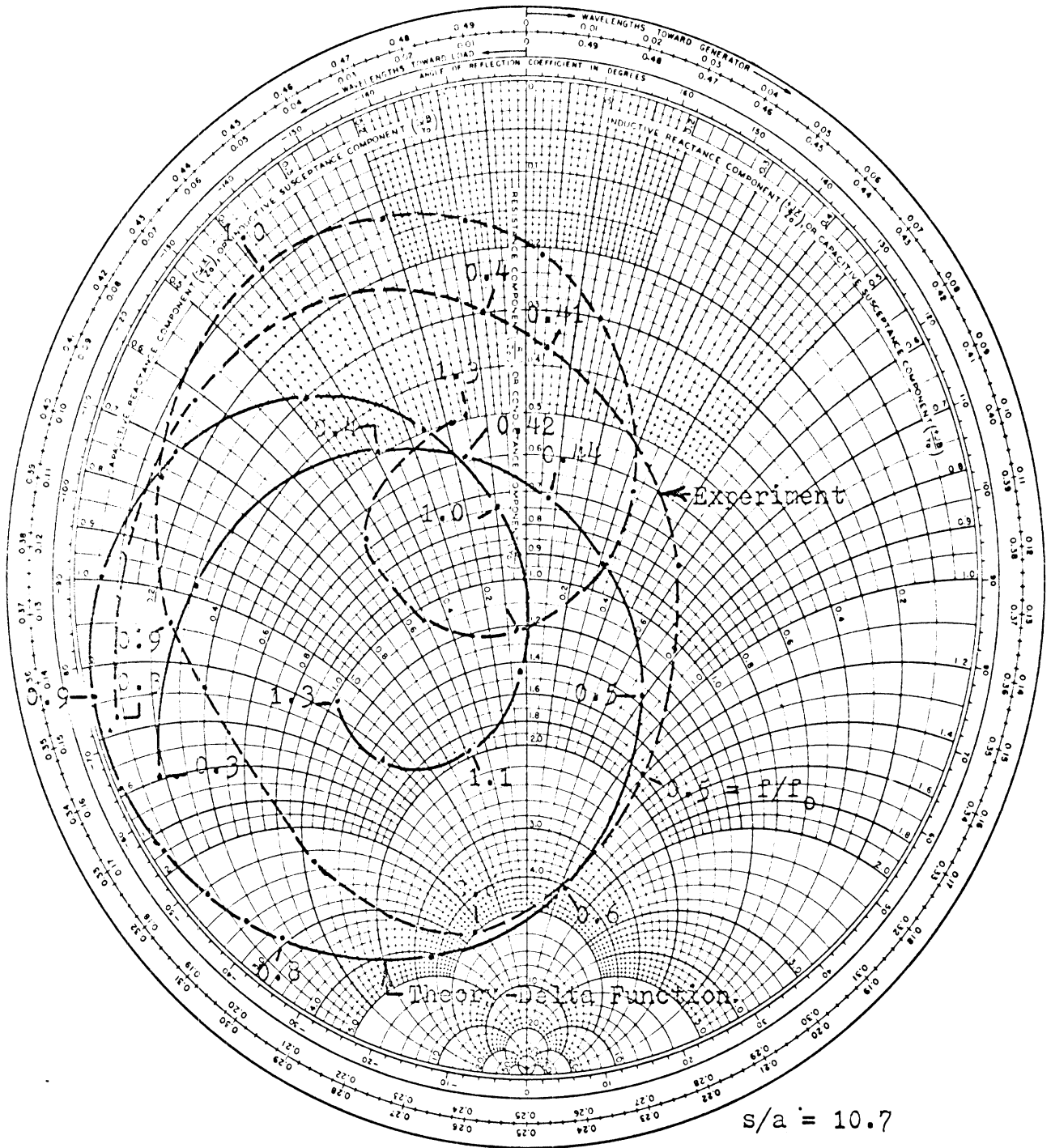


Figure 4-9: Input Impedance of a Trap Antenna with a 34.8 Ohm Transmission Line Trap

Figure 4-10 compares theoretical and experimental input impedances for a 2x4 antenna with a lumped inductor-capacitor trap. Agreement between theory and experiment is not as good as for the copper tube models, but this is not surprising. First, the accuracy of the measurement equipment used for the 2x4 models is not as good as that of the equipment used for measuring the copper tubing models. Second, the ground plane used as a counterpoise for the 2x4 models is really quite small, only a wave length on a side when measured in terms of the anti-resonant frequency of the trap. Regrettably, a larger ground plane was not available, nor was there sufficient room to construct a larger one. Third, 100 MHz., the anti-resonant frequency of the trap, is close to the upper useful limit at which lumped element traps can successfully operate. Attempts to build inductor-capacitor traps anti-resonant much above 100 MHz. resulted in traps whose impedance did not agree well with theory.

Selected linear power radiation patterns for a 34.8 ohm transmission line trap antenna are shown in Figure 4-11. Note that at the first two resonant frequencies, the antenna has essentially the same radiation pattern.

Figure 4-12 shows the amplitude and Figure 4-13 the phase of the current distribution on a copper tube trap antenna at f_0 , the anti-resonant frequency of the trap. Note the close agreement between experiment and theory corrected for the trap gap capacitance. Furthermore, note that the amplitude of the current distribution from the



$Z_0 = 50$ Ohms - Experimental $Z_0 = 100$ Ohms - Theory

Figure 4-10: Input Impedance of a Trap Antenna with a 53 Ohm L-C Trap

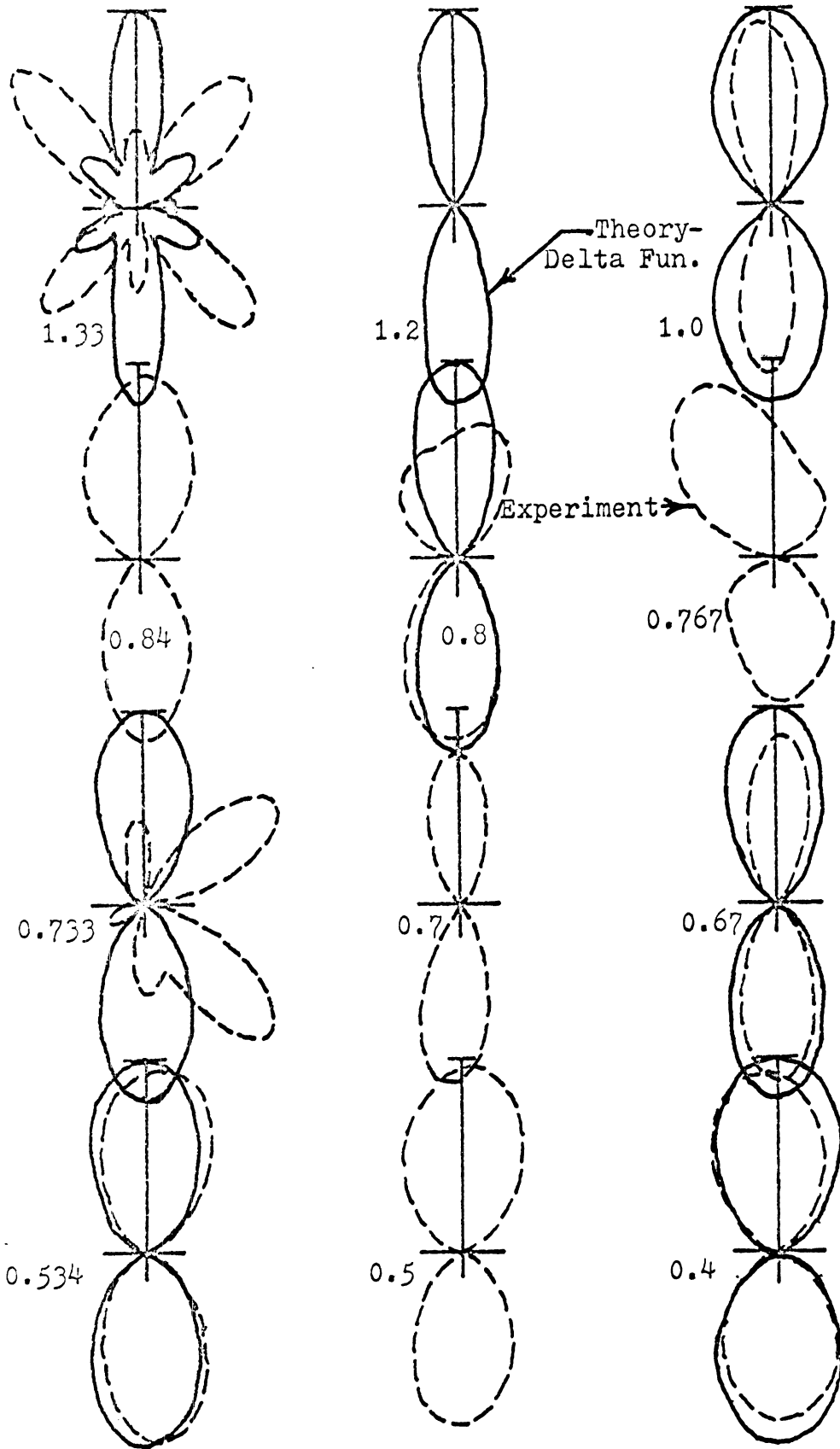
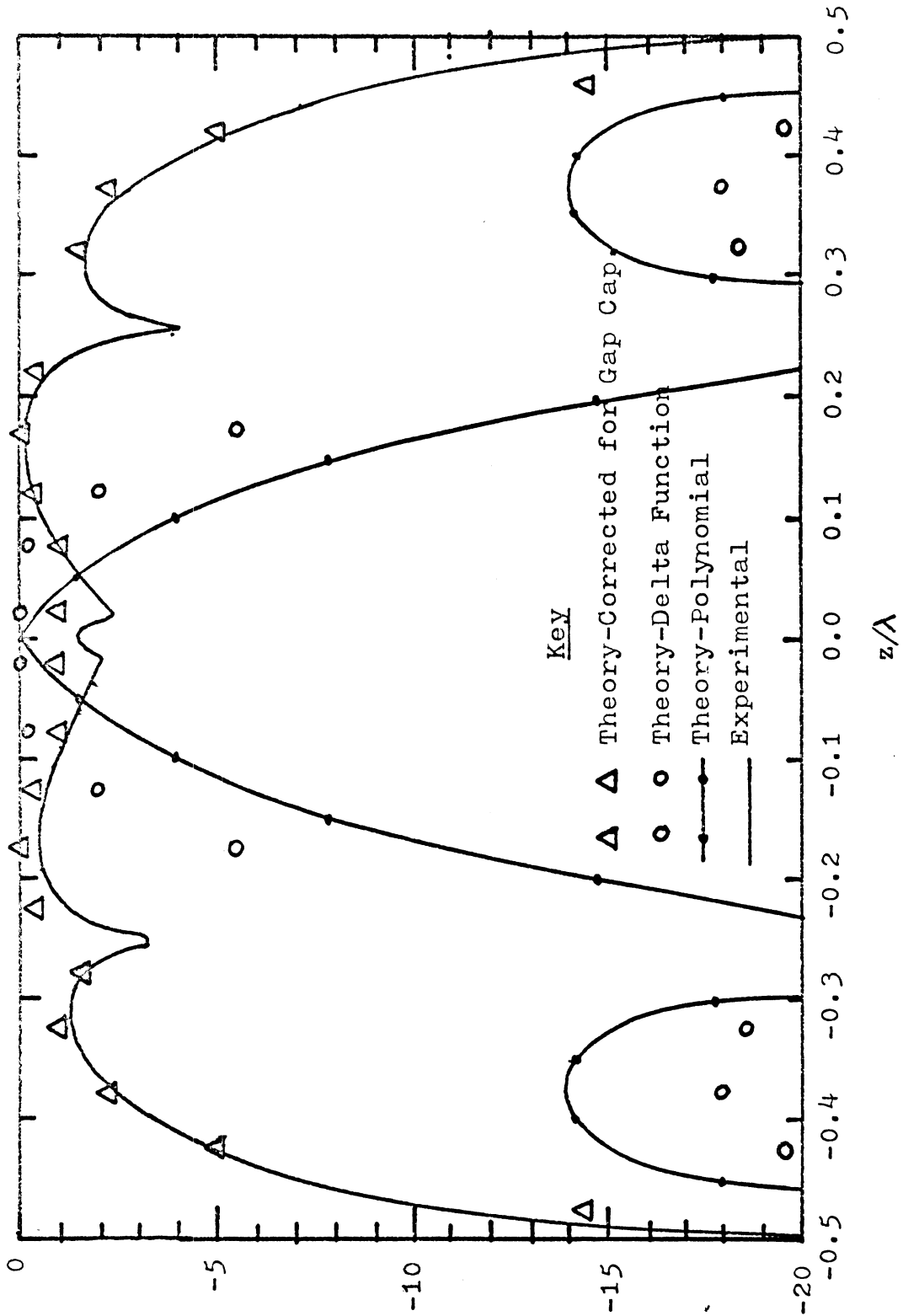


Figure 4-11: Linear Power Radiation Patterns of a Trap Antenna as a Function of Frequency Normalized to the Anti-Resonant Frequency of the Trap ($a/L = 10.7$)



Relative Amplitude in db

Figure 4-12: Amplitude of the Current Distribution on a Trap Antenna at the Anti-Resonant Frequency of the Trap.

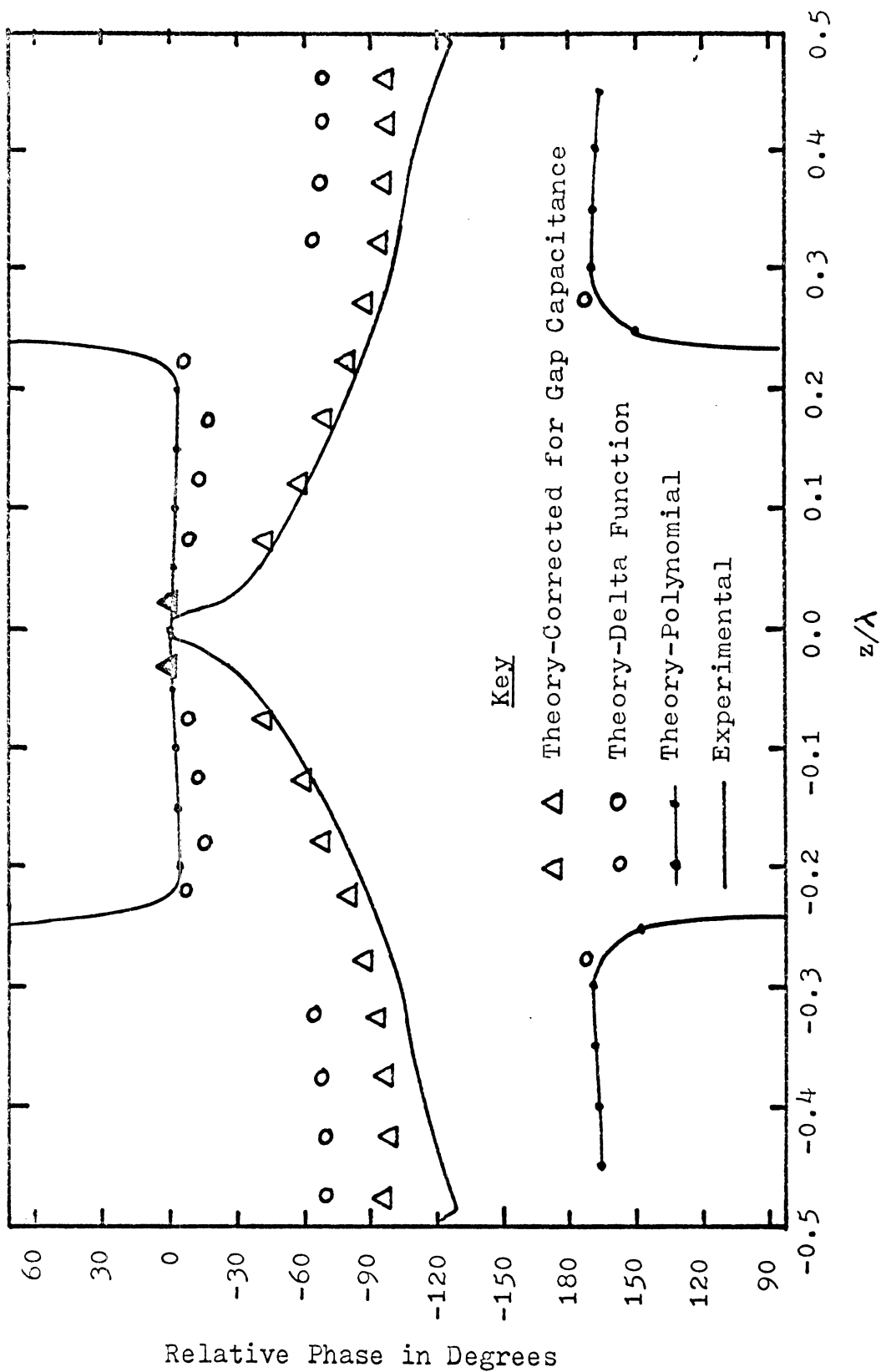


Figure 4-13: Phase of the Current Distribution on a Trap Antenna at the Anti-Resonant Frequency of the Trap

trap to the ends of the antenna is indeed suppressed by the trap.

Figures 4-14 and 4-15 show the input impedance of a 34.8 ohm transmission line trap Franklin antenna and Figure 4-16 shows the input impedance of a 53 ohm inductor-capacitor trap antenna. Again note that correcting the experimental results in Figure 4-15 for a slight feed gap capacitance would give good agreement between theory and experiment.

Figure 4-17 shows selected linear power radiation patterns for a Franklin antenna with a 34.8 ohm transmission line trap. Note that the expected radiation pattern, a pattern similar to a co-linear array of three half-wave length dipoles, does not occur at the anti-resonant frequency of the trap, $f/f_0=1.0$, but at about $f/f_0=0.8$ for the theoretical patterns and at approximately $f/f_0=0.7$ for the experimental curves where, of course, the trap is detuned due to the trap gap capacitance.

The reason for this rather surprising result can be seen in Figures 4-18 and 4-19 which show the amplitude and phase of the current distribution for a Franklin antenna at the anti-resonant frequency of the trap. While the maximum of the amplitude in the outer sections is only 1 or 2 db down from the maximum of the amplitude in the center section, the trap fails to force the phase reversal necessary to produce the expected co-linear dipole array pattern.

As Figures 4-20 and 4-21 show, this is apparently

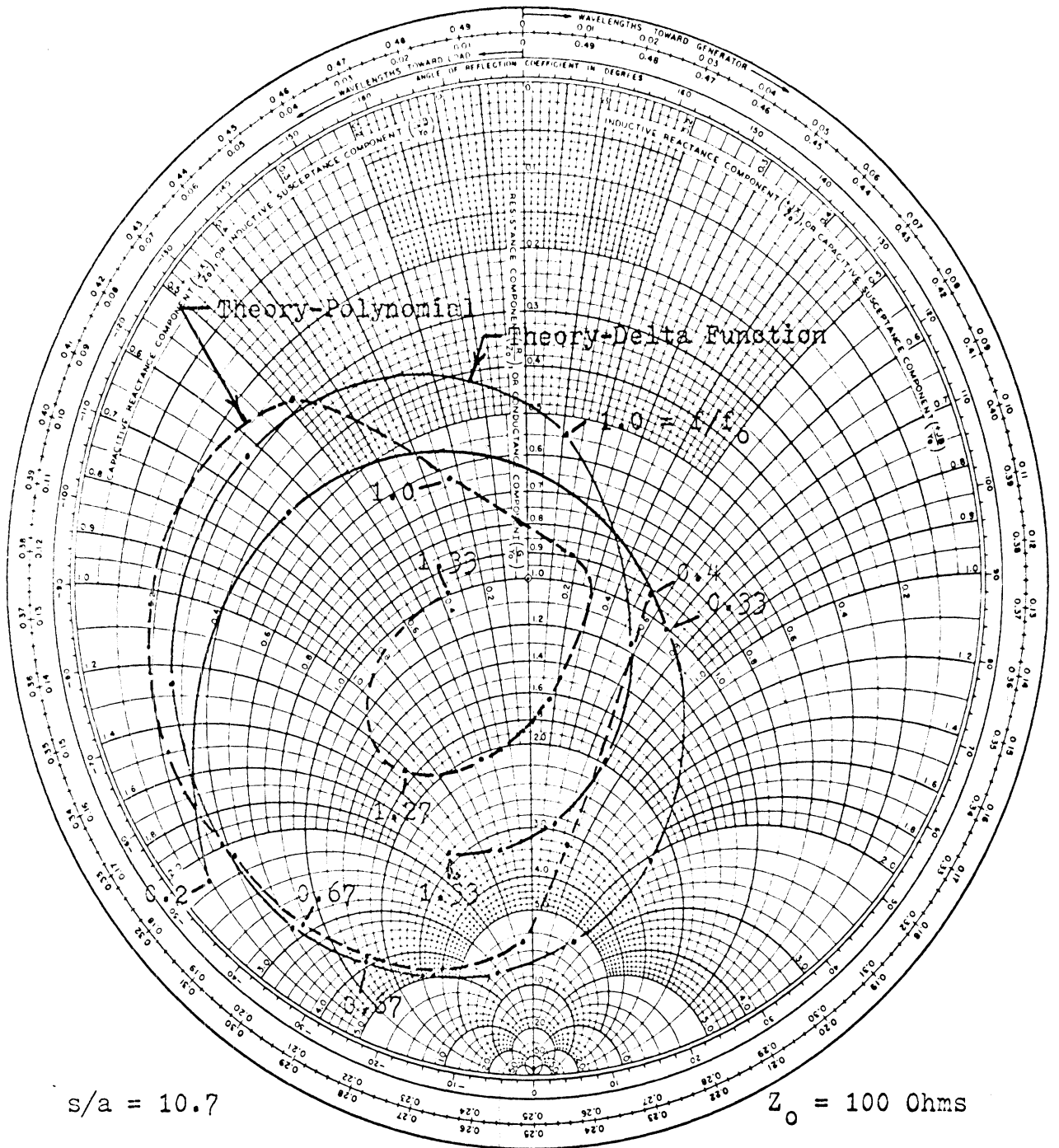


Figure 4-14: Input Impedance of a Franklin Antenna with
a 34.8 Ohm Transmission Line Trap

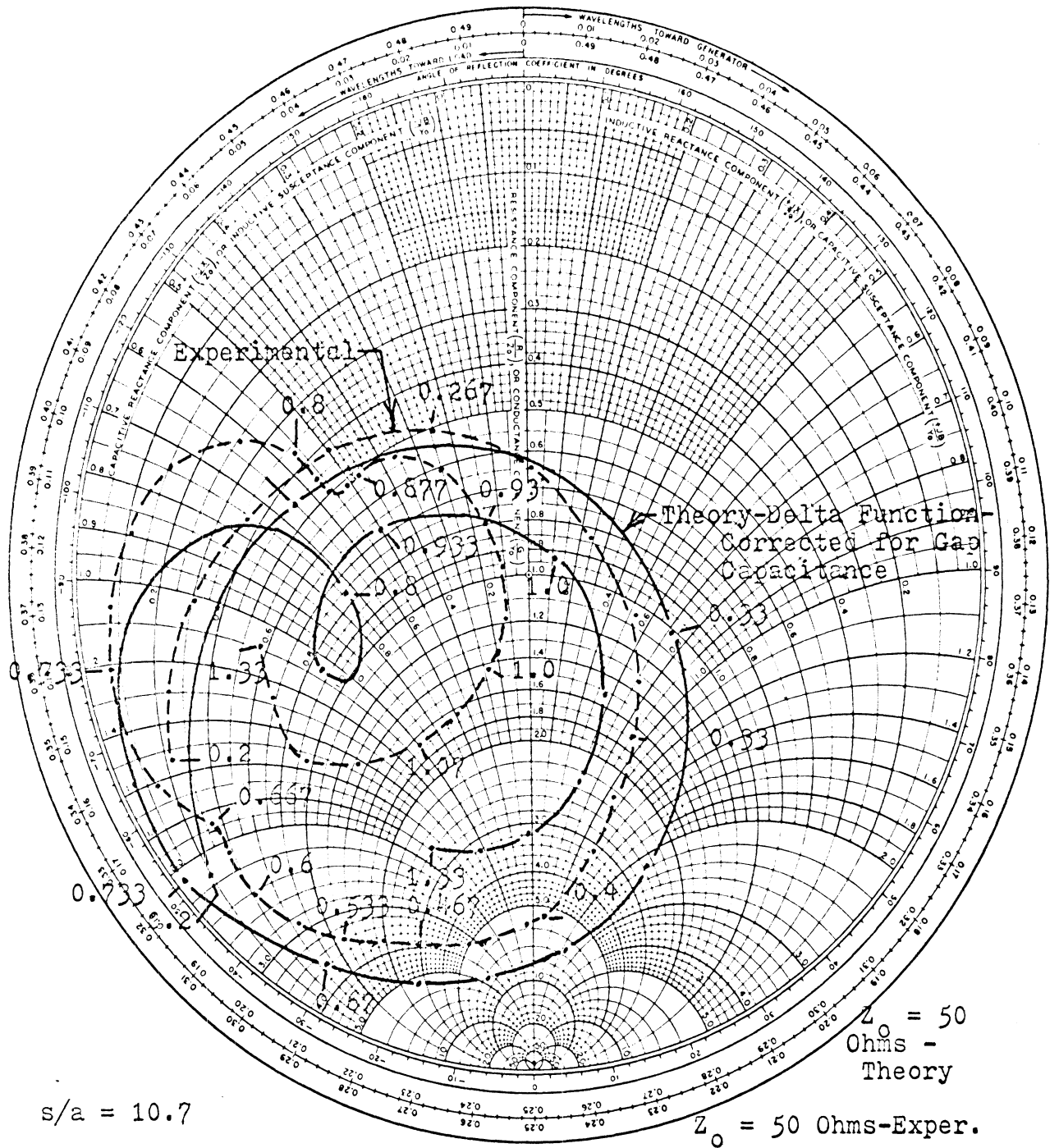


Figure 4-15: Input Impedance of a Franklin Antenna with a 34.8 Ohm Transmission Line Trap

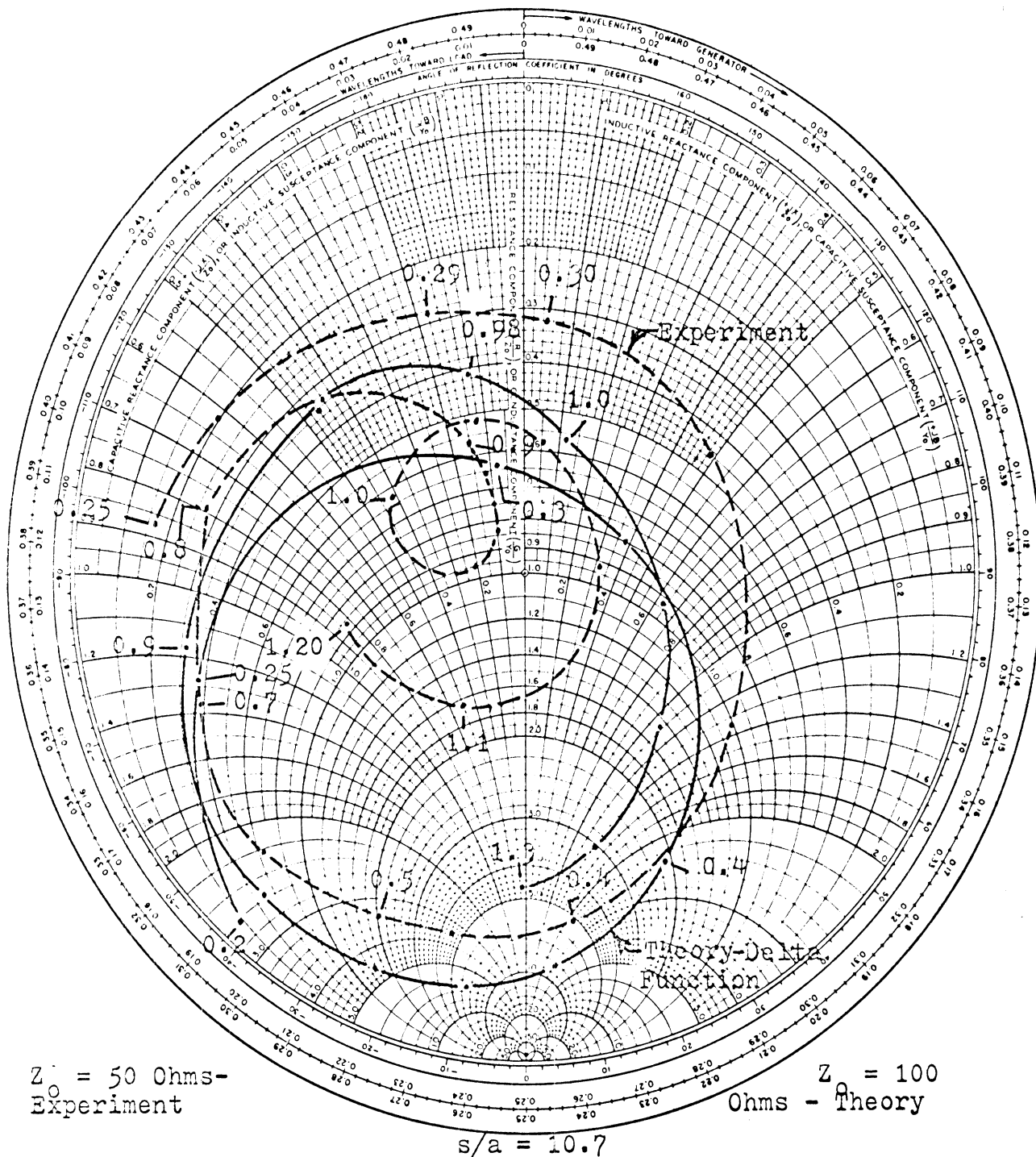


Figure 4-16: Input Impedance of a Franklin Antenna with a 53 Ohm L-C Trap

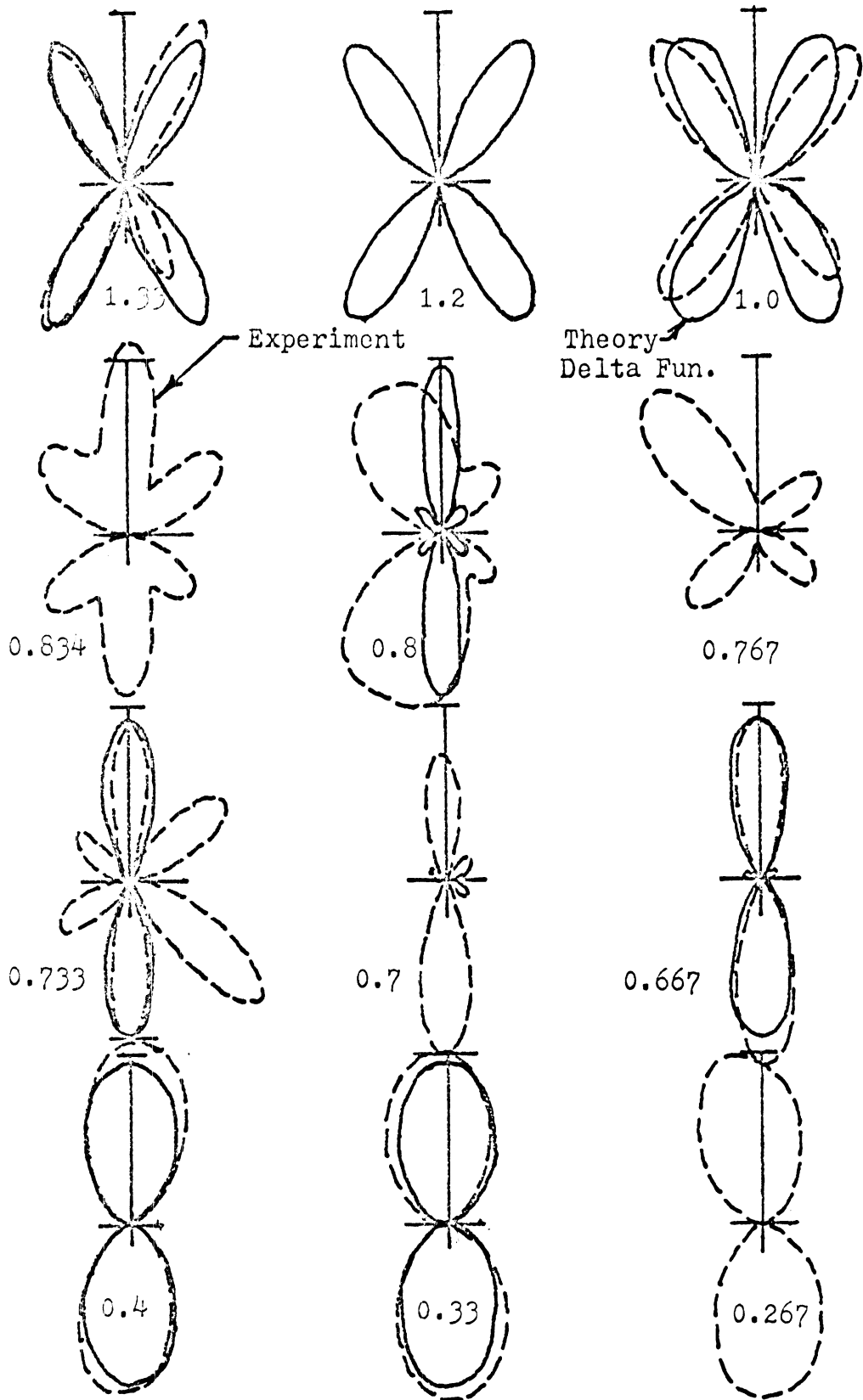


Figure 4-17: Linear Power Radiation Patterns of a Franklin Antenna as a Function of Frequency Normalized to the Anti-Resonant Frequency of the Trap ($s/a=10.7$)

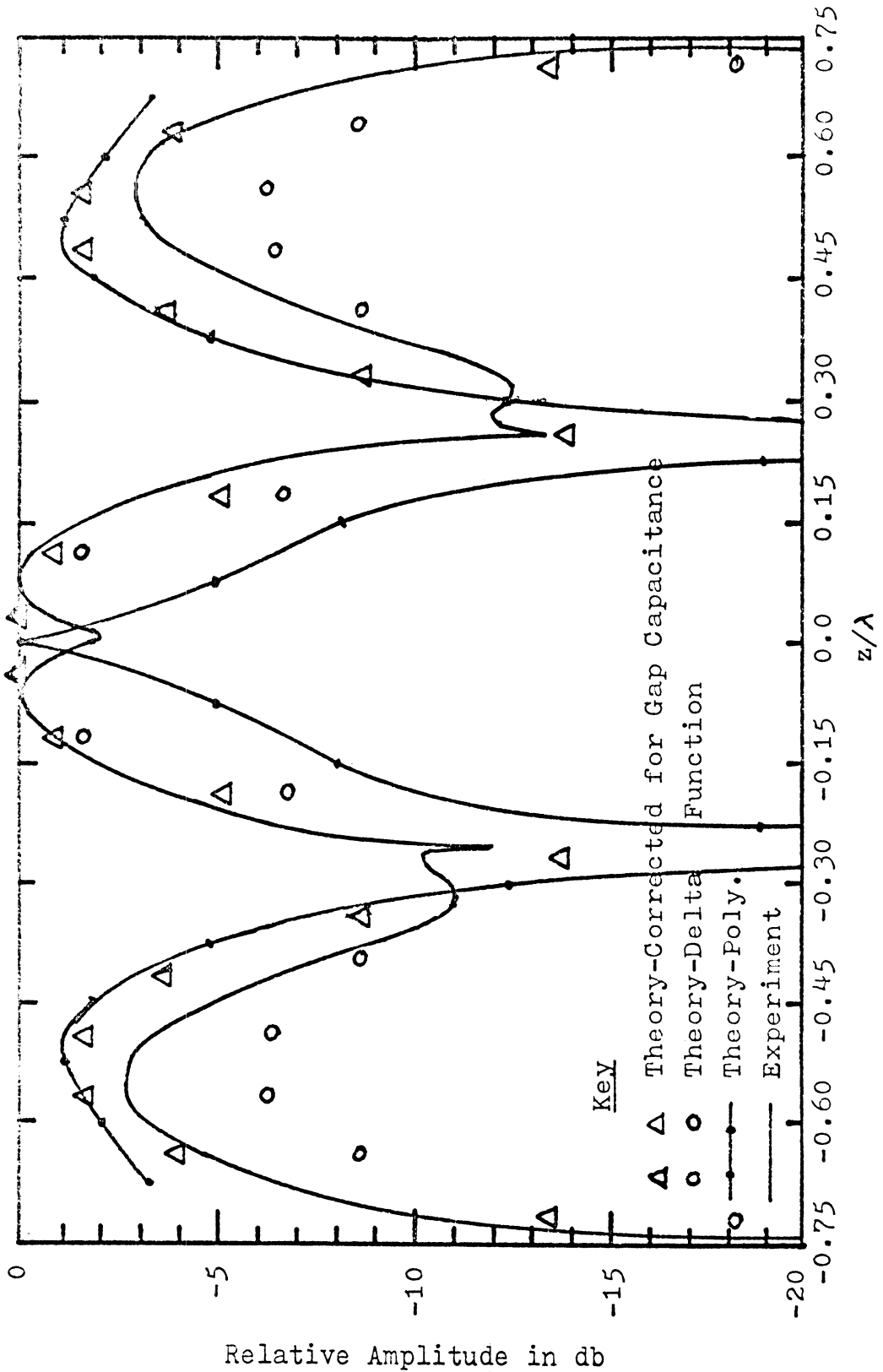


Figure 4-18: Amplitude of the Current Distribution on a Franklin Antenna at the Anti-Resonant Frequency of the Trap

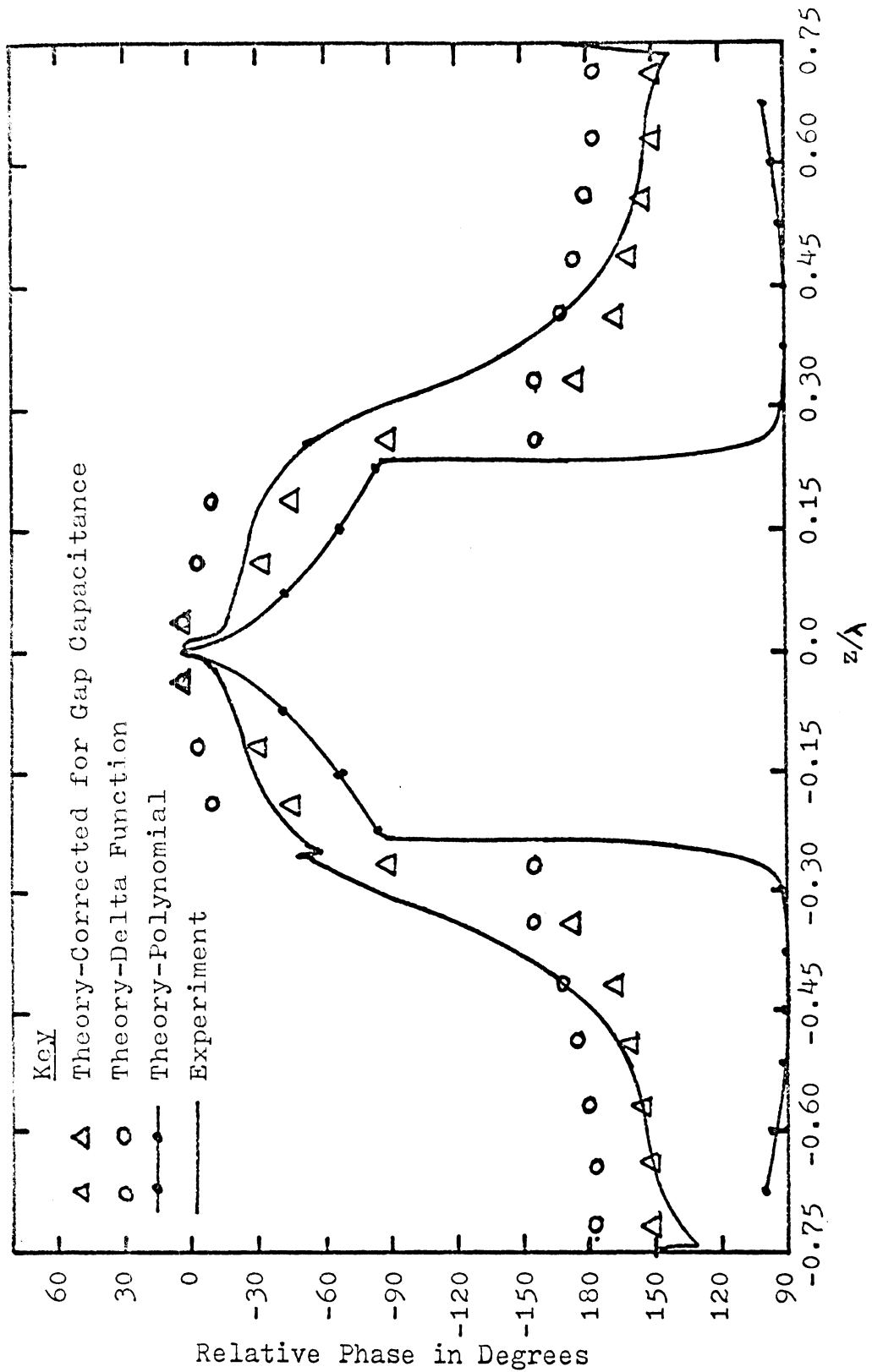


Figure 4-19: Phase of the Current Distribution on a Franklin Antenna at the Anti-Resonant Frequency of the Trap

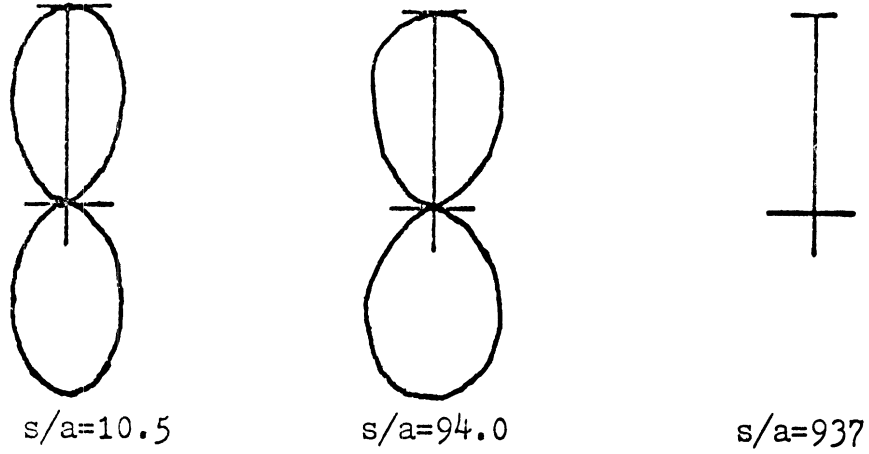


Figure 4-20: Linear Power Radiation Patterns of a Trap Antenna When the Trap is Anti-Resonant (Theory)

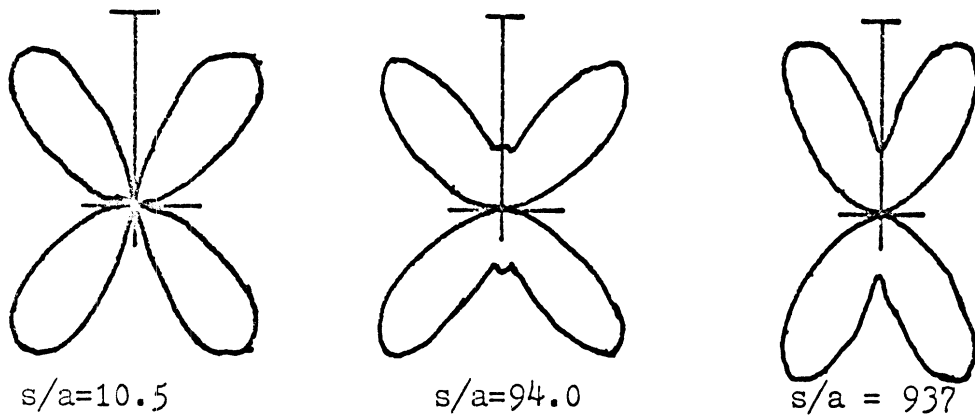


Figure 4-21: Linear Power Radiation Patterns of a Franklin Antenna When the Trap is Anti-Resonant (Theory)

a phenomenon that becomes more pronounced for larger antenna radii. As Figure 4-21 clearly illustrates, the radiation pattern of a Franklin antenna tends to become more broadside as the radius of the cylinder becomes smaller.

The Franklin antenna could be operated below the anti-resonant frequency of the trap to obtain the desired broadside pattern. However, this results in a highly capacitive, low resistive input impedance.

Another approach, as Figure 4-22 illustrates, is to shorten the length, L , and the trap location, s , by the same amount. The pattern with maximum directivity is produced near $L = 0.6375 \lambda_0$, where λ_0 is the wave length of the anti-resonant frequency of the trap. The effect this has on the input impedance is illustrated in Figure 4-23. Note that the input impedance still becomes capacitive, but not nearly as much as would be obtained by operating a Franklin antenna below the anti-resonant frequency of the trap. Furthermore, the input impedance has a higher resistive component.

Several other trap-loaded cylindrical antennas were studied. These antennas had outer section lengths intermediate to the trap and Franklin antennas, different inner section lengths, different diameters, different trap characteristic impedances and different trap or feed gaps. The remaining figures in this chapter summarize how these parameters affected the trap-loaded cylindrical

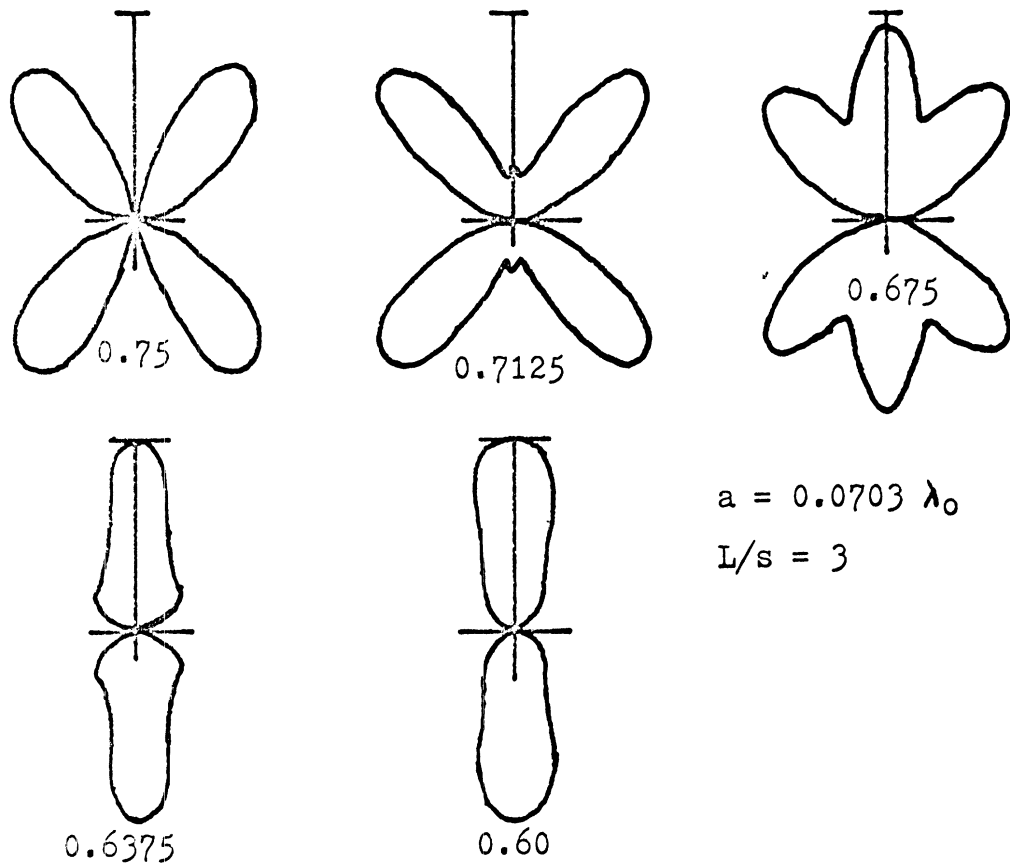


Figure 4-22: Linear Power Radiation Patterns of a Franklin-Like Trap-Loaded Cylindrical Antenna as a Function of Length When the Trap is Anti-Resonant (Theory)

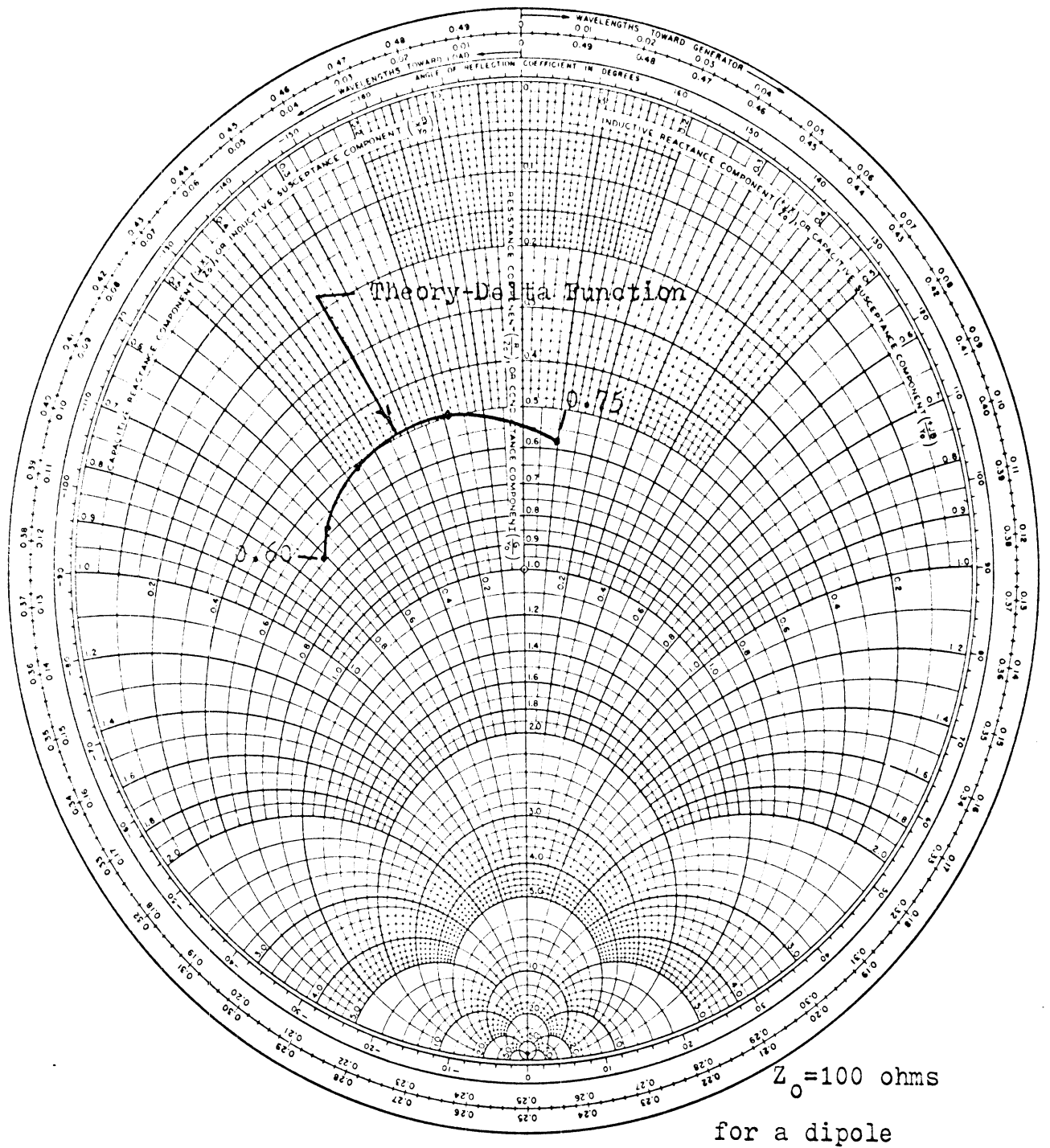


Figure 4-23: Input Impedance for a Franklin Antenna as a Function of L/λ_0 . Where the Trap is Anti-Resonant (Theory) "

antenna's performance.

In these figures, the resonant frequencies were taken to be the first and third crossings of the real axis by the impedance curve as frequency was increased. If the curve was too capacitive to cross the real axis a third and fourth time, the point where it came closest to the real axis was considered the resonant frequency.

Plots of the input impedances from which the summary plots were derived are included in Appendix A. Selected radiation patterns are included in Appendix B and some interesting current distributions are included in Appendix C.

Figure 4-24 shows how the first two resonant frequencies of a 34.8 ohm transmission line trap-loaded cylindrical antenna vary as a function of the length of the antenna, L , while the length of the inner section, s , is held constant. The antenna length, L , is normalized to λ_0 , the wave length in free space corresponding to the frequency, f_0 , where the trap is anti-resonant. The data were measured on a series of copper tubing antennas with a 34.8 ohm characteristic impedance transmission line trap.

The discrepancy between theory and experiment for the upper resonant frequency is due to the detuning effect of the trap gap capacitance. Modifying the theoretical solution to account for the trap gap capacitance affects only the second resonant frequency, not the first. Hence close agreement between theory and experiment exists for the first resonant frequency.

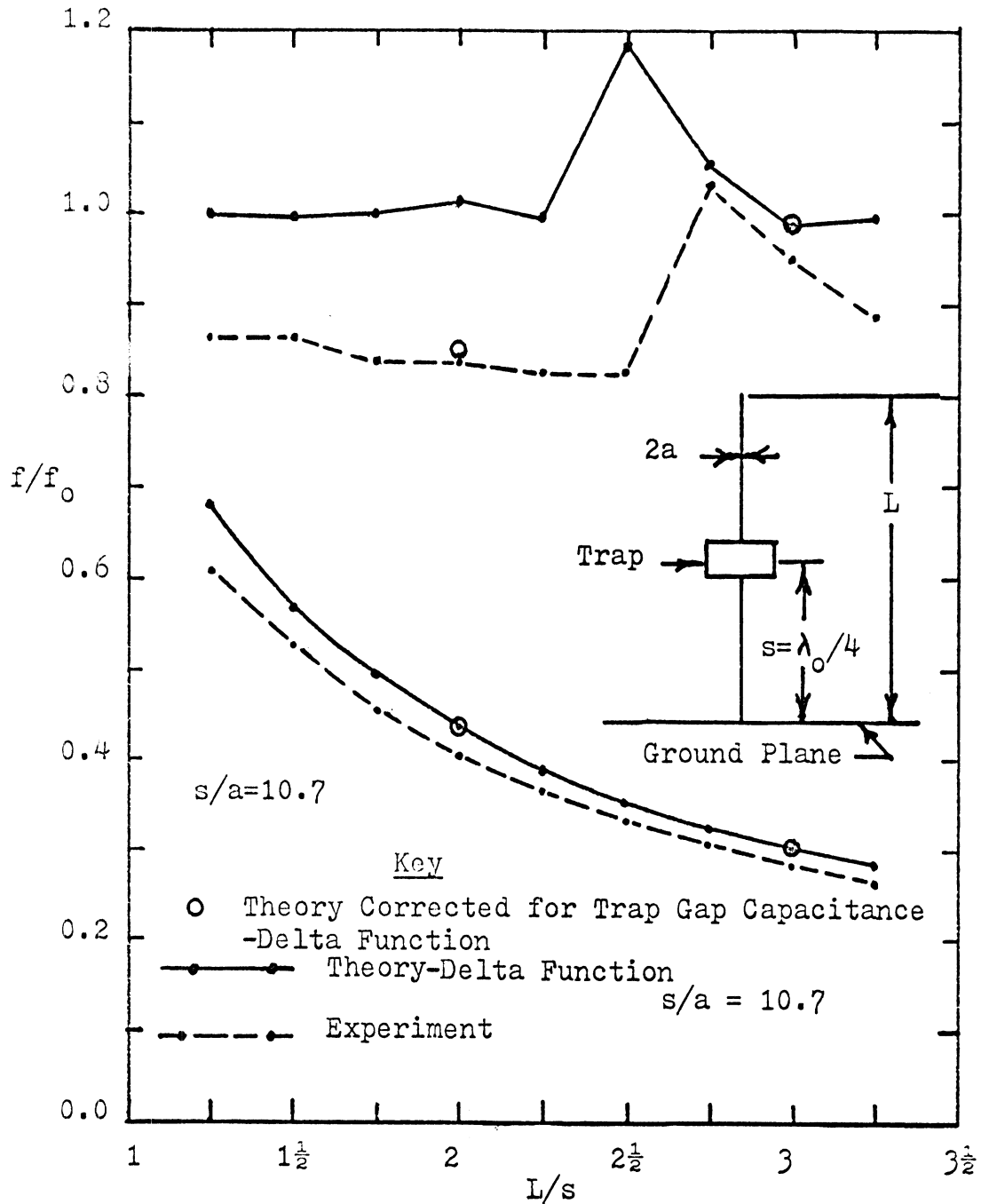


Figure 4-24: The First Two Resonant Frequencies of a Trap-Loaded Cylindrical Antenna as a Function of the Length of the Outer Arm (f_0 Is The Anti-Resonant Frequency of the Trap)

Note that the second resonant frequency remains practically constant as a function of the length of the outer section, except for L/s in the vicinity of $2\frac{1}{2}$. Since the first resonant frequency seems to vary somewhat linearly with respect to the length of the outer section, the length of the outer section can be adjusted to tune the lower frequency without greatly affecting the second resonance.

Figure 4-25 shows how the first two resonant frequencies of a 34.8 ohm transmission line trap-loaded cylindrical antenna vary as the length of the inner section, s , varies while the length of the outer section, $(L - s)$, remains constant. Both the first and second resonant frequencies seem to vary linearly with the length of the inner section. Hence, varying the length of the inner section does not seem to provide any advantage in designing trap-loaded cylindrical antennas. Note also that when the trap gap capacitance is taken into account in the theory, it agrees well with experiment.

Figure 4-26 illustrates how the first two resonant frequencies of a transmission line trap antenna vary as a function of the characteristic impedance of the trap. Note that the second resonant frequency remains essentially constant as a function of the characteristic impedance of the trap, while the lower frequency seems to vary linearly as a function of the trap characteristic impedance. Hence the characteristic impedance of a transmission line trap, or the inductance-capacitance ratio of an inductor-capacitor

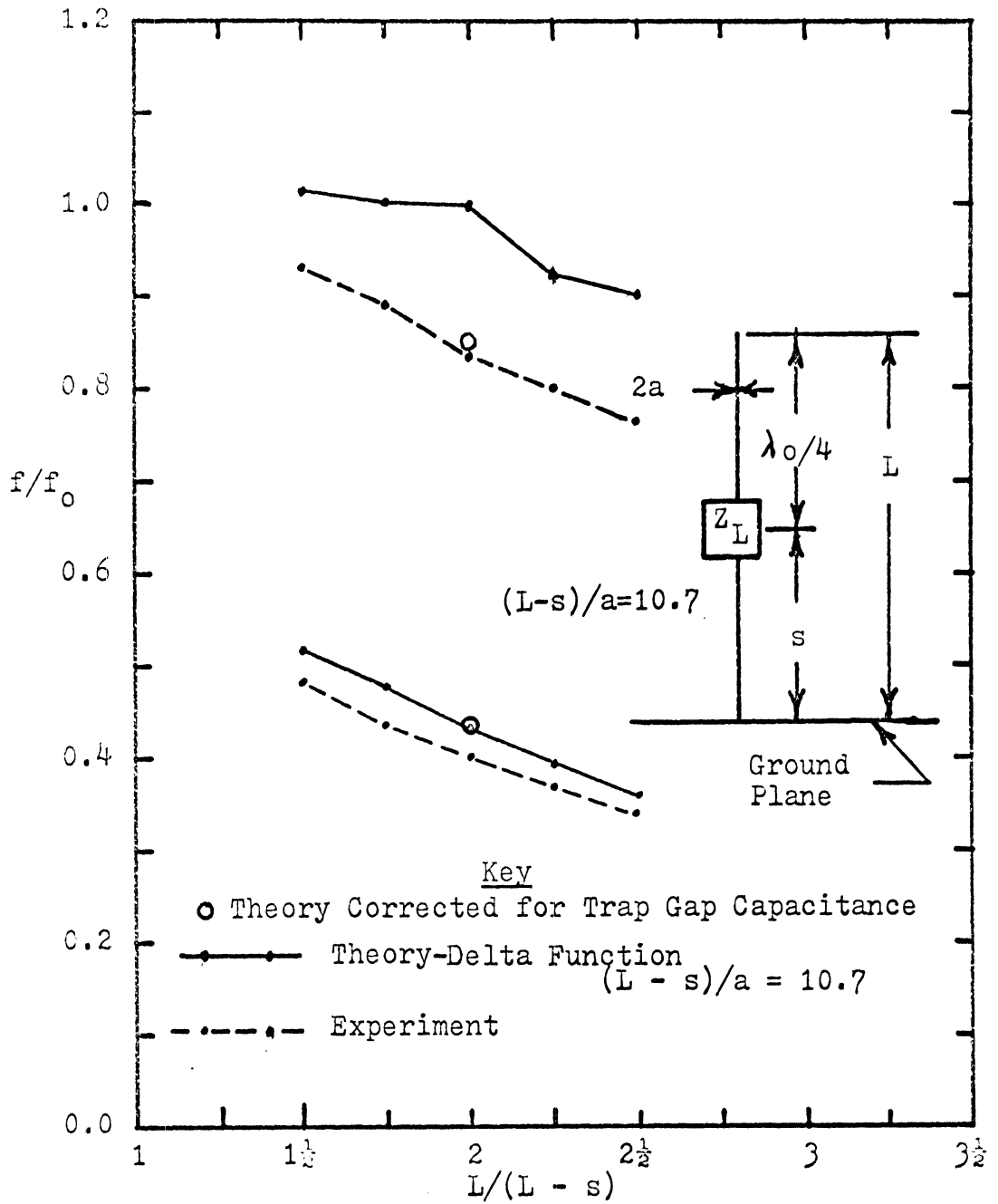


Figure 4-25: The First Two Resonant Frequencies of a Trap-Loaded Cylindrical Antenna as a Function of the Length of the Inner Arm (f_0 Is the Anti-Resonant Frequency of the Trap)

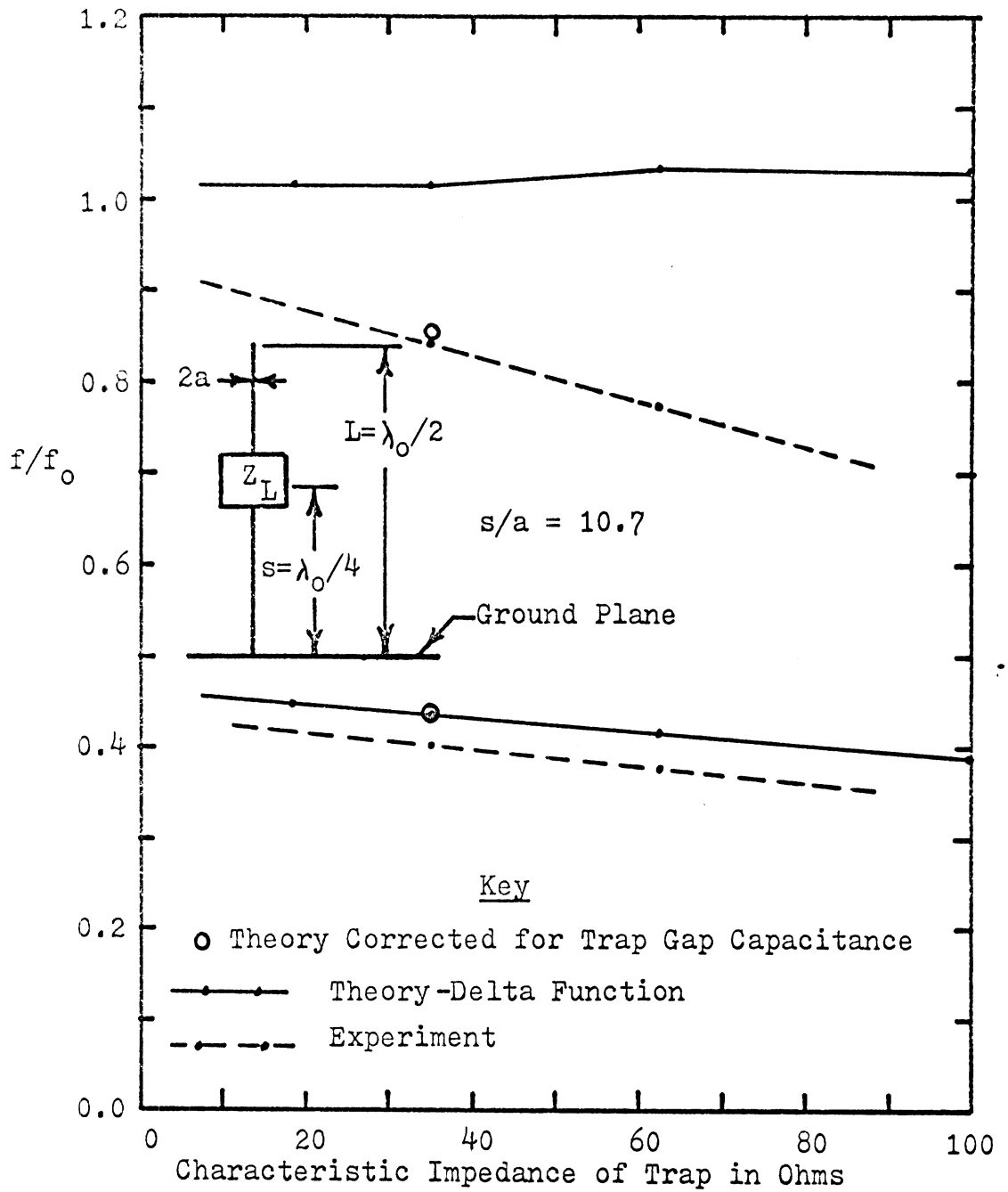


Figure 4-26: The First Two Resonant Frequencies of a Trap-Loaded Cylindrical Antenna as a Function of the Characteristic Impedance of the Trap (f_0 Is the Anti-Resonant Frequency of the Trap)

trap, can be used as a parameter to adjust the first resonant frequency of a trap-loaded cylindrical antenna.

To make this data universally applicable to both transmission line and inductor-capacitor traps, the first resonant frequency has been replotted in Figure 4-27 as a function of the equivalent inductance of the trap at resonance. Also included in Figure 4-27 are data obtained from inductor-capacitor traps. Note that the agreement is very good between the data from both types of trap-loaded antennas.

Figures 4-28 and 4-29 show, respectively, how the first two resonant frequencies vary as a function of the feed and trap gap for a 34.8 ohm transmission line trap antenna. The gap widths were increased by adding additional washers on the assumption that the resulting increase in the total length of the antenna would be negligible. The effect on the second resonance of the trap width is most noticeable and due to the detuning effect of the trap gap capacitance. The effect of the trap gap on the first resonance is minimal. Furthermore, the effect of the feed gap on both resonances is also minimal and appears to be due to the slight lengthening of the antenna.

All of the design information presented so far (except Figure 4-27) is based on transmission line traps and rather thick antennas. As Figures 4-30 and 4-31 show, the resonant frequencies are not very sensitive to the monopole length to radius ratio, L/a . These data are based on the

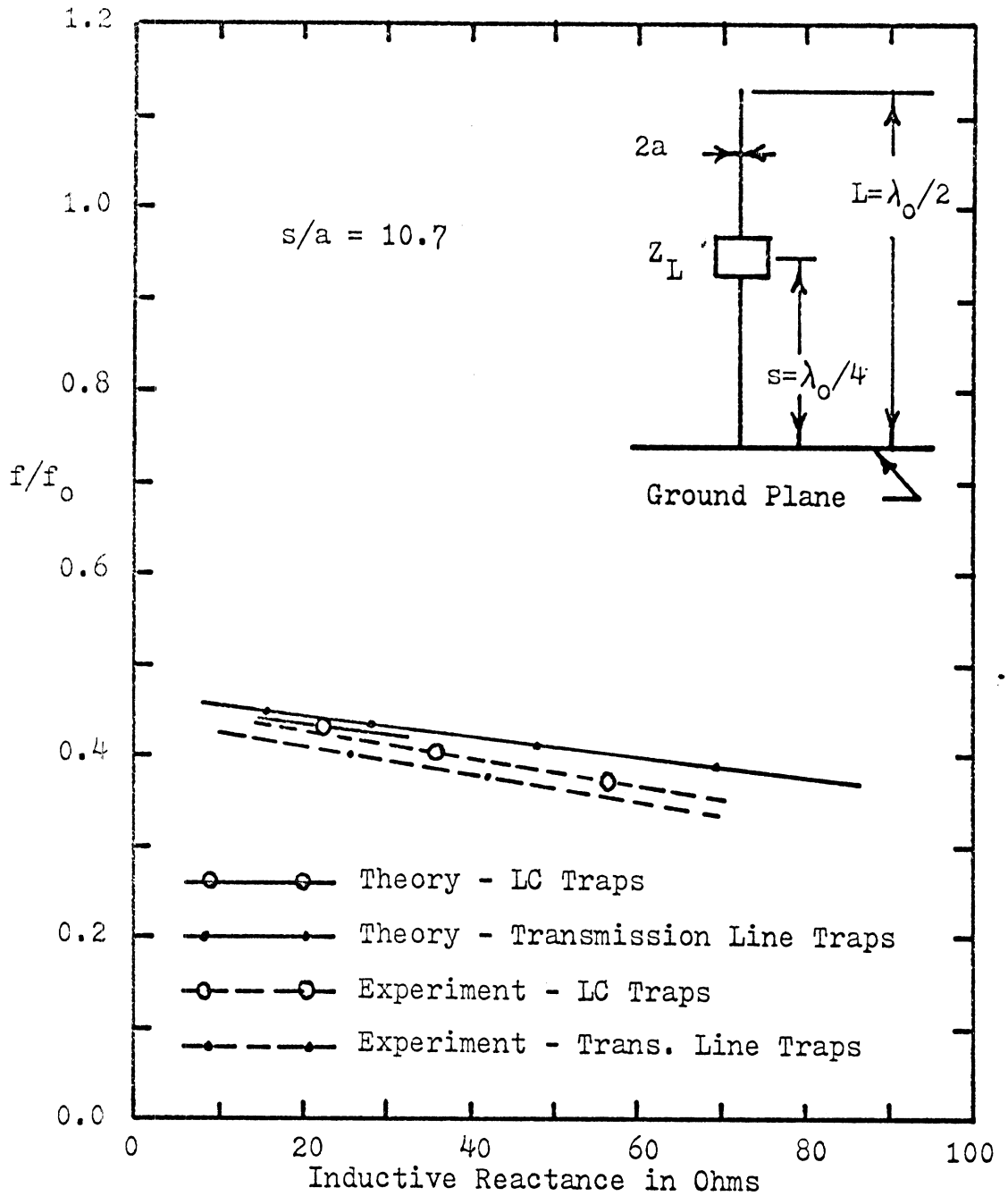


Figure 4-27: The First Resonant Frequency of a Trap Antenna as a Function of the Inductive Reactance of the Trap (f_0 Is the Anti-Resonant Frequency of the Trap)

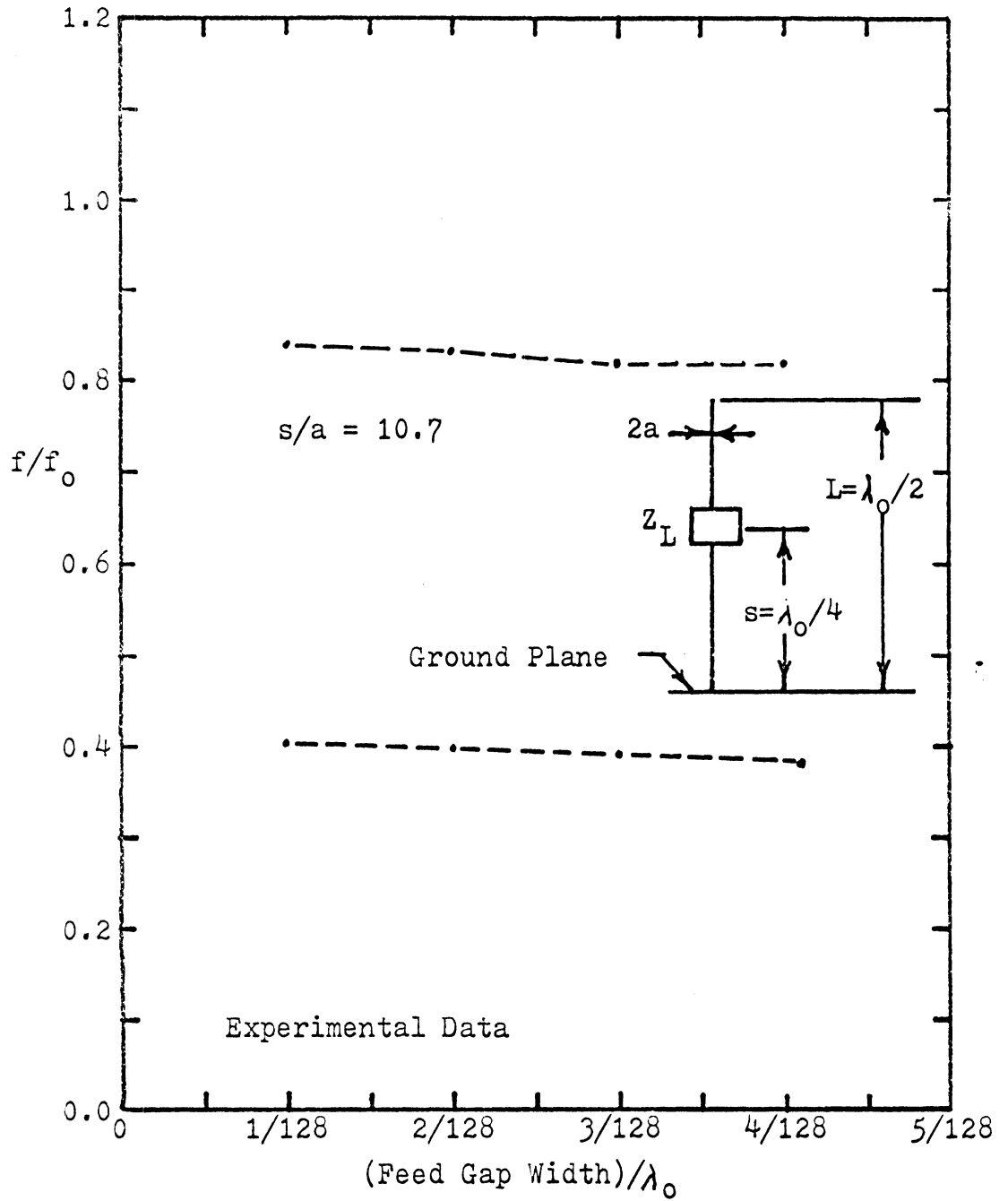


Figure 4-28: The First Two Resonant Frequencies of a Trap Antenna as a Function of the Feed Gap Width (f_0 is the Anti-Resonant Frequency of the Trap)

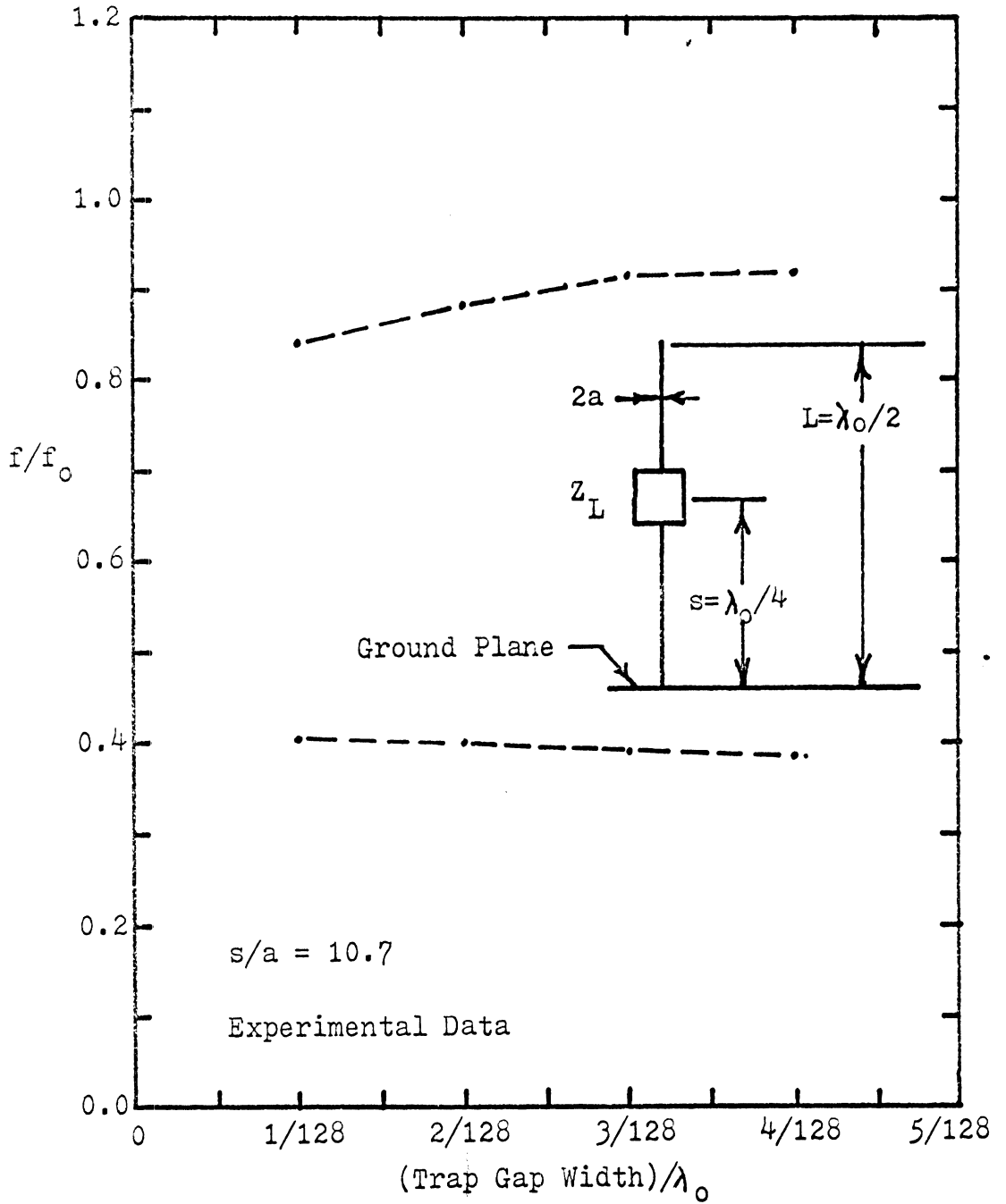


Figure 4- 29: The First Two Resonant Frequencies of a Trap Antenna as a Function of the Trap Gap Width (f_0 is the Anti-Resonant Frequency of the Trap)

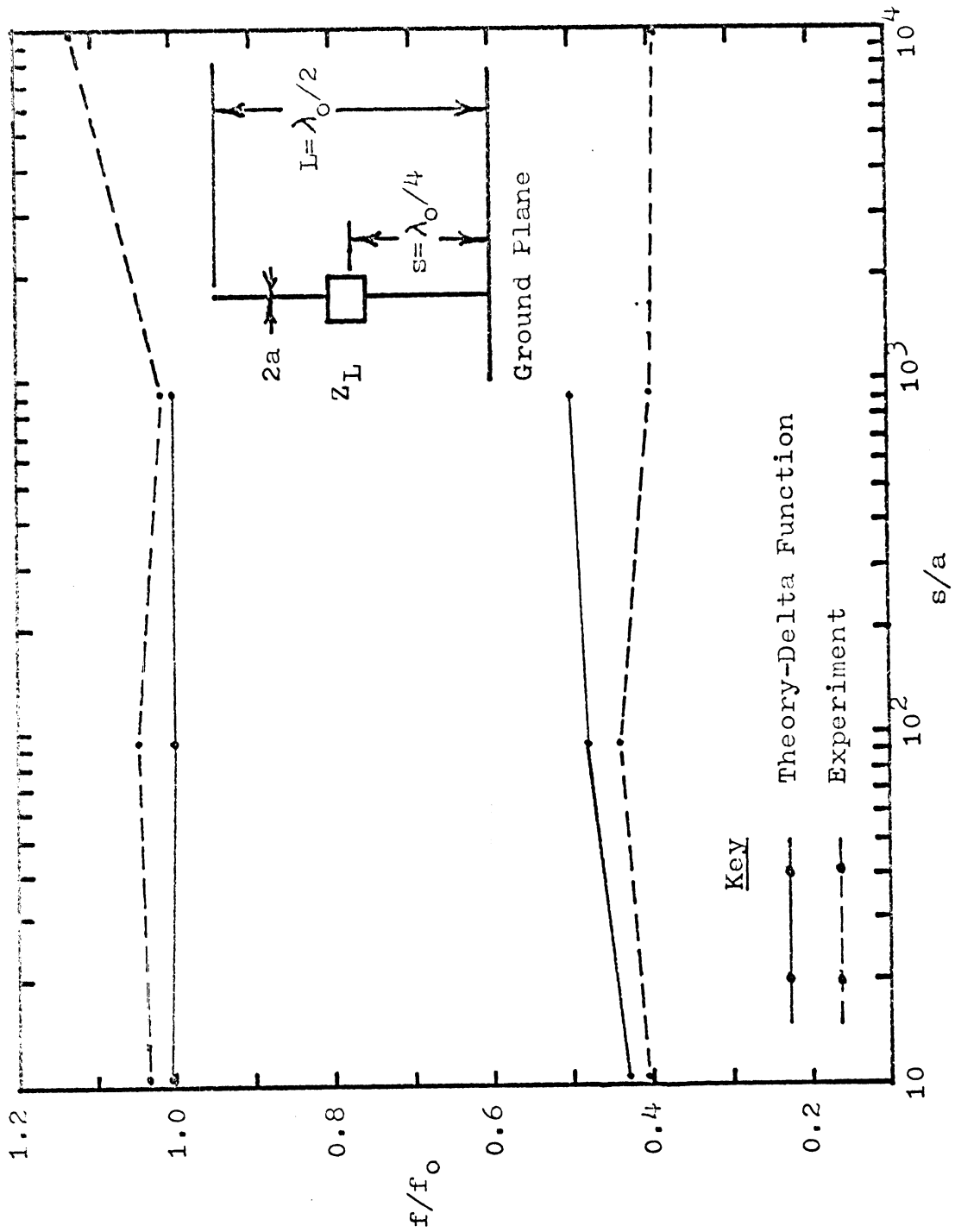


Figure 4-30: The First Two Resonant Frequencies of a Trap Antenna as a Function of the Antenna Radius (f_0 is the Anti-Resonant Frequency of the Trap)

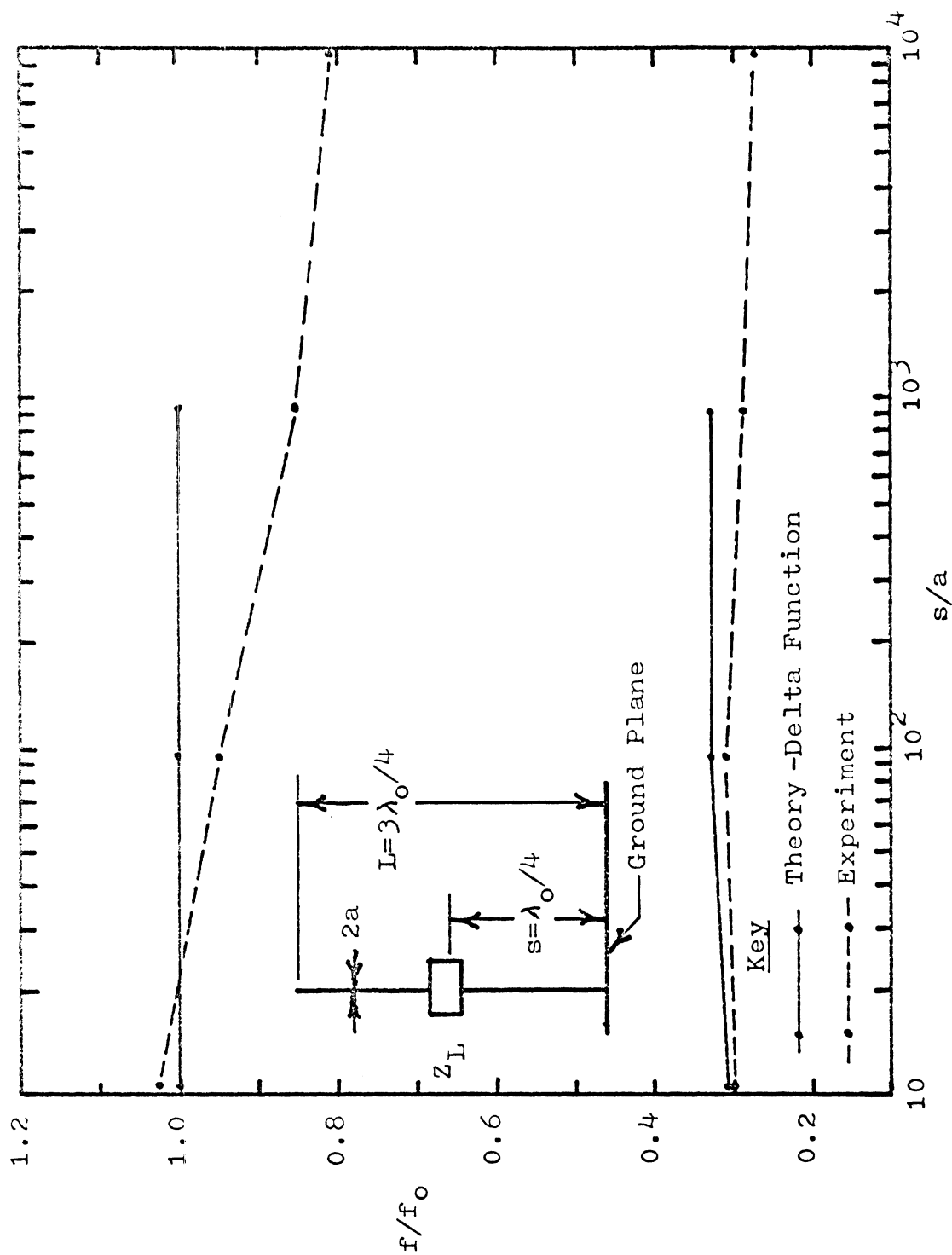


Figure 4-31: The First Two Resonant Frequencies of a Franklin Antenna as a Function of the Antenna Radius (f_0 is the Anti-Resonant Frequency of the Trap)

2x4 series of antennas and lumped inductor-capacitor traps. The lack of theoretical data for $s/a = 9.84 \times 10^3$ is a result of the high Q of the antenna. Off resonance, the input impedance is very highly reactive and would show up as infinity on an impedance chart. Near resonance, the matrix equation is close to being singular and cannot be solved numerically.

As can be seen from the figures, the second resonant frequency is essentially independent of the antenna radius. The first resonant frequency, however, does seem to increase slightly as the radius decreases. Thus the design data available for $s/a = 10.7$ is generally applicable to trap-loaded cylindrical antennas thinner than this.

CONCLUSIONS

The following conclusions can be made about the trap antenna.

1) Greenberg's (1956) design procedure (adjusting the anti-resonant frequency of the trap to control the upper resonant frequency of the antenna and adjusting the length of the outer section to control the lower resonant frequency) is indeed valid even though not confirmed in the original paper. The information in Figure 4-24 was not in Greenberg's paper and should prove useful when using his procedure.

2) In addition, the inductance-capacitance ratio of an inductor-capacitor trap, or the characteristic impedance of a transmission line trap, can also be used to control the first antenna resonant frequency. Figure 4-27 should prove useful in designing trap antennas using this technique.

3) Varying the length of the inner section gives no design advantage since both the first and the second resonant frequencies are altered. Figure 4-25 illustrates this relationship.

4) Data taken for antennas with $s/a=10.7$ are generally applicable to thinner antennas, as Figures 4-30 and 4-31 illustrate.

5) Radiation patterns similar to those of a half-wave dipole are obtainable at the second resonant frequency for $1\frac{1}{2} \leq L/s \leq 2\frac{1}{2}$. Figure B-1 illustrates the radiation patterns and Figure 4-24 illustrates the location of the

second resonant frequency.

6) The trap does indeed tend to suppress the current on the outer section of the antenna at the anti-resonant frequency of the trap. Figure 4-12 illustrates this phenomenon.

The following conclusions can be made about the Franklin antenna.

1) The Franklin antenna must be operated somewhat below the nominal design frequency (Figure 4-17) or the lengths of the sections must be shortened somewhat (Figure 4-22) to obtain a radiation pattern similar to a colinear array-like radiation pattern.

2) When the antenna is adjusted to give a colinear array-like radiation pattern, the input impedance has low resistive and highly capacitive reactive components as Figures 4-14, 4-15 and 4-23 illustrate.

3) The thicker the antenna, the more the radiation pattern at the nominal design frequency deviates from the desired pattern (Figure 4-21).

4) As Figure 4-18 illustrates, the current magnitude distribution at the nominal design frequency is similar to a colinear array of half-wave dipoles, although the maximum of the current on the outer sections is 1 or 2 dB down from the maximum in the center section. However, Figure 4-19 clearly illustrates that the traps do not give the desired phase reversal.

REFERENCES

- Altshuler, Edward (1961), "The Traveling-Wave Linear Antenna," IRE Trans. AP-9, n. 4, pp. 324-329.
- ARRL (1968), The A. R. R. L. Antenna Book, 11th Ed., The American Radio Relay League, Newington, Conn.
- Bell, Wesley M. (1963), "A Trap Collinear Antenna," QST v. 47 n. 8 pp. 30-31.
- Carnahan, Brice and James O. Wilkes (1968), Introduction to Algorithms and Numerical Methods, The University of Michigan, Ann Arbor.
- Greenberg, Arthur (1956), "Simple Trap Construction for the Multiband Antenna," QST v. 40 n. 10 pp. 18-19, 120.
- Harrington, Roger F. (1967), "Matrix Methods for Field Problems," Proc. of IEEE v. 55 n. 2 pp. 136-149.
- Harrington, Roger F. (1968), Field Computation by Moment Methods, Macmillan, New York.
- Harrison, Charles W., Clayborne D. Taylor, Edward E. O' Donnell, Eugene A. Aronson (1967), "On Digital Computer Solutions of Fredholm Integral Equations of the First and Second Kind Occurring in Antenna Theory," Radio Science v. 2 n. 9 pp. 213-220.
- Hickman, C. E., F. W. Stallman, J. D. Tillman (1966), "Gaussian Quadrature Solution of Integral Equation for the Current Distribution and Terminal Impedance of a Cylindrical Antenna," IEEE International Antenna and Propagation Symposium Digest, pp. 213-220.
- Jasik, Henry, Ed. (1961), Antenna Engineering Handbook, McGraw-Hill, New York.
- King, Ronold W. P. (1967), "The Linear Antenna -- Eighty Years of Progress," Proc. of IEEE v. 55 n. 1 pp. 2-16.
- Lin, C.J., D.P. Nyquist, K. M. Chen (1970), "Short Cylindrical Antennas with Enhanced Radiation of High Directivity," IEEE Trans. AP-18 n. 4 pp. 576-580.
- Liu, Yu-Ping and Dipak L. Sengupta (1971), "Resistively Loaded Linear Antenna: Current Distribution and Far Field," University of Michigan Radiation Laboratory Memo 004940-507-M. A more available reference is: Yu-Ping Liu, Dipak L. Sengupta and Chen-To Tai, "Numerical Investigation of Wave Forms Radiated by a

Pulse Excited Resistively Loaded Linear Antenna,"
University of Michigan Radiation Laboratory Report
RL-545.

Mei, K. K. (1965), "On the Integral Equations of Thin
Wire Antennas," IEEE Trans. AP-13 n. 3 pp. 374-378.

Popovic, B. D. (1970), "Polynomial Approximation of Current
Along Thin Symmetrical Cylindrical Dipoles," Proc. IEE
v. 117 n. 5 pp. 873-878.

Richmond, Jack H. (1965), "Digital Computer Solutions of
Rigorous Equations for Scattering Problems," Proc. of
IEEE v. 53 n. 8 pp. 796-804.

Schelkunoff, Sergi A. and Harald T. Friis (1952), Antennas
Theory and Practice, John Wiley and Sons, New York.

Shafer, David P. (1958), "Four-Band Dipole with Traps,"
QST v. 42 n. 10 pp. 38-40.

Ullman, Nelly and Robert Ullman (1966), "Numerical Solutions
of Singular Fredholm Equations," Jour. of Math. Phy.
v. 7 n. 9 pp. 1743-1748.

Van Bladel, J. (1964), Electromagnetic Fields, McGraw-Hill,
New York.

Westman, H. P. Ed. (1964), Reference Data for Radio Engineers,
International Telephone and Telegraph Co., New York.

Williams, H. Paul (1950), Antenna Theory and Design, Sir
Isaac Pitman and Sons, London.

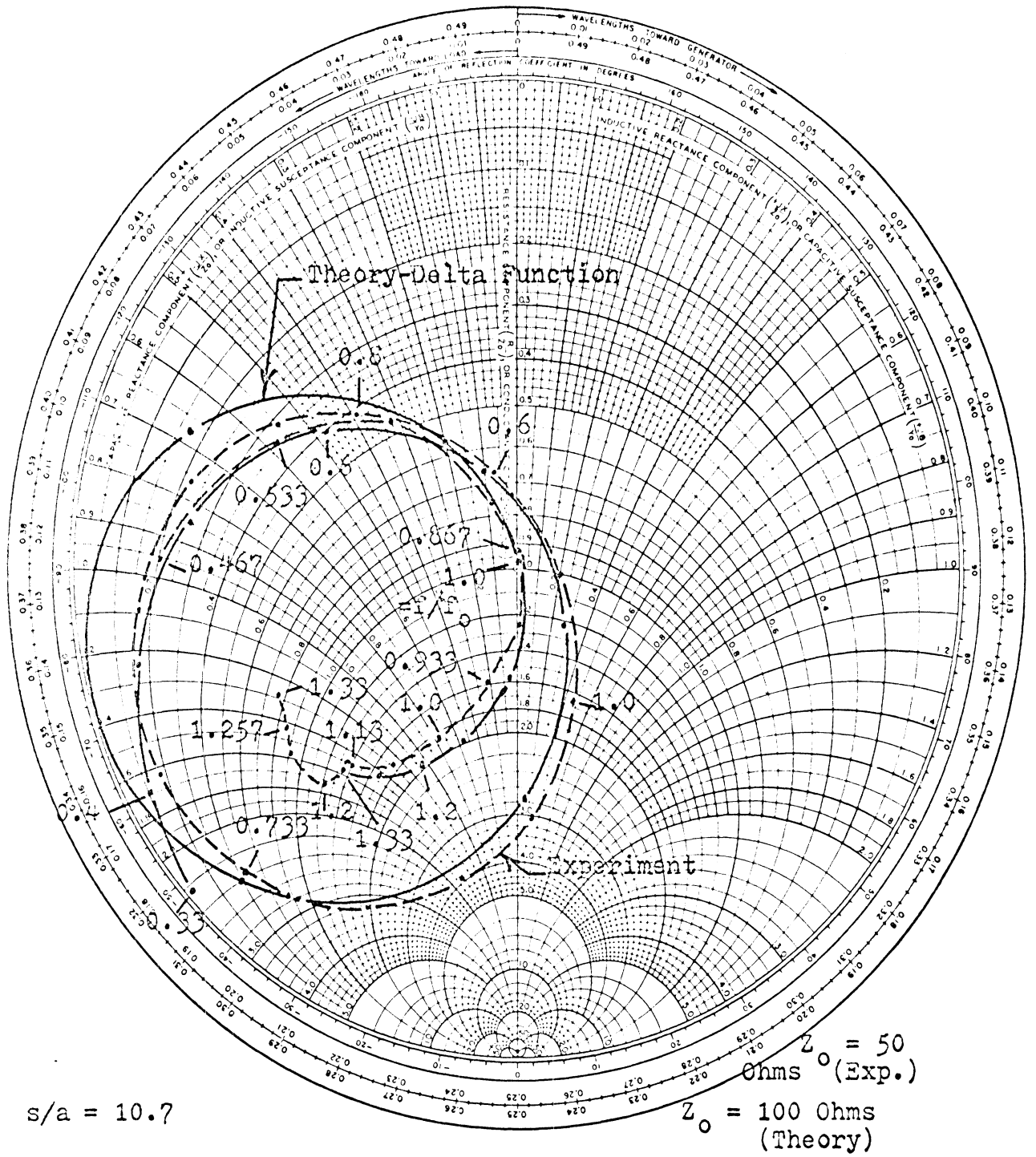
APPENDIX A

ADDITIONAL INPUT IMPEDANCE PLOTS

Figures A-1 through A-7 contain the impedance plots that resulted from the study of how the length of the outer section affected the impedance of a trap-loaded cylindrical antenna. Figures A-8 through A-11 contain the plots that resulted from varying the length of the inner section.

Figures A-12 through A-14 give the input impedance of several trap antennas of different diameters and Figures A-15 through A-17 the input impedance of several Franklin antennas of different diameters all with 53 ohm inductor-capacitor traps. Figures A-18 and A-19 give two more trap antennas and Figures A-20 and A-21, two more Franklin antennas but this time with 88.5 ohm inductor-capacitor traps.

Figures A-22 through A-25 contain the input impedances of several trap antennas and Figures A-26 and A-27 the input impedances of two Franklin antennas all containing transmission line traps but with different characteristic impedances. Figures A-28 through A-30 give the results obtained by varying the feed gap width and Figures A-31 through A-33 the results obtained by varying the trap gap width of a trap antenna with a 34.8 ohm transmission line trap.



s/a = 10.7

Z_o = 50 Ohms (Exp.)

Z_o = 100 Ohms (Theory)

Figure A-1: Input Impedance of a Trap-Loaded Cylindrical Antenna with a 34.8 Ohm Transmission Line Trap, $L/s = 1\frac{1}{4}$, $s = \lambda_0/4$

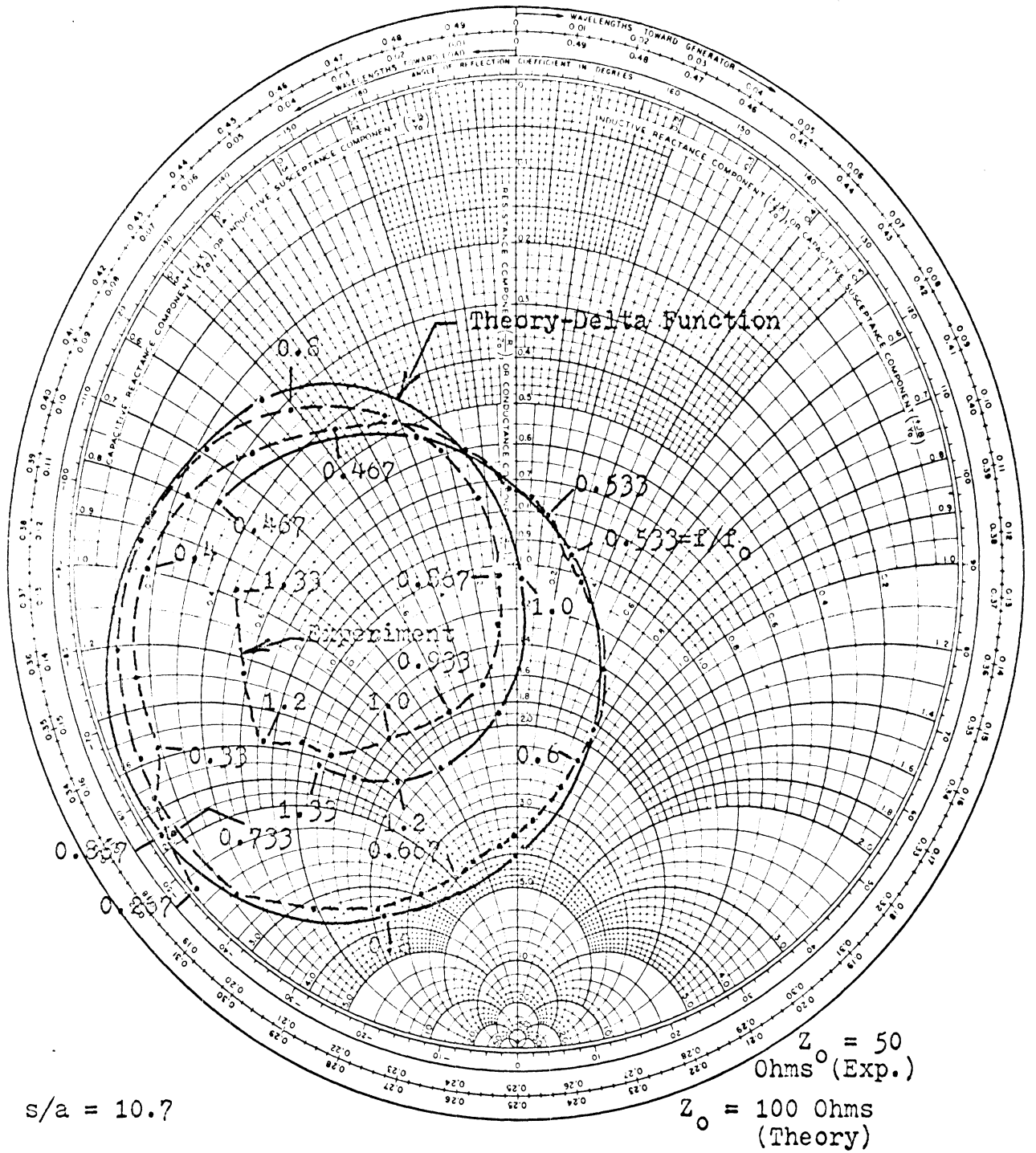
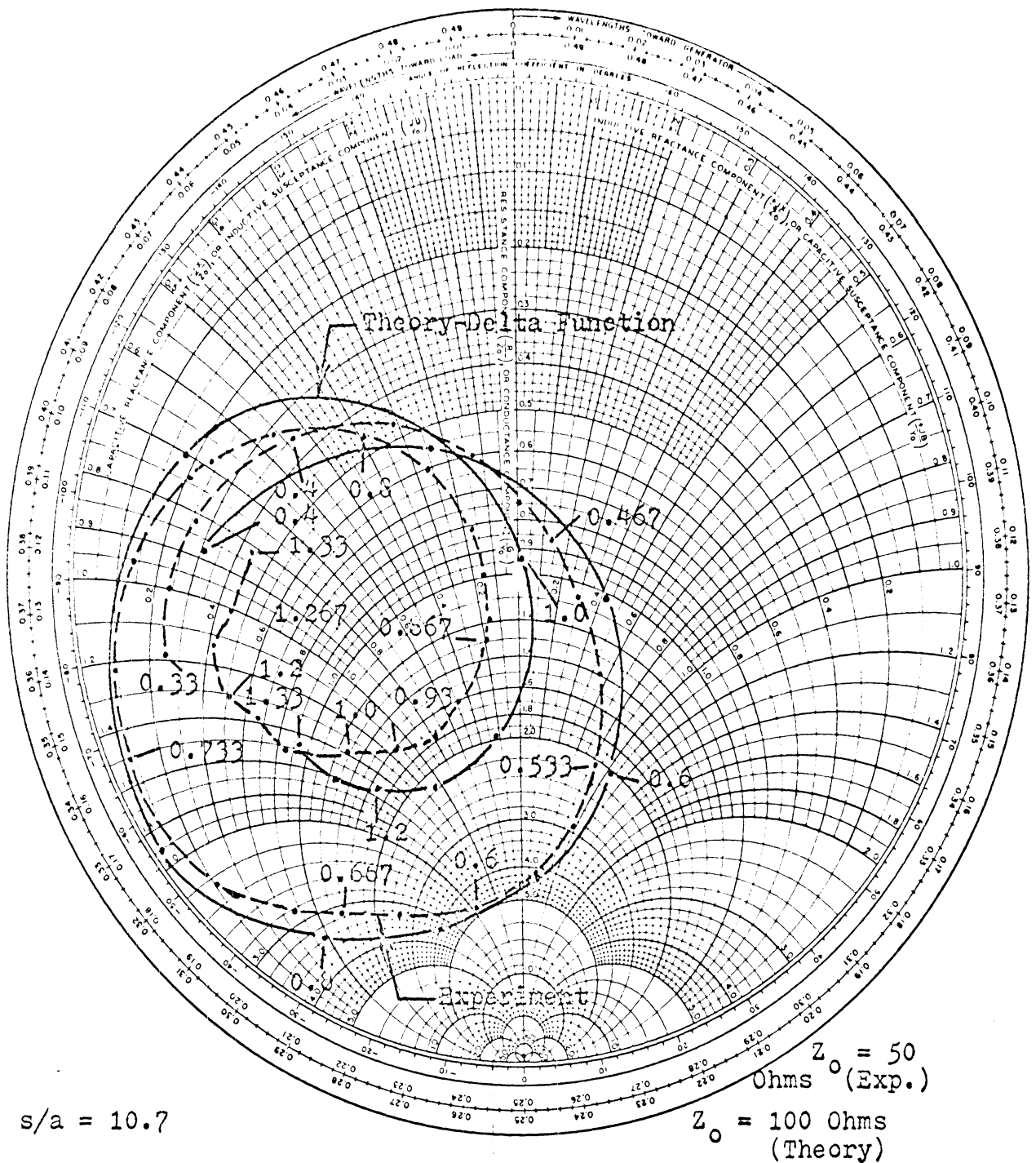


Figure A-2: Input Impedance of a Trap-Loaded Cylindrical Antenna with a 34.8 Ohm Transmission Line Trap, $L/s = 1\frac{1}{2}$, $s = \lambda_0/4$



$s/a = 10.7$

$Z_0 = 50$
Ohms (Exp.)
 $Z_0 = 100$ Ohms
(Theory)

Figure A-3: Input Impedance of a Trap-Loaded Cylindrical Antenna with a 34.8 Ohm Transmission Line Trap, $L/s = 1-3/4$, $s = \lambda_0/4$

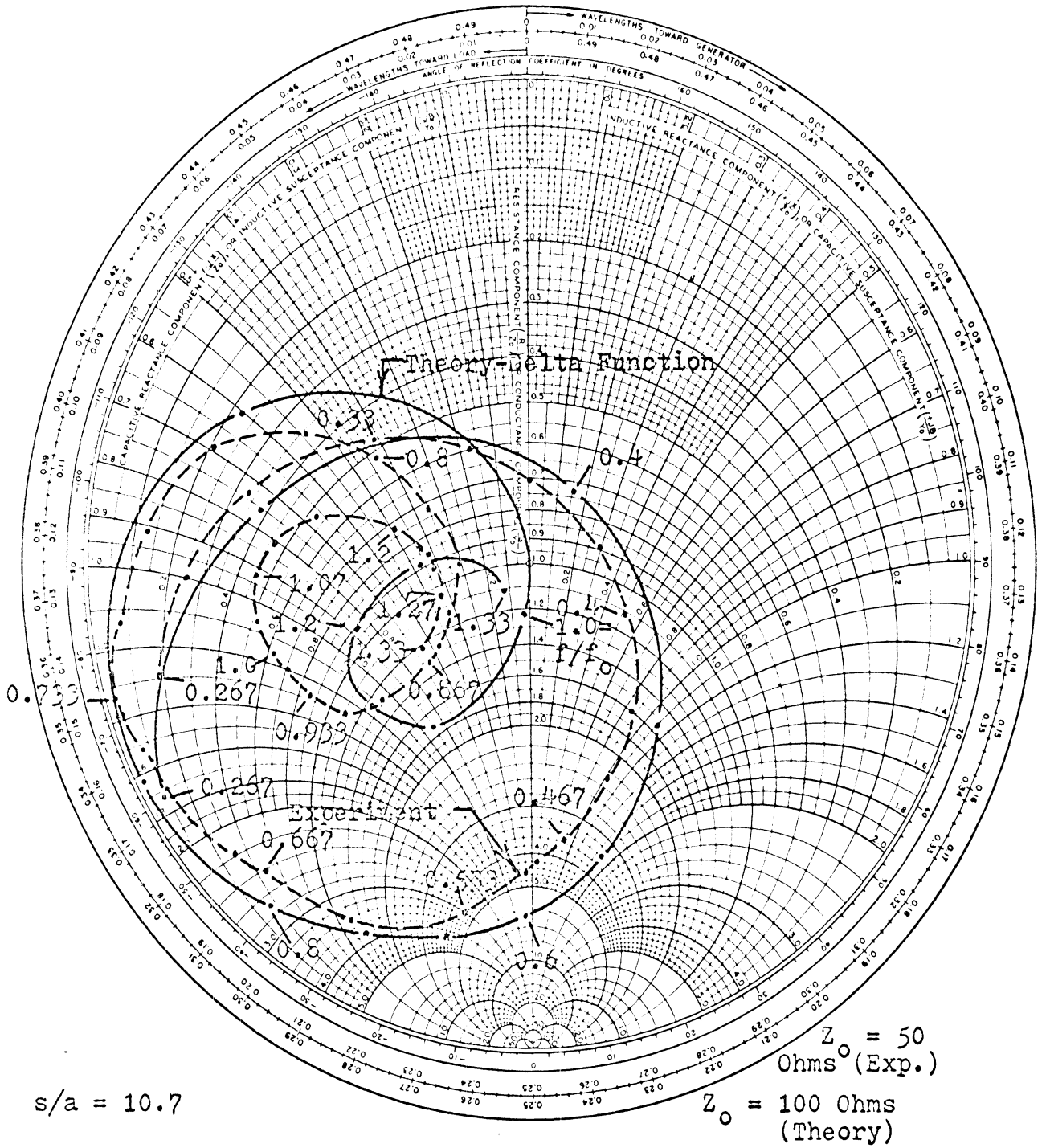


Figure A-4: Input Impedance of a Trap-Loaded Cylindrical Antenna with a 34.8 Ohm Transmission Line Trap, $L/s = 2\frac{1}{2}$, $s = \lambda_0/4$

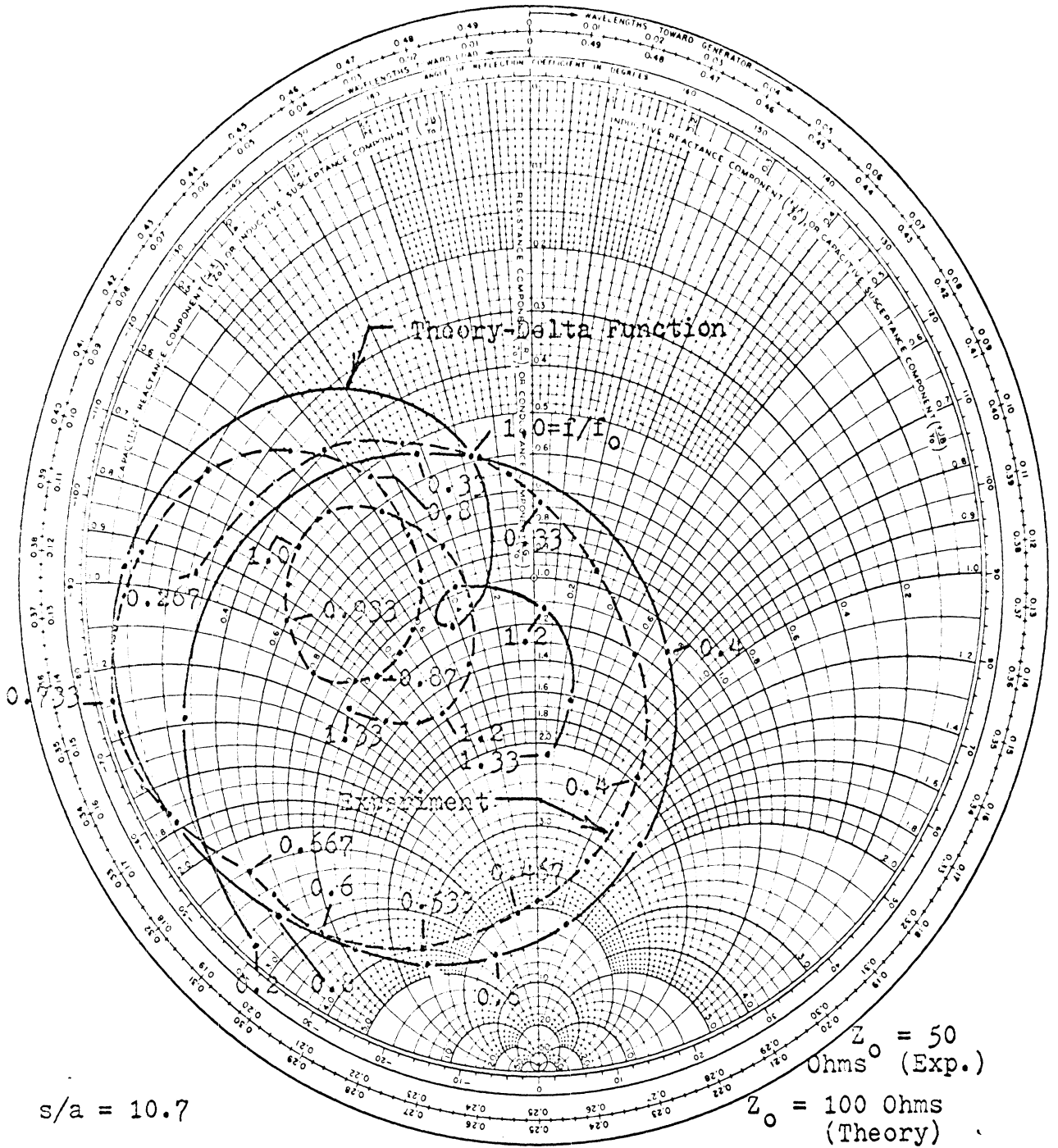


Figure A-5: Input Impedance of a Trap-Loaded Cylindrical Antenna with a 34.8 Ohm Transmission Line Trap, $L/s = 2\frac{1}{2}$, $s = \lambda_0/4$

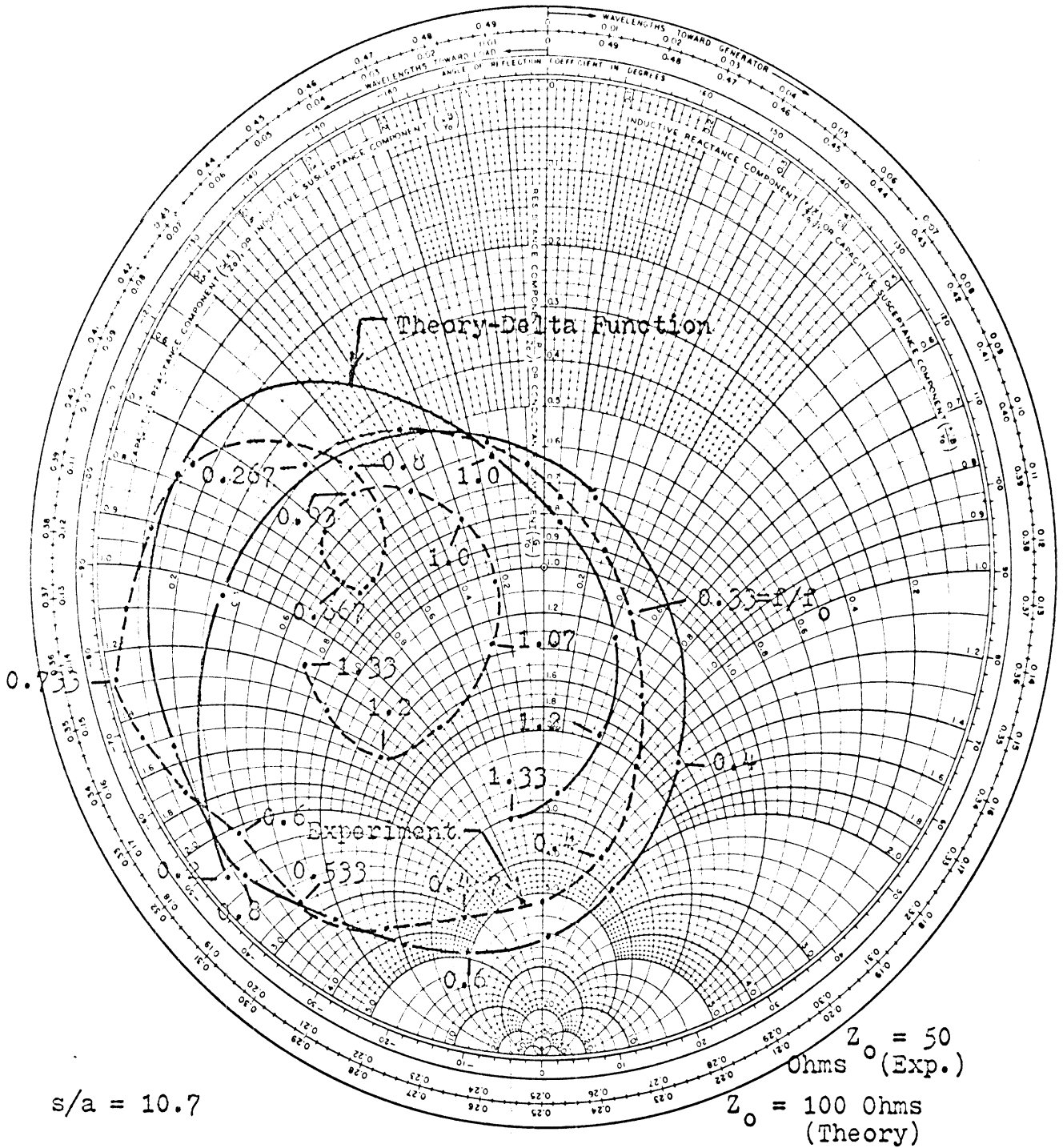


Figure A-6: Input Impedance of a Trap-Loaded Cylindrical Antenna with a 34.8 Ohm Transmission Line Trap, $L/s = 2-3/4$, $s = \lambda_0/4$

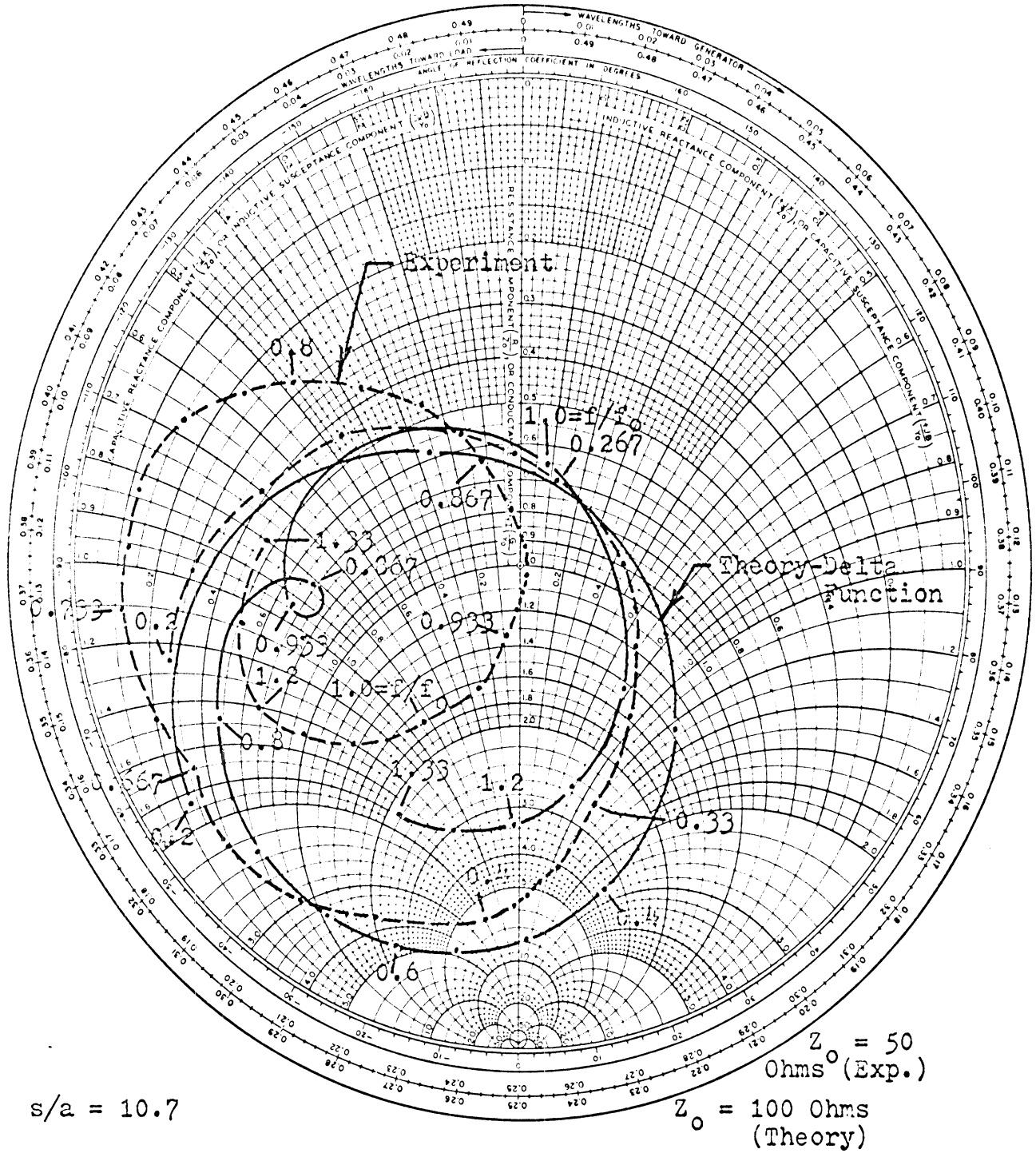


Figure A-7: Input Impedance of a Trap-Loaded Cylindrical Antenna with a 34.8 Ohm Transmission Line Trap, $L/s = 3\frac{1}{4}$, $s = \lambda_0/4$

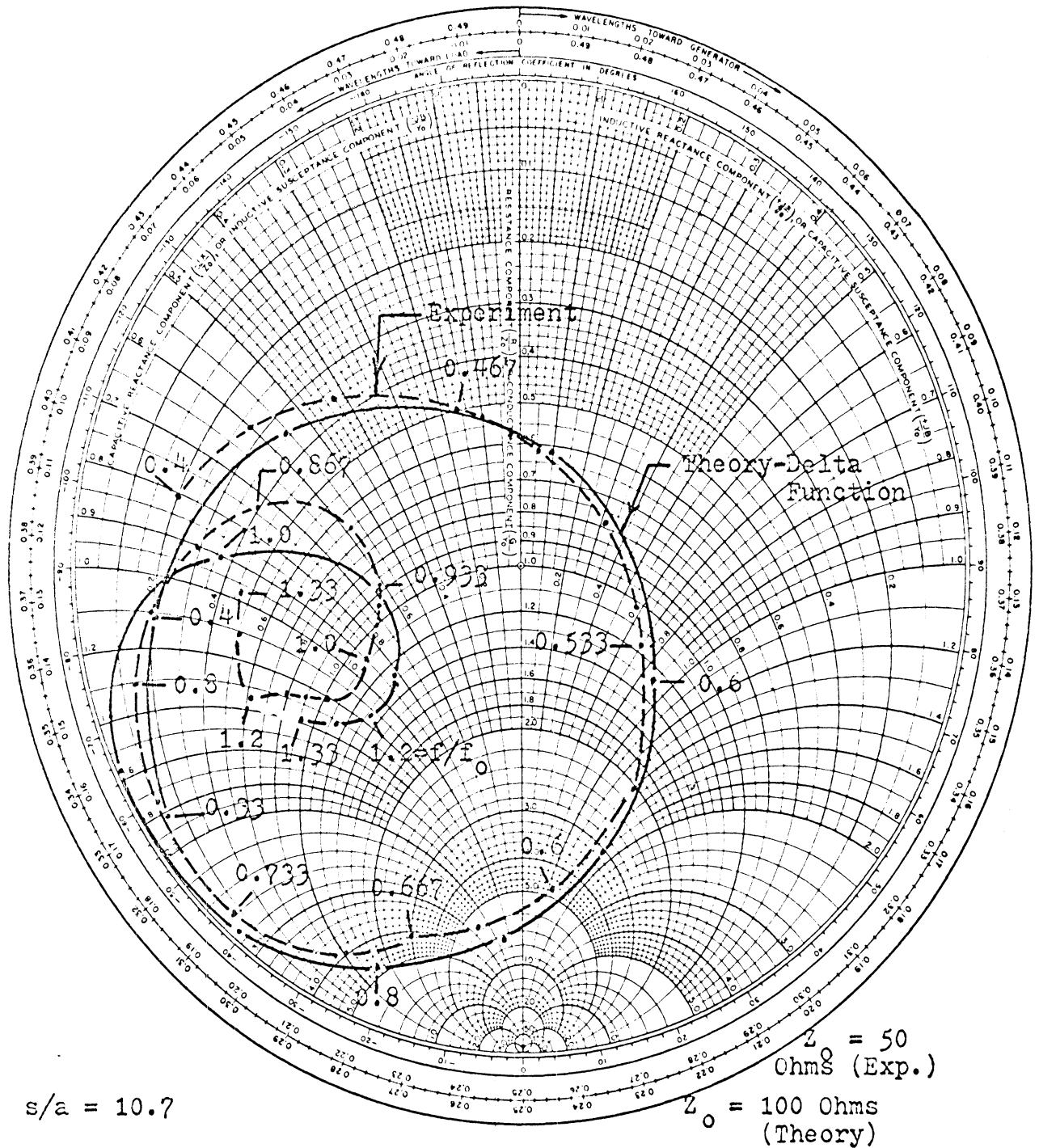


Figure A-8: Input Impedance of a Trap-Loaded Cylindrical Antenna with a 34.8 Ohm Transmission Line Trap, $L/(L - s) = 1\frac{1}{2}$ and $(L - s) = \lambda_0/4$

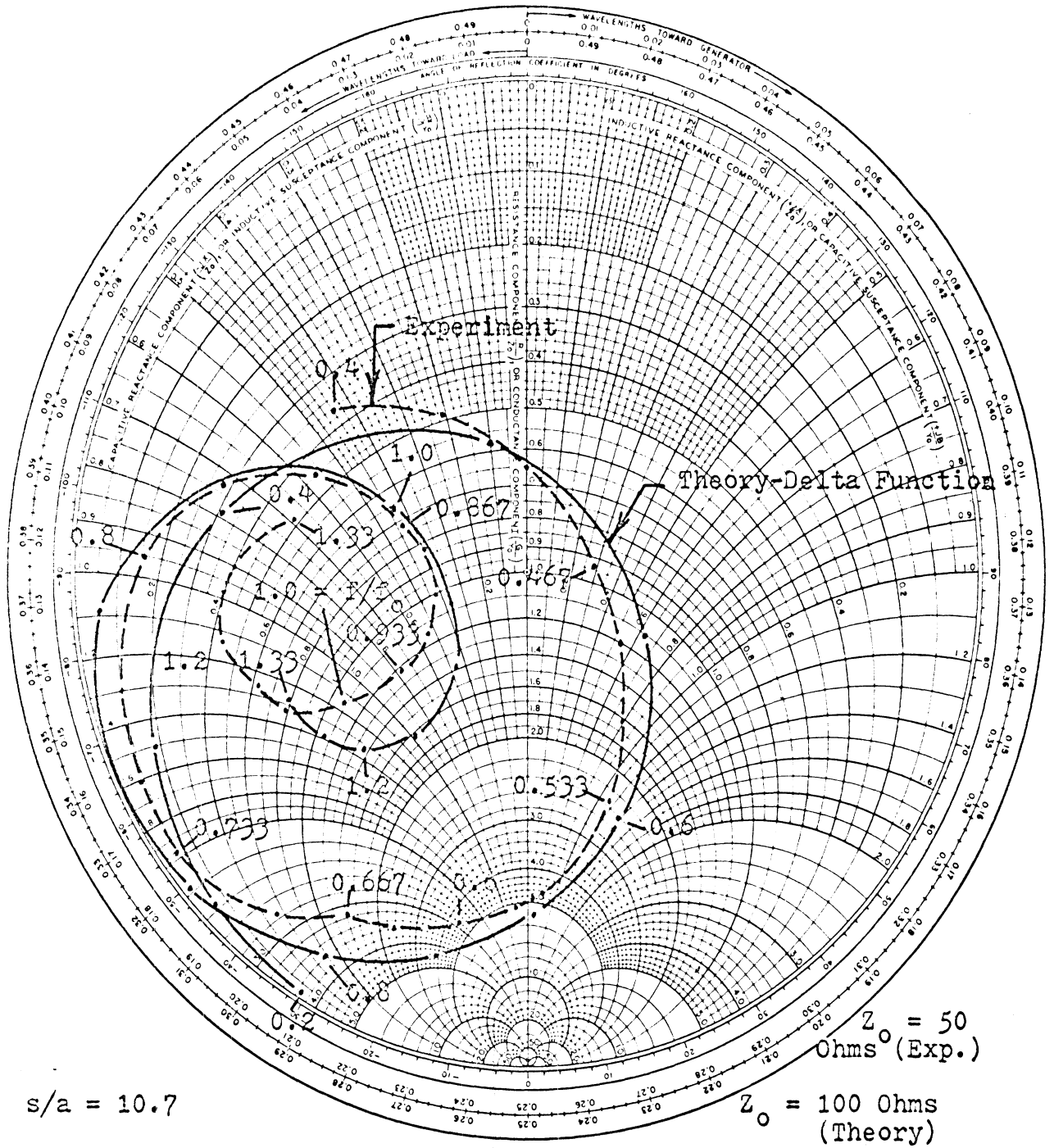


Figure A-9: Input Impedance of a Trap-Loaded Cylindrical Antenna with a 34.8 Ohm Transmission Line Trap, $L/(L - s) = 1-3/4$ and $(L - s) = \lambda_0/4$

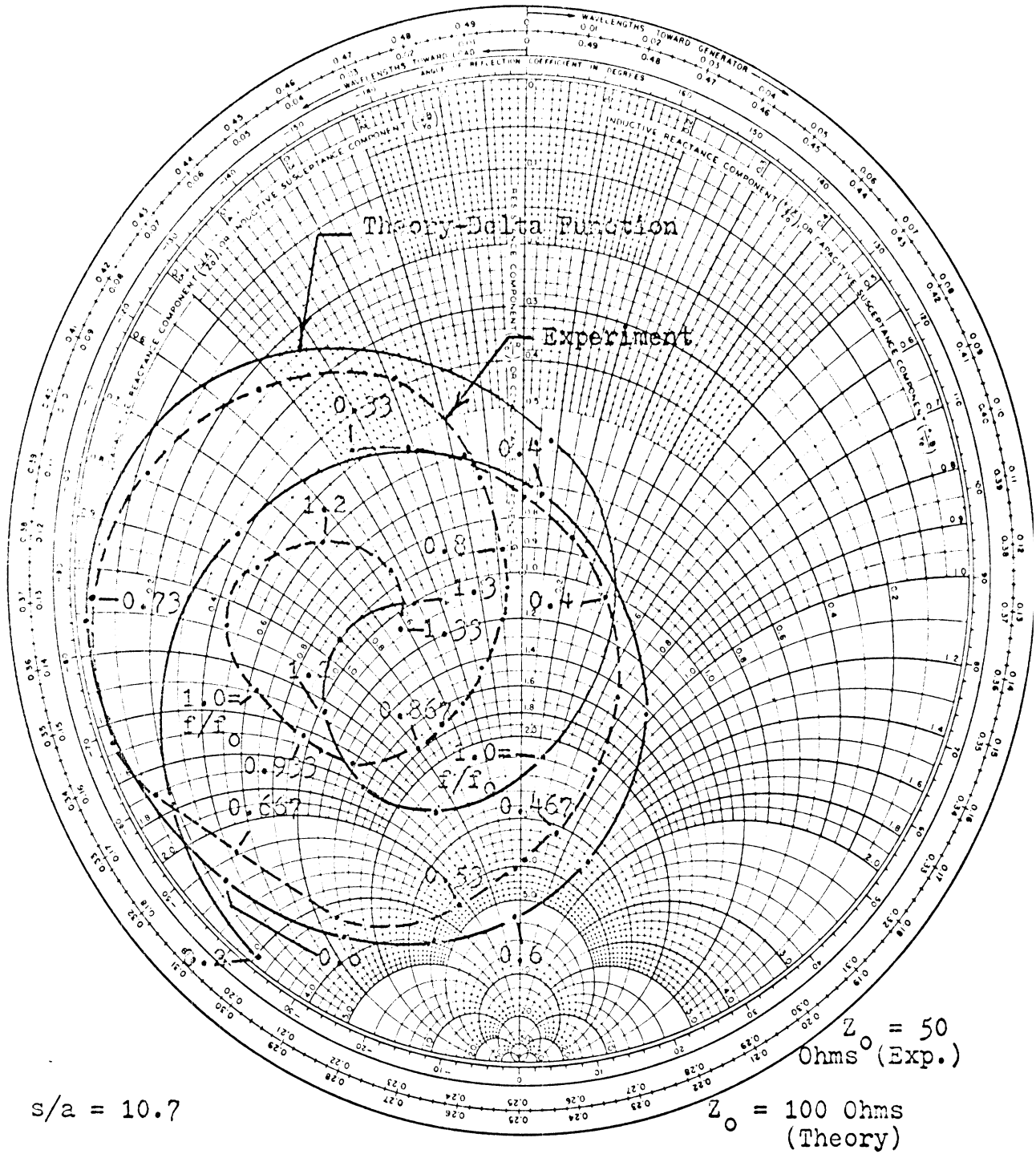


Figure A-10: Input Impedance of a Trap-Loaded Cylindrical Antenna with a 34.8 Ohm Transmission Line Trap, $L/(L - s) = 2\frac{1}{2}$ and $(L - s) = \lambda_0/4$

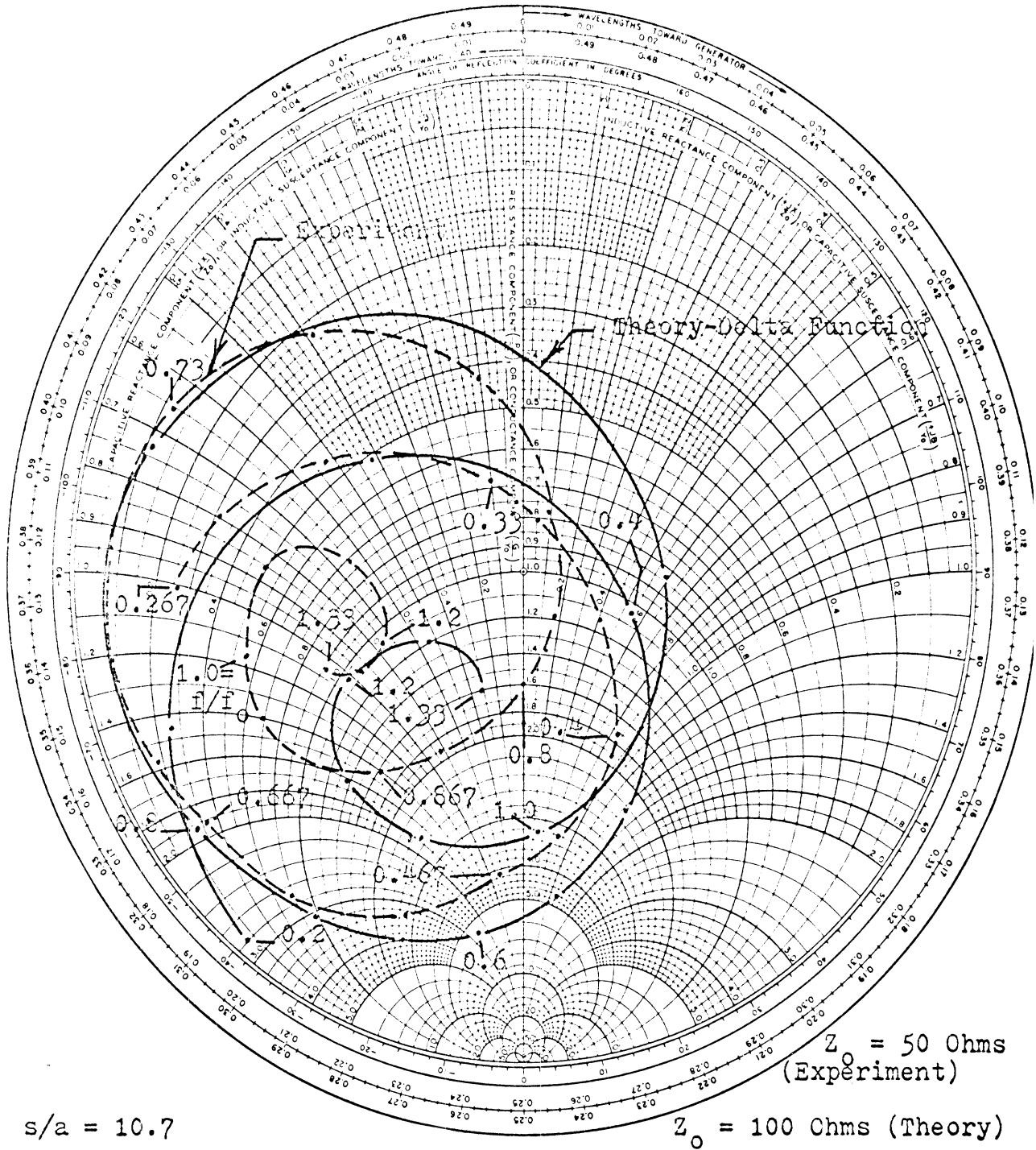
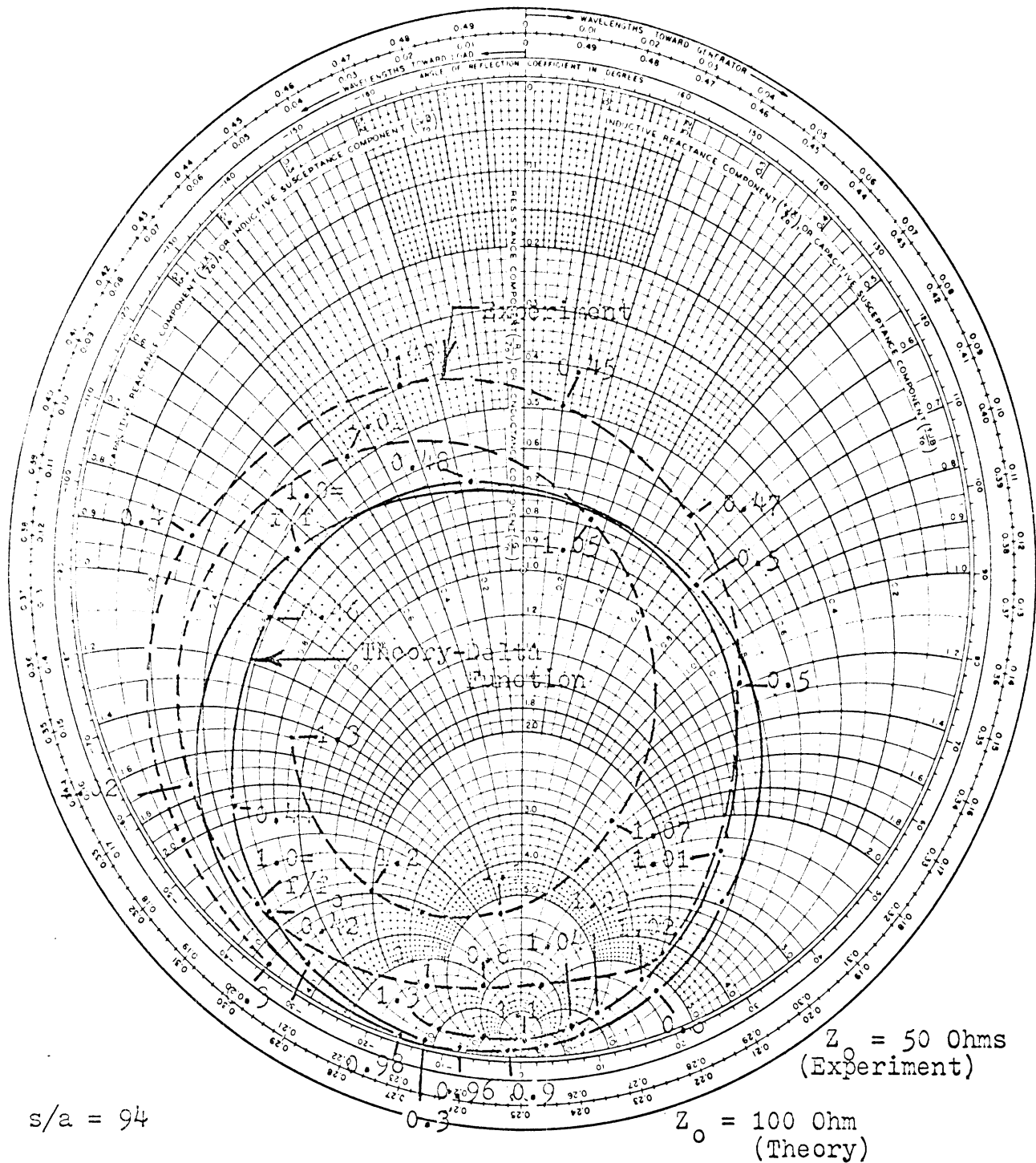


Figure A-11: Input Impedance of a Trap-Loaded Cylindrical Antenna with a 34.8 Ohm Transmission Line Trap, $L/(L - s) = 2\frac{1}{2}$ and $(L - s) = \lambda_0/4$



$s/a = 94$

$Z_0 = 100 \text{ Ohm}$
(Theory)

$Z_0 = 50 \text{ Ohms}$
(Experiment)

Figure A-12: Input Impedance of a Trap Antenna with a 53 Ohm Inductor-Capacitor Trap

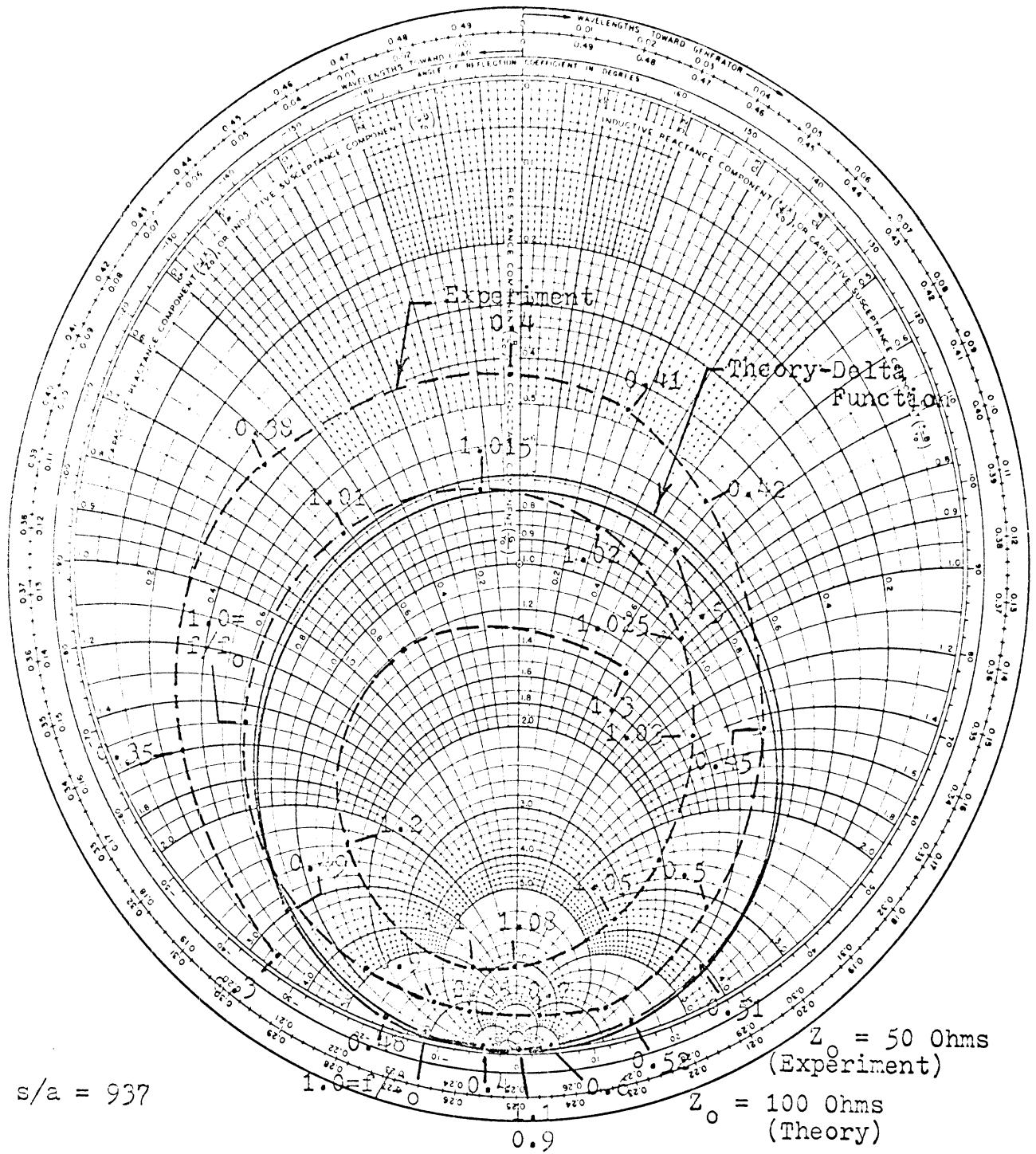


Figure A-13: Input Impedance of a Trap Antenna with a 53 Ohm Inductor-Capacitor Trap

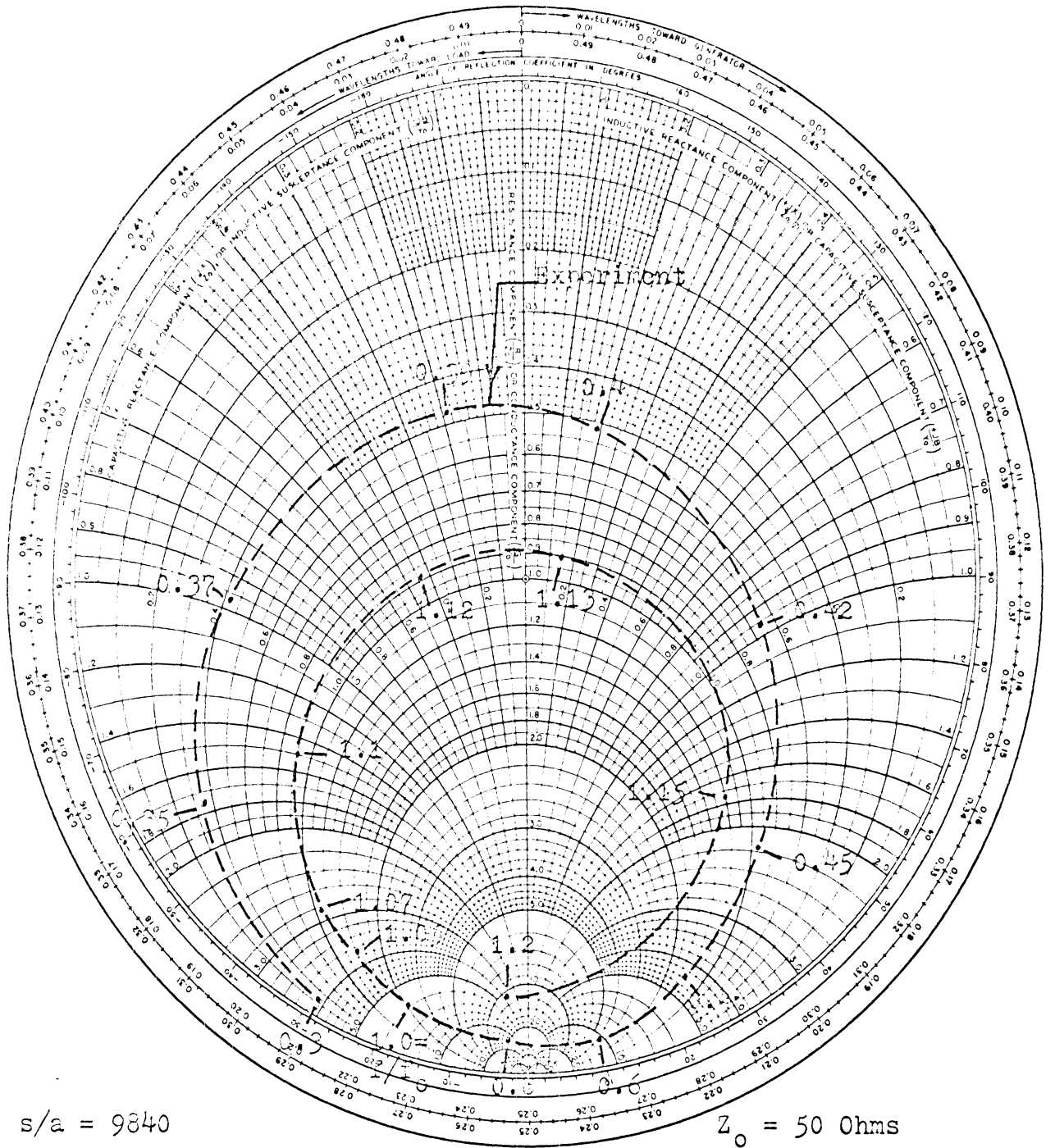


Figure A-14: Input Impedance of a Trap Antenna with a 53 Ohm Inductor-Capacitor Trap

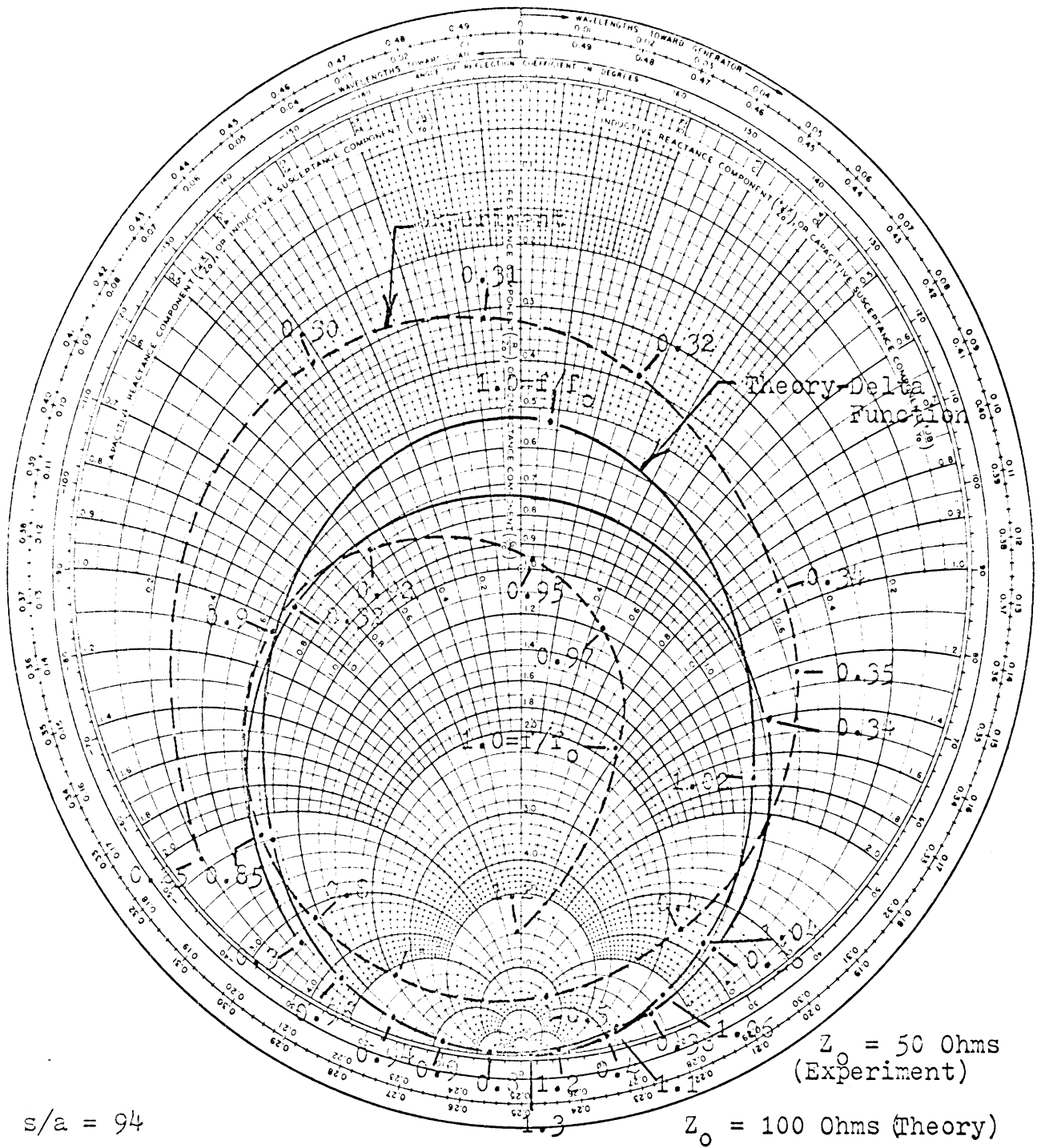


Figure A-15: Input Impedance of a Franklin Antenna with a 53 Ohm Inductor-Capacitor Trap

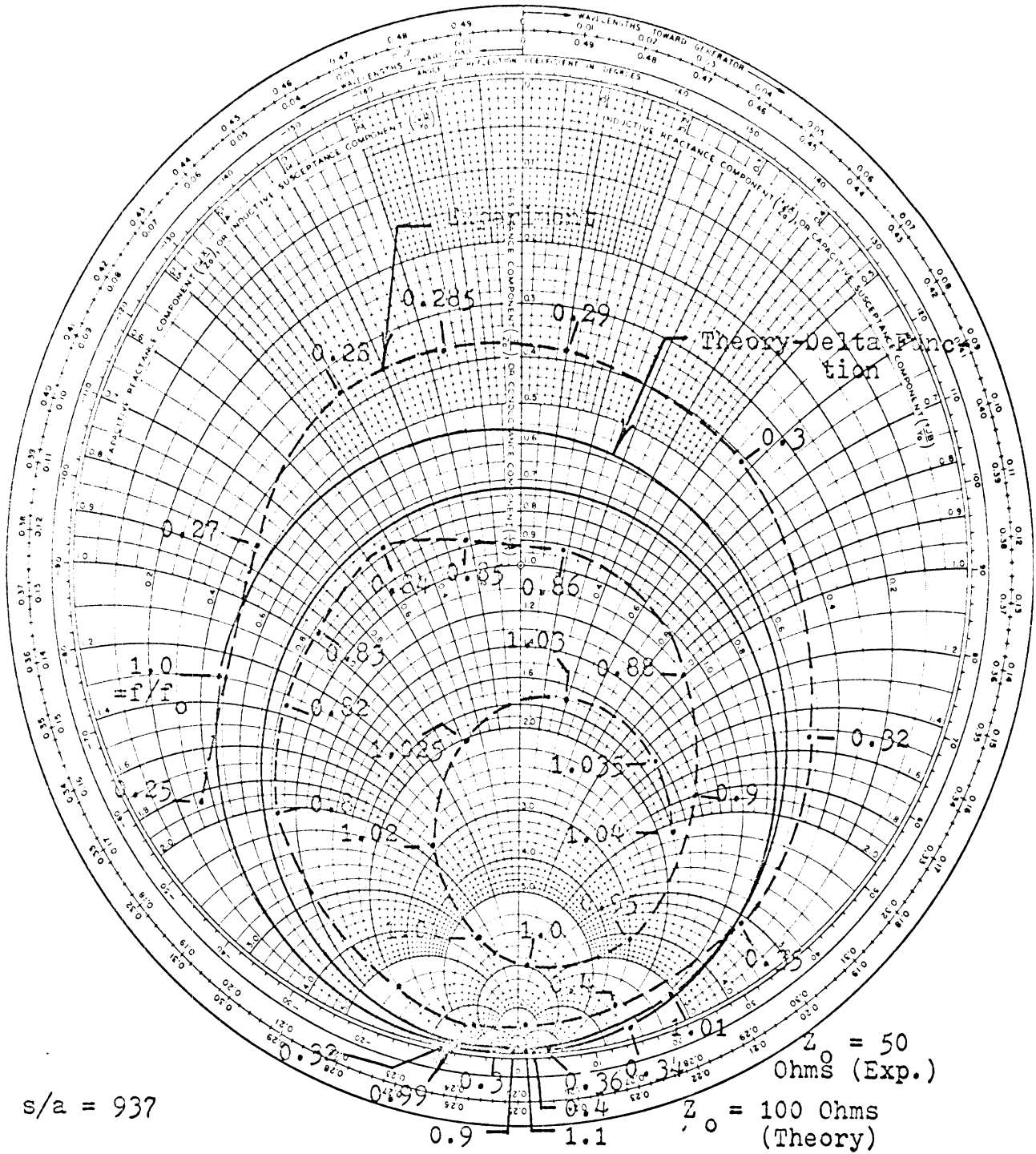
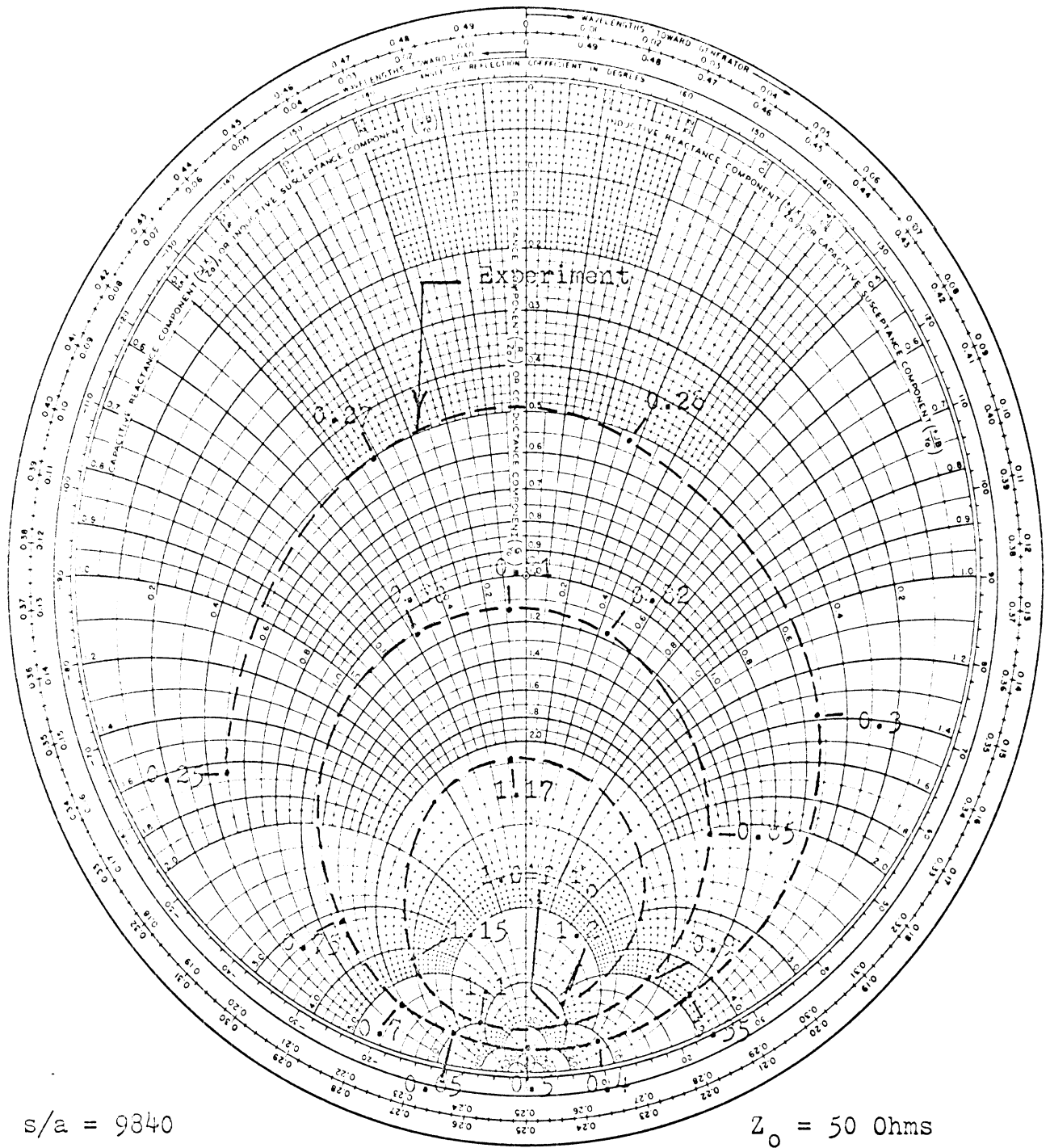


Figure A-16: Input Impedance of a Franklin Antenna with a 53 Ohm Inductor-Capacitor Trap



s/a = 9840

Z₀ = 50 Ohms

Figure A-17: Input Impedance of a Franklin Antenna with a 53 Ohm Inductor-Capacitor Trap

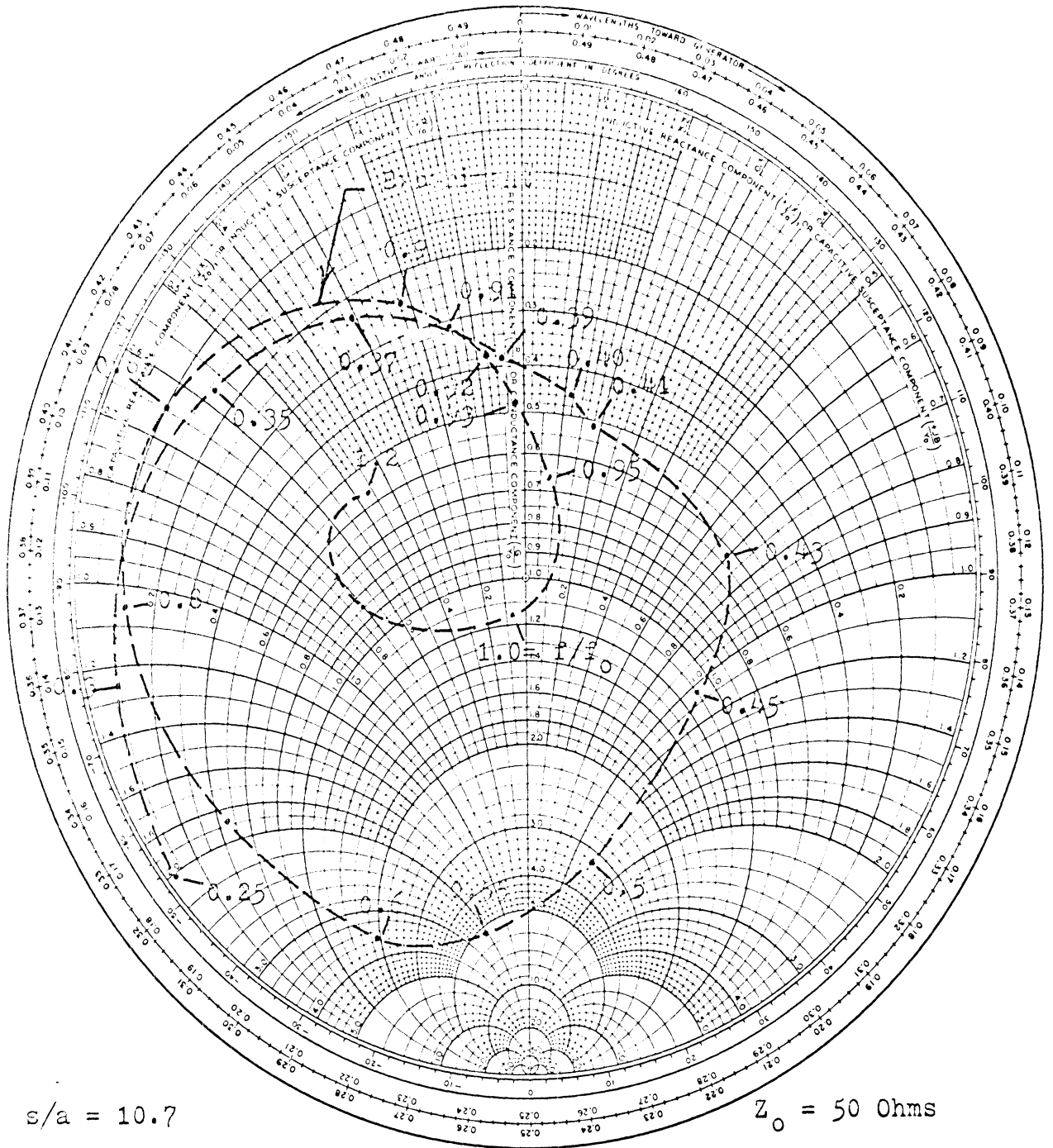


Figure A-18: Input Impedance of a Trap Antenna with a 88.5 Ohm Inductor-Capacitor Trap

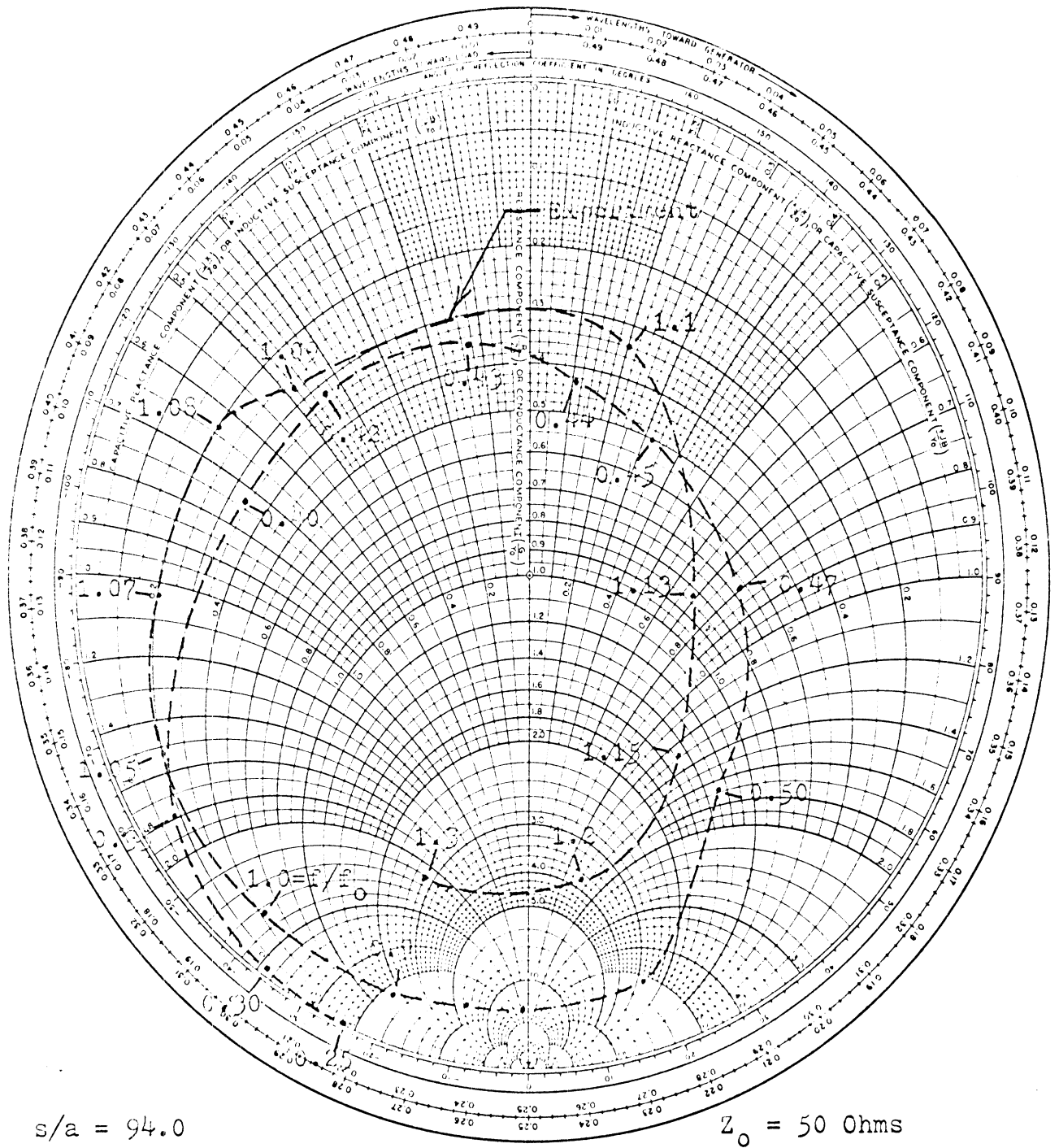


Figure A-19: Input Impedance of a Trap Antenna with a 88.5 Ohm Inductor-Capacitor Trap

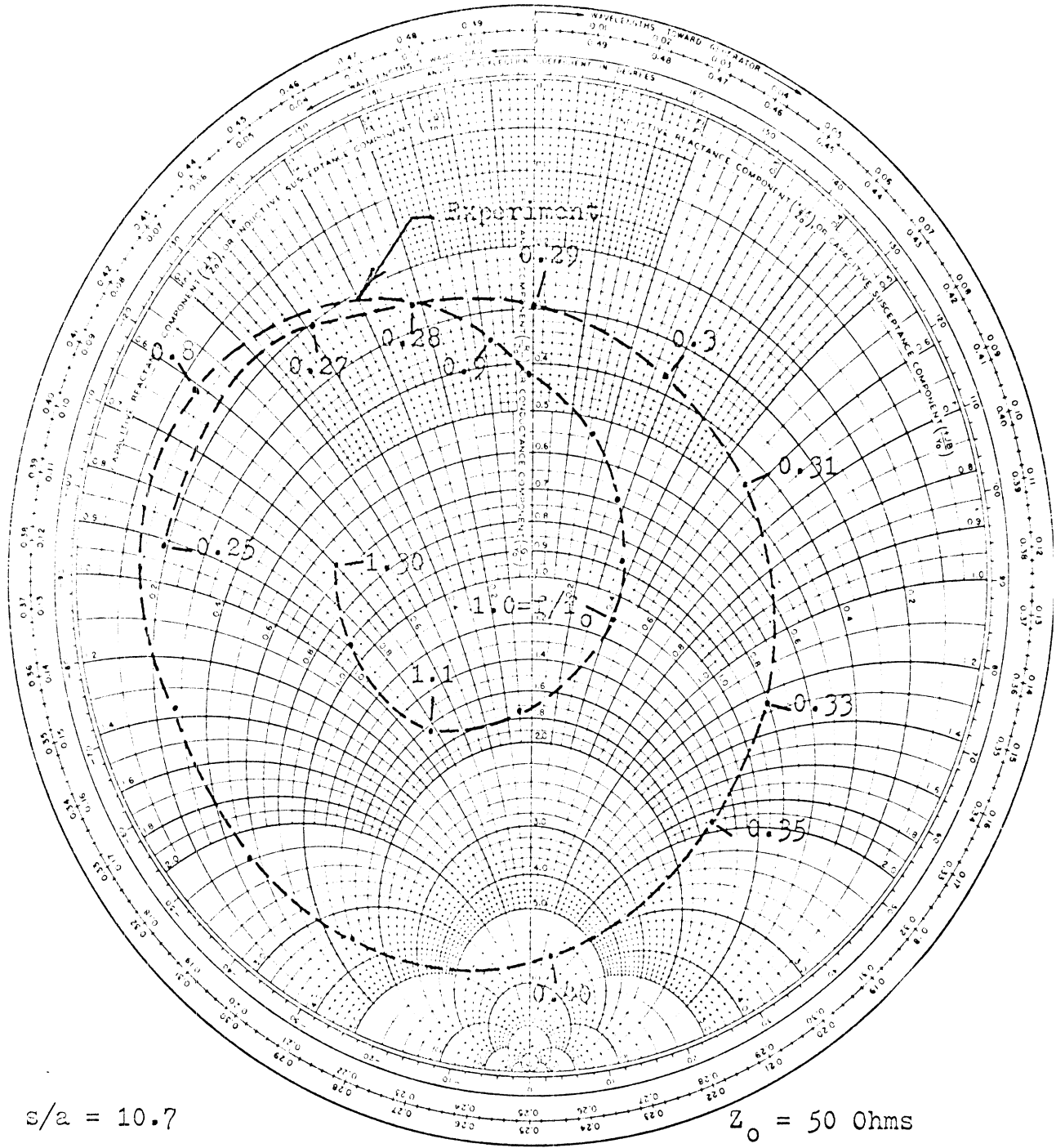
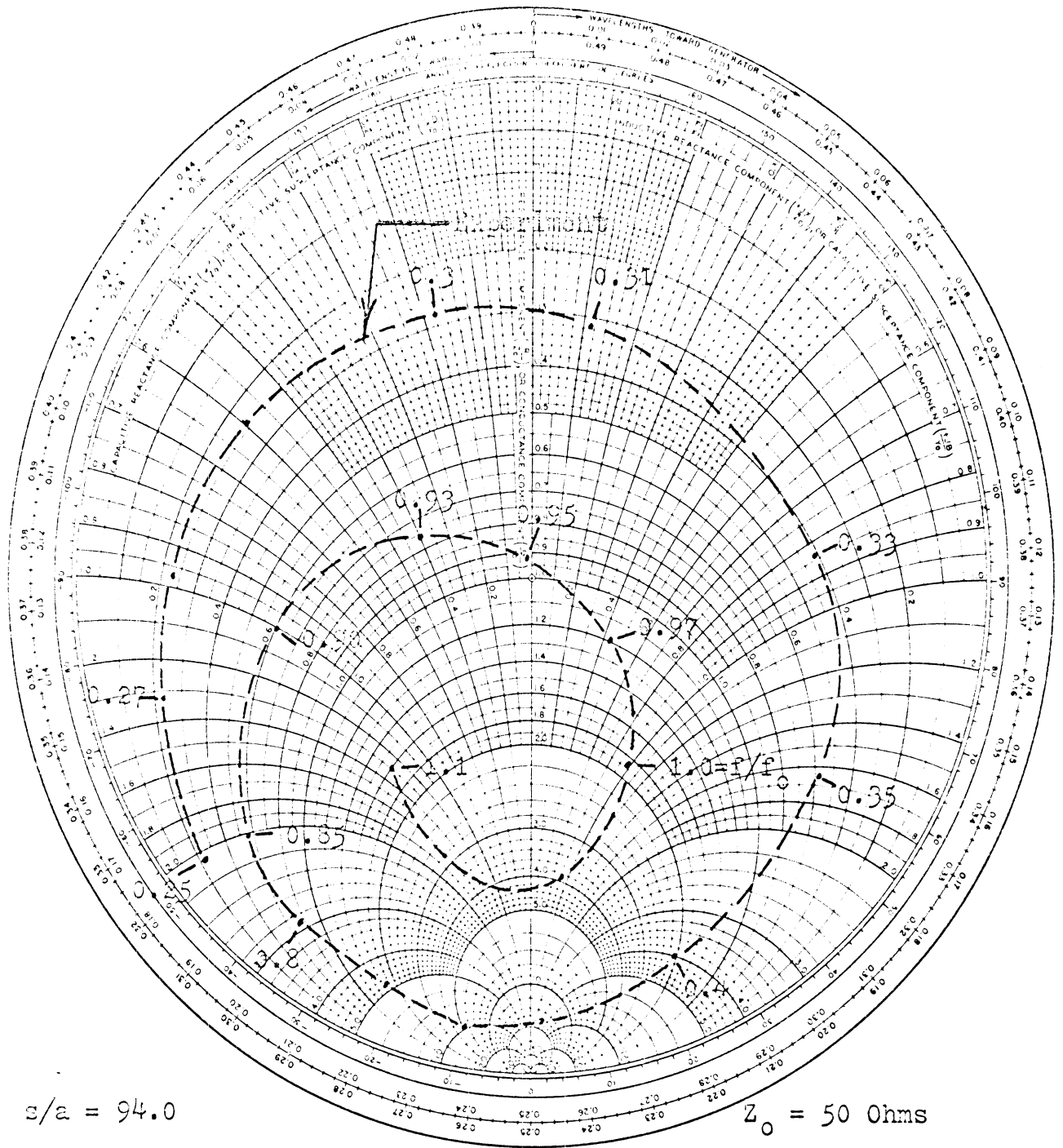


Figure A-20: Input Impedance of a Franklin Antenna with a 88.5 Ohm Inductor-Capacitor Trap



$c/a = 94.0$

$Z_0 = 50 \text{ Ohms}$

Figure A-21: Input Impedance of a Franklin Antenna with a 88.5 Ohm Inductor-Capacitor Trap

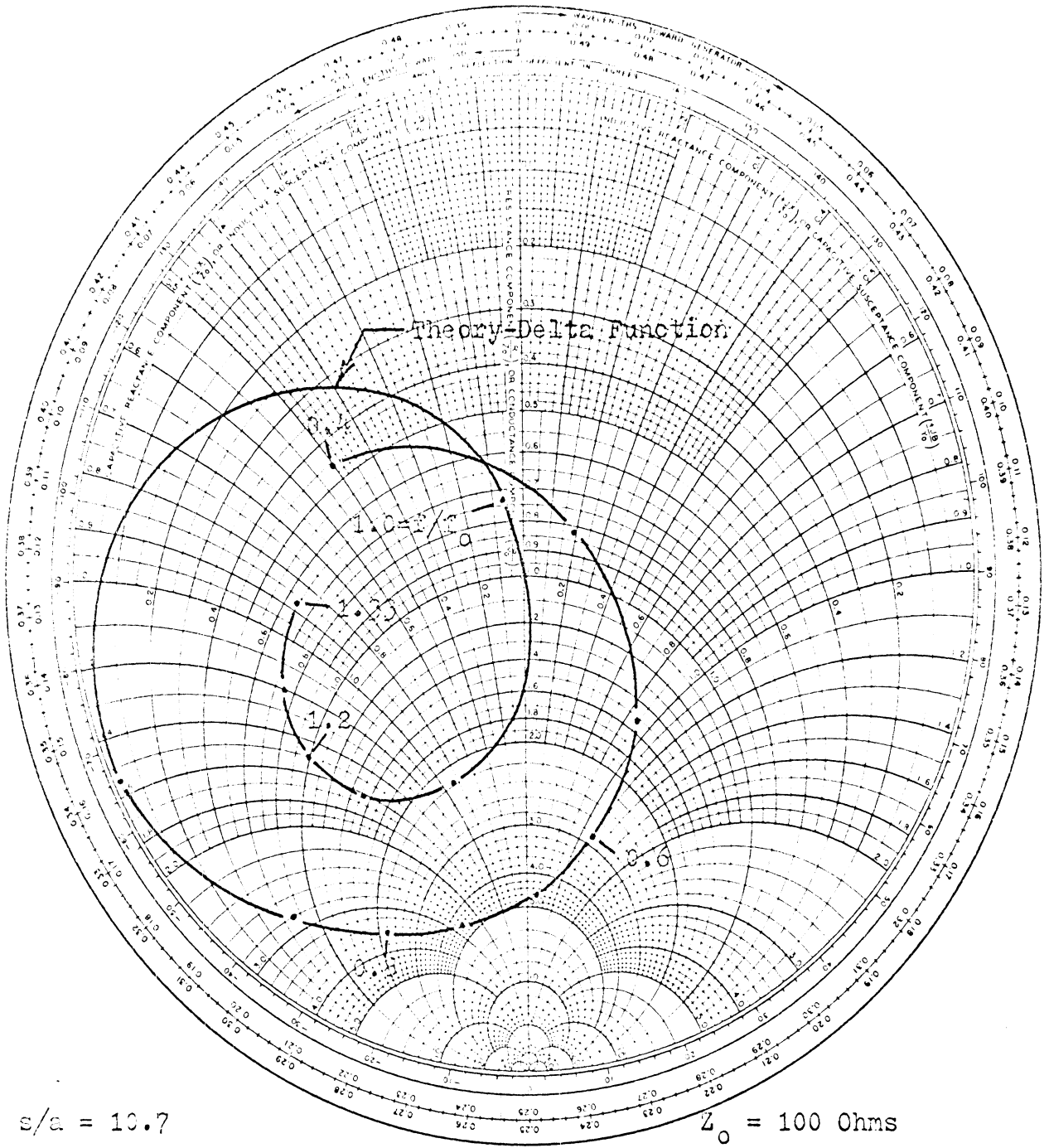


Figure A-22: Input Impedance of a Trap Antenna with a 18.5 Ohm Transmission Line Trap

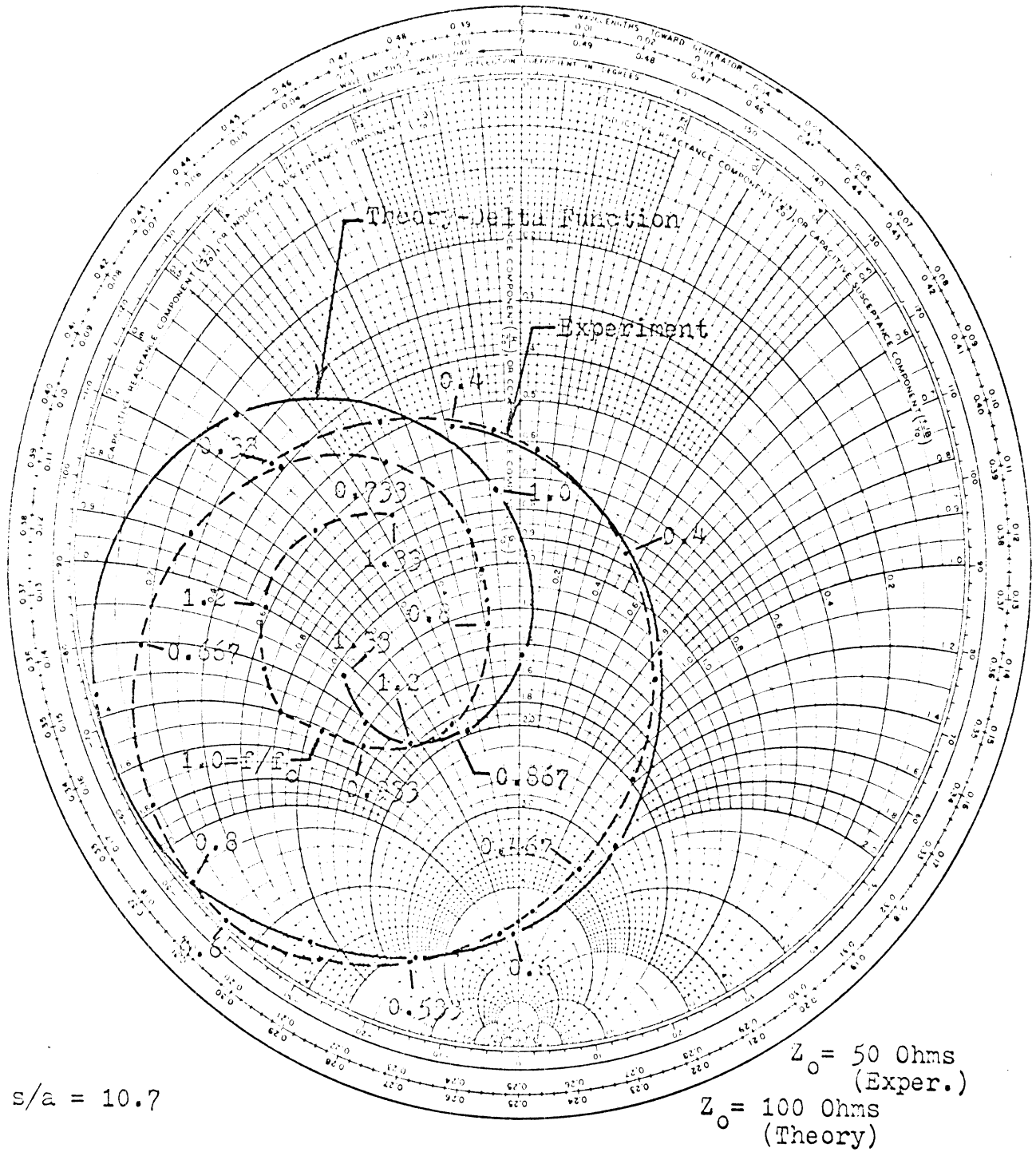


Figure A-23: Input Impedance of a Trap Antenna with a 62.5 Ohm Transmission Line Trap.

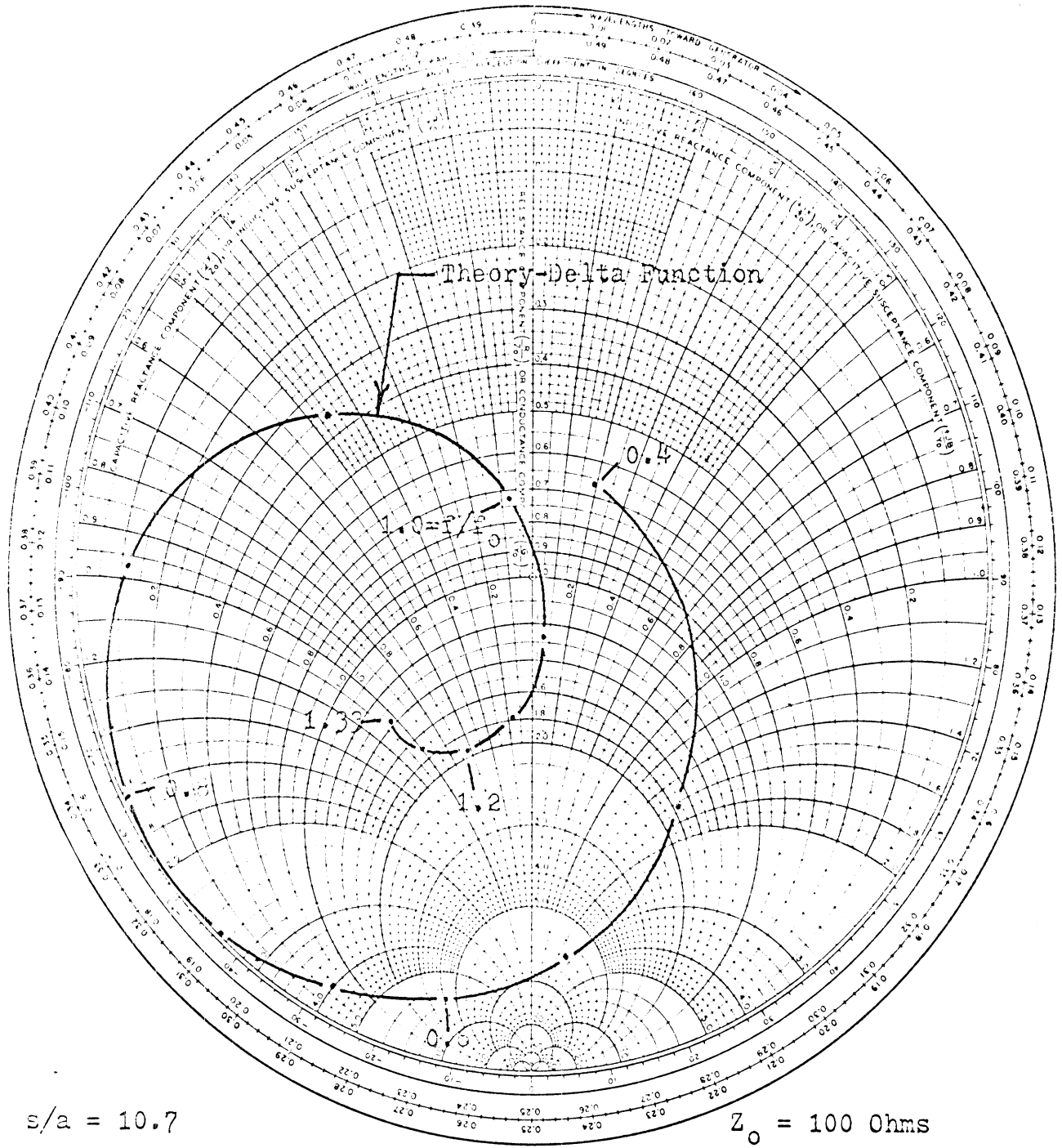


Figure A- 24: Input Impedance of a Trap Antenna with a 100 Ohm Transmission Line Trap

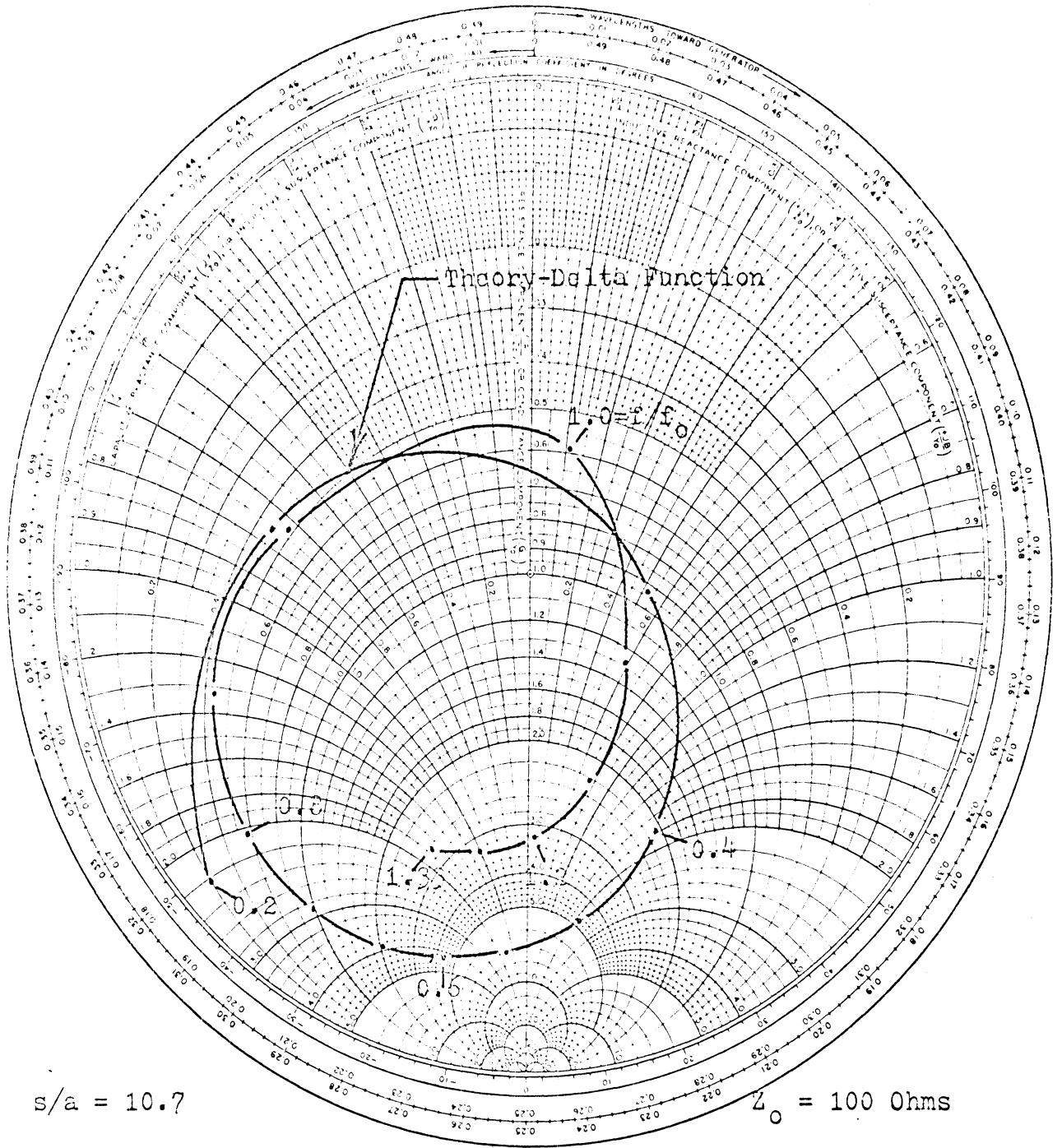


Figure A-25: Input Impedance of a Franklin Antenna with a 18.5 Ohm Transmission Line Trap

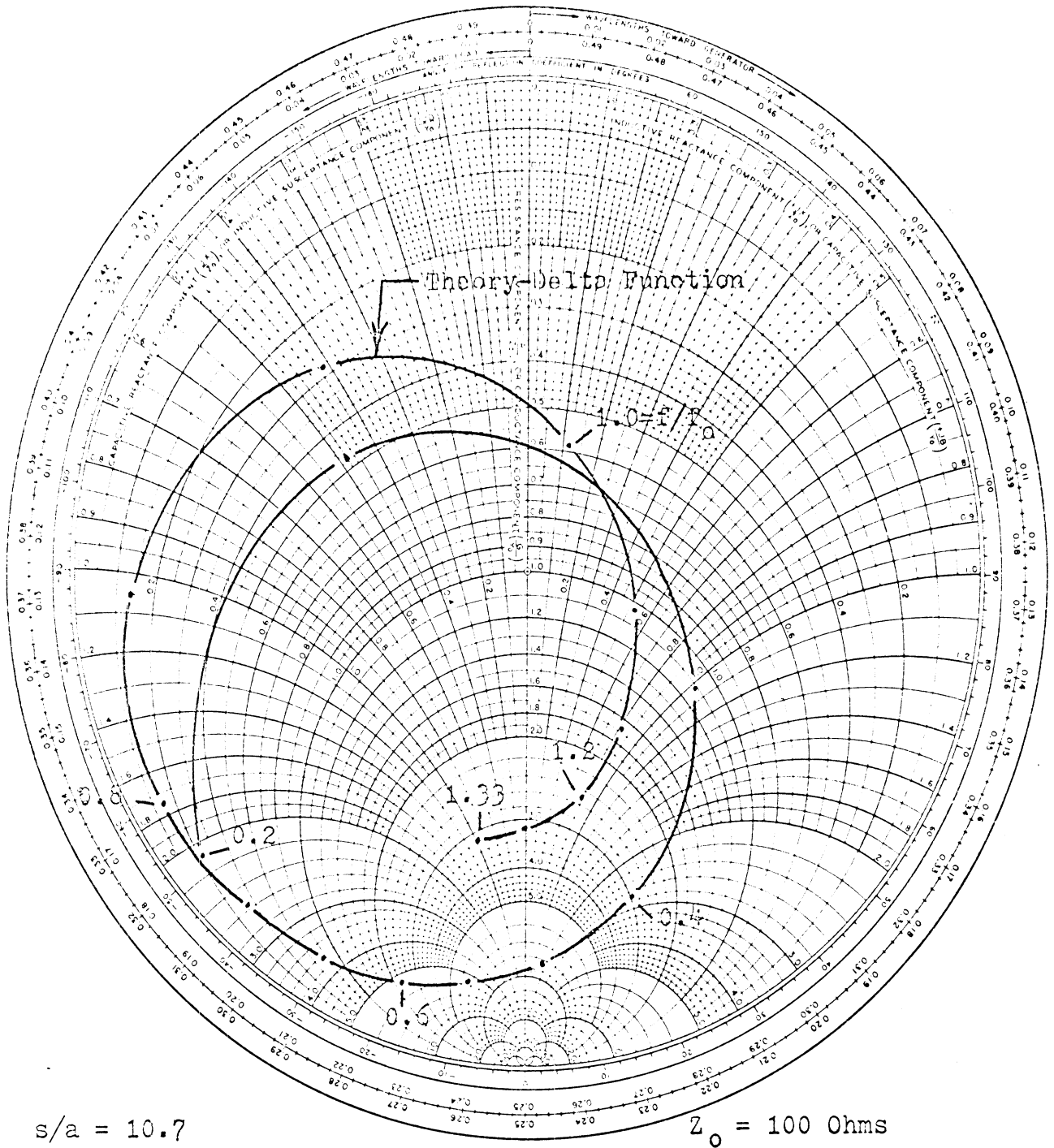


Figure A-26: Input Impedance of a Franklin Antenna with a 62.5 Ohm Transmission Line Trap

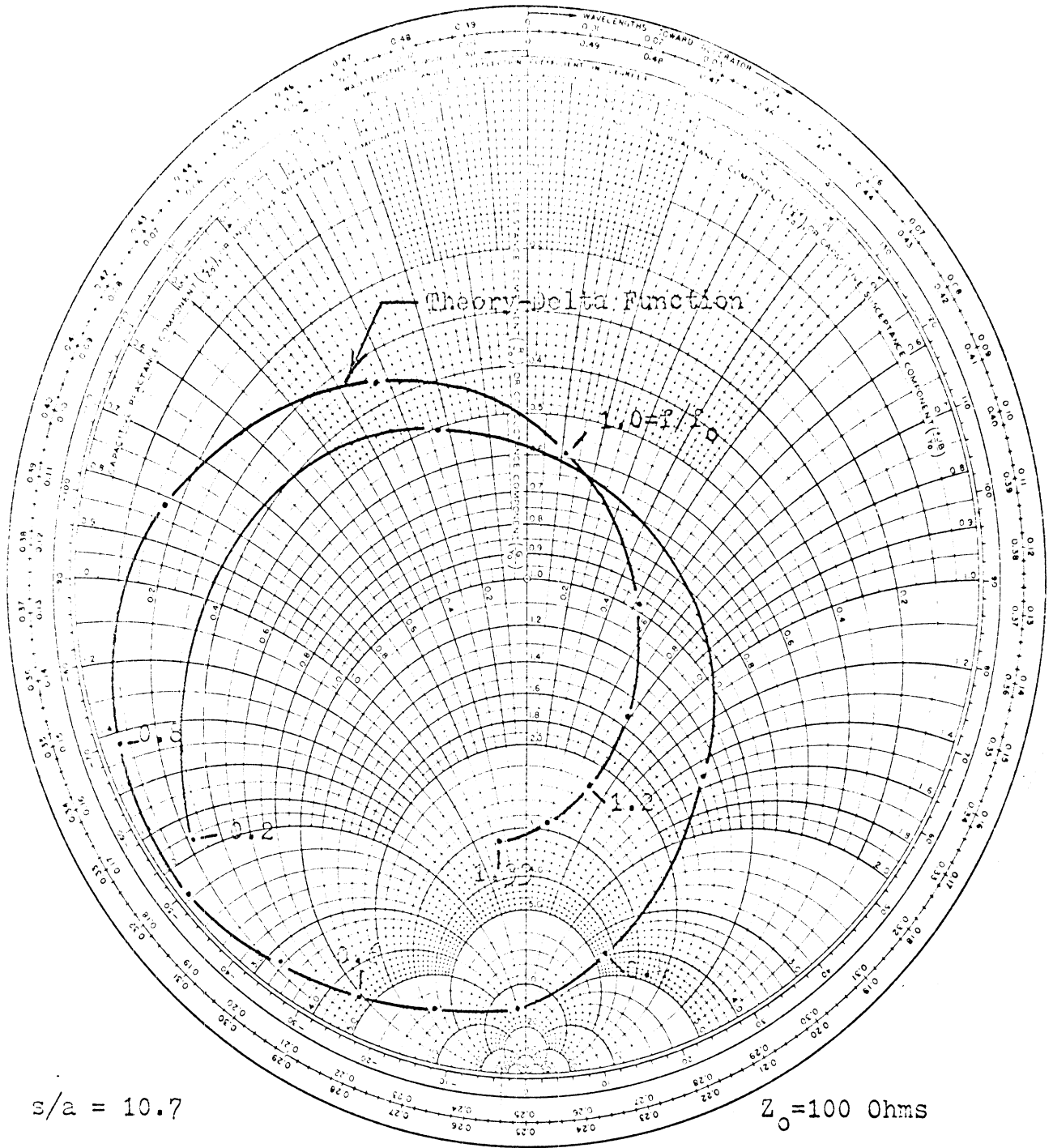


Figure A-27: Input Impedance of a Franklin Antenna with a 100 Ohm Transmission Line Trap

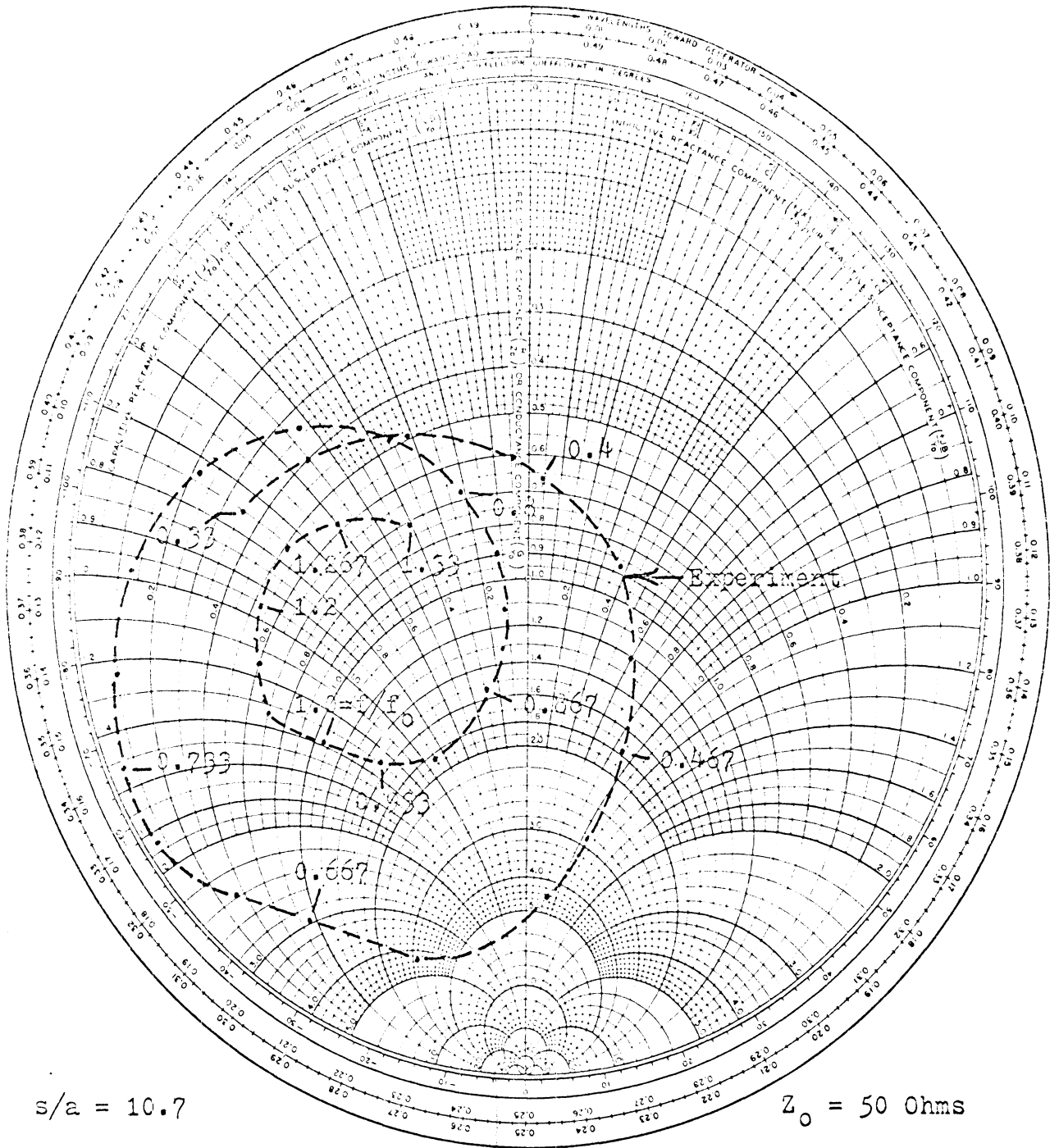


Figure A- 28: Input Impedance of a Trap Antenna with a 34.8 Ohm Transmission Line Trap and a 2/16 Inch Feed Gap Width

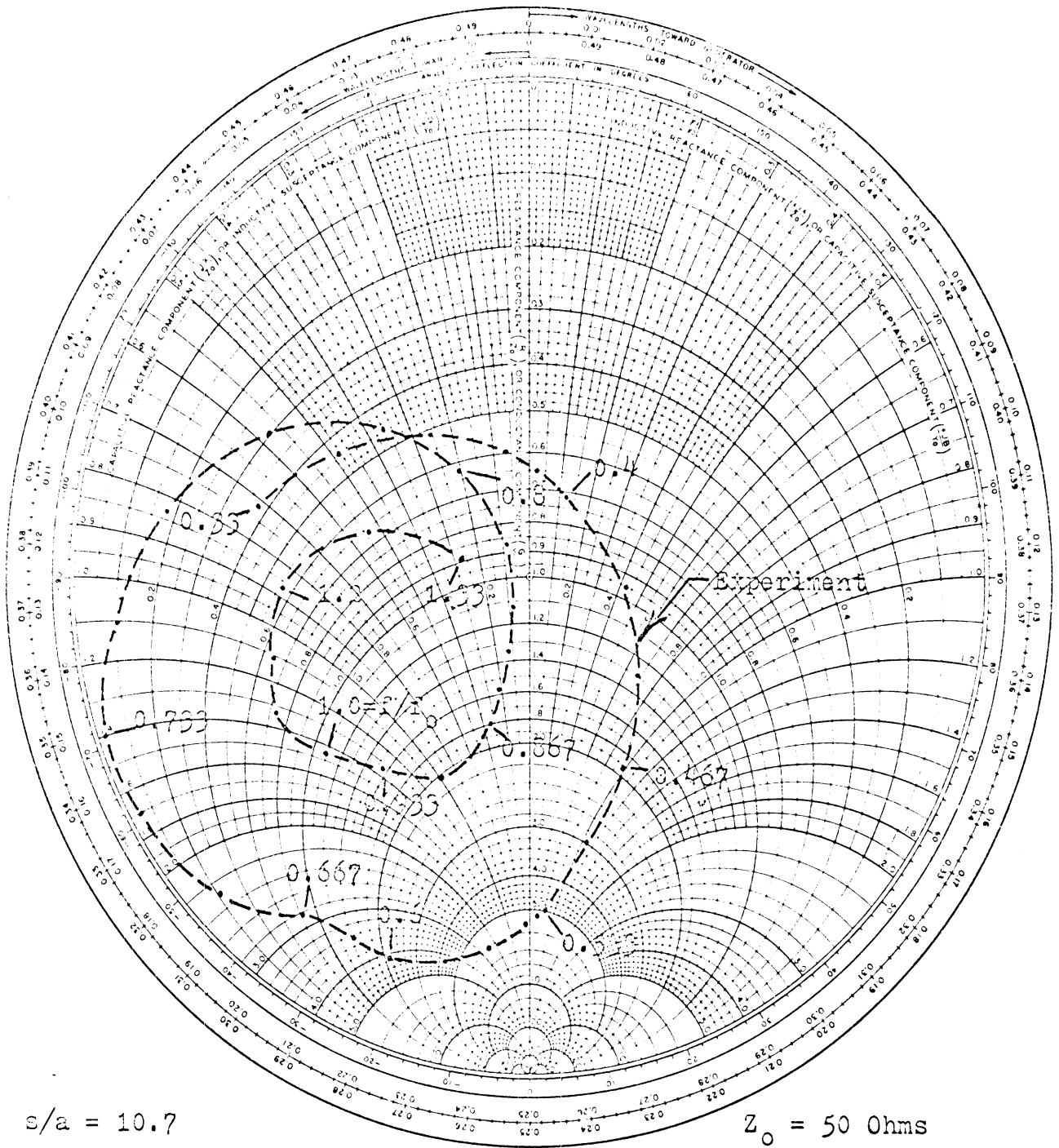


Figure A-29: Input Impedance of a Trap Antenna with a 34.8 Ohm Transmission Line Trap and a 3/16 Inch Feed Gap Width

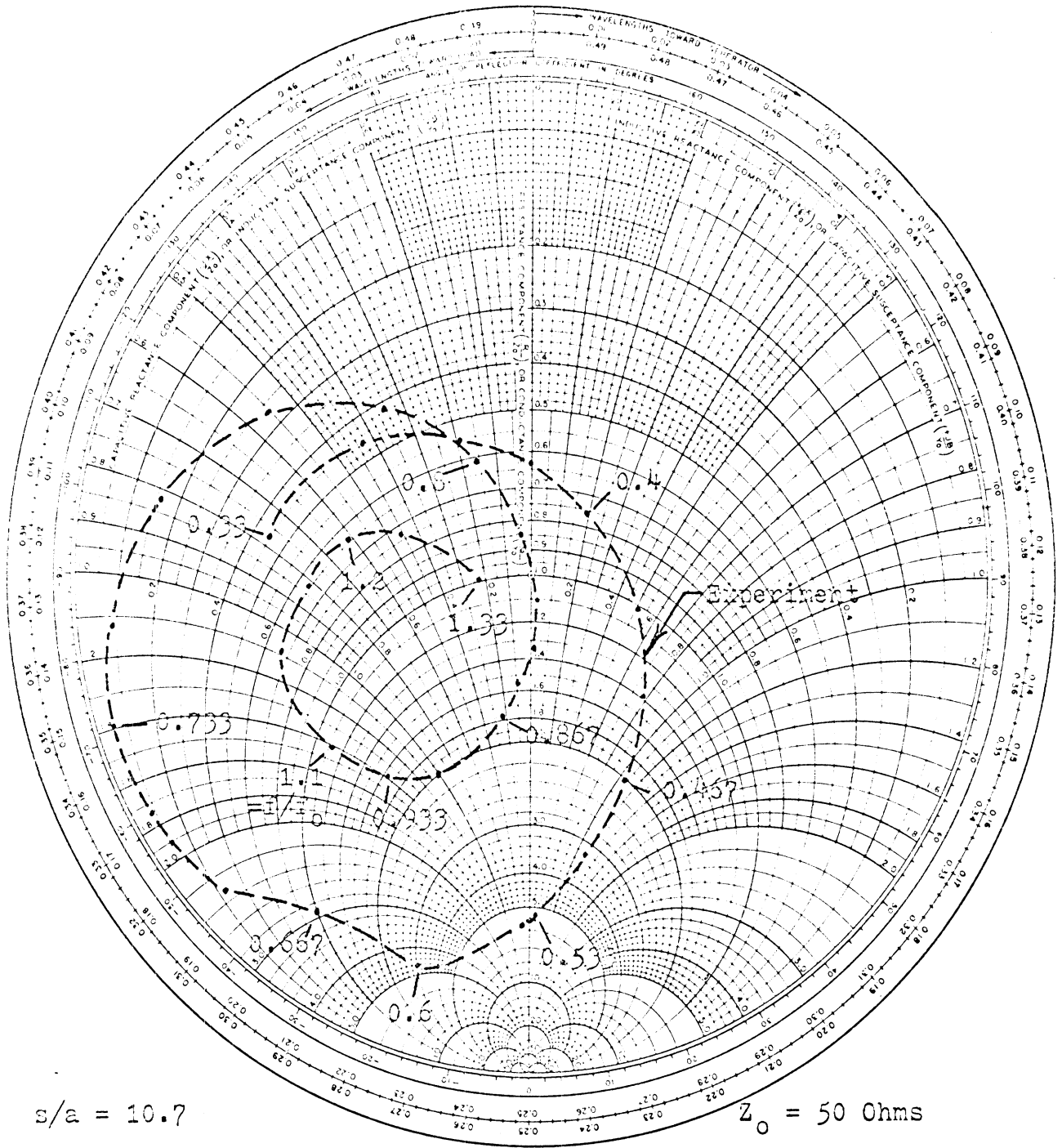


Figure A-30: Input Impedance of a Trap Antenna with a 34.8 Ohm Transmission Line Trap and a 4/16 Inch Feed Gap Width

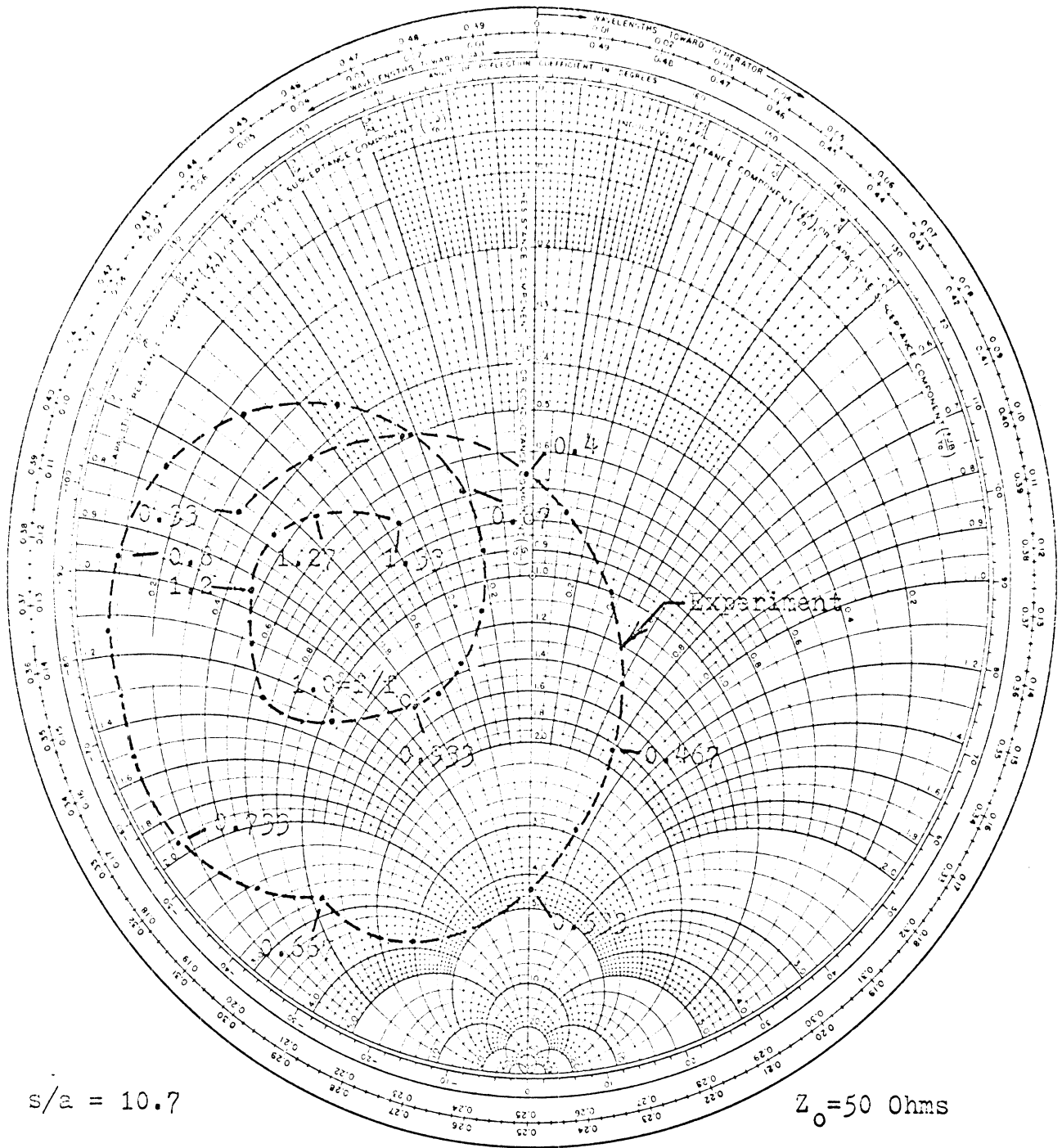


Figure A-31: Input Impedance of a Trap Antenna with a 34.8 Ohm Transmission Line Trap and a 2/16 Inch Trap Gap Width

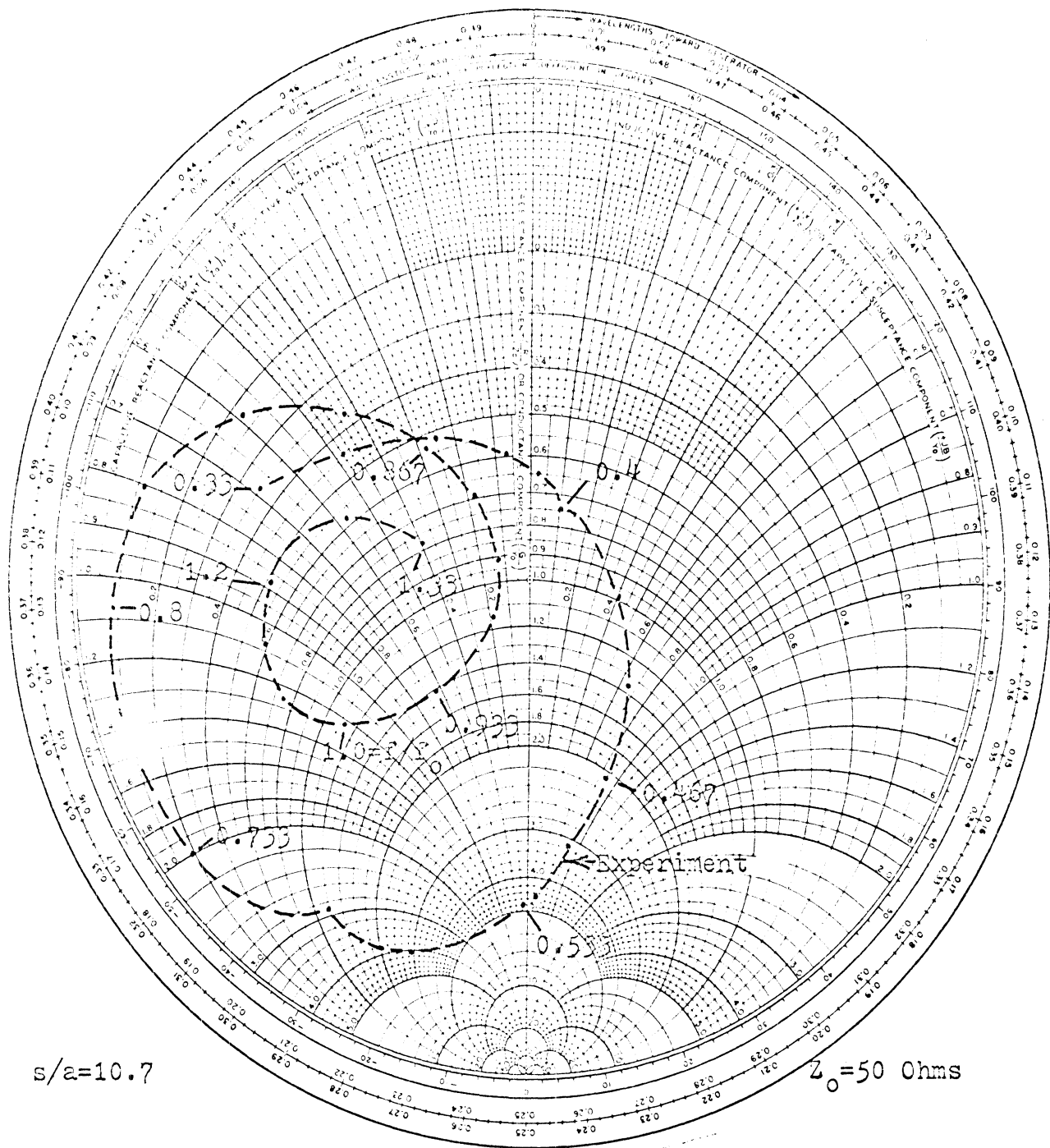


Figure A- 32: Input Impedance of a Trap Antenna with a 34.8 Ohm Transmission Line Trap and a 3/16 Inch Trap Gap Width

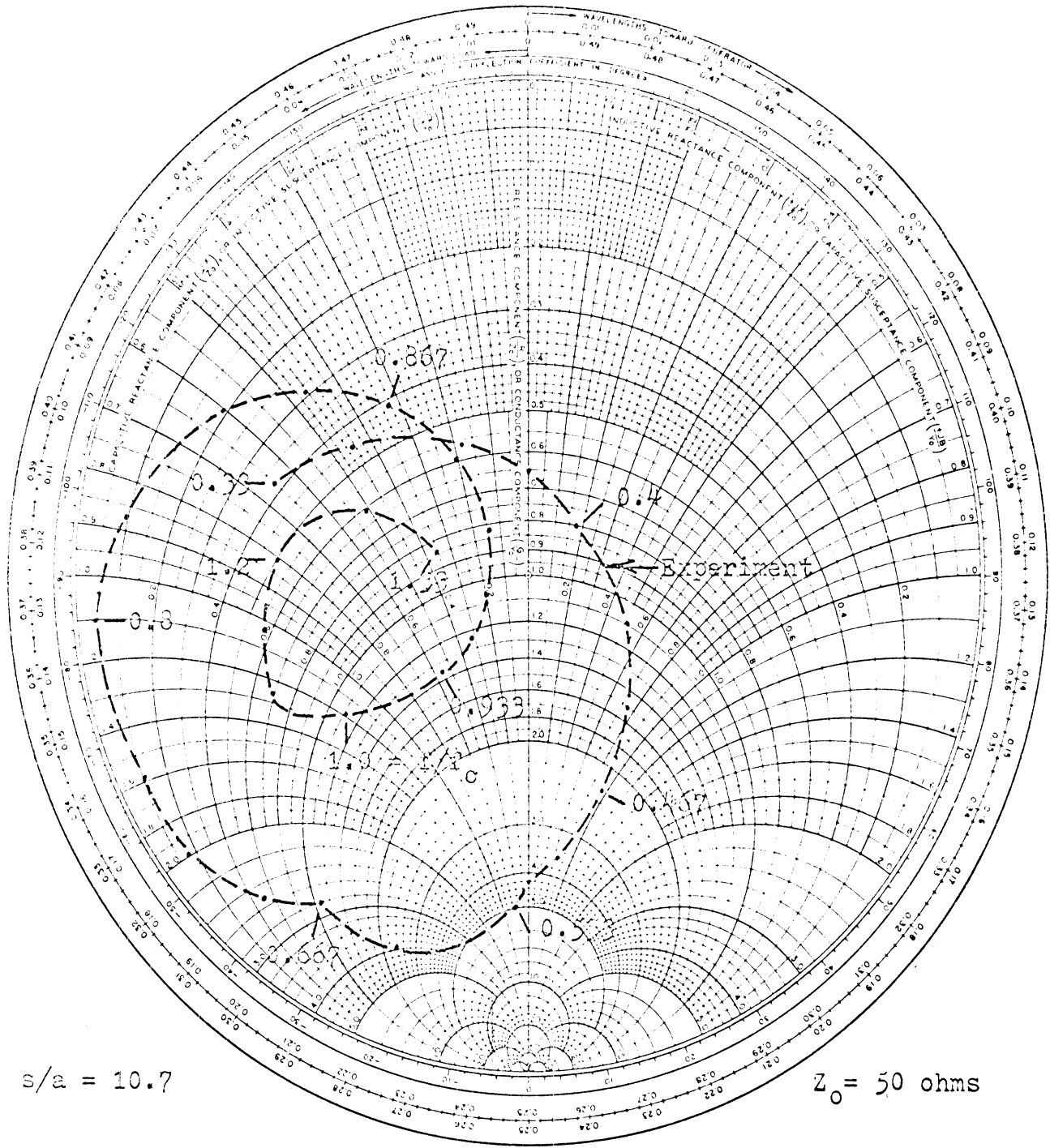


Figure A-33: Input Impedance of a Trap Antenna with a 34.8 Ohm Transmission Line Trap and 4/16 Inch Trap Gap Width

APPENDIX B
SELECTED RADIATION PATTERNS

Figure B-1 illustrates how the radiation pattern at the anti-resonant frequency of the trap of a trap-loaded cylindrical antenna changes as a function of the length of the outer element. Figure B-2 illustrates how the radiation pattern at the anti-resonant frequency of the trap of a trap-loaded cylindrical antenna varies as a function of the length of the inner section.

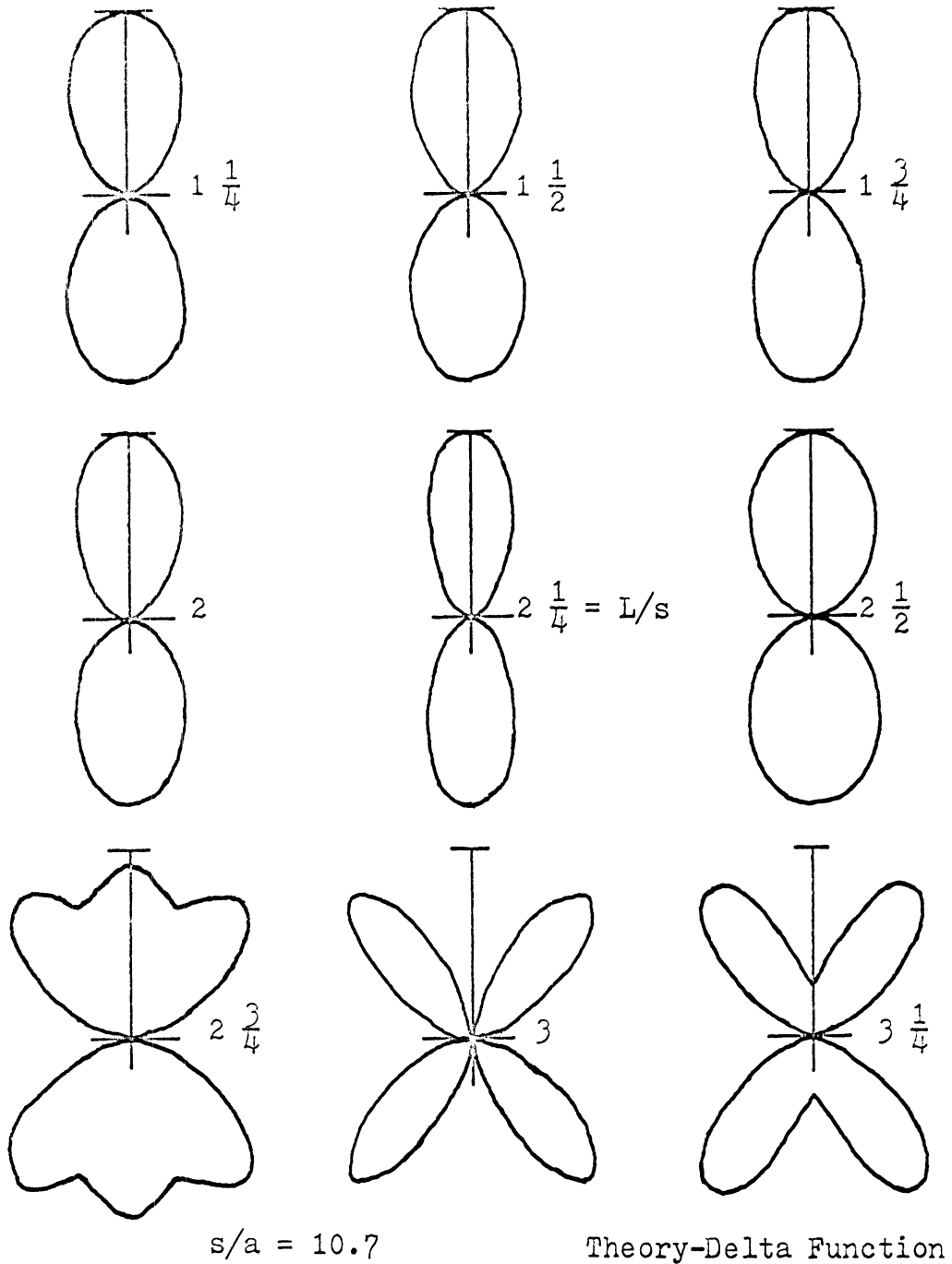


Figure B-1: Linear Power Radiation Patterns of a Series of Trap-Loaded Cylindrical Antennas at the Anti-Resonant Frequency of the Trap as a Function of the Antenna Length to Trap Location Ratio

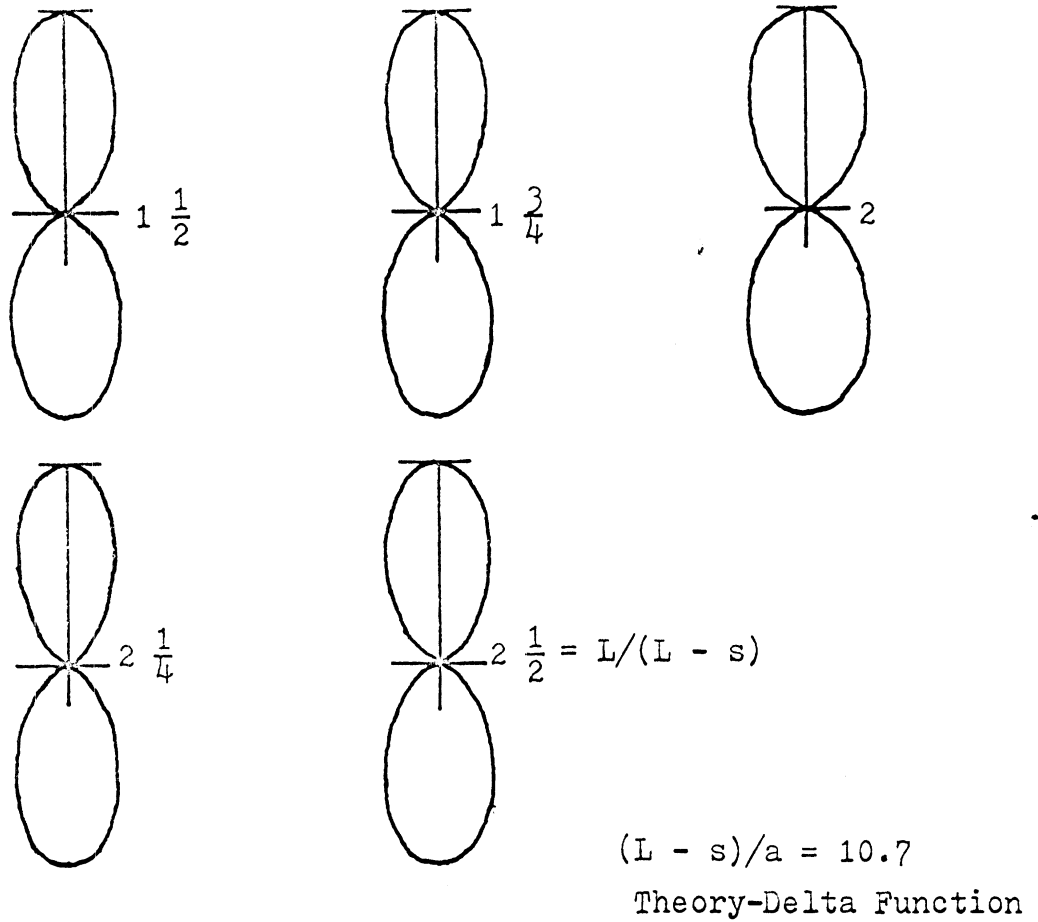


Figure 3-2: Linear Power Radiation Patterns of a Series of Trap-Loaded Cylindrical Antennas at the Anti-Resonant Frequency of the Trap as a Function of the Antenna Length to Outer Section Length Ratio

APPENDIX C

SELECTED CURRENT DISTRIBUTIONS

Figures C-1 through C-9 show plots of the amplitude and phase of the current distribution at the anti-resonant frequency of the trap on a trap-loaded cylindrical antenna as the length of the outer section is varied. Figures C-10 through C-13 show plots of the amplitude and phase of the current distribution at the anti-resonant frequency of the trap on a trap-loaded cylindrical antenna as the length of the inner section is varied.

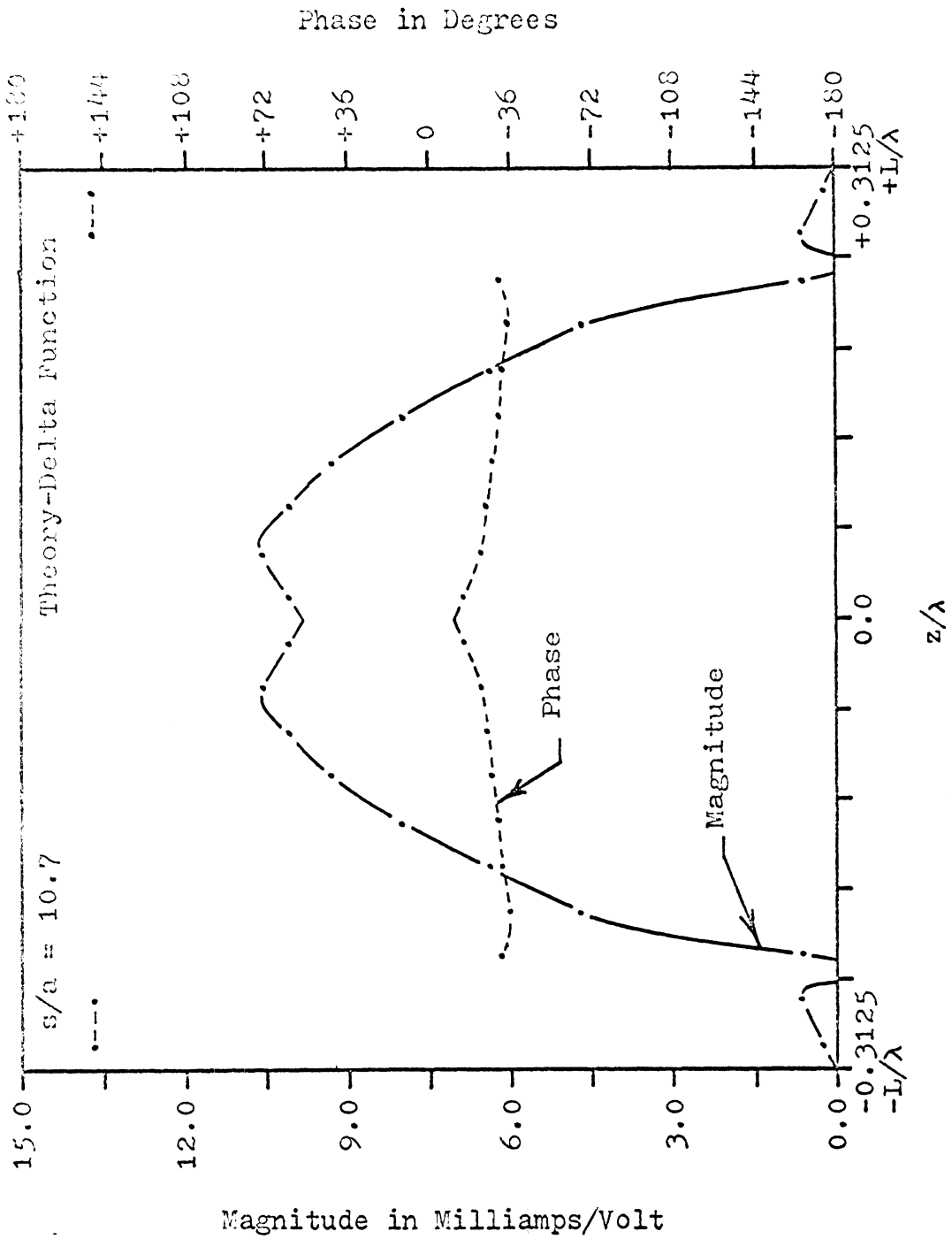


Figure C-1: Current Distribution for a Trap-Loaded Cylindrical Antenna at the Anti-Resonant Frequency of the Trap, $L = (5/16)\lambda$, $L/s = 1\frac{1}{4}$

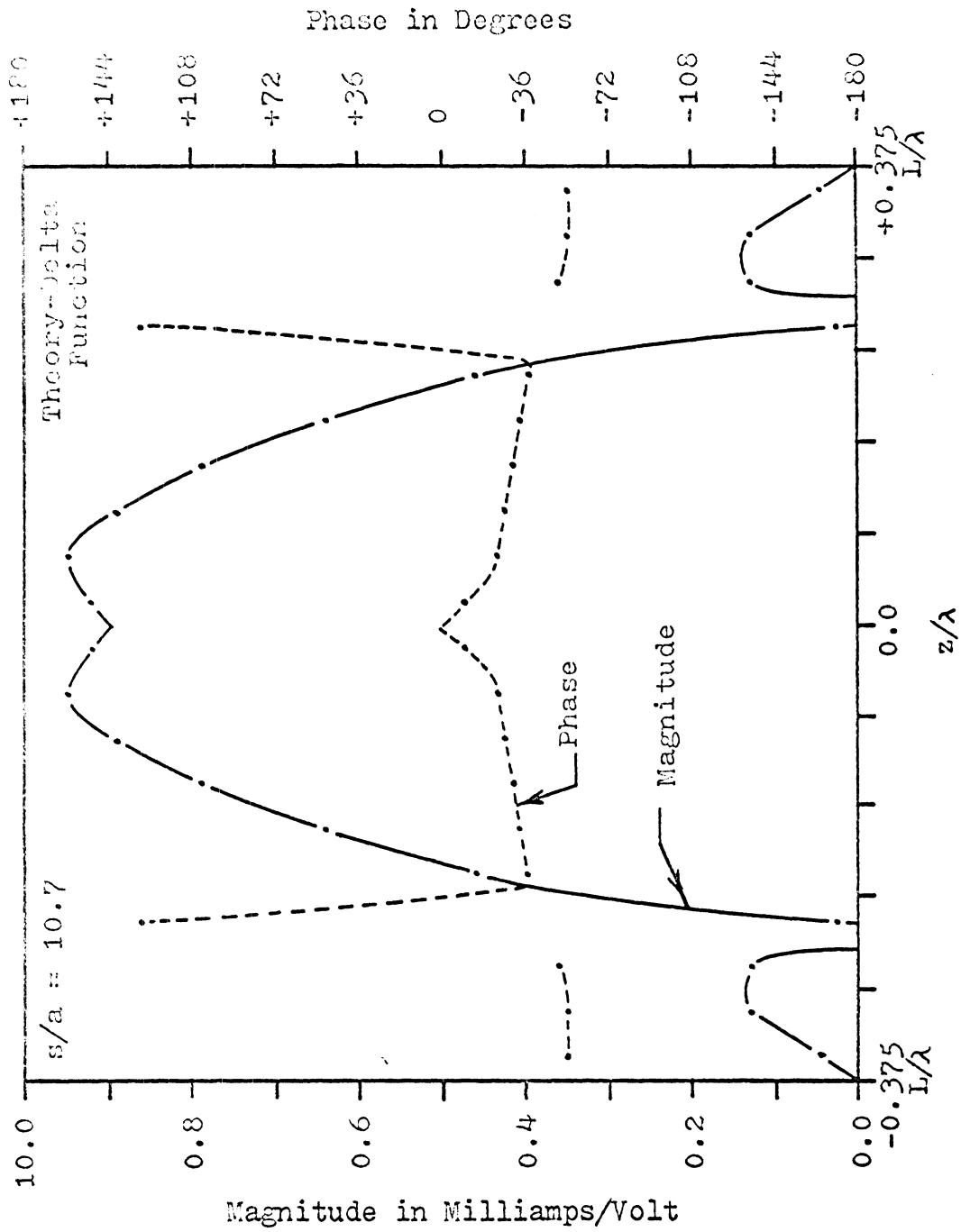


Figure C-2: Current Distribution for a Trap-Loaded Cylindrical Antenna at the Anti-Resonant Frequency of the Trap, $L = (3/8)\lambda$, $L/s = 1\frac{1}{2}$

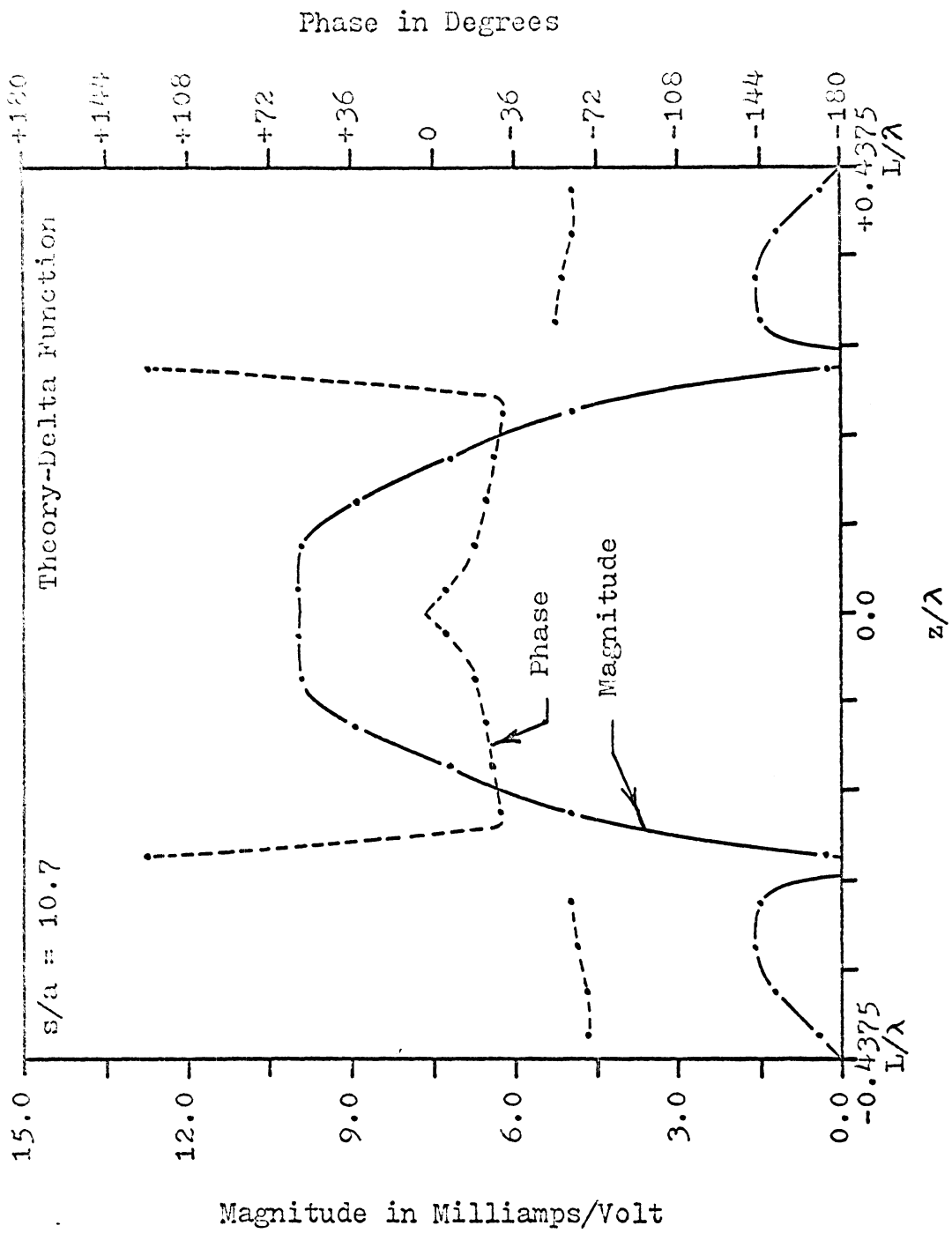


Figure C-3: Current Distribution for a Trap-Loaded Cylindrical Antenna at the Anti-Resonant Frequency of the Trap, $L = (7/16)\lambda$, $L/s = 1-3/4$

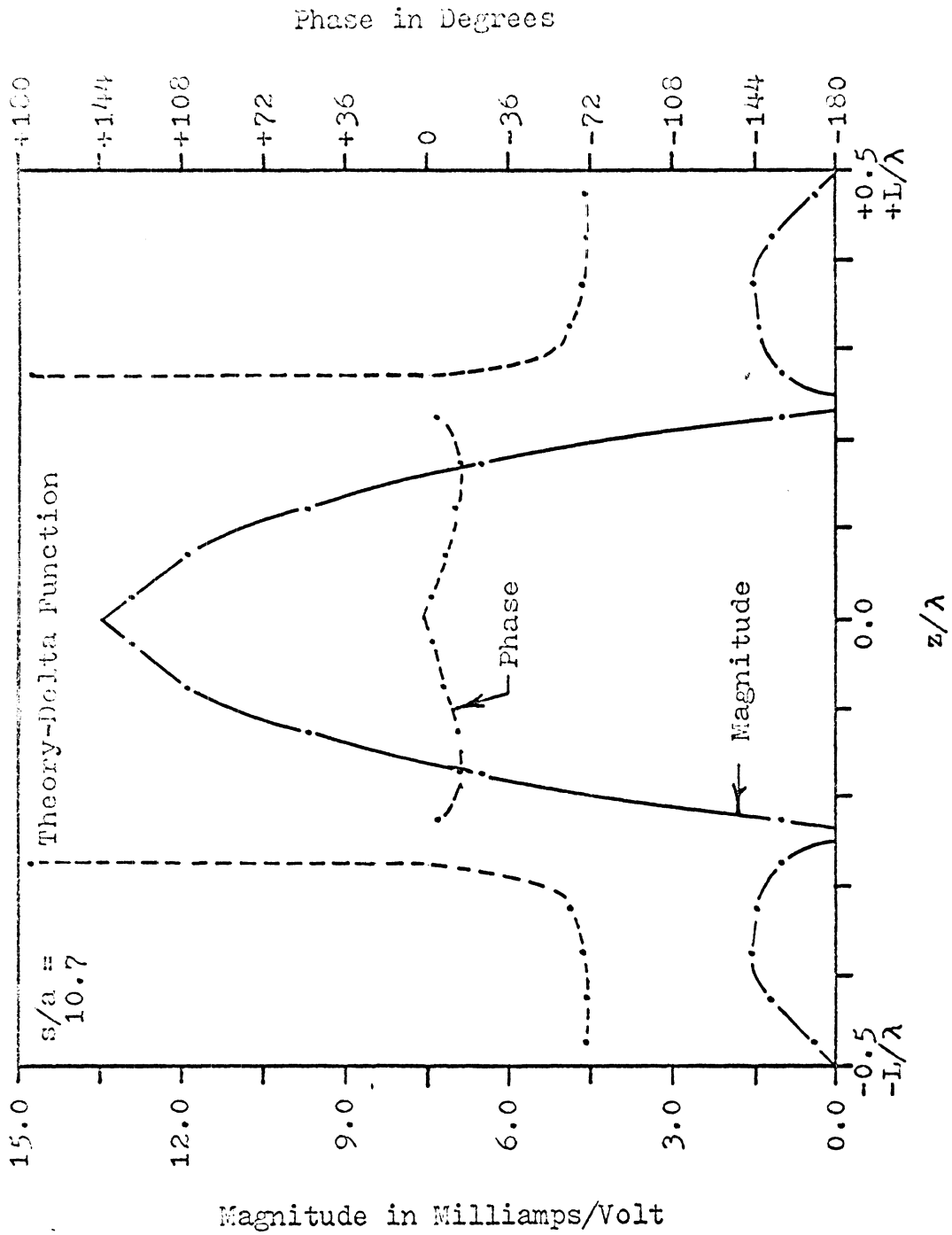


Figure C-4: Current Distribution for a Trap-Loaded Cylindrical Antenna at the Anti-Resonant Frequency of the Trap, $L = (1/2) \lambda$, $L/s = 2$

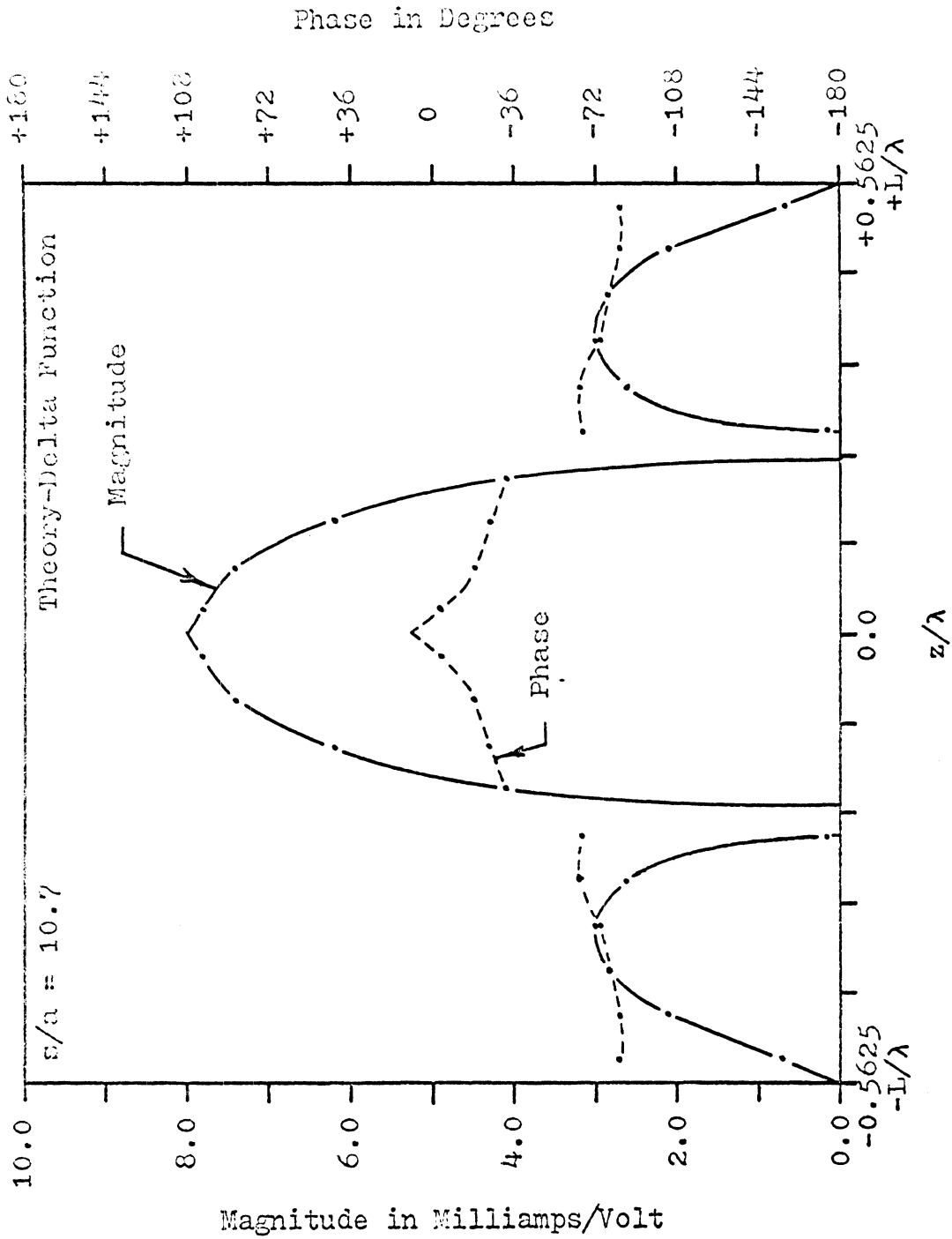


Figure C-5: Current Distribution for a Trap-Loaded Cylindrical Antenna at the Anti-Resonant Frequency of the Trap, $L = (9/16)\lambda$, $L/s = 2\frac{1}{4}$

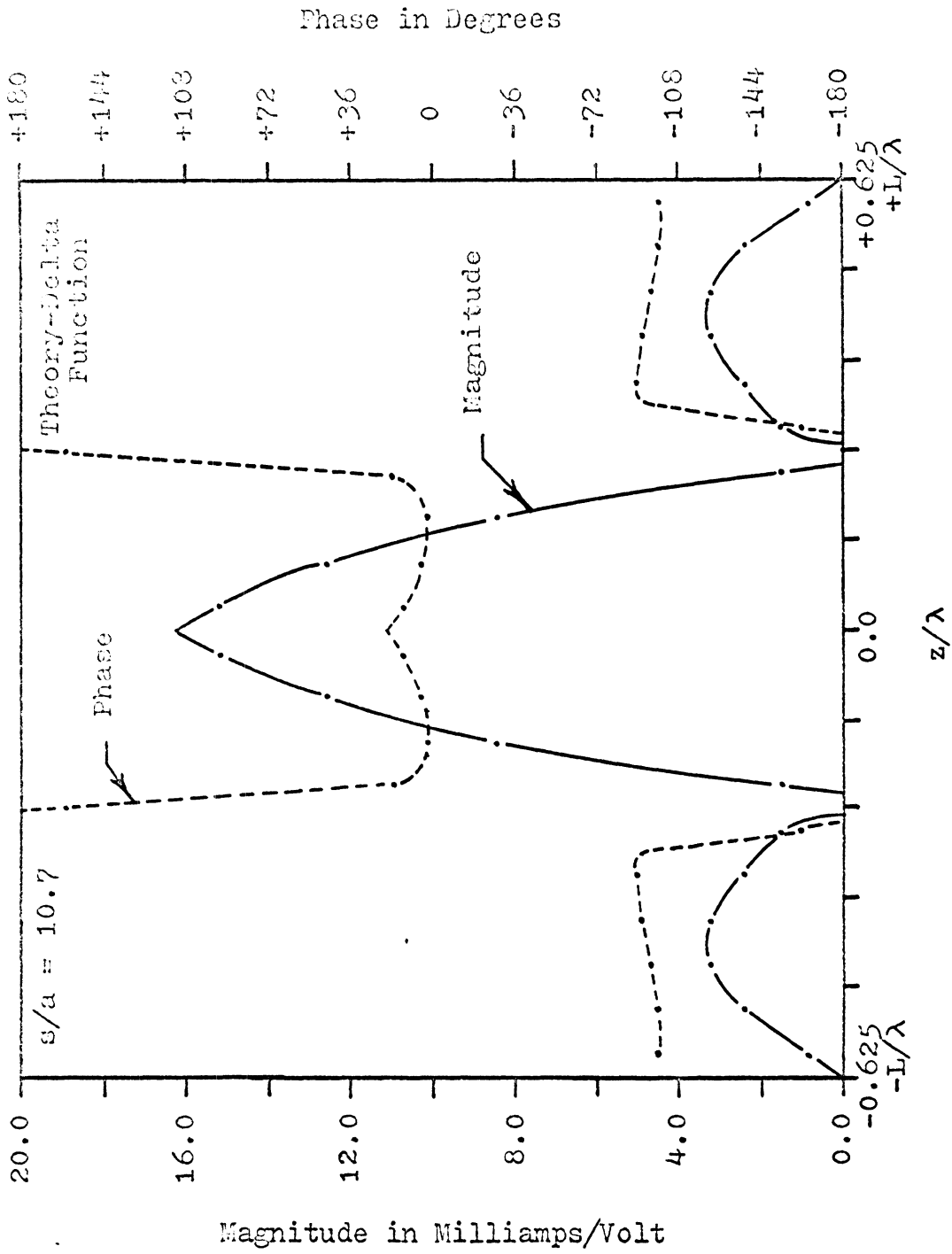


Figure C-6: Current Distribution for a Trap-Loaded Cylindrical Antenna at the Anti-Resonant Frequency of the Trap, $L = (5/8)\lambda$, $L/s = 2\frac{1}{2}$

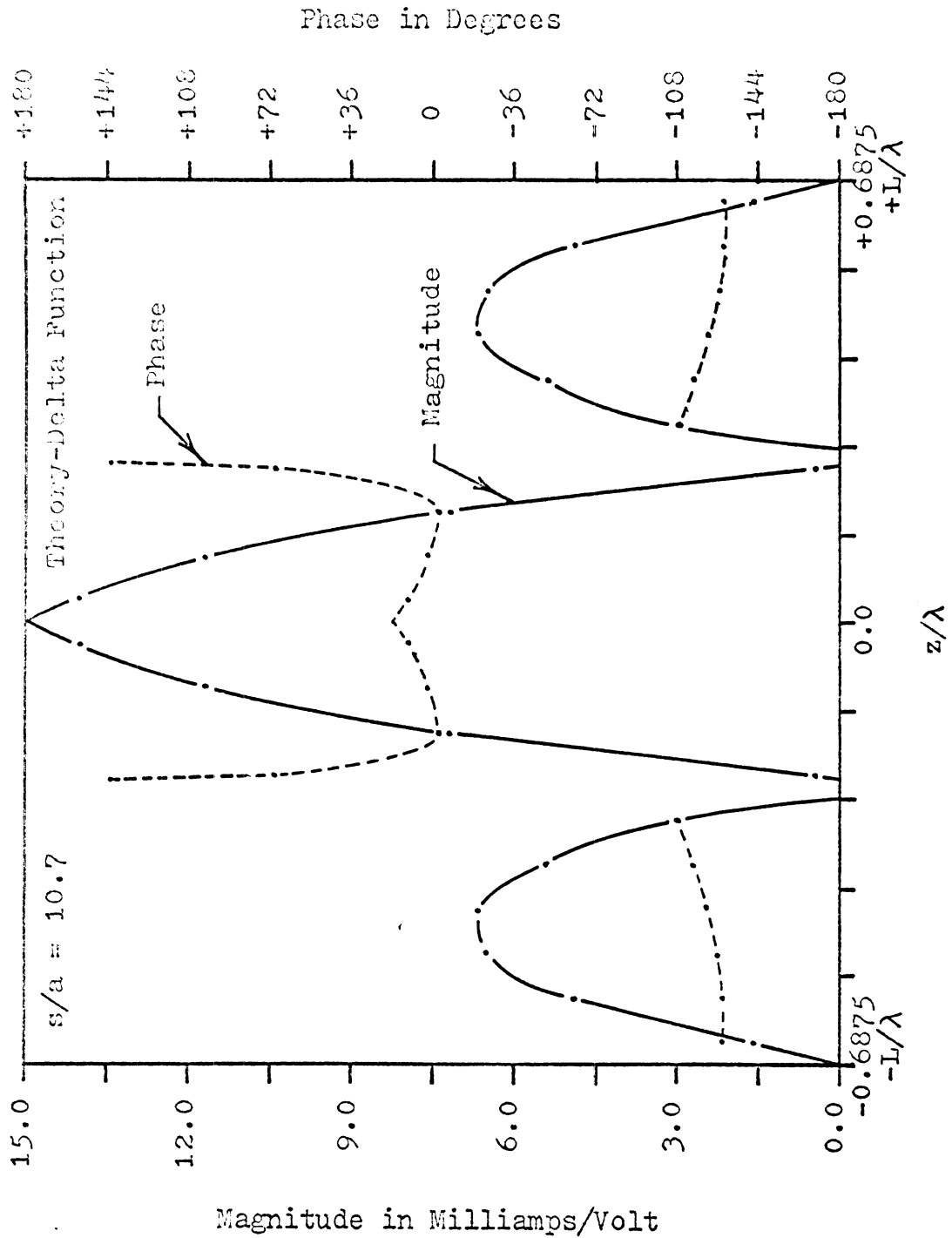


Figure C-7: Current Distribution for a Trap-Loaded Cylindrical Antenna at the Anti-Resonant Frequency of the Trap, $L = (11/16) \lambda$, $L/s = 2-3/4$

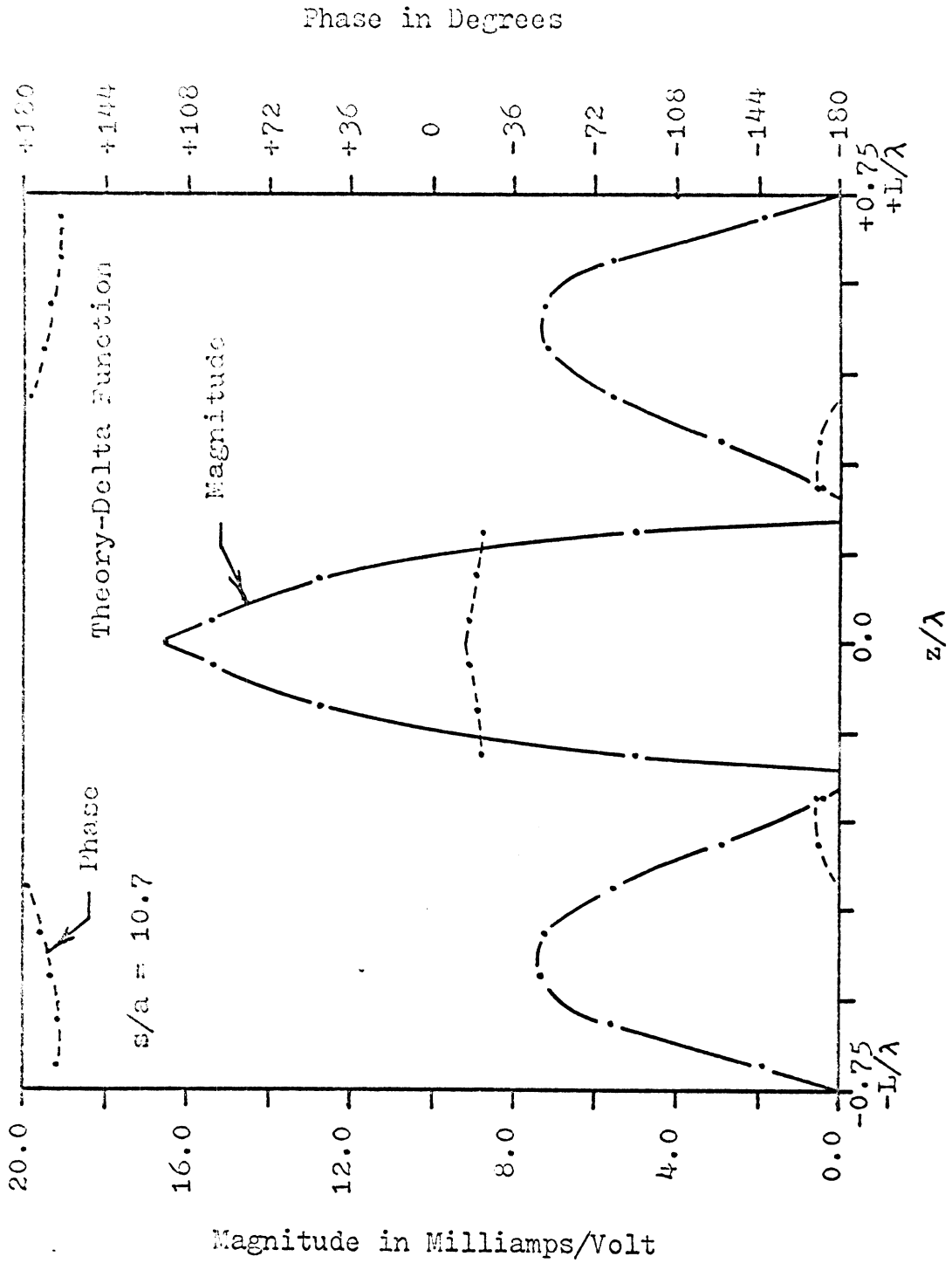


Figure C-8: Current Distribution for a Trap-Loaded Cylindrical Antenna at the Anti-Resonant Frequency of the Trap, $L = (3/4)\lambda$, $L/s = 3$

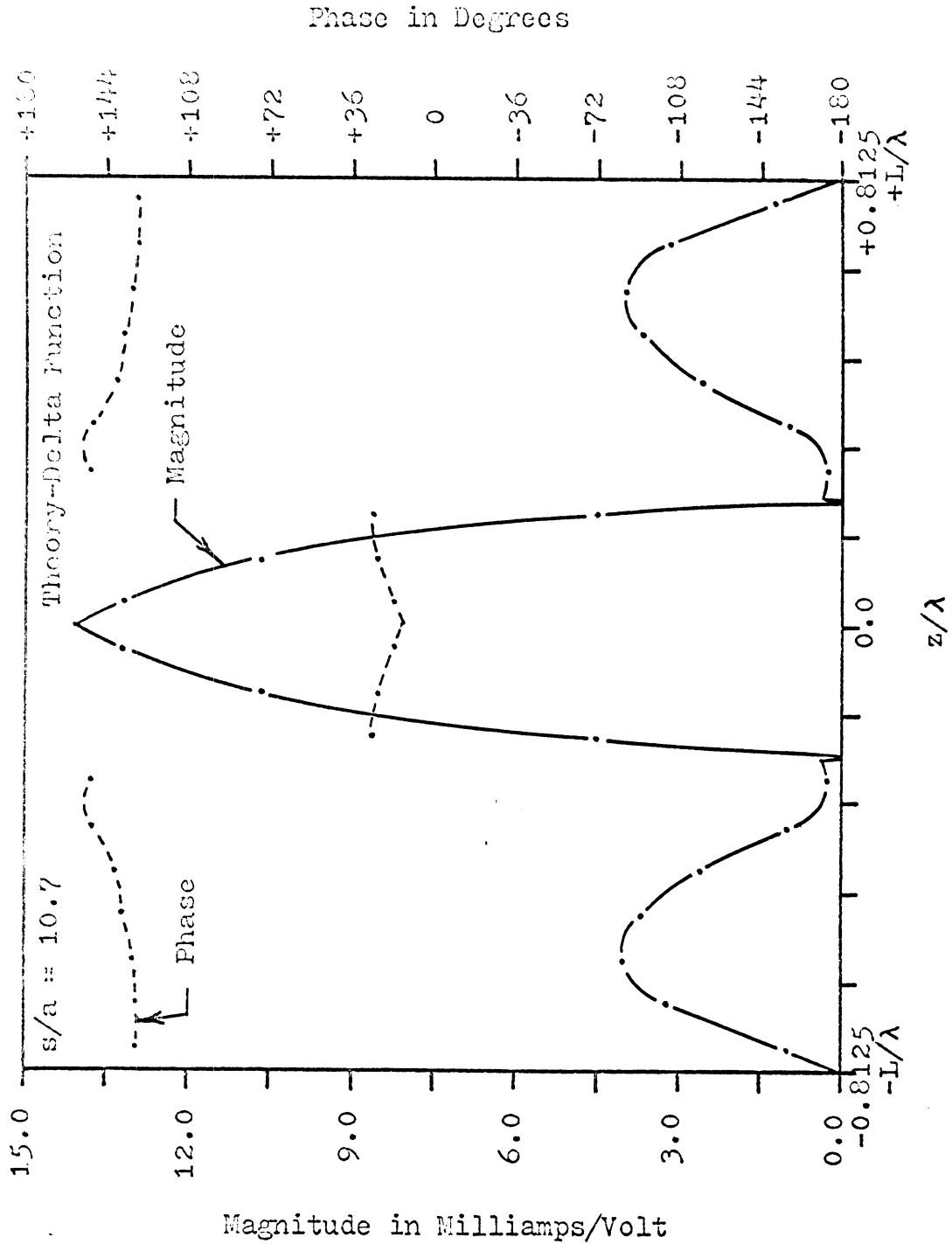


Figure C-9: Current Distribution for a Trap-Loaded Cylindrical Antenna at the Anti-Resonant Frequency of the Trap, $L = (13/16) \lambda$, $L/s = 3\frac{1}{4}$

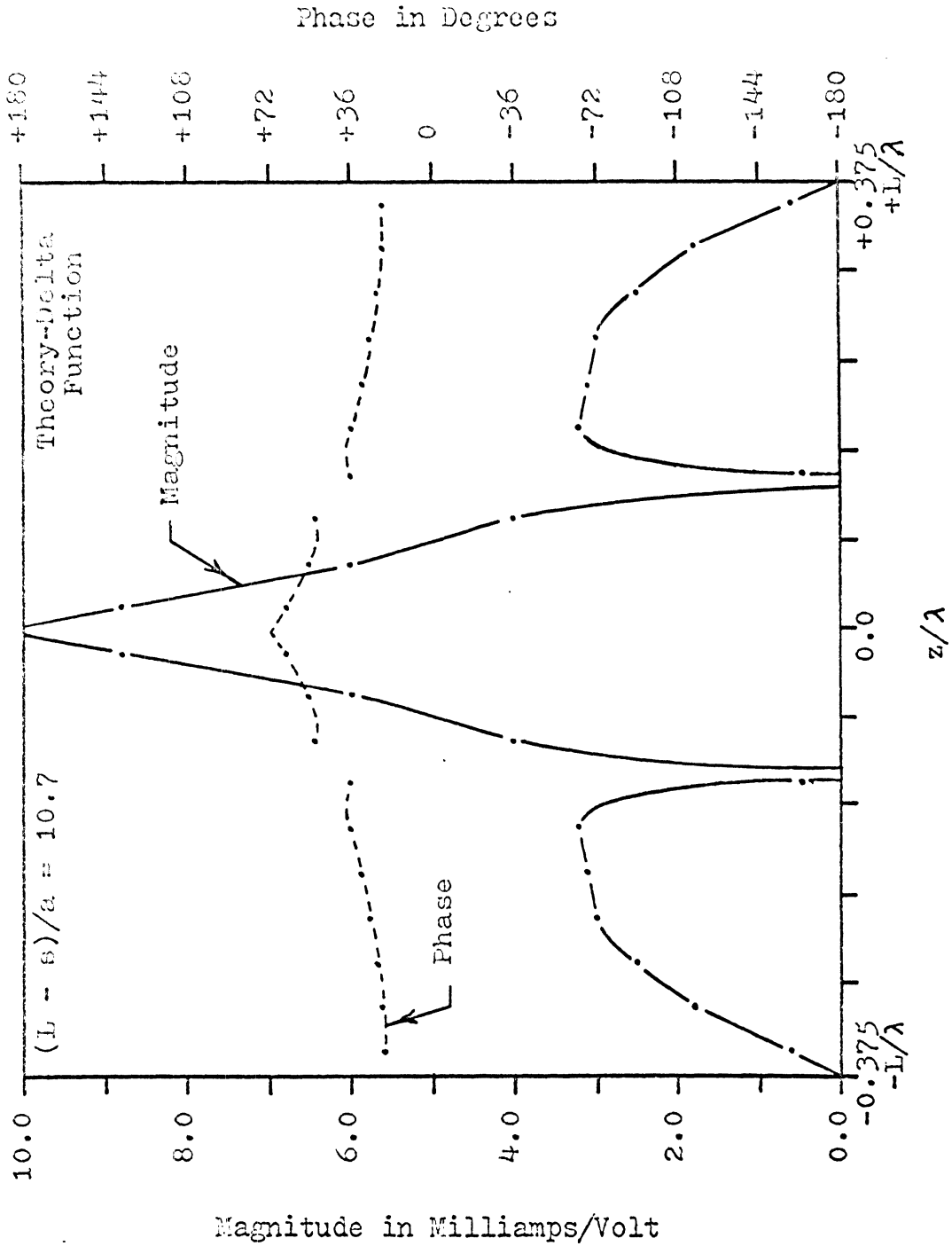


Figure C-10: Current Distribution for a Trap-Loaded Cylindrical Antenna at the Anti-Resonant Frequency of the Trap, $L = (3/8)\lambda$, $L/(L-s) = 1\frac{1}{2}$

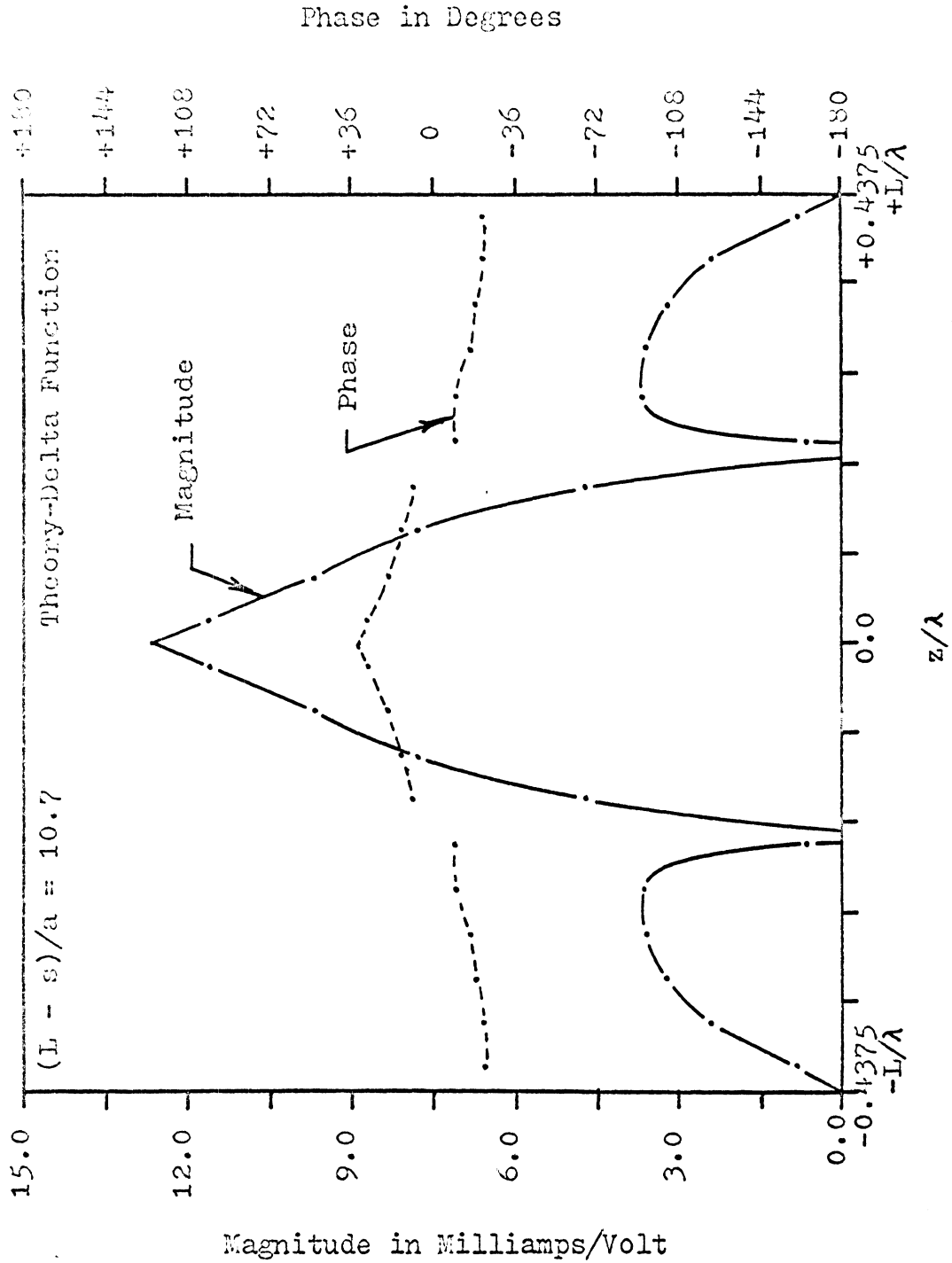


Figure C-11: Current Distribution for a Trap-Loaded Cylindrical Antenna at the Anti-Resonant Frequency of the Trap, $L = (7/16)\lambda$, $L/(L-s) = 1-3/4$

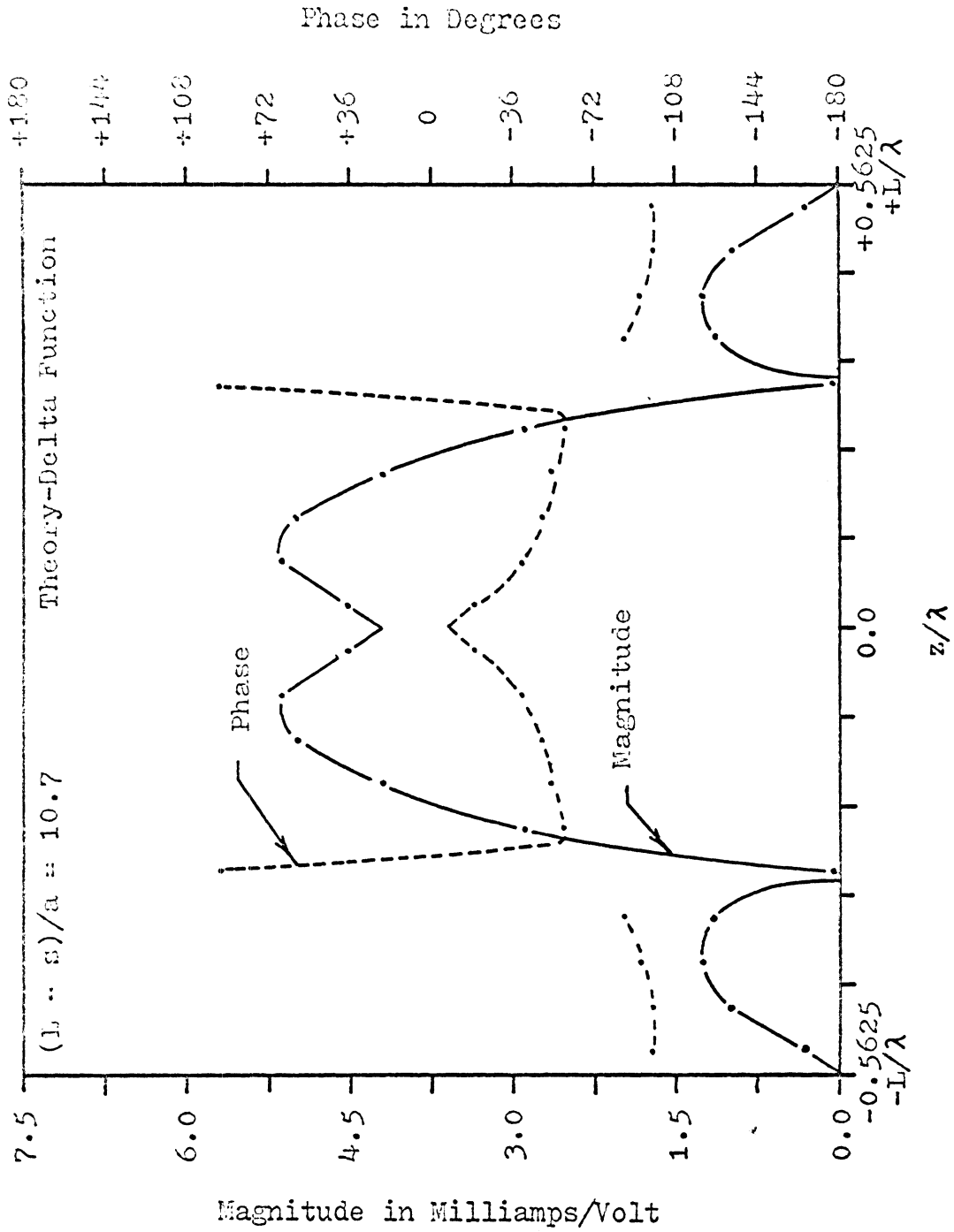


Figure C-12: Current Distribution for a Trap-Loaded Cylindrical Antenna at the Anti-Resonant Frequency of the Trap, $L = (9/16)\lambda$, $L/(L-s) = 2\frac{1}{4}$

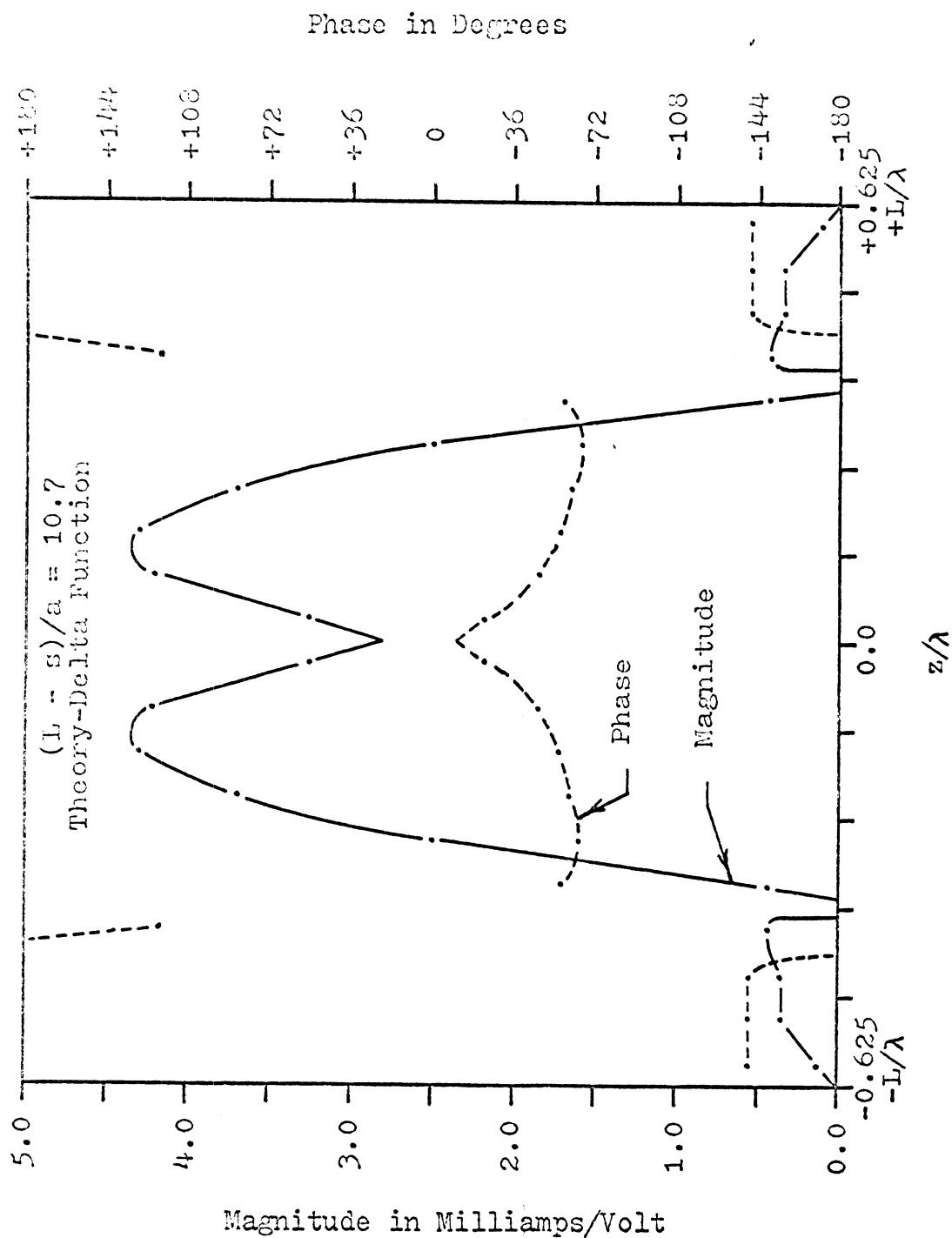


Figure C-13: Current Distribution for a Trap-Loaded Cylindrical Antenna at the Anti-Resonant Frequency of the Trap, $L = (5/8)\lambda$, $L/(L-s) = 2\frac{1}{2}$

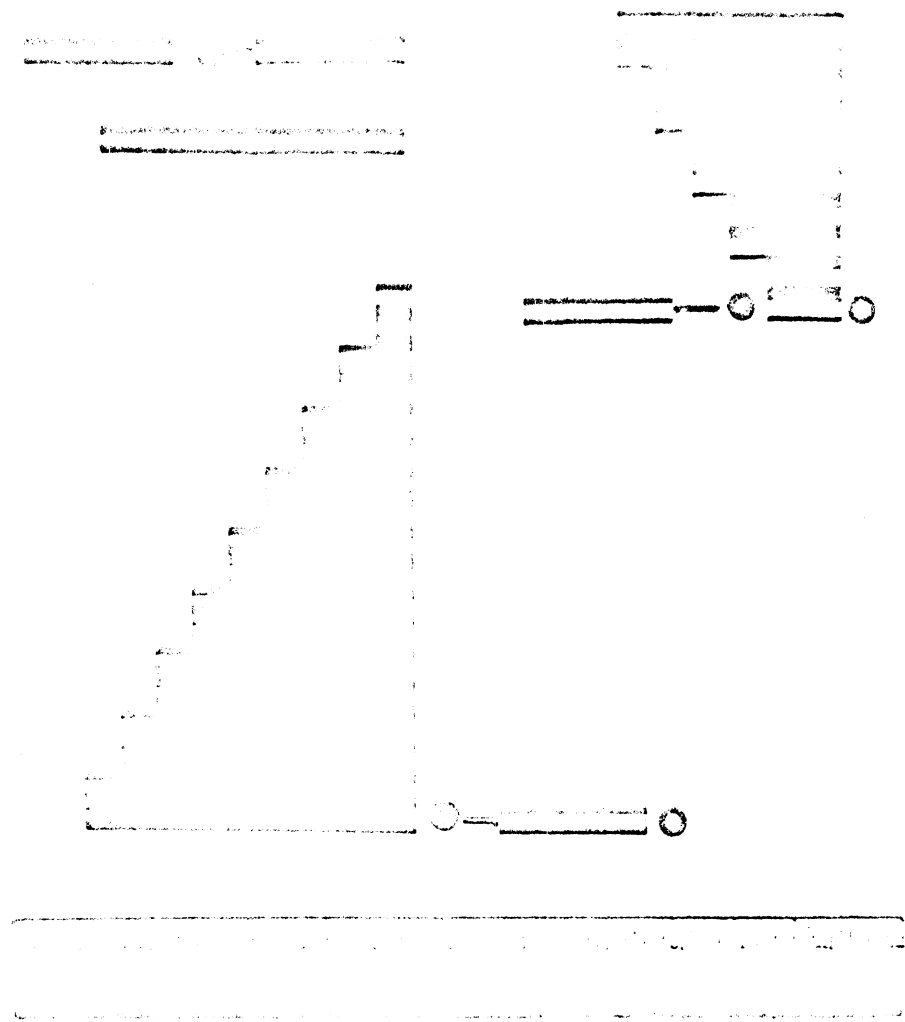


Figure D-1: Copper Tubing Series of Antennas

APPENDIX D
PHOTOGRAPHS

Photographs of several features of the experimental models are included in Figures D-1 through D-8.

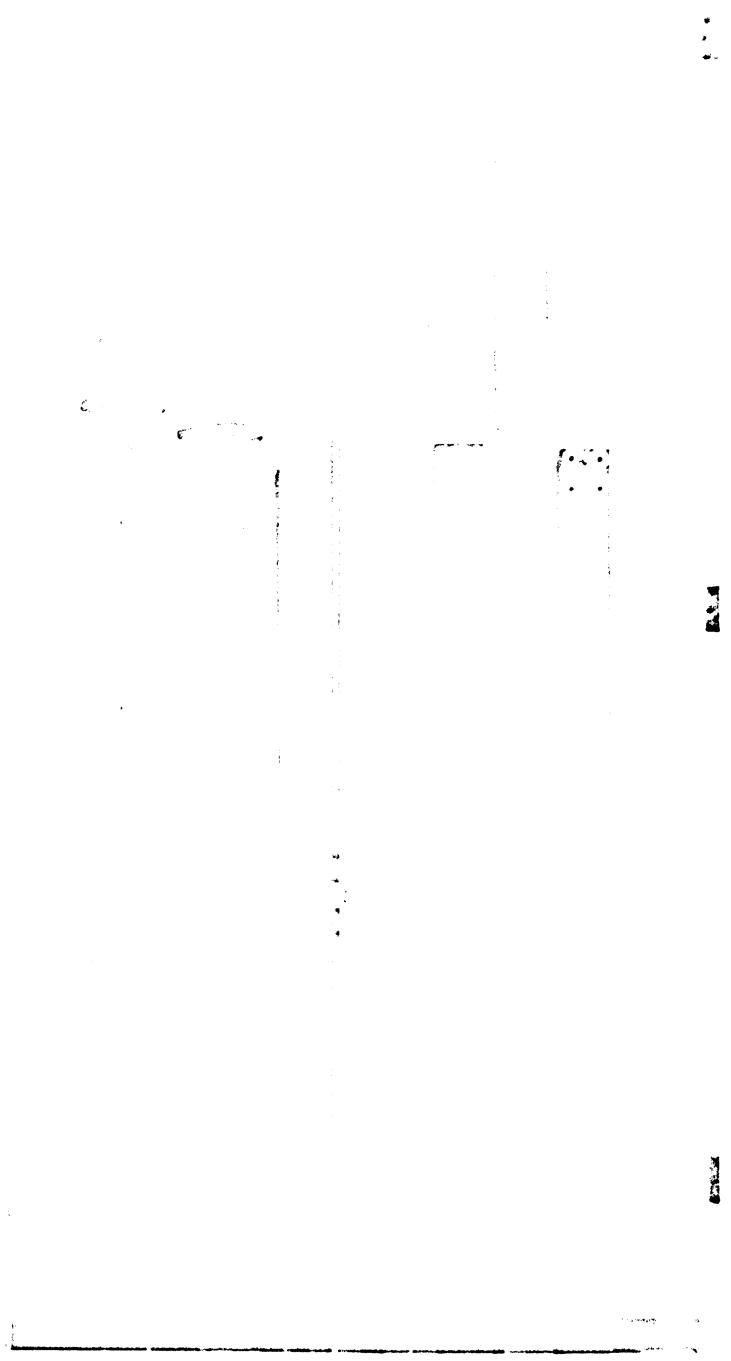


Figure D-2: 2x4 Series of Antennas



Figure D-3: 2x4 Antenna Mounted on Ground Plane



Figure D-4: Inductor-Capacitor Trap

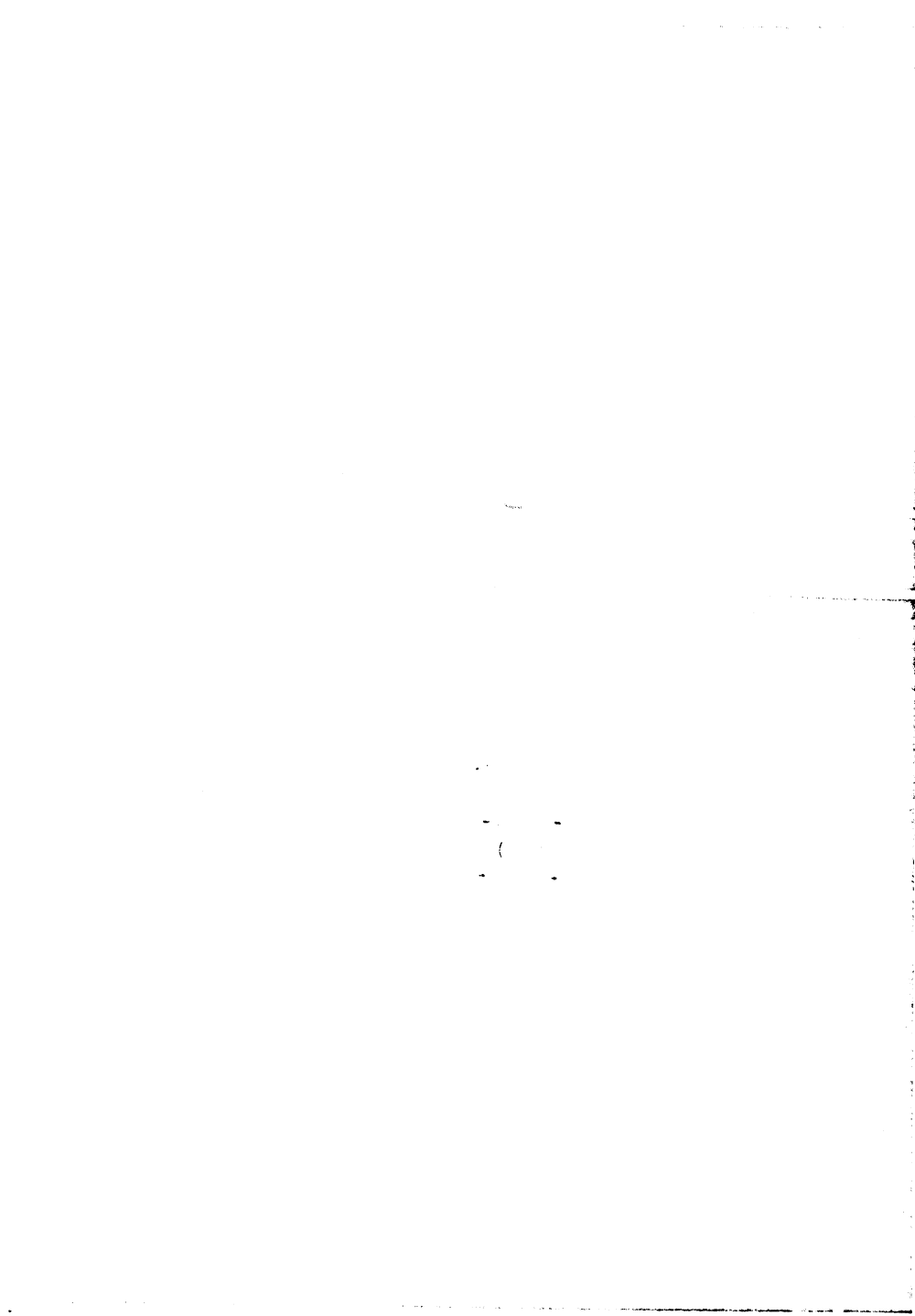


Figure D-5: Copper Tubing Trap Antenna Mounted on
Ground Plane

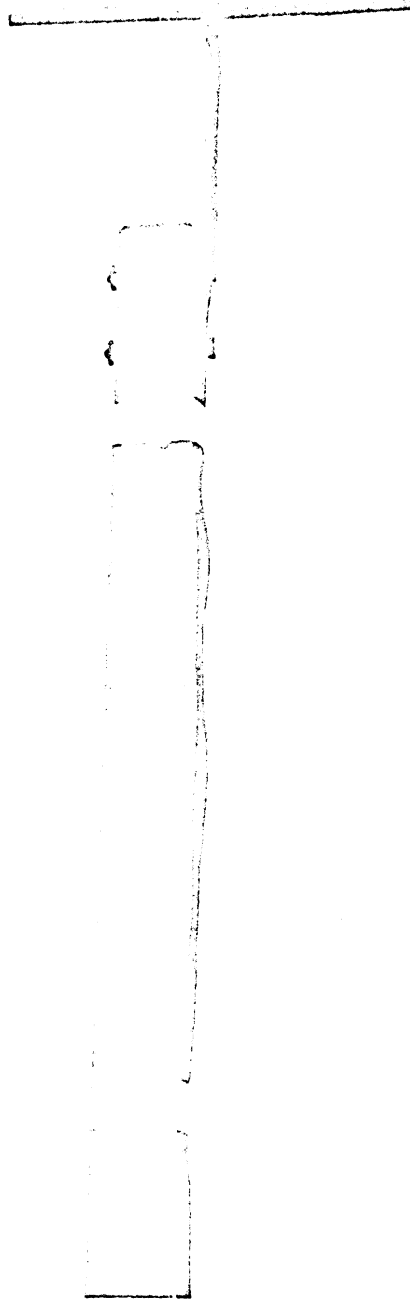


Figure D-6: Radiation Pattern Measurement on a Trap Antenna

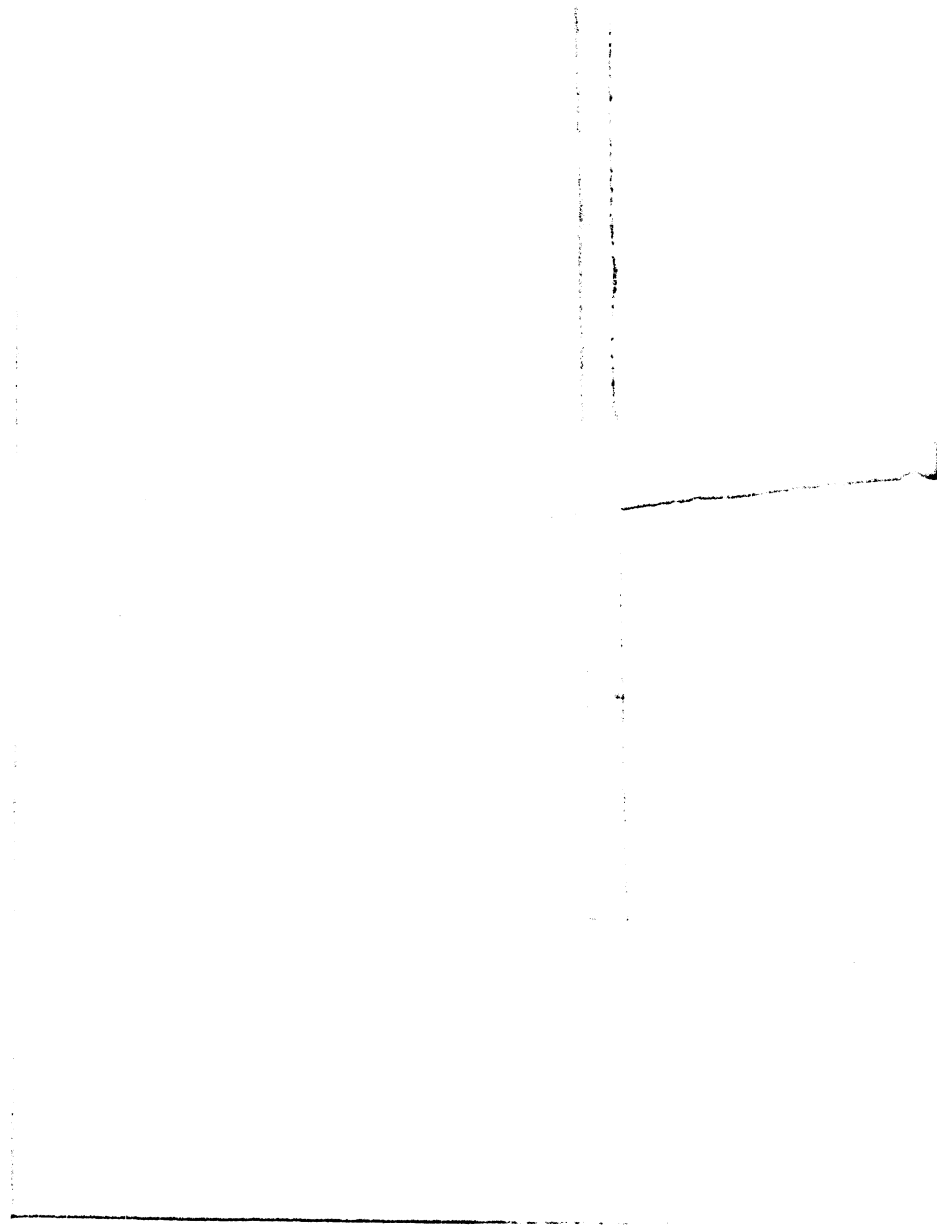


Figure D-7: Current Probe and a Trap Antenna

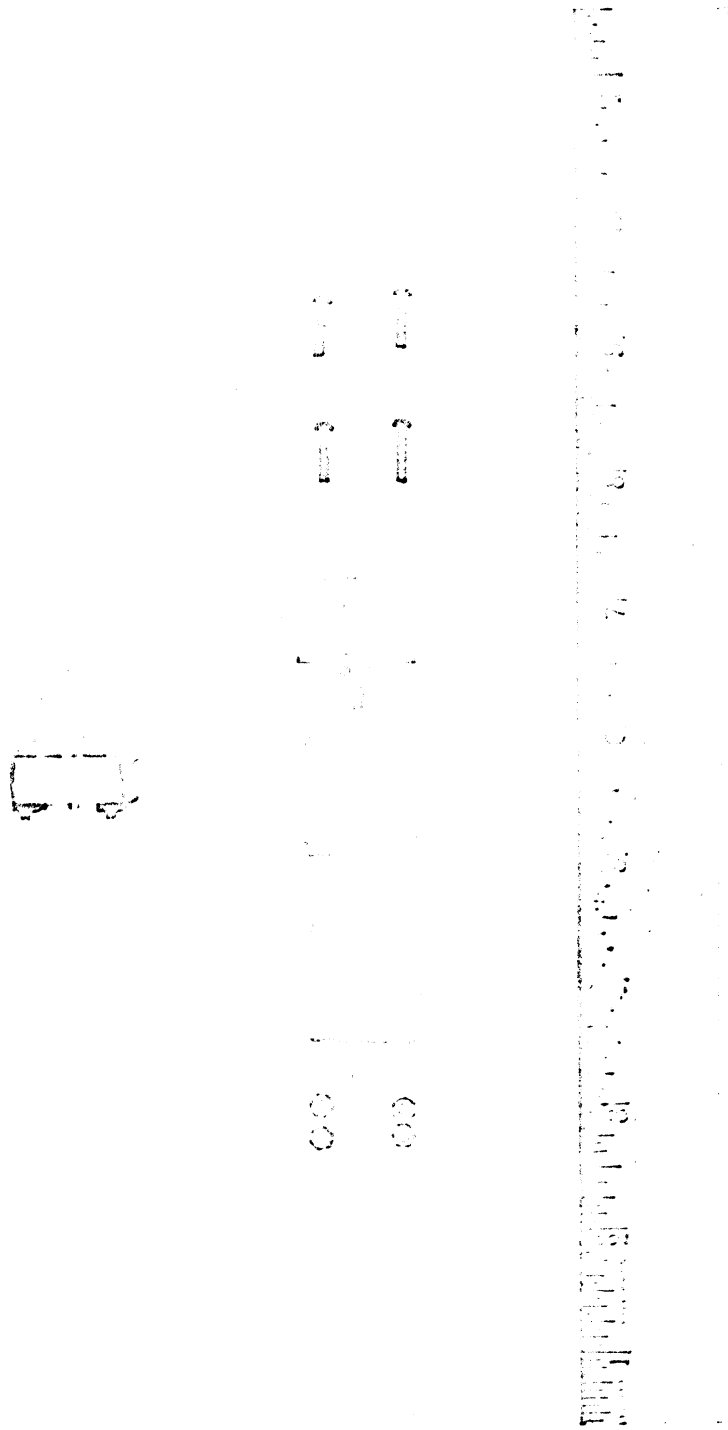


Figure D-8: Assembled and Dis-Assembled Special Short Circuit